TARGETED RESOURCE RECOVERY FROM MINE WATERS BY SELECTIVE ION EXCHANGE

A THESIS SUBMITTED IN PARTIAL FULFILMENT
OF THE REQUIREMENTS FOR THE DEGREE OF

DOCTOR OF PHILOSOPHY

BY

ALEX LLOYD RILEY, MSC

Department of Chemical & Biological Engineering
Faculty of Engineering
The University of Sheffield

SUPERVISED BY

DR. MARK D. OGDEN
DR. HENRIETTE S. JENSEN

SUBMITTED
January 2020

SUMMARY

Waste stockpiles generated as a result of mining cause long-term damage to the environment and can continue to act as a source of pollution for decades beyond mine closure. Current treatment options tend to focus predominantly on Fe removal and may not properly target other trace metal species that may also be present, e.g. Ni, Mn, Co, Cu; metals with an intrinsic recovery value. As such, this thesis explores the potential application of ion exchange resins to selectively recover metals from mine waters, with the hope that by viewing the wastes as a resource rather than a problem, an incentive is provided to deal with this globally significant pollution source.

A range of commercially available ion exchange resins of different chemical functionality were screened for their selective metal recovery performance under a range of pH and [SO_4^{2-}] conditions. Of the most suitable resins, fixed-bed breakthrough modelling was used to describe their extractive abilities under dynamic operation, and to define optimum operating conditions. Of particular note, a resin was identified which was capable of truly selective Cu recovery from the complex waste stream. The extent to which metals could be recovered from resins after extraction was determined through elution studies, and the composition of eluents was tailored to maximise the concentration of solutions recovered. For one of the resins, a two-stage elution process was proposed for the selective recovery of Co and Ni as two separate, concentrated product streams; a highly desirable separation given the high value of each metal. The reusability of each resin was determined through cyclic adsorption and desorption studies to assess process sustainability, and where appropriate, resin degradation mechanisms were explored. Finally, a bench-scale system was operated to explore the potential of a coupled-column system design for continuous treatment and resource recovery.

ACKNOWLEDGMENTS

The work presented in this thesis would not have been possible without the contribution of the many people who I have been fortunate enough to work alongside throughout my doctoral studies. I must begin by first acknowledging the efforts of my primary supervisor, Dr. Mark D. Ogden, who willingly accepted a muddy-booted environmental scientist with no chemical laboratory experience and shaped me to become the researcher that I am today. His guidance and knowledge have been critical throughout my time at The University of Sheffield, and this final product would not have been possible without him. I must also thank my second supervisor, Dr. Henriette Jensen, particularly for the excellent advice given to me during the write-up process, which I have used daily.

I am also indebted to the generosity of Dr. Will Mayes (University of Hull) and Dr. Chris Porter (R.S. Bruce Ltd.) for providing me with free access to ICP-OES analysis during the first and final years of my studies during times when the AAS operated strictly in 'random number generator' mode. Furthermore, I am grateful to the members of the Separations and Nuclear Chemical Engineering Research (SNUCER) Group, past and present, who have made my time at Sheffield truly enjoyable and have taught me more in the last four years than they realise. I wish them all the best for the future.

There are also people who have supported me personally throughout my PhD studies. I thank my parents and family, without whose constant encouragement throughout my university education I would have never been able to reach this point. Finally, I thank my wonderful wife, Lauren, for her endless support and reassurance over the past four years, which has been invaluable to me.

TABLE OF CONTENTS

LIST OF FIGURES

LIST OF TABLES

1 INTRODUCTION

1.1 MINE POLLUTION IN THE UK

One of the major challenges currently facing humanity is the need to provide an adequate quantity of high-quality water to support a rapidly growing population. Despite the abundance of water on earth, only around 2.5 % of total global water is freshwater; the majority of which (approximately 69 %) is held in glaciers and ice caps and therefore inaccessible for drinking water abstraction. The remaining freshwater must provide for a rapidly accelerating population yet is being increasingly polluted by human activities. While there are many contributors to global water pollution, such as eutrophication from irresponsible farming practices, and the increasing prevalence of emerging contaminants (e.g. pharmaceuticals) in natural waters, a common cause of water quality degradation stems from mining operations (WHO/UNEP, 1997).

Worldwide, mining activities are responsible for mobilising 50×10^9 tonnes of geological material per year (Schwarzenbach, et al., 2010), which after metal/mineral extraction results in the heaping of enormous quantities of waste. The pollution generated by these wastes have been conservatively estimated to have detrimentally affected around 20,000 km of rivers and 70,000 ha of lakes and reservoirs globally (Johnson & Hallberg, 2005). On a national scale, the discharge of contaminated waters from mines and associated waste heaps is the most severe issue facing water quality within the United Kingdom (Jarvis & Younger, 2000). The release of problematic metals from past and present mining activities adversely affects receiving streams through damage to ecological community structure (Armitage, et al., 2007, Jarvis & Younger, 1997) and degradation of chemical water quality. Mine pollution also acts as a barrier to reaching strict legislative environmental targets, with UK mine waters commonly exceeding environmental quality standards by several orders of magnitude for key metal concentrations (Jarvis, et al., 2014).

The UK has a long and rich history of metal mining, ranging from early Bronze Age copper and tin mines through to modern iron and coal extraction. Mining efforts greatly accelerated throughout the industrial revolution and reached their peak in the early 20th century (Younger, et al., 2002). The majority of modern metal mining activities in the UK ceased to operate prior to 1999 (Jones, et al., 2013), when an alteration to the Water Resources Act (WRA 91) stated that mine operators were thereafter responsible for any enduring pollution emitted from the mines upon closure (Johnston, et al., 2008). Poor environmental management surrounding historical mining activities coupled with rapid abandonment of mining operations during the 20th century resulted in the creation of a nationally significant mine water pollution problem.

The effects of this pollution are widespread, with more than 700 km of UK streams and rivers affected (Jarvis & Younger, 2000). A more recent study which aimed to identify and prioritise the management of non-coal mine sites reported that 6% of all surface water bodies in England and Wales are affected by metal mine discharge (Mayes, et al., 2009), while in Scotland the issue of mine-related freshwater pollution is second only to that of sewage (Younger, 2001).

The spatial distribution of streams and rivers affected by mine water discharges is linked closely to areas which have long histories of mining (Figure 1.1), notably the orefields of southwest England, North and Western Wales, the Lake District, and the Pennines (Mayes, et al., 2009). The widespread distribution of watercourses affected by abandoned mine discharges highlights the need to employ effective remediation strategies at legacy pollutant sites. Similarly, the legislative responsibility of mine operators for long-term pollution emphasises the importance of environmental remediation in current post-closure management plans. In order to address this pollution issue, it is first important to understand the processes governing the formation of mine-wastes, and the pollution arising from their disposal.
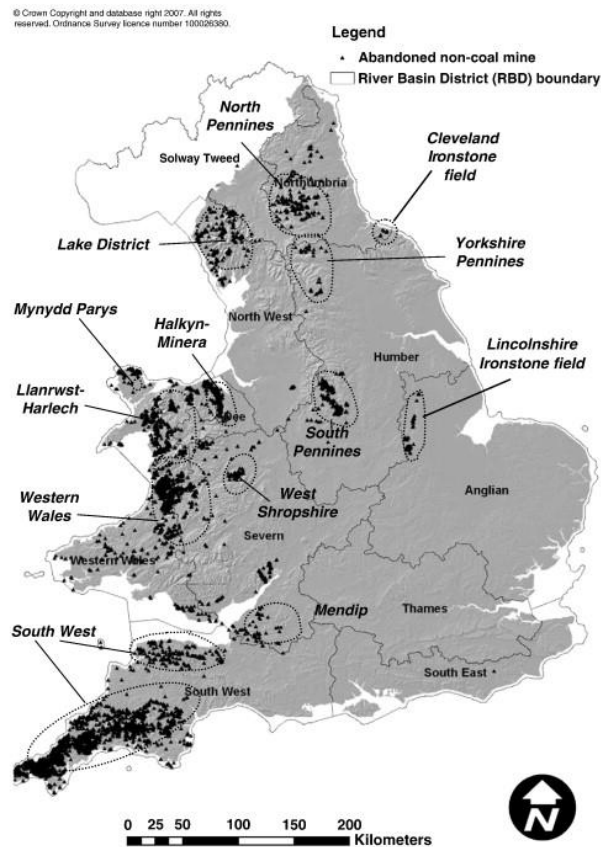
Figure 1.1. National distribution of abandoned non-coal mines and associated River Basin Districts (used with permission from Mayes *et al.*, 2009)

1.2 FORMATION AND COMPOSITION OF MINE WATERS

During active operation, mine shafts are continuously pumped of groundwater to maintain access to ore deposits below the water table (Blowes, et al., 2013). The removal of ore from host rock reveals previously unexposed minerals, particularly pyrite (FeS_2), to atmospheric oxygen. When mines are abandoned, it is often the case that water pumps are switched off (Westermann, et al., 2017), allowing natural resurgence of groundwater and eventually the uncontrolled release of metalliferous waters to the environment (Banks, et al., 2017). This process of draining and flooding is key to mine water formation and is described through Equations 1.1-1.4 for pyrite (Kruse, et al., 2013; Younger, et al., 2002).

The pyritic oxidation process occurs in four stages; 1) oxidation and hydrolysis of exposed pyrite (Equation 1.1), 2) conversion of ferrous to ferric iron (Equation 1.2), 3) hydrolysis of ferric iron (Equation 1.3), and 4) further oxidation of pyrite by ferric iron (Equation 1.4).

Equation 1.1. Oxidation and hydrolysis of pyrite.

$$2FeS_{2\ (s)} + 7O_{2\ (g)} + 2H_2O_{(l)} \rightarrow 2Fe^{2+}_{(aq)} + 4SO^{2-}_{4\ (aq)} + 4H^+_{(aq)}$$
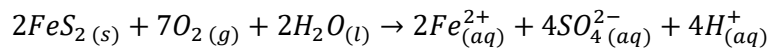
Equation 1.2. Oxidation of ferrous iron to ferric iron.

$$2Fe^{2+}_{(aq)} + 0.5O_{2\ (aq)} + 2H^+_{(aq)} \rightarrow 2Fe^{3+}_{(aq)} + H_2O_{(l)}$$
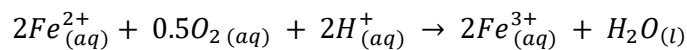
Equation 1.3. Hydrolysis of ferric iron.

$$2Fe^{3+}_{(aq)} + 6H_2O_{(l)} \leftrightarrow 2Fe(OH)_{3\ (s)} + 6H^+_{(aq)}$$
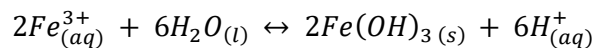
Equation 1.4. Further oxidation of pyrite by aqueous ferric iron.

$$14Fe^{3+}_{(aq)} + FeS_{2(s)} + 8H_2O_{(l)} \rightarrow 2SO^{2-}_{4(aq)} + 15Fe^{2+}_{(aq)} + 16H^+_{(aq)}$$
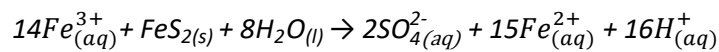
The mineral oxidation reactions detailed are abiotic and occur in both anaerobic and aerobic environments. However, the presence of certain species of lithotrophic bacteria in aerobic mine systems can accelerate mineral dissolution processes through regeneration of ferric iron to further attack pyrite (Equation 1.5; Johnson & Hallberg, 2003).

Equation 1.5. Bacterially-catalysed regeneration of ferric iron.

$$4Fe^{2+}_{(aq)} + O_{2(g)} + 4H^+_{(aq)} \rightarrow 4Fe^{3+}_{(aq)} + 2H_2O_{(l)}$$
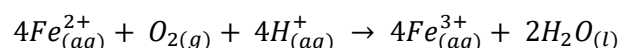
The products of mineral weathering processes detailed in Equations 1.1-1.5 are responsible for the geochemical characteristics of mine waters. The production of H^+ ions in solution is accountable for a

decrease in solution pH within the mine, which in turn aids further dissolution of metal-bearing ores (Wolkersdorfer, 2008). Consequently, the trace metal composition of waters which drain abandoned mines are highly variable and characteristic of the unique mineralogical formations within the host rock of each mine. Increased concentrations of metals such as copper, cobalt, iron, manganese, nickel, and zinc are commonly observed, alongside aluminium where clay deposits are present (Banks, et al., 1997). An example of the variability of concentrations within different sources is provided in Table 1.1, evidenced by large ranges between minimum and maximum values. The resulting metal-rich, acidic leachates are commonly referred to as acid mine drainage (AMD) and can be responsible for both chemical and biological degradation downstream of discharge (e.g. Mayes *et al.*, 2010; Armitage *et al.*, 2007).

Table 1.1. Typical concentrations (mg/L) of selected metals within mine waters from abandoned mines alongside legislative limits (Environment Agency Environmental Quality Standards (EQS) for protection of surface water quality; µg/L). Data summarised from multiple sources (Gombert, et al., 2019; Banks, et al., 1997; Blowes, et al., 2013; Gandy & Jarvis, 2006, Mayes, W.M.).

	Min mg/L	Max mg/L	Mean mg/L	EQS µg/L
Al	2.58	885	302	200
Co	0.05	1.5	1.03	100
Cu	0	43.1	0.53	10
Fe	0	1650	39.3	1000
Mn	0.001	250	4.80	300
Ni	0.001	260	0.07	20
Zn	0.002	7840	4.08	50

In addition to the discharge of contaminated waters from mine workings directly, similar pollution can arise from the weathering of mine tailings. Mine tailings are the fine-grained residual materials that remain after processing of the extracted ore to remove the target mineral. Historically, ores were crushed and milled near the point of extraction, after which the valuable fraction was taken for further processing and gangue material placed in large heaps on site. Tailings heaps are subject to atmospheric weathering and given the generally high sulfide content are liable to the same

geochemical reactions outlined in Equations 1.1-1.5. A representation of pollution formation within a mine system is presented in Figure 1.2.
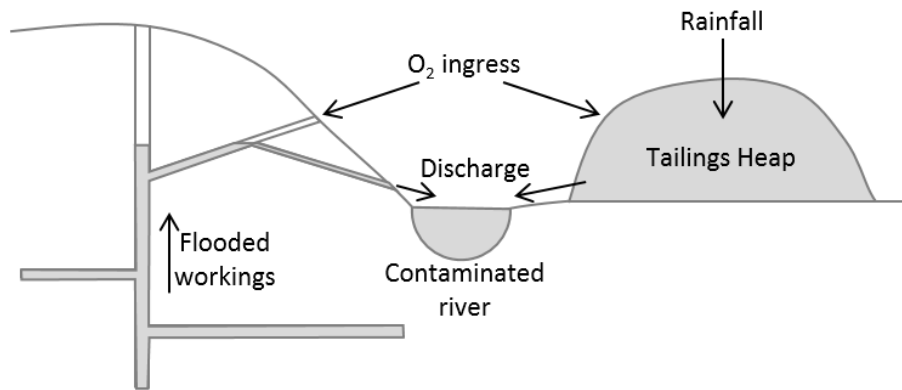
Figure 1.2. Schematic representation of sources and pathways governing mine water formation and release in a typical mine system (after Younger et al., 2002)

1.3   IMPACTS OF MINE WATER POLLUTION

The release of AMD has significant impacts on surrounding aquatic environments. These impacts are often related to the increased metal concentrations within leachates and propensity for mineral precipitation. The abundance of ecotoxic metals and low pH within mine waters have been shown to adversely impact the environment through depletion of species diversity (Jarvis & Younger, 1997). Significant quantities of dissolved metals are released to the environment each year from abandoned metal mines in the UK; an estimated flux of 551 tonnes Fe, 193 tonnes Zn, 72 tonnes Mn, and 19.1 tonnes Cu per annum (Mayes, et al., 2010). This highlights the magnitude of mine leachates as sources of metal pollution to the environment.

In addition to toxicity, where ferruginous mine waters exist it is common for rapid precipitation of amorphous iron hydroxides (Equation 1.3). Ochre precipitation smothers riverbeds downstream of

mine discharge and has caused complete collapse of ecological community structures due to the preclusion of photosynthesis and subsequent loss of primary producers (Younger, 2000).

Biological and chemical quality of rivers and streams are both parameters used for the assessment of environmental health through legislative acts such as the Water Framework Directive. As such, it follows that the effects of mine wastes, which substantially diminish both qualities, should be minimised. A possible solution for this issue is in the removal of problematic metal species from mine wastes to limit the release of dissolved metals to the environment.

1.4   RATIONALE FOR RESEARCH

The removal of metals from aqueous wastes is not solely a requirement for environmental remediation. In hydrometallurgical circuits, for example, methods such as chemical precipitation (Khatri, et al., 2017), membrane separation (Scott & Hughes, 1996), and solvent extraction (Dupont, et al., 2015) are widespread. However, where environmental remediation is concerned the focus is often towards using lower-cost technologies that exploit naturally occurring energy sources, such as aeration cascades (Oh, et al., 2015) and constructed wetlands (Mayes, et al., 2009). Though the treatment of mine waters by these methods has been effective at several sites, the resource recovery potential of these is low, given the generation of large volumes of solid wastes containing multiple metals (Simate & Ndlovu, 2014). Ion exchange resins are commonly used in hydrometallurgical circuits and offer a means of selectively extracting problematic metal species at low concentration (Hubicki & Kołodyńska, 2012). This technology could be applied towards mine water treatment. Further, the extracted metals could be recovered from the metal-loaded resins to produce a highly concentrated aqueous product for recycling (Sole, et al., 2018). Through the selective recovery of metals from what would otherwise be considered a waste, there is potential for

'closing the loop' (Figure 1.3) within the mining industry in the context of a circular economy; shifting the focus towards treating mining residues as 'anthropogenic ores' (Sapsford, et al., 2016).

While commonly used in the hydrometallurgical industry, the application of ion exchange resins for environmental remediation has to date been limited. An investigation into the applicability of ion exchange resins for treatment of mine waters and tailings leachates is an important step to expanding the currently available arsenal for tackling a nationally significant pollution problem.
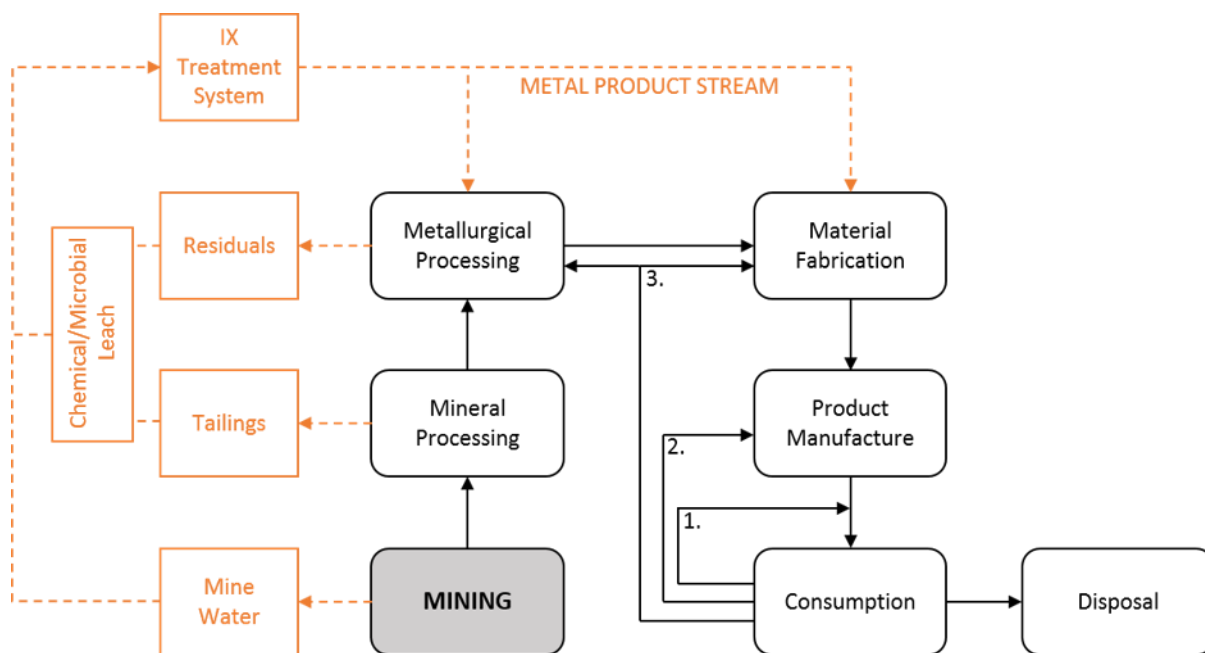
Figure 1.3. An overview of current mineral extraction/processing/consumption routes (black solid lines), and how the proposed treatment system will integrate with waste management (orange dashed lines); 1. Reuse/Repair, 2. Remanufacturing, 3. Recycling. (Adapted a

2 LITERATURE REVIEW

2.1 REVIEW OF MINE WATER TREATMENT SYSTEMS

Management options for the remediation of metal mine waters are commonly categorised as either active or passive treatments. In general, active remediation strategies require prolonged efforts to achieve the desired outcome; often requiring higher capital investment and resource consumption (Williams, 2011). Conversely, passive approaches to remediation utilise naturally available energy sources (e.g. gravity, biological processes) in low-maintenance systems to remediate pollution at a lower long-term cost (PIRAMID Consortium, 2003) (Younger, 2000). A review of the more commonly utilised mine water treatment options is provided in this chapter, with specific focus on the benefits and shortcomings of each technology.

2.1.1 Chemical dosing (pH alteration)

Commonly, the active treatment of mine waters involves dosing of affected waters with alkaline materials (e.g. CaO, $CaCO_3$, NaOH) to neutralise waters and promote metal attenuation through precipitation (Brown, et al., 2002; Mohajane, et al., 2014). Often preceded by a cascade to oxidise ferric iron, the increase of pH by carbonate/hydroxyl addition has a dual effect of lowering the solubility of problematic metal species whilst promoting rapid precipitation of secondary metal hydroxide minerals (Younger, 2000). The minimum pH values for the hydroxide precipitation of commonly encountered metals are provided in Table 2.1.

Table 2.1. Minimum pH required for precipitation (as hydroxides) of selected mine water pollutants (adapted from Brown *et al*. (2002) and Djoudi *et al*. (2019))

Metal Ion	Min. pH
Fe^{3+}	4.3
Pb^{2+}	6.3
Co^{2+}	6.9
Cu^{2+}	7.2
Zn^{2+}	8.4
Mn^{2+}	9.0
Ni^{2+}	9.3
Fe^{2+}	9.5
Cd^{2+}	9.7

The precipitation of amorphous ferric minerals (e.g. ferrihydrite, ferric sulfate) is also able to reduce metal concentrations through the coagulation and binding of other metal oxides into large agglomerates; a flocculation process (Fu & Wang, 2011; Mackie, et al., 2016; Nariyan, et al., 2017). The drawbacks to using a pH modification approach for mine water treatment are primarily due to the cost of constant chemical addition, and the formation of large amounts of sludge with high water content (Tolonen, et al., 2014). Where gypsum is used as the neutralising agent, the residual sulfate concentrations due to gypsum dissolution often exceeds the permissible limits for direct release to effluent waters (Al-Zoubi, et al., 2010). Additionally, the rapid precipitation resulting from alkali dosing forms a sludge containing a variety of metal species, hindering the resource recovery potential from the waste due to difficulties in recycling (Chen, et al., 2014; Kefeni, et al., 2017).

2.1.2   Aerobic wetlands

Much of the published research on the passive treatment of mine-affected waters has focussed on the use of constructed aerobic wetland systems (e.g. Kusin, et al., 2010; Mayes, et al., 2009). Such systems are particularly well suited to net-alkaline waters and have the primary aim of reducing iron concentrations. This is achieved through oxidation and hydrolysis of contaminants (Jarvis, et al.,

2012) followed by sedimentation and filtration of the secondary mineral phases, in addition to direct metal uptake by wetland plants (Mayes, et al., 2009).

Wetland treatment of mine waters is very effective for iron removal through ochre formation, but less well suited for trace metals, which are of great concern in mine water discharges. The attenuation of other metal species by adsorption and co-precipitation with ochre is observed in aerobic wetlands, but the area-adjusted removal rates are orders of magnitude below that for iron (approximately 0.05 g/d/m^2 for Cu, Ni, and Zn, compared to approximately 10 g/m^2/day for Fe (PIRAMID Consortium, 2003)).

The applicability of wetlands for treatment of Zn-contaminated waters was studied at laboratory scale by Gillespie, et al. (1999). Using two wetland microcosms, initial results of 81% and 70% Zn removal were obtained with a 24-hour retention time, of which 98% was sequestered within the soil matrix. Although these results appeared promising, the experiment was only conducted for two months, while the adsorption capacity of wetland soils often becomes exhausted after 3 to 6 months (Jarvis, et al., 2012). In a separate study, a full-scale aerobic wetland achieved 13% Zn removal (Scholes, et al., 1998), though this comparatively lower removal efficiency could have been a result of lower influent Zn concentrations in this study compared to that performed by Gillespie et al. (1999) (21-65 μg/L and 1.76 mg/L, respectively). A laboratory-scale wetland for treatment of lead mine drainage assessed the removal of a range of contaminants over 300 days (Song, et al., 2001). Favourable removal efficiencies of Zn, Pb, and SO$_4^{2-}$ were recorded, but high residence times within the system led to low area-adjusted removal rates of 0.003 g/m^2/day (Song, et al., 2001); comparable to those encountered by Scholes et al. (1998) of 0.002 g/m^2/day. Removal rates such as these are unfavourably low for application in passive mine water treatment systems in the UK where the availability of large amounts of land with suitable topography is limited, particularly considering the upland setting of most abandoned mine sites (Figure 1.1; Mayes, et al., 2009).

2.1.3 Compost wetlands

Another type of wetland treatment system, compost wetlands have similar appearance to traditional aerobic wetlands but have a thick layer of anoxic substrate; bridging the gap between aerobic and anoxic treatment systems. The compost layer promotes bacterial sulfate reduction and results in the precipitation of insoluble metal monosulphides (generally of Fe) within the substrate. However, it has been suggested that under certain conditions, the complex biological substrate may act to release previously sequestered metals, and as such these systems are rarely recommended (PIRAMID Consortium, 2003).

One drawback of wetland treatment in general (aerobic and anaerobic) is the difficulty of removing metal sludges once the system has reached its capacity given the dense root structures of wetland plants. To reduce the frequency at which dredging is required, wetlands are often preceded by settlement lagoons to reduce the suspended solid content of influent waters, which ultimately requires additional land area for effective treatment.

2.1.4 Anoxic Limestone Drains (ALDs)

In cases where iron concentrations are low, anoxic limestone drains (ALDs) can be used to treat mine waters. ALDs consist of buried trenches packed with limestone gravel and capped with a layer of clay to maintain anoxic conditions (Brown, et al., 2002). The dissolution of $CaCO_3$ within the limestone bed serves to raise the pH of waters through the production of bicarbonate alkalinity (RoyChowdhury, et al., 2015; Brown, et al., 2002). The anoxic nature of ALDs ensures reducing conditions within the system and prevents mineral precipitation and subsequent armouring of the limestone bed. Given the lack of metal attenuation within the system itself, ALDs are commonly used as a pre-conditioning step for subsequent aerobic treatment cells (such as wetlands or settlement lagoons) where mineral precipitation occurs. The drawback of ALDs lie within the requirements for

input water to have below 2 mg/L Fe and <1 mg/L dissolved oxygen; conditions that are rarely met in European mine waters (PIRAMID Consortium, 2003).

2.1.5   Reducing and Alkalinity Producing Systems (RAPS)

To overcome the issue of excess dissolved oxygen and iron concentrations, ALDs can be modified with a layer of anoxic compost, through which the water must first pass, to create a 'reducing and alkalinity producing system' (RAPS). In this system, the compost layer promotes reducing conditions and aids dissolved oxygen removal by decomposition of organic matter. In addition, alkalinity production is promoted through the metabolism of certain sulfate reducing bacteria (Brown, et al., 2002). Beneath the compost layer, limestone ($CaCO_3$) dissolution acts to produce further bicarbonate alkalinity. As for ALDs, the focus of RAPS is acidity consumption and alkalinity generation, and as such must be followed by further metal removal systems (Younger, et al., 2003). However, by adopting a vertical flow-through design and anoxic substrate, RAPS require approximately 20% of the area that a compost wetland would for the same results and has a higher tolerance to increased Fe and Al concentrations.

As for most gravity-fed systems, the development of hydraulic 'short-circuits' (Taylor, et al., 2016) within the substrate can have negative effects on the retention time, and therefore the treatment capabilities, of RAPS. Another potential drawback specific to RAPS is the prerequisite for approximately 2.5 metres of relief below mine water discharge point to account for hydraulic head losses and precipitate accumulation over time. However, this could be avoided through pumping, which would render the system *semi-passive* (PIRAMID Consortium, 2003).

2.1.6   Vertical Flow Reactors (VFRs)

Other passive technologies focus on the removal of dissolved metals through adsorption and co-precipitation mechanisms. After observing the accumulation of ochre precipitates on the surface of RAPS, a novel vertical flow reactor (VFR) was developed by Sapsford, et al. (2007). Running in parallel to a more traditional lagoon-based treatment system at Taff Merthyr, South Wales, the VFR was employed to treat net-alkaline coal mine waters high in dissolved iron (7.2 mg/L). The VFR consisted of a steel tank (66 m^2 footprint), at the bottom of which was a sandstone gravel bed suspended above a void space. Mine water was diverted into the tank, and iron hydroxide deposits were allowed to build up, forming a bed through which the water drained. Iron removal rates were reported to be much higher than in the neighbouring lagoon system, with the key removal mechanisms being the physical filtration of suspended iron flocs, and the surface-catalysed oxidation of iron leading to further precipitation of iron hydroxides and co-removal of other pollutants (e.g. manganese (Sapsford, et al., 2007)). However, as for RAPS, the development of preferential flow pathways was also encountered during field trials of this VFR system, which was attributed to the coarseness of the gravel initially used.

Another study focussed on the remediation of circum-neutral metal mine waters using pelletised ochre, recovered from coal mine water treatment, bound together with Portland cement (Mayes, et al., 2009). A pilot treatment tank was installed containing 180 kg of ochre pellets, through which mine water passed. This column-style VFR yielded Zn removal rates of 3.7 g/m^2/day; orders of magnitude higher than those previously reported for wetlands (Scholes, et al., 1998; Song, et al., 2001). The primary removal mechanisms within the system were identified as sorption to the charged surface of the ochre in addition to co-precipitation of Zn within secondary carbonate precipitates: formed through dissolution of portlandite from the cement binders used (Mayes, et al., 2009). While the high pH generated by portlandite dissolution aids metal removal from solution, precipitation of carbonate minerals can cause issues for systems such as this through armouring of, in this case, the ochre pellets (Jarvis, et al., 2012). Armouring of reactive media by mineral formation

14

was also encountered by Cortina, et al. (2003) in a treatment column containing caustic magnesia (MgO with trace amounts of CaO and quartz sand). In this instance, armouring of caustic magnesia grains led to a reduction in solution pH and remobilisation of previously sequestered metals. It is worth noting that this problem was overcome by addition of 50% quartz sand to the column to aid porosity (Cortina, et al., 2003), though presumably this would effectively double the size of column required for equivalent treatment potential.

2.1.7   Permeable Reactive Barriers

While the technologies reviewed previously focussed solely on the treatment of surface waters, mine-related wastes also have potential to contaminate groundwater, which in the worst-case scenario can polluted aquifers designated for drinking water abstraction (e.g. the contamination of the Magnesian Limestone Aquifer following cessation of mine dewatering in County Durham; Neymeyer, et al., 2007). Permeable reactive barriers (PRBs) are commonly used to protect groundwater resources from pollution and typically consist of buried trenches backfilled with reactive media (often zero valent iron or activated carbon), which intercept the migrating pollutant plume (Blowes, et al., 2000). To ensure interception of the whole plume, PRBs either rely on naturally impermeable sub-strata (e.g. clay) or artificial impermeable walls to direct groundwater to the reactive media (Phillips, 2009). While PRBs have been shown to be highly effective over a long period (one source reporting a lifespan of 62 years; Roehl, et al., 2005), they are also subject to the problems encountered by ALDs, RAPS, and VFRs; namely the build-up of precipitates over time which 'smother' the reactive material and reduce the porosity of the barrier (Phillips, 2009).

Although PRBs are generally filled with either low-cost and/or waste materials, a novel piece of research carried out by Vilensky, et al. (2002) investigated the feasibility of a PRB packed with ion exchange resins to remove metal ions from contaminated groundwaters. Additionally, owing to the high hydraulic conductivity of ion exchange resins, an alternative to the standard 'continuous wall' of

reactive media was proposed by the researchers; the new design consisting of clusters of wells to intercept contaminant plumes, gain access to deeper groundwaters, and reduce costs associated with PRB installation. Due to the high exchange capacity offered by ion exchange resins (reportedly an order of magnitude higher than conventional PRB media, e.g. zeolites), Vilensky, et al. (2002) concluded that 1 kg of resin (Amberlite IRA-96) could suitably treat 1 m^3 of groundwater containing 200 µg/L Cd; a concentration typical of Cd contaminated groundwaters, and much higher than typical concentrations in UK mine-affected surface waters.

2.2   ION EXCHANGE FOR SELECTIVE METAL RECOVERY

2.2.1   Rationale for an ion exchange approach

Metal mining and subsequent mineral processing inevitably produces large volumes of waste material, often highly reactive due to fine particle size and reactive mineral content (Falagán, et al., 2017). Given the relative inefficiencies of historic mineral processing practices, such wastes and their leachates often contain resources of an economically viable concentration to warrant recovery using modern processes, particularly base metals such as copper, cobalt, manganese, nickel, and iron (Hardwick & Hardwick, 2016). The same is true of waters draining historic mine systems, whereby the same metals are present as in the tailings waste. In a circular economy context, the recovery of metals from waste heaps and waters is preferential to primary resource extraction, and so waste reprocessing technologies are required to improve overall sustainability in the mineral supply chain (Lèbre, et al., 2017). Furthermore, the storage of residues from the traditional passive treatment systems detailed previously (i.e. metal-rich sludges) may also pose environmental risks through metal mobilisation, particularly for metals such as Fe, Al, Ni, Zn, and Mn (Jouini, et al., 2020).

Ion exchange technology is often viewed as an alternative or complimentary technology to solvent extraction. However, the metal concentrations required for effective recovery are generally lower for

ion exchange when compared to solvent extraction, meaning that such an approach can still be economically viable when feed concentrations would be too low for other technologies (Hardwick & Hardwick, 2016). Additionally, the use of a solid-state extraction technique can prevent the issues with organic waste disposal and undesired phase formation encountered in solvent extraction circuits (Bezzina, et al., 2018).

2.2.2   Ion exchange for mine water treatment

While the use of ion exchange resins in the hydrometallurgical industry is widespread (e.g. Van Deventer, 2011), the treatment of mine waste waters by this method is rare, and ion exchange is often viewed as a supplementary technology (e.g. García, et al., 2014). As such, a paucity of thorough studies focussing on ion exchange for mine water treatment exist in the published literature. A selection of literature which investigates ion exchange resins for metal recovery from mine waters is provided here to give an insight to the current state of research in this area.

Research into the treatment of acid mine drainage from a South African gold mine focussed on the use of dual technology; metal precipitation by $Ca(OH)_2$ dosing, followed by ion exchange for effluent desalination (Feng, et al., 2000). The resin used in this case was Amberlite IR120H, a strong aid exchange resin with sulfonic acid functionality, and was used to remove residual cations produced in the metal precipitation stage. Initial screening of the resin indicated a high operating capacity for calcium ions (55 mg Ca^{2+}/mL resin) with preference for pH > 6 (Feng, et al., 2000). The adsorption kinetics for calcium uptake were favourable, with equilibrium being reached within 3 hours of solution contact time. When treating effluents from the precipitation process (823 mg/L Ca^{2+}, 556 mg/L K^+, 348 mg/L Mg^{2+}, and 345 mg/L Na^+), the sulfonic acid resin exhibited strong selectivity towards calcium and magnesium ions, with lower affinity for potassium and sodium. For the case of all cations, 80 mL of exchange resin was sufficient to reduce residual concentrations to below the

respective water quality standards, and calcium reduction required only half of this amount (Feng, et al., 2000).

While the research of Feng et al. (2000) used ion exchange as a secondary treatment technique, it is possible for ion exchange to be used as a stand-alone technology. For example, a dual-temperature approach was investigated to selectively separate copper from aluminium in acidic mine waters by Muraviev et al (1997). In this work, a carboxylic acid resin (Lewatit R 250-K) and iminodiacetic acid resin (Lewatit TP207) were used for adsorption. It was determined that temperature control could be used to selectively elute metals from resin columns by introducing mine waters at 20 and 80°C, removing the requirement for chemical eluents (Muraviev, et al., 1997). However, while the heating of process waters by solar irradiation, as suggested, could potentially be feasible in the Rio Tinto region of Spain, where mine to be treated was located, the artificial heating of waters is unlikely to be economically viable in the UK, especially considering the limited budget available for abandoned mine water treatment.

The removal of inorganic mercury from mine wastewaters was investigated by Monteagudo & Ortiz (2000) using three commercially available exchange resins; Dowex XVS/M, Amberlite 252/M, and Dowex XZS-1/G, all of which with sulfonic acid functionality. The mine waters used contained a suite of metals at various concentrations, with approximately 80 mg/L of mercury. The efficacy of the resins for mercury removal was determined through static equilibrium studies as well as column breakthrough determinations, where capacities of 3.9 – 4.4 meq/g were calculated. Mercury concentration was reduced from influent concentrations of 80 mg/L to less than 34 μg/L in effluent waters, highlighting the effectiveness of the resin for this application. The feasibility of the operation was tested by cyclic adsorption and elution of a resin-packed column which suggested minimal loss of capacity over five repeated cycles (Monteagudo & Ortiz, 2000). While mercury is seldom the key problem in UK mine waters, the systematic approach in this paper provided the means for effectively

assessing the resin for its suitability towards the desired application and is an overarching method which will be used in the present work.

A study of copper recovery from nickel laterite leachates (Perez, et al., 2019) used a similar approach when assessing the suitability of Dowex XUS 43605 (hydroxypropylpicolylamine (HPPA)). By transitioning from a batch setup to a fixed-bed setup the authors were able investigate the effect of flow rate on metal extraction under dynamic adsorption conditions, which are more likely to be used in current hydrometallurgical applications. While this was one of the few papers to focus on flow rate effects under dynamic operation (other notable examples include Amphlett, et al., (2018), Hamdaoui (2009), and Tavakoli, et al., (2013), though these are not mine water focussed), the breakthrough profiles were not modelled and as such it was not possible to determine any changes in capacity as a function of flow rate. Despite this, the value of using chelating resins for selective metal recovery from mine waters was demonstrated, and so it became apparent that a selection of chelating functionalities should be screened in this work.

The majority of publications in this research area are laboratory-based, however, a novel field trial of an ion exchange based mine water treatment system was presented at the International Mine Water Association Symposium (Leipzig, 2016); the first trial of such a system in the UK, so far as the author is aware. The semi-continuous system consisted of a 5000 L holding tank, from which untreated mine waters were pumped to a 60 L exchange reactor containing 30 rotating permeable discs coated with a mixture of cationic (weak carboxylic acid), anionic (amine), and chelating (oxime) functional groups supported by a cross-linked polymer matrix. The water treated had a trace metal composition of approximately 50 ppm Zn, 0.14 ppm Cd, and 0.06 ppm Pb. The system was run for 170 days during which time, average removal efficiency for Zn was 64%, with 22% cadmium removal and 75% lead removal, in addition to removal of acidity, alkalinity, and conductivity.

While initial results were promising, the risks of operating a pilot scale system without first completing thorough laboratory-scale resin screening studies were apparent. Upreti, et al. (2016)

report that the removal of metals continued after exhaustion of the ion exchange capacity, suggesting another removal mechanism, which was identified as sorption and co-precipitation of aqueous metals to secondary precipitates that had formed on the surface of the discs. Subsequent analysis of the solids revealed that 77% of the zinc, 47% of the cadmium, and 63% of the total sequestered lead was removed via this mechanism. While this side-effect of the system was beneficial to the overall aim of indiscriminate metal removal from the water, the co-precipitation of metals would be unfavourable for a truly selective metal extraction and remediation system such as the one proposed in this project. In an ideal scenario, the metals would be removed entirely through interaction with resin functionality to allow the subsequent elution of a relatively 'pure' (i.e. single-metal) waste stream without the need for post-processing of solid residual mineral wastes and the associated costs of doing so.

2.3 SCOPE FOR RESEARCH

It is evident that the current options for mine water remediation do not provide a complete solution and tend to focus solely on removal of iron. While slight attenuation of other metals (e.g. Ni, Al, Zn) is observed in wetland systems, the area requirements for designated wetland treatment of such metals would be unfeasible. The proposed ion exchange-based system aims to address the limitations of current remediation options, specifically by focussing on removal of those metals which, although present at lower concentrations, have potential for greater environmental damage and mobility (e.g. Zn, Ni, Al, Mn, Cu). Given the high selectivity of chelating resins, it is expected that targeted resins will be identified, and a system developed that can selectively extract problematic and/or valuable metals effectively and provide opportunity for resource recovery. In doing so, this will provide an alternative to the 'blanket' metal removal offered by current treatment techniques. Meeting site-specific metal removal requirements will reduce and/or prevent the need for the system to be followed by subsequent treatment units and produce effluent waters of suitable quality

for environmental release. Additionally, the strong chelating effect of resins will provide a secure sink for toxic and valuable metals prior to elution, preventing the secondary metal releases associated with, for example, compost wetlands. The high exchange capacity of resins will allow development of a low-footprint system, combatting the area requirements of conventional approaches such as settlement lagoons and wetlands, and allow treatment at a greater number of mine sites – particularly where land availability is low.

Furthermore, for the literature where ion exchange resins were investigated for their role in mine water treatment there remained a lack of systematic investigation, with most published works investigating this issue through seemingly arbitrary selection of adsorbent functionalities. Therefore, it became apparent that a 'bottom up' approach was required, starting with a thorough screening of candidate resin materials, and working methodically to investigate each aspect of resin implementation within a coupled system. Such investigations are not only required for ultimately producing a more robust treatment system, but will also provide a contribution to the academic literature which has remained relatively under-studied.

3 RESEARCH AIMS

It is evident from the review of currently-employed mine water treatment techniques that the opportunity for resource recovery from these waste streams is not currently exploited to its full potential. As such, it is of value to explore technologies that could accomplish metal removal from contaminated waters in a manner which would allow for their recovery as a saleable resource. Not only would such a solution aid in the treatment and remediation of mine-affected waters, but it would also valorise the waste and ascribe a value, and therefore commercial interest, to what would otherwise be considered only as an environmental burden.

This thesis aims to explore the potential role of ion exchange resins for resource recovery from mine waters using fixed-bed adsorption techniques, and will do so by tackling the overarching research question;

"Can problematic metals present in mine water leachates be recovered through targeted ion exchange to produce a product stream capable of valorising the waste?"

This overarching research question may be split further to a number of hypotheses and sub-hypotheses, as presented below, which will be addressed in this thesis.

1. Can the dissolved metals present in mine wastes be selectively extracted by ion exchange functionalities?

    a. Is resin performance resilient towards changes in solution pH, and is effective recovery achievable under these conditions?

    b. Where effective recovery is observed, is selective extraction feasible under the high sulfate concentrations anticipated?

2. For the identified resin functionalities, is an acceptable level of performance maintained when used in dynamic fixed-bed operation?

    a. Does solution flow rate affect metal extraction performance, and are any issues encountered under changing flow rates?

3. Can a concentrated product stream be acquired from loaded resins that is suitable for process valorisation?

    a. If target metals are not selectively extracted, is a selective elution approach achievable?

    b. Can adsorbent materials be reused with no degradation in resin performance?

4. Can columns be coupled to achieve targeted extraction and separation of metals in a continuous process?

    a. To what extent can the fate of bound metals be controlled when coupling ion exchange columns together?

    b. Where eluents have been previously optimised, are these still effective when used on columns from a coupled system?

4 EXPERIMENTAL AND ANALYTICAL METHODS

4.1 PREPARATION OF STOCK SOLUTIONS

While the exact composition of mine waters and tailings leachates varies depending on factors previously discussed, synthetic solutions were prepared to represent metals typically encountered in such wastes. Given that the aim of screening experiments in this case was to determine the behaviour of different resin functionalities under different operational conditions, a decision was made to simplify the working solutions and to keep concentrations of each metal species equal. This allowed determination of the selectivity of each functional group without interference that could arise from differences in relative concentration ratios.

Table 4.1. Mass of metal salts used to prepare 1 L of mixed-metal spike solution at 2000 mg/L.

Chemical Formula	Mass added (g)	mol/L
$Al_2(SO_4)_3.16H_2O$	23.364	0.037
$CoSO_4.7H_2O$	9.539	0.034
$CuSO_4.5H_2O$	7.858	0.031
$FeSO_4.7H_2O$	9.956	0.036
$MnSO_4.H_2O$	6.152	0.036
$NiSO_4.6H_2O$	8.958	0.034
$ZnSO_4.7H_2O$	8.796	0.031

A mixed metal stock solution was prepared using the sulfate salts of Al (III), Co (II), Cu (II), Fe (III), Mn (II), Ni (II), and Zn (II) (Table 4.1). All metal salts used were of analytical grade and purchased from Sigma-Aldrich. Salts were dissolved in deionised water and acidified to pH 1 using H_2SO_4, such that the final concentration of each metal was 2000 mg/L. Aliquots of this were taken and diluted to produce the pregnant liquor solutions (PLS) that were used in experimental procedures. The preparation of specific PLS used in experiments is detailed in the respective experimental chapters.

Working from a stock solution ensured continuity in metal concentrations between batches of PLS, and hence minimise variation in solutions between resin contacts.

4.2 RESIN PRECONDITIONING

The resins used in experimental investigations were either donated by Purolite International Ltd (Puromet MTS9100, MTS9140, MTS9200, MTS9301, MTS9501, MTS95700, MTS9850) or purchased from Sigma-Aldrich (Dowex M4195, M31). Functional group structure of resins used is presented in Figure 4.1. All received resins were supplied in the form of dried spherical beads, with specific characteristics reported in Appendix Table 11.1. When working with ion exchange resins it is desirable to have all functional groups present in a single form, i.e. for each functional group to be associated with the same counter-ion. Given that the form in which different resins are sold can vary, it is common practice to precondition resins before use to ensure uniformity. Resins were preconditioned to their proton (H^+) form through contact with excess 1 M H_2SO_4 for 24 hours while being agitated on an orbital shaker. Five batch washing cycles using excess deionised water ensured complete removal of residual acid from the preconditioning process. Resins were then stored under deionised water until required so that they remained in their hydrated form.
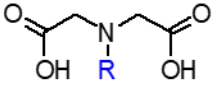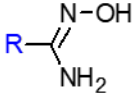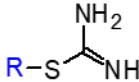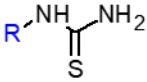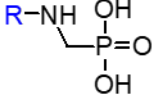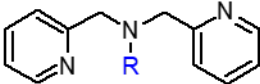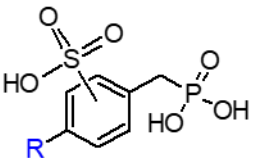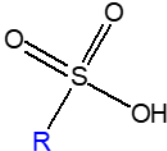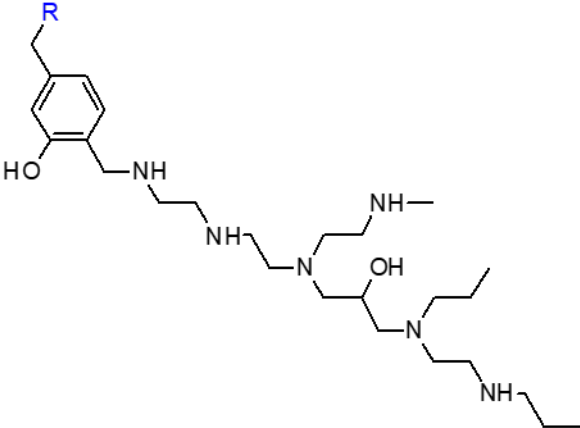
Figure 4.1. Resin functional group structures (R = resin backbone – see polymer matrix in Appendix Table 11.1 for details).

4.3   STATIC EQUILIBRIUM EXPERIMENTS

Static equilibrium experiments are performed by contacting a fixed amount of resin with a constant

volume of solution and allowing the system to equilibrate over a suitably long period of time. All

resins were measured out volumetrically by pipetting a hydrated resin and water slurry into a 10 mL measuring cylinder, inverting the cylinder to promote particle size mixing, then allowing resins to settle under gravity (referred to herein as 'wet settled resin'). For batch screening experiments, 2 mL of wet settled resin was measured, transferred to a plastic container, and contacted with 50 mL of PLS. Containers were placed on an orbital shaker to promote thorough mass transfer between the solution and adsorbent, and contacted for 24 hours to ensure equilibrium was reached. Upon reaching equilibrium, supernatant solution was decanted, and an aliquot taken for elemental analysis and pH measurement.

4.4   DYNAMIC (COLUMN) EXPERIMENTS

In contrast to static equilibrium experiments, where batches of resin and solution are contacted and allowed to equilibrate, dynamic experiments use a packed column of resin through which the solution is pumped. The key difference in this case is that due to the constant displacement of forward-reaction products, the adsorbent/solution system does not operate under equilibrium (Harland, 1994).

4.4.1   Breakthrough determination

Small-scale columns were completely packed with ion exchange resin and capped at either end with Teflon frits, resulting in a total bed volume of 5 mL wet settled resin. Columns were intermittently agitated during the packing process to promote homogeneous distribution of resin particle size throughout the bed. To ensure efficient mass transfer between solution and resin, and to reduce the risk of 'channelling' (Harland, 1994) a reverse-flow setup was employed, whereby the PLS was introduced at the bottom of the vertical column and pumped against the force of gravity (Figure 4.2).

The setup was slightly modified for elution studies and coupled column breakthrough experiments where smaller scale columns (1.4 mL) were used to reduce backpressure in pump tubing.
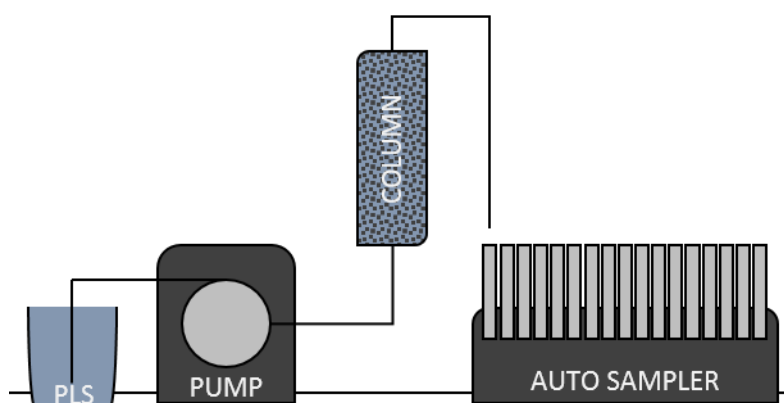
Figure 4.2. Laboratory setup of dynamic breakthrough experiments using a reverse-flow pump setup.

Peristaltic pumps were used for their ability to provide consistent low flow rates, and to minimise potential contamination which could arise through other pumping techniques where solution is in contact with the pump mechanism itself. One of two peristaltic pumps were used during experimentation, either; a Heidolph Hei-Flow Value 01 pump with Heidolph SP Quick pump head, or a BioRad Econo Gradient Pump. Both pumps were able to achieve the low flow rates required for experimental work, depending on the choice of peristaltic tubing used. Verification of solution flow rates was achieved by pumping deionised water through each packed column for a set time and using the mass of water collected to calculate flow in bed volumes per hour (BV/hour).

Given that resins were used in their hydrated form and measured volumetrically as a slurry when packing columns, it was necessary to calculate the density of each resin to use as a conversion factor to aid with data modelling. This was achieved by measuring out 2 mL of each protonated resin in triplicate (as per the procedure mentioned in Section 4.3) and placing in an oven at 50 °C overnight to dry. Dry resin samples were then weighed using an analytical balance, from which their density was calculated (Table 4.2).

Table 4.2. Mean density of each resin studied (protonated form).

Resin	Mean (g/mL)	S.D.
S910	0.375	0.001
S914	0.308	0.004
S920	0.322	0.006
S930	0.357	0.006
S950	0.293	0.006
S957	0.261	0.004
S985	0.383	0.006
M4195	0.300	0.001

4.4.2   Column elution profiles

For determination of resource recovery potential, various eluents were explored for metal elution from loaded columns. Specific details of eluents used are provided in the respective experimental chapter. There are two variations for the setup of elution experiments; *co-flow*, whereby the flow direction of the eluent is the same as the loading cycle, and *counter-flow* regeneration, where the cycle directions oppose. While notable differences may only become apparent at industrial-scale processes, a counterflow regeneration cycle was employed during elution experiments. During counterflow regeneration, fresh eluent solution first encounters resin which is least exhausted (assuming the column was not entirely saturated during loading), and ions present are likely to be those with lowest affinity to the resin functionality due to chromatographic separations that occur during column loading (Harland, 1994). Columns were loaded as per Figure 4.2 then rinsed with DI water, removed, inverted, and reattached to pump tubing before eluent introduction.

4.5   SAMPLE ANALYSIS

4.5.1   Aqueous Elemental Analysis

4.5.1.1   Sampling and pH Measurements

For static batch experiments, samples of pre- and post-contact solutions were taken and diluted using a 1 wt.% nitric acid solution (prepared through dilution of analytical grade 70 wt.% HNO_3 stock) prior to metals analysis. All sampling was carried out using regularly calibrated pipettes, using fresh sterile tips for each distinct solution. Raw solutions were diluted such that theoretical maximum metal concentrations in analytical samples were below 10 ppm for subsequent elemental analysis. Sampling error was determined through triplicate sampling and analysis of the pre-contact solution phase and applied to post-contact phases accordingly. Post-contact solution pH measurements were achieved using a silver/silver chloride reference electrode calibrated from pH 1 – 10 using standard buffer solutions.

For column experiments, sample collection was automated using a BioRad Model 2110 fraction collector set to advance at specified time intervals, calculated during calibration of pump flow rate. As soon as possible following completion of each column run, aliquots of each collected fraction were diluted using the 1% HNO_3 solution before metals analysis using either inductively coupled plasma optical emission spectrometry (ICP-OES), or more commonly, flame atomic absorption spectroscopy (AAS).

4.5.1.2   Inductively Coupled Plasma Optical Emission Spectrometry

When available, full elemental analysis by ICP-OES was performed using a regularly calibrated Perkin Elmer Optima 5300 DV model or Spectro Arcos model ICP-OES depending on the location that samples were analysed. A schematic diagram of typical ICP-OES setup is provided in Figure 4.3.
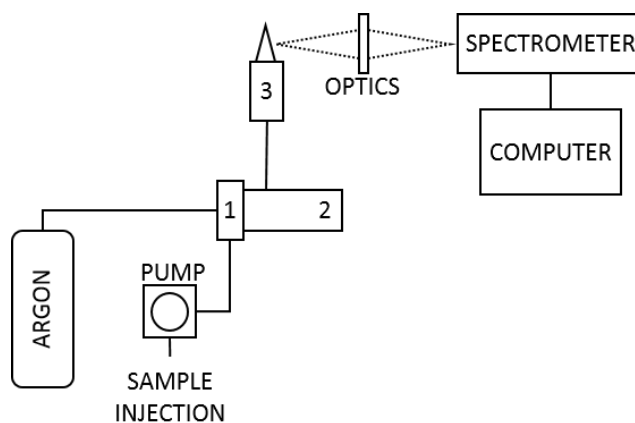
Figure 4.3. Schematic diagram of an ICP-OES; 1. Nebuliser, 2. Spray chamber, 3. ICP torch. Adapted from Boss & Fredeen (2004)

During ICP-OES the solution to be analysed is nebulised, to produce an aerosol of the sample. A carrier gas, often argon, is mixed with the nebulised sample which is then transported to the ICP torch and heated to approximately 10,000°C. This is the point at which atom excitation occurs. The principle is that atoms in their *ground state*, i.e. where electrons in the atom are closest to the nucleus and therefore more stable, absorb energy from the torch and shift to a higher energy level (an *excited state*). Given the relative instability of excited atoms, electrons shift back to ground state and in doing so release energy in the form of a photon, which is detected and measured by the spectrometer and converted to concentration (Boss & Fredeen, 2004). Many elements have potential for more than one electron to shift energy levels, resulting in multiple wavelength emission lines for the same element. Given the variation of electron arrangements between elements, it is possible to identify the presence and concentration of multiple elements concurrently through simultaneous observation of different wavelengths of emission. Due to the presence of multiple emissions from elements, careful selection of wavelengths can minimise or avoid spectral overlap (where emission lines are too similar for separate measurement) and provide a more accurate measurement of concentration. Wavelength selection was made with guidance from Method 200.7 of the US

Environmental Protection Agency (Bradshaw, 2013) to ensure use of the most sensitive wavelength for each analyte.

4.5.1.3 Atomic Absorption Spectrometry (AAS)

Most of the analytical results presented were obtained using AAS, specifically a Perkin Elmer AAnalyst 400 model spectrometer in conjunction with an air/acetylene flame. A simplified schematic of the instrument is provided in Figure 4.4.
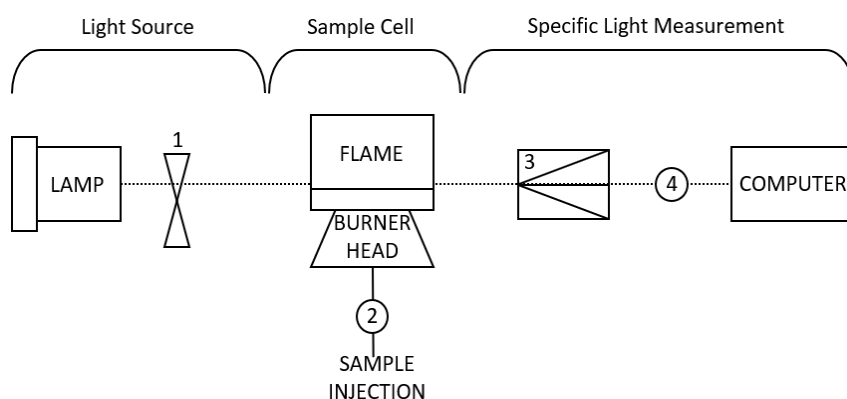
Figure 4.4. Schematic diagram of an atomic absorption spectrometer; 1. modulator, 2. nebuliser, 3. monochromator, 4. Detector; dotted line represents path of light. Adapted from Perkin Elmer Inc. (1996).

The principle of AAS analysis is in measuring the absorption of light after passing through the sample cell (Figure 4.4). A hollow cathode lamp containing an alloy of the analyte metal produces light of a specific wavelength and intensity, as defined in the program method file. The light then passes through the sample cell where an air-acetylene flame burns a nebulised mist of the sample to be analysed. As for ICP-OES, energy provided by the lamp causes ground state atoms to become excited (Perkin Elmer, Inc., 1996); a process which consumes energy. After passing through a monochromator, the detector analyses a specific wavelength of light associated with the metal

species and determines its concentration in solution. This determination is based on the principle that a higher number of metal atoms shifting to the excited state in the flame results in a higher degree of light absorption.

Calibration of the instrument was performed at the start of each analysis period using a set of four calibration standards prepared by the dilution of certified mixed- or single-metal standards with 1% nitric acid (to ensure a match in matrix between samples and standards). The analysis of periodic check standards, often the 5 mg/L standard, between samples allowed any 'drift' in instrument performance to be quickly identified, as described in Section 4.6. Regular setup and maintenance of burner head position and nebuliser flow rate, as recommended by the manufacturer, ensured reliable instrument performance.

4.5.1.4   Ion Chromatography (IC)

Fundamentally, ion chromatography analysis relies upon the natural variation in relative affinity between anions present in a sample and the separation column resin. Following sample injection, continuous pumping of an eluent phase allows for analytes to move through the column at different rates, relative to their affinity; i.e. ions with lower affinity to the column will travel faster through the column and therefore be detected first at the column outlet (Moustafa & Morsi, 2013). After sample analysis, the regenerant solution is pumped through the separation column to remove any remaining analytes adsorbed to the column and prepare the system for the next analytical run.
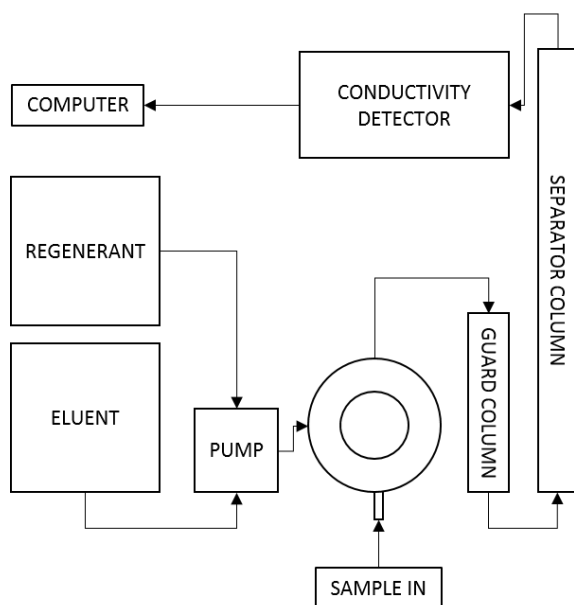
Figure 4.5. Schematic diagram of an ion chromatography system.

Anion composition analysis of effluent samples was achieved using a Metrohm 883 Basic IC Plus Instrument fitted with a 'Metrosep A Supp 5' column (PVA-quaternary ammonium). A carbonate eluent was prepared through dissolution of Na_2CO_3 to a concentration of 4.5 mM and $NaHCO_3$ to 803 μM. The choice of carbonate eluent was made given that the formation of carbonic acid (H_2CO_3, pK_a 6.36) within the suppressor allows for Cl^- and SO_4^{2-} to remain fully deprotonated (SeQuant, 2007), and therefore allow efficient detection. A regenerant solution of 0.1 M H_2SO_4 was also prepared and used during IC analysis. The instrument was calibrated using certified analytical standards of Cl^-, SO_4^{2-}, and ClO_3^- prepared across a calibration range from zero to 200 mg/L. For experiments where IC was employed, samples and standards were diluted using 18 MΩ water, which was also used as the blank calibration standard, to eliminate peaks which may arise from the diluent composition.

4.5.2   Solid State Analysis

4.5.2.1   X-Ray Photoelectron Spectroscopy (XPS)

Determination of Puromet MTS9140 elemental composition and the oxidation state of adsorbed Cu was achieved by X-ray photoelectron spectroscopy (XPS) using a Kratos AXIS Supra instrument with a monochromated Al source. Specific experimental procedures are provided in the relevant chapter. Fundamentally, XPS is a method which analyses the kinetic energy spectrum of photoelectrons from the surface and near-surface (5-10 nm) of a solid sample after excitation by an X-ray source (Konno, 2016). A schematic of typical XPS instrumentation is provided in Figure 4.6. The kinetic energy is used by the instrument to calculate the binding energy between the emitted photoelectron and the sample, which in turn is directly related to the chemical environment of the atom within the sample. Given that different elements emit photoelectrons at different x-ray energies (eV), and that binding energy increases with increased chemical state number, XPS is a powerful technique which can be used to determine both elemental composition and metal speciation within solid-state samples.
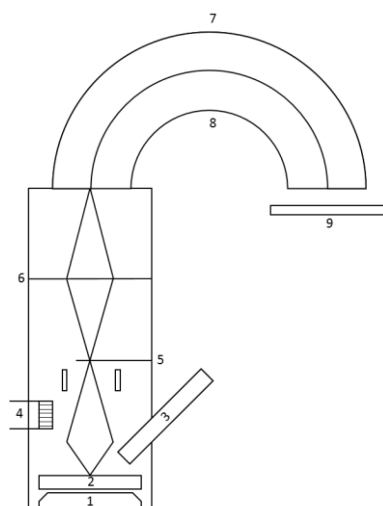
Figure 4.6. Schematic diagram of an X-ray photoelectron spectroscopy system; 1. Magnetic lens, 2. Sample, 3. X-ray source, 4. Charge neutraliser, 5. Spot size aperture, 6. Electrostatic lens, 7. Outer hemisphere, 8. Inner hemisphere, 9. Detector. Adapted from Teignmouth Science and Technology Centre (2017).

4.6 ERROR MINIMISATION

While the introduction of a certain degree of error is inevitable, efforts were made to keep experimental and analytical errors to a minimum. Experimental error was minimised using, for example, clean volumetric glassware, calibrated pipettes with fresh pipette tips, and an analytical balance during solution preparation and measurement. Triplicate sampling and analysis of PLS batches and pre-contact solutions allowed variation and error within sampling procedures to be quantified, and data were used to produce error bars as necessary. Quality assurance of data was maximised during sample analysis by calibrating analytical instruments (ICP-OES, AAS, and IC) at the start of each batch of samples and running regular check standards throughout to monitor instrumental drift. Where check standards were beyond 5% from their expected concentration, the instrument was re-calibrated and previous samples re-analysed to ensure the accuracy and quality of collected data.

5   STATIC RESIN FUNCTIONALITY SCREENING[1]

5.1   CHAPTER INTRODUCTION

Commercially, ion exchange resins are sold with a wide range of functional groups; generally categorised as weak acid, weak base, strong acid, strong base, and chelating functionalities. Given the diversity of available resins and given that they are often developed with specific applications in mind, screening a range of resin functionalities for their suitability towards desired separations is an important first step in the development of a treatment system, and can identify potential applications not previously considered by the manufacturer.

Ion exchange resin screening studies are a valuable tool for determining adsorbent effectiveness and are predominantly performed under static conditions, whereby 'static' refers to a batch of resin and solution in contact at, or approaching, equilibrium. Through changing solution characteristics in a controlled system, it is possible to determine the effects that single parameters have upon resin selectivity and extraction efficiencies towards multiple metals. Given the typically low pH and high sulfate concentration of mine waters and leachates following sulfuric acid leaches of hydrometallurgical wastes, it was decided that pH and sulfate concentration were the most important variables to explore during initial screening studies. This chapter represents one of the first comprehensive published resin screening studies using a complex multi-metal waste stream, with the aim of assessing resin suitability towards selective metal extraction. Further to this, the data generated is intended to allow researchers to understand the behaviour of several resin functionalities towards a range of transition metals ions under comparable conditions; a rarity in the published literature.

5.2 SPECIFIC METHODS

5.2.1 Static Screening Experiments

Using the mixed metal stock solution prepared in Chapter 4, a series of PLS were produced by dilution with deionised water such that final metals concentrations in solutions were 200 ppm for each metal. While such concentrations are higher than those typically encountered in mine waters and tailings leachates, the decision to use equal and artificially high concentrations was made based on several key considerations; a) equal concentrations ensured that observed differences in adsorption were a result of resin selectivity and not differences in relative metal concentrations, b) solution volumes could be reduced to allow more efficient testing at benchtop scale, and c) as samples required dilution prior to analysis, a heightened starting concentration ensured that final sample concentrations were in acceptable ranges for AAS analysis. Adjustments to pH were made through addition of concentrated sulfuric acid, prior to final dilution volume being reached, such that solutions of a range of pH were obtained.

Through the process previously outlined, 2 mL of each wet settled resin was contacted with 50 mL of each PLS in a clean plastic beaker and placed on an orbital shaker to equilibrate for 24 hours. After contact, supernatant solutions were sampled and diluted for metals analysis by ICP-OES. As a change in pH is expected during proton exchange, equilibrium pH was used as the x-axis variable in pH screening plots. For studying the effects of sulfate concentration, ammonium sulfate ($(NH_4)_2SO_4$) was added to PLS solutions such that concentrations ranged from $0.02 - 4$ M SO_4^{2-}. Resins and solutions were contacted as per the pH screening, and supernatant solutions analysed by ICP-OES. Following analysis of samples from the static experiments described previously, metal extraction efficiency was calculated for each resin using Equation 5.1, where C_o is the initial metal concentration (mg/L), and C_e is the concentration at equilibrium (mg/L). Further to this, for the strong acid and weak acid resins, where metal extraction involved the exchange of H^+ ions, the number of protons involved in this exchange was estimated using the relationship between pH and the logarithm of the distribution

coefficient (D). Distribution coefficients were calculated as per Kononova, *et al.* (2014), by first

calculating the working exchange capacity (WEC, Equation 5.2) and applying this to Equation 5.3.

Equation 5.1. Metal extraction efficiency calculation (C_o = PLS metal concentration (mg/L), C_e = equilibrium metal concentration (mg/L)).

$$Extraction\ efficiency = \left(\frac{C_o - C_e}{C_o}\right) * 100$$

Equation 5.2. Calculation of working exchange capacity (WEC (mg/g)), V = volume of PLS used (L), m = mass of resin used (g).

$$WEC = \frac{(C_o - C_e)\ V}{m}$$

Equation 5.3. Calculation of distribution coefficient (D) using WEC.

$$D = \frac{WEC}{C_e}$$

5.2.2. XPS Sample Preparation and Analysis

To determine the Cu oxidation state after extraction by S914, a 5 mL sample of hydrated S914 was

contacted with 1 L of 200 mg/L Cu solution (as $CuSO_4$) to ensure complete Cu loading and prepared

for X-Ray Photoelectron Spectroscopy (XPS) analysis. A small sample of resin was homogenised in a

clean pestle and mortar using a small amount of deionised water to form a paste. This was gently

dried overnight at 50 °C to produce a fine powder of ground resin and was submitted to the Sheffield

Surface Analysis Centre where it was pressed into indium foil prior to analysis. Analyses were

performed using a Kratos AXIS Supra instrument with a monochromated aluminium source, focused

on two analysis points (area: 700 μm by 300 μm). Survey scans were carried out between 1200 – 0 eV

energy resolution, and one 300 second sweep. High resolution C 1s, Cu 2p, and Cu LMM scans were collected at their appropriate energy ranges at 0.1 eV energy resolution, with a 300 second sweep for C and three 300 second sweeps for the Cu 2p and Cu LMM scans.

Collected data was calibrated in intensity using a transmission function characteristic of the instrument (determined using software from NPL) to make the values instrument independent and allow better comparison to published literature. All data was calibrated relative to a C 1s position of 285 eV for C-C/C-H type environments.

5.2.3. Criteria for Resin Progression

The overall aim of this chapter is to identify the functional groups which are most appropriate for effective and selective metal recovery, and so a number of semi-quantitative criteria were set to aid decision-making in relation to which resins were selected for further study. Using the experimental methods detailed, several characteristics were elucidated related to resin performance; predominantly resin selectivity, and their extractive resilience under varying pH and sulfate concentration. Table 5.1 explains the importance of each characteristic in terms of process design, and details the acceptable ranges used in decision making following data analysis. The interconnectivity of these criteria meant that trade-offs were required, and these are detailed at the appropriate discussion sections.

Table 5.1. Criteria for resin progression/elimination following completion of screening study.

Characteristic	Importance for System Design	Assessment
Selectivity	Preferential extraction of certain species over others would allow for tailored treatment to target metals of key concern. In-situ separation of metals to discrete columns reduces resource recovery complexity (post-processing) given fewer metals present in product streams. Bulk (low-selectivity) extraction has benefits for final effluents treatment to ensure environmental limits are not exceeded.	Ideal: One metal species preferentially extracted over all others – selectivity apparent by large separation in y-axis on extraction efficiency figures. Acceptable: Two/three metals with high difference in extraction % from rest of metals IF extracted metals are of particular interest for resource recovery (e.g. Ni, Co). Acceptable: low degree of selectivity between metals IF extraction efficiency is high.
Extraction resilience	A high extraction is indicative of efficient metal removal from solution. A more efficient extraction means less adsorbent is required, ultimately reducing material costs.	Acceptable: Extraction efficiency of selectively-extracted metals above >80% in the range of 0.01 – 0.1 M H^+ (i.e. the less-extreme and therefore more probable conditions encountered)

5.3 RESULTS

5.3.1 Dowex M4195 (WBA)
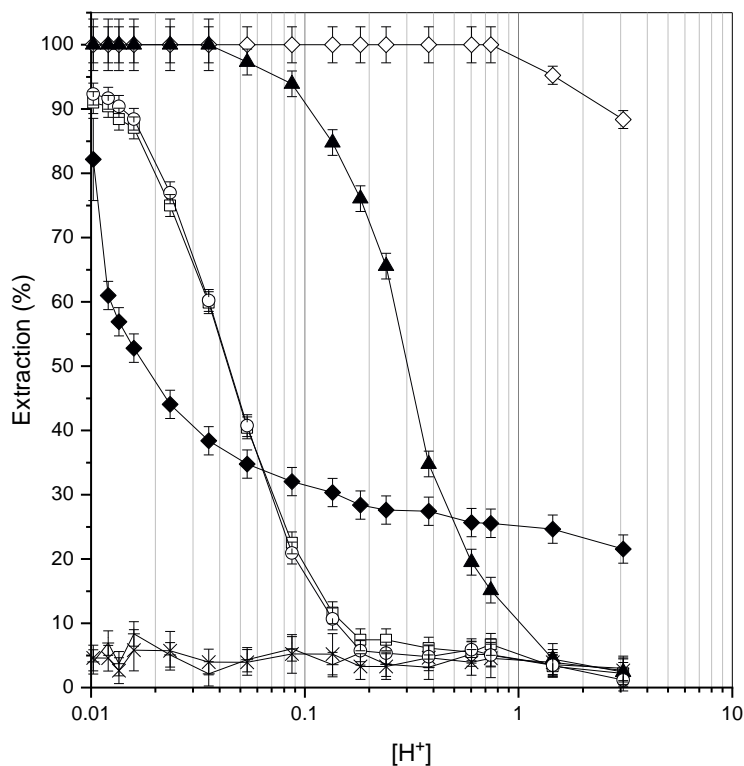
Figure 5.1. Extraction of metal ions as a function of sulfuric acid concentration on M4195. Al(III) = +, Co(II) = □, Cu(II) = ◇, Fe(III) = ◆, Ni(II) = ▲, Mn(II)= ×, Zn(II) = ○.

The weak base anionic (WBA) bispicolylamine functionalised resin, Dowex M4195, exhibited very high Cu selectivity across the studied pH range, evidenced by the complete extraction observed below 1 M H^+ (Figure 5.1). For other metals, distinct pH-dependent uptake behaviour was observed. Removal of Ni was shown to greatly affected by increasing proton concentration, dropping from 100% extraction at 0.01 M H^+ to almost zero uptake beyond 1 M H^+ (Figure 5.1). Similar extraction profiles for Co, Zn, and Fe were observed, though not to the same extent as for Ni. Removal of Al and

Mn was minimal under all conditions of pH, indicating poor selectivity towards these metals by

bispicolylamine functional groups. As such, the selectivity series for M4195 may be defined as Cu >>

Fe > Ni > Co = Zn = Mn = Al at 1M H$^+$, switching to Cu = Ni > Zn = Co > Fe > Mn = Al at lower proton

concentration (0.2 M H$^+$).
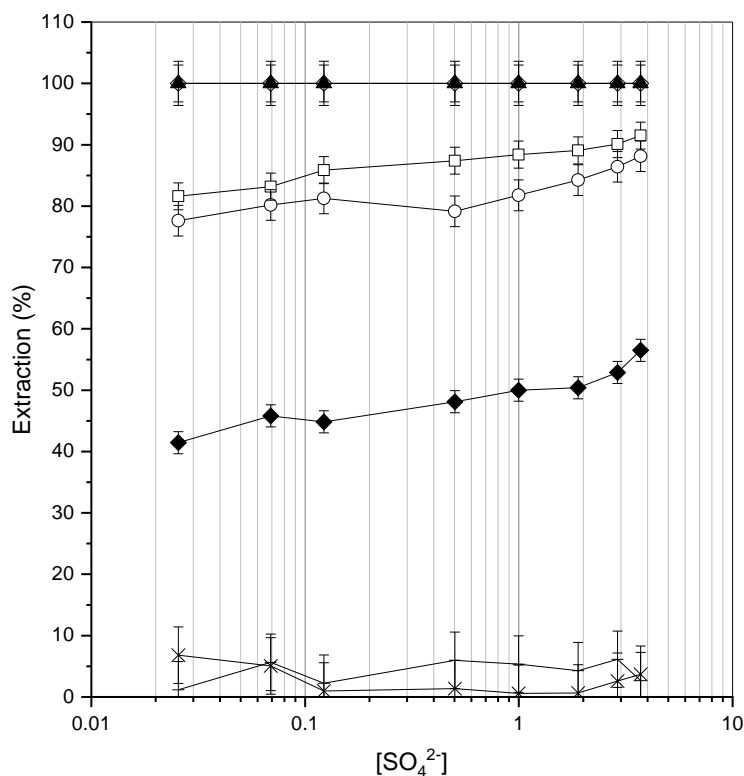
Figure 5.2. Extraction of metal ions as a function of ammonium sulfate concentration on M4195 at 0.027 M H$^+$.
Al(III) = $+$, Co(II) = □ , Cu(II) = ◇, Fe(III) = ◆, Ni(II) = ▲, Mn(II)= ✕, Zn(II) = ◯.

A pH of 1.57 (0.027 M H$^+$) was chosen for sulfate screening experiments given that M4195 displayed

effective extraction for a range of metals at this pH. Sulfate screening results for M4195 are

presented in (Figure 5.2). The addition of ammonium sulfate to the PLS did not strongly affect the

selectivity towards Cu and Ni, with continued quantitative extraction of these metals. For Co, Zn, and

Fe, increases in sulfate concentration were accompanied by modest increases in their extraction,

with improvements of approximately 8%, 10%, and 16%, respectively (Figure 5.2). Extraction of Al

and Mn remained low, with little response to sulfate addition. As such, it was observed that the

selectivity of M4195 was not notably affected by increases in sulfate concentration and exhibited

robust performance towards Cu and Ni with increased ionic strength.

A parameter that can be explored to indicate the strength of interaction between a metal species

and the resin functional group is through comparison of pH_{50} values; the pH at which 50% metal

extraction occurs (Amphlett *et al.*, 2018; Eldridge *et al*, 2015). In general, a lower pH_{50} value is

indicative of a stronger interaction between metal and resin, as a greater concentration of proton

would be required to inhibit the metal interaction. Interpretation of pH_{50} values for M4195 suggests

that Cu has the strongest interaction with the bis-picolylamine groups followed by Ni, with similar

interaction for Zn, Co, and Fe (Table 5.2). This relates strongly to the pH profiles presented in Figure

5.1, as the metal species with lower pH_{50} values were extracted to a higher degree by M4195.

Table 5.2. pH_{50} values for the extracted metal ions as a function of pH for Dowex M4195 (*predicted from extrapolation of data points).

Metal	pH_{50}
Cu^{2+}	-0.51*
Ni^{2+}	0.54
Zn^{2+}	1.40
Co^{2+}	1.41
Fe^{3+}	1.82

5.3.2   Puromet MTS9850 (WBA)

Puromet MTS9850 (S985), a polyamine functionalised resin, was not effective for metal removal

from sulfuric acid media regardless of solution pH, with extraction rarely exceeding 20% over the

studied range (Figure 5.3). Differences in extraction percentage between metals was also very small,

indicating poor selectivity under the studied range of pH for the metals in the PLS. Given the poor

selectivity of S985 towards the metal species studied, the effect of sulfate concentration was not

investigated, as having high capacity towards at least one metal in the PLS was an essential criterion

for resin progression to further screening experiments.
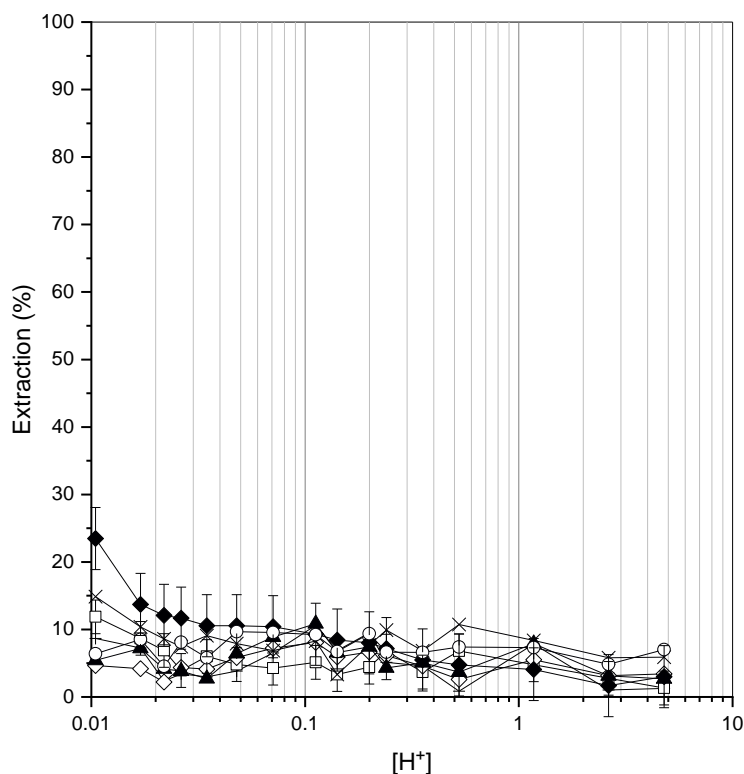
Figure 5.3. Extraction of metal ions as a function of sulfuric acid concentration on S985. Al(III) = $+$, Co(II) = $\square$, Cu(II) = $\diamondsuit$, Fe(III) = $\blacklozenge$, Ni(II) = $\blacktriangle$, Mn(II)= $\times$, Zn(II) = $\bigcirc$.

5.3.3   Puromet MTS9100 (WBA)

The effects of pH on the extraction of metals from PLS by the amidoxime functionalised resin,

Puromet MTS9100 (S910), is provided in Figure 5.4. It was observed that the resin was most selective

for Fe (pH$_{50}$ 2.15), with poor extraction of other metals over the studied range. An increase in Fe

extraction was observed between 0.05 and 0.5 M H$^+$, indicative of a change in extraction mechanism

at this point, but this had little effect on the extraction of the other metals in solution. As only Fe

extraction was affected, it is likely that an alteration in metal speciation is the cause of this change,

rather than a change in, for example, degree of protonation within the resin functionality, which

would likely affect the uptake of other metal species also. This change in Fe speciation was observed

during geochemical modelling (Appendix Figure 11.1), where $FeHSO_4^+$ became the predominant Fe

species beyond 0.1 M H^+, concurrent with the change in extractive behaviour in Figure 5.4. At lower

proton concentration, Cu extraction did increase to approximately 28%, but Fe was still preferentially

extracted (Figure 5.4). While a tendency towards Fe extraction was observed by this resin, at the

point of greatest selectivity compared to other metals (0.2 M H^+), Fe extraction was only 40% and

deemed unsuitable for effective recovery.
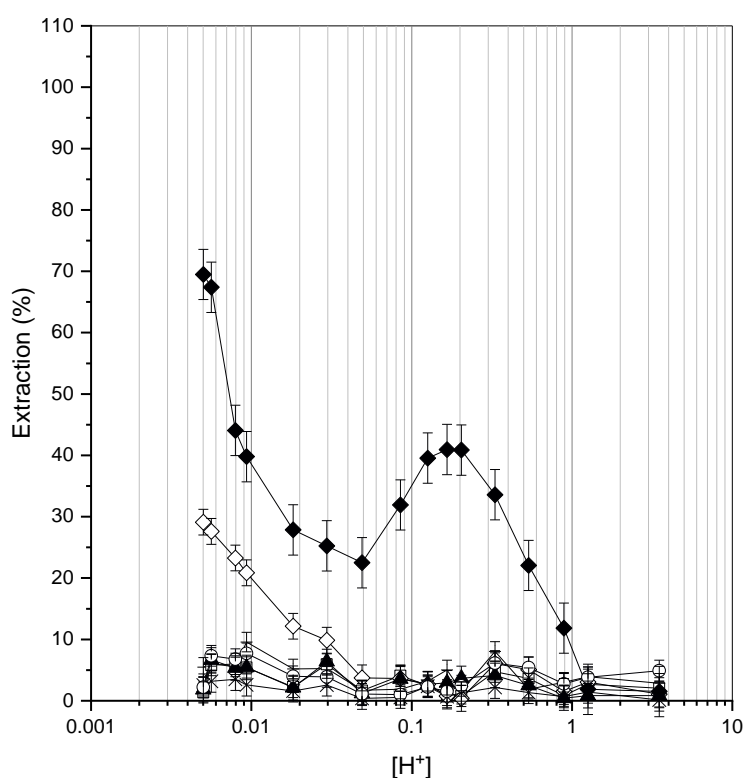
Figure 5.4. Extraction of metal ions as a function of sulfuric acid concentration on S910. Al(III) = $+$, Co(II) = $\square$, Cu(II) = $\diamondsuit$, Fe(III) = $\blacklozenge$, Ni(II) = $\blacktriangle$, Mn(II)= $\times$, Zn(II) = $\bigcirc$.

5.3.4   Puromet MTS9501 (WAC)

The extraction of metals from PLS using the weak acid cationic resin Puromet MTS9501

(aminophosphonic acid functionality), is displayed in Figure 5.5. A distinct preference towards the

extraction of Fe and Al is exhibited by S950, with complete extraction of Fe irrespective of pH, and

extraction of Al only diminishing by 20% under high acid concentration (Figure 5.5).
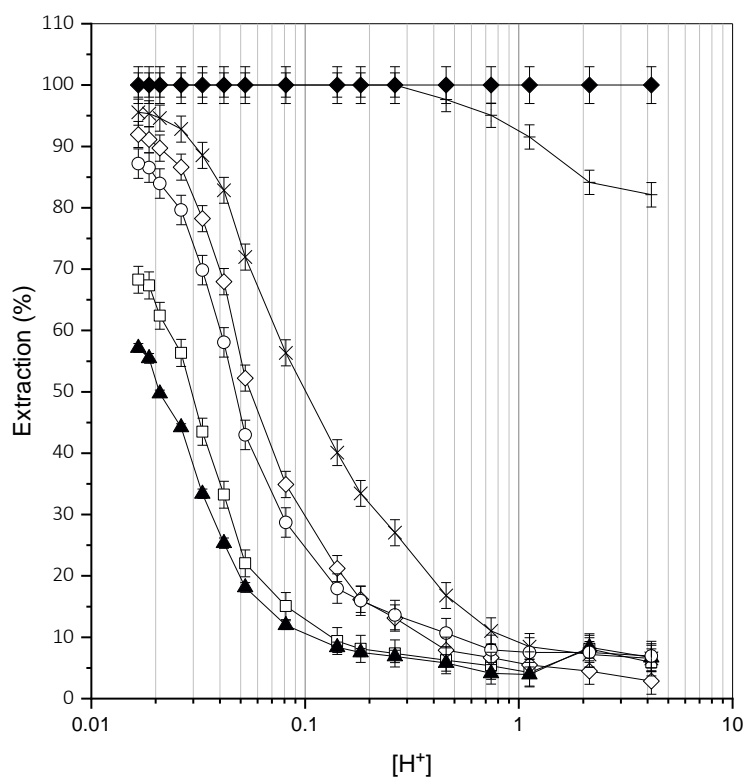
Figure 5.5. Extraction of metal ions as a function of sulfuric acid concentration on S950. Al(III) = ＋, Co(II) = □,
Cu(II) = ◇, Fe(III) = ◆, Ni(II) = ▲, Mn(II)= ✕, Zn(II) = ○.

The extraction of other elements in solution was suppressed gradually as proton concentration

increased, with almost exclusive extraction of Fe and Al beyond 2 M H+. The affinity towards Fe and

Al by S950 is evident from Figure 5.5, and by combining this observation with the increasing order of

pH$_{50}$ values reported in Table 5.3, a selectivity series for S950 under the studied conditions can be

determined as Fe > Al > Mn > Cu > Zn > Co > Ni.

Table 5.3. pH50 values for the extracted metal ions as a function of pH for Puromet MTS9501.

Metal	pH$_{50}$
Mn^{2+}	0.94
Cu^{2+}	1.19
Zn^{2+}	1.31
Co^{2+}	1.51
Ni^{2+}	1.60

Linear regression of logD values (Equation 5.3) when plotted against pH can provide indication of the

number of protons involved in metal exchange reactions for weak and strong acid resins, which work

via proton exchange mechanisms. The resulting slopes for S950 are presented in Figure 5.6, with

results of regression analyses in Table 5.4, where the gradient of the slope approximately equates to

the number of protons exchanged per metal cation extracted.
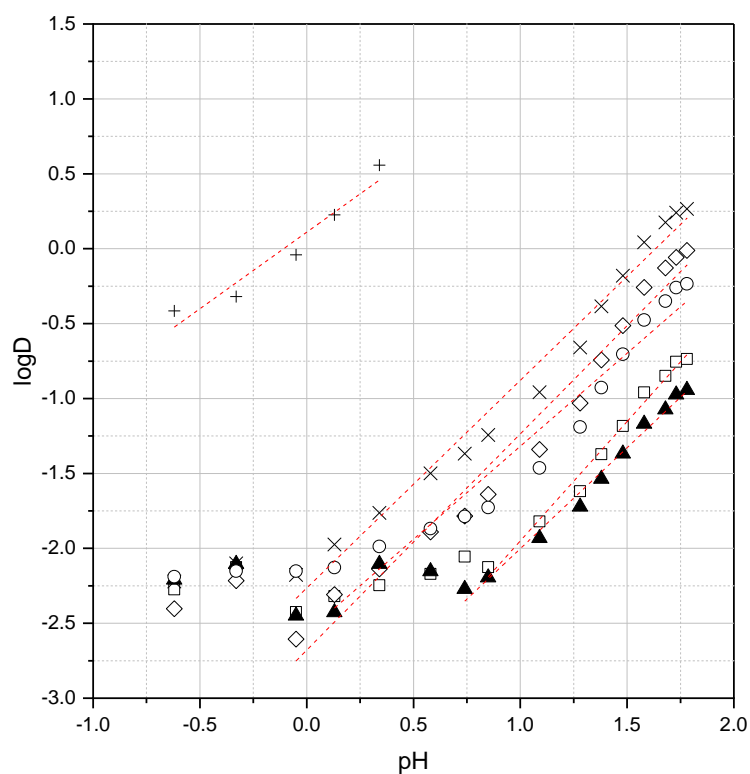
Figure 5.6. pH vs. logD for S950. Al(III) = +, Co(II) = □, Cu(II) = ◇, Ni(II) = ▲, Mn(II)= ✕, Zn(II) = ○. Dashed lines represent portion used in linear regression analyses.

Table 5.4. Linear regression analysis of pH vs. logD curves for S950.

	Al	**Co**	**Cu**	**Mn**	**Ni**	**Zn**
Intercept	-4.525	-4.484	-2.663	-3.932	-4.304	-3.397
Slope	1.395	1.705	2.672	0.971	2.021	0.948
R²	0.892	0.981	0.988	0.842	0.993	0.929

The addition of ammonium sulfate to solutions at pH 1.43 (0.037 M H⁺) had no effect on the Fe

extraction efficiency of S950 (Figure 5.7). As sulfate concentration increased to 2 M, the extraction of

all other metal ions was suppressed, before increasing again above 2 M sulfate for Mn, Cu, and Zn,

potentially suggesting an alternate extraction mechanism under such conditions. The extraction of

Co and Ni does not increase above 2 M sulfate and remains inaccessible to resin functionality.
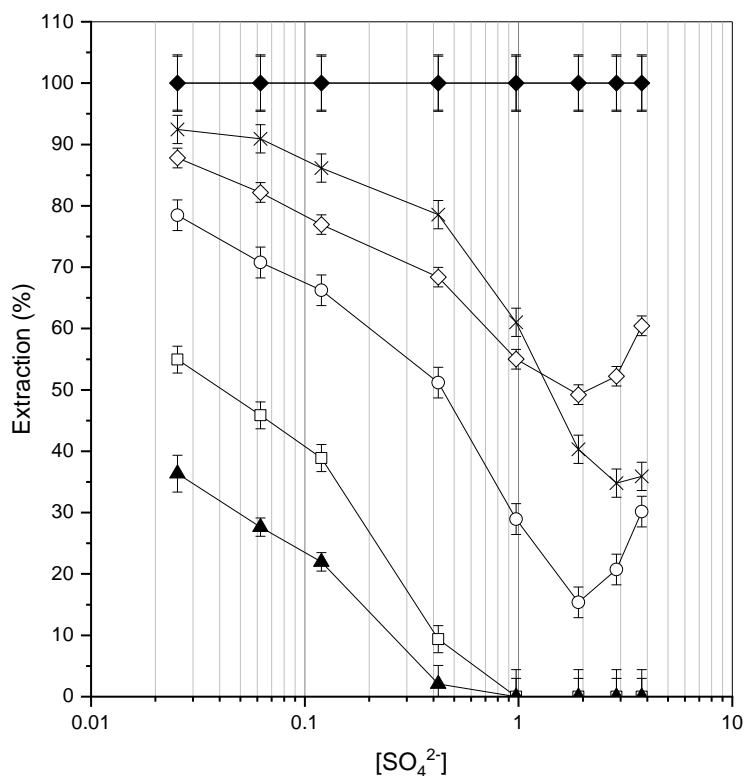
Figure 5.7. Extraction of metal ions as a function of ammonium sulfate concentration on S950 at 0.027 M H$^+$.
Al(III) = $+$, Co(II) = $\square$, Cu(II) = $\diamond$, Fe(III) = $\blacklozenge$, Ni(II) = $\blacktriangle$, Mn(II)= $\times$, Zn(II) = $\bigcirc$.

5.3.5   Puromet MTS9301 (WAC)

The results of pH screening for the iminodiacetic acid functionalised resin is presented in Figure 5.8.

At lower [H$^+$] Puromet MTS9301 (S930) shows high selectivity towards Cu and Fe, with reasonable Ni

extraction also. The addition of sulfuric acid to the PLS has a drastic adverse effect on metal removal

capabilities of this resin, with extraction under 8% for all studied metals beyond 1 M H$^+$ (Figure 5.8).

As such, this resin would be more suitable for operation in the region of 0.1 M H$^+$ or lower, where

metal extraction is less hindered by proton concentrations. Using Figure 5.8 in conjunction with pH$_{50}$

values in Table 5.5, it is possible to infer the selectivity series for S930, based upon strength of interaction between metal ions and the iminodiacetic functional groups, as being Cu > Fe > Ni > Co > Zn > Al = Mn.
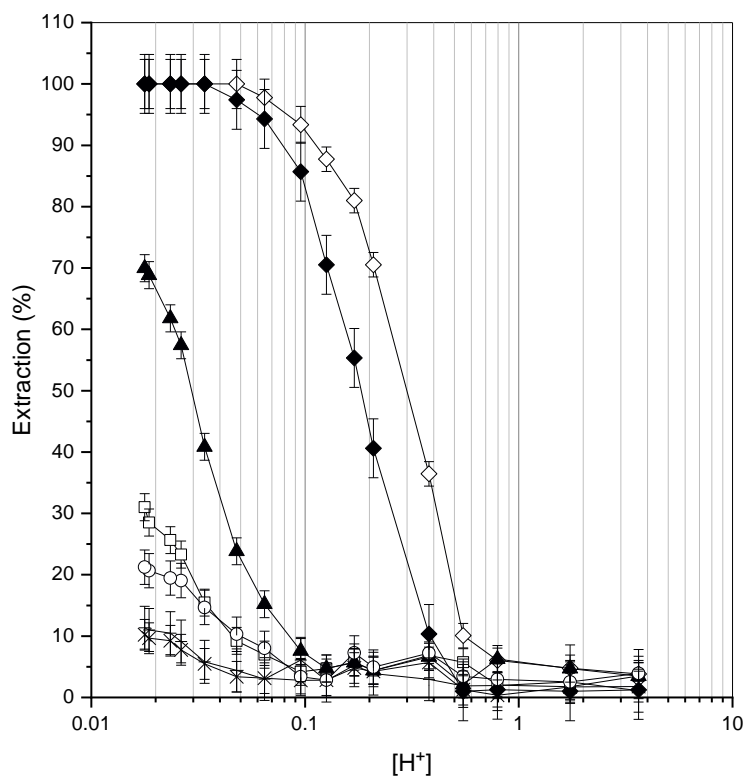
Figure 5.8. Extraction of metal ions as a function of sulfuric acid concentration on S930. Al(III) = $+$, Co(II) = $\square$, Cu(II) = $\diamond$, Fe(III) = $\blacklozenge$, Ni(II) = $\blacktriangle$, Mn(II)= $\times$, Zn(II) = $\bigcirc$.

Table 5.5. pH50 values for the extracted metal ions as a function of pH for Puromet MTS9301 (*predicted from linear extrapolation of data points).

Metal	pH_{50}
Cu^{2+}	0.51
Fe^{3+}	0.74
Ni^{2+}	1.53
Co^{2+}	2.08*
Zn^{2+}	2.80*
Al^{3+}	3.06*
Mn^{2+}	3.72*

Analysis of logD values as a factor of pH (Figure 5.9) indicated that for the two most favourably exchanged ions, Cu and Fe, the exchange stoichiometry between ion and proton was approximately 1:2 (Table 5.6), with Ni also being exchanged for proton on this basis. Linear regression of log distribution curves for Al and Mn was unsuccessful, as evidenced by low R^2 values, given the relatively poor extraction of these metals by S930 (Figure 5.8).
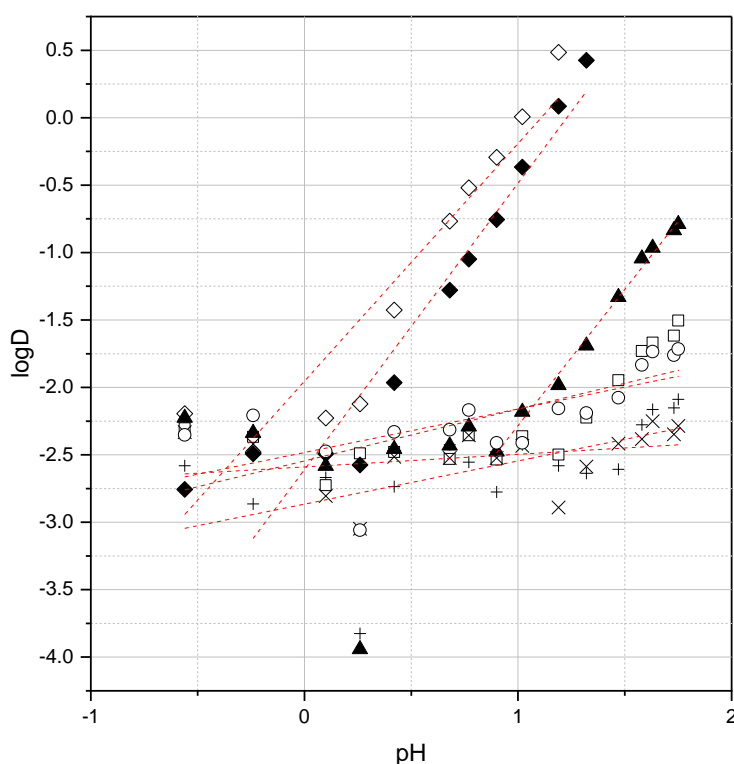
Figure 5.9. pH vs. logD for S930. Al(III) = $+$, Co(II) = $\square$, Cu(II) = $\diamond$, Fe(III) = $\blacklozenge$, Ni(II) = $\blacktriangle$, Mn(II)= $\times$, Zn(II) = $\bigcirc$. Dashed lines represent portion used in linear regression analyses.

Table 5.6. Linear regression analysis of pH vs. logD curves for S930.

	Al	Co	Cu	Fe	Mn	Ni	Zn
Intercept	-2.865	-2.035	-1.411	-1.509	-2.589	-1.656	-2.127
Slope	0.320	0.737	1.897	1.972	0.093	2.021	0.488
R^2	0.326	0.965	0.961	0.989	0.089	0.990	0.917

The effect of ammonium sulfate addition on the uptake efficiencies of S930 towards metals was studied at pH 1.48 (Figure 5.10). Increased concentrations of sulfate in solution resulted in a steady improvement of Ni, Co, and Zn removal, with little effect on Al extraction. Mn removal was low under all conditions, with a notable decrease in removal with increased sulfate concentration. Quantitative extraction was observed for Cu and Fe under all sulfate concentrations below 4 M sulfate, at which point minor suppression of Fe extraction was observed but remained high at 95% (Figure 5.10).
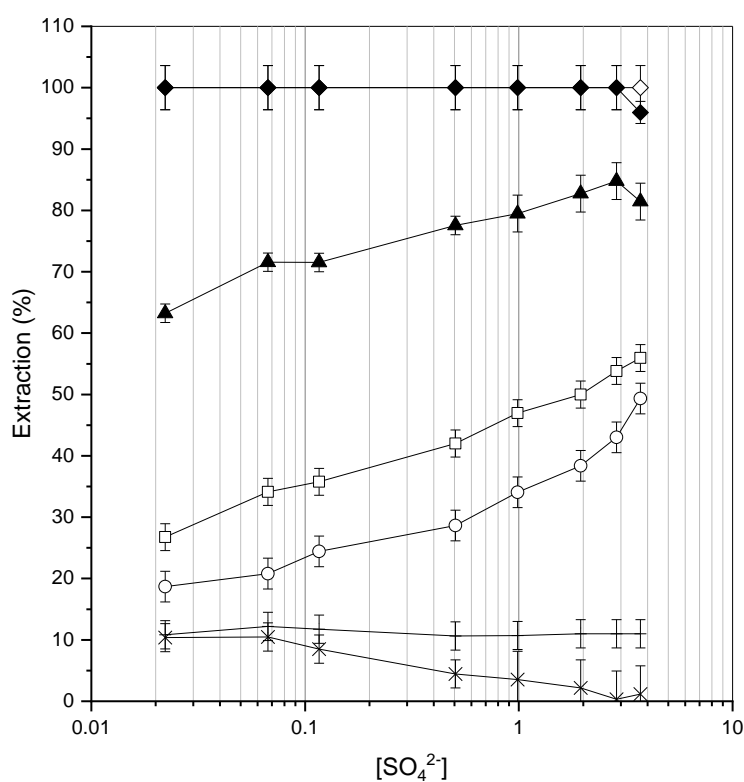
Figure 5.10. Extraction of metal ions as a function of ammonium sulfate concentration on S930 at 0.03 M H⁺. Al(III) = ╋, Co(II) = ▫ , Cu(II) = ◇, Fe(III) = ◆, Ni(II) = ▲, Mn(II)= ✕, Zn(II) = ◯.

5.3.6   Puromet MTS9570 (SAC/WAC)

Puromet MTS9570 is a bifunctional resin, containing strongly acidic sulfonic acid functional groups in addition to weakly acidic phosphonic acid groups (Figure 4.1). The extraction of metals as a factor of

[H⁺] is shown in Figure 5.11. A high Fe selectivity was observed compared to all other metals in the PLS, along with reasonable Al extraction. A sharp reduction in extraction capability for most metals, except for Fe, occurs as the pH of solutions decreases. The strong acid functionality of S957 shows little separation capability between first row transition metals, evidenced by the similar extraction percentages and behaviour reported. Reading Figure 5.11 in conjunction with the pH_{50} values calculated in Table 5.7, a selectivity series of Fe >> Al > Cu > Mn > Co > Zn > Ni can be determined for S957.
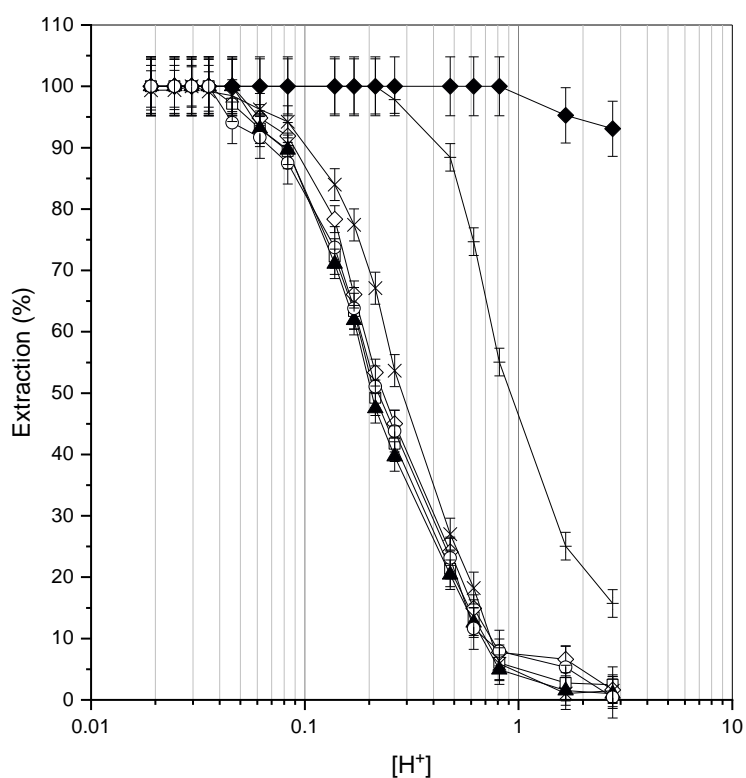
Figure 5.11. Extraction of metal ions as a function of sulfuric acid concentration on S957. Al(III) = $+$, Co(II) = $\square$, Cu(II) = $\diamond$, Fe(III) = $\blacklozenge$, Ni(II) = $\blacktriangle$, Mn(II)= $\times$, Zn(II) = $\bigcirc$.

Table 5.7. pH50 values for the extracted metal ions as a function of pH for Puromet MTS9570.

Metal	pH$_{50}$
Al^{3+}	0.04
Cu^{2+}	0.51
Mn^{2+}	0.64
Co^{2+}	0.66
Zn^{2+}	0.66
Ni^{2+}	0.68

Figure 5.12 indicated a strong positive correlation between pH and logD values for S957, suggesting that proton-metal ion exchange is the dominant process for metal removal by this resin. R^2 values for regression analysis of distribution curves were generally high (Table 5.8), and so the estimations of exchange stoichiometry between protons of the functional group and metal ions in solution are accurate.
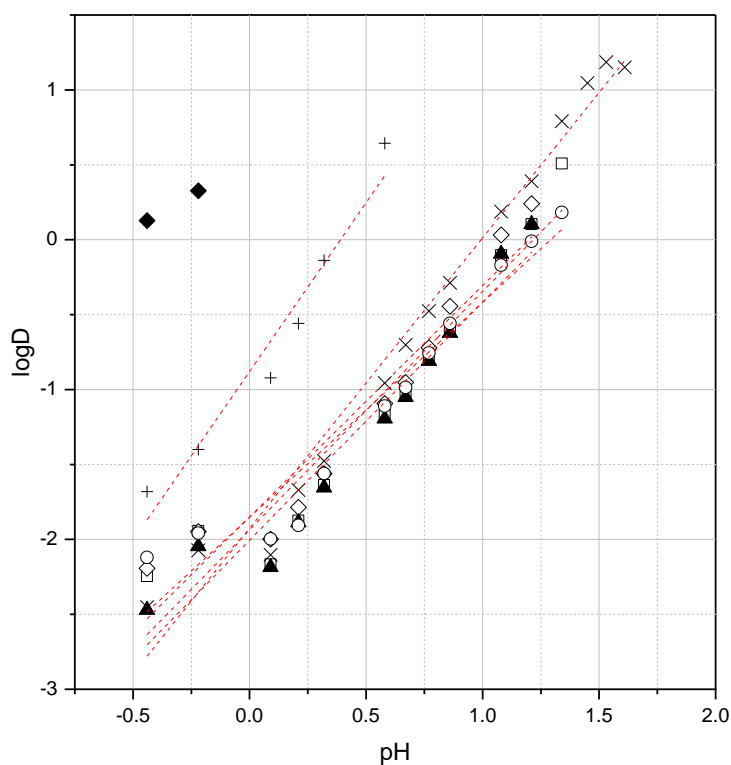
Figure 5.12. pH vs. logD for S957. Al(III) = $+$, Co(II) = $\square$, Cu(II) = $\Diamond$, Fe(III) = $\blacklozenge$, Ni(II) = $\blacktriangle$, Mn(II)= $\times$, Zn(II) = $\bigcirc$. Dashed lines represent portion used in linear regression analyses.

Table 5.8. Linear regression analysis of pH vs. logD curves for S957.

	Al	Co	Cu	Fe	Mn	Ni	Zn
Intercept	-0.879	-1.935	-1.850	NA	-1.926	-2.005	-1.85233
Slope	2.253	1.590	1.544	NA	1.940	1.588	1.434
R²	0.954	0.925	0.928	NA	0.980	0.942	0.938

Sulfate screening experiments for S957 were performed at pH 1.37 and presented in Figure 5.13. The effects of ammonium sulfate addition appears to have little effect on the extraction of Fe and Al, with only minor suppression of Al uptake beyond 1 M sulfate. A significant decrease in the extraction

performance for other metals present in the PLS was revealed, with final metal extraction under 20% beyond 1 M sulfate.
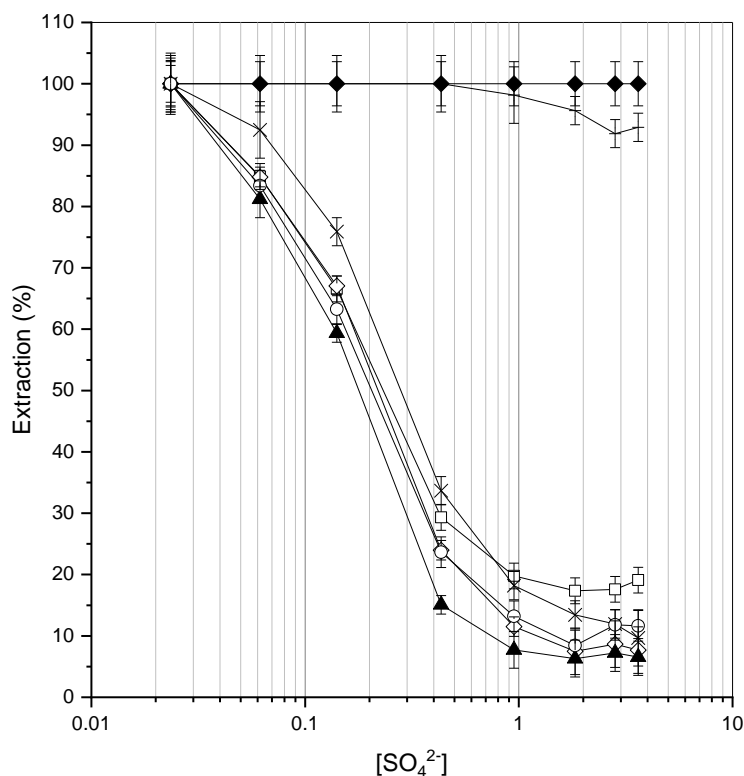
Figure 5.13. Extraction of metal ions as a function of ammonium sulfate concentration on S957 at 0.04 M H$^+$.
Al(III) = $+$, Co(II) = $\square$, Cu(II) = $\diamond$, Fe(III) = $\blacklozenge$, Ni(II) = $\blacktriangle$, Mn(II)= $\times$, Zn(II) = $\bigcirc$.

5.3.7 Dowex M31 (SAC)

The effect of increased [H$^+$] on metal extraction by the strongly acidic sulfonic acid functionalised resin, Dowex M31, is presented in Figure 5.14. This resin proved highly effective for the removal of all metal species present in the simulant solution, with higher extraction percentages at lower [H$^+$]. However, as the pH of the solution decreased, a sharp decline in its capacity for removal was observed, falling below 20% beyond 1 M H$^+$ (Figure 5.14). The marginally higher extraction of Al, Fe, and Mn by S957 was confirmed by marginally lower pH$_{50}$ values for these metals (Table 5.9); indicative of a stronger interaction with the resin functionality.

57
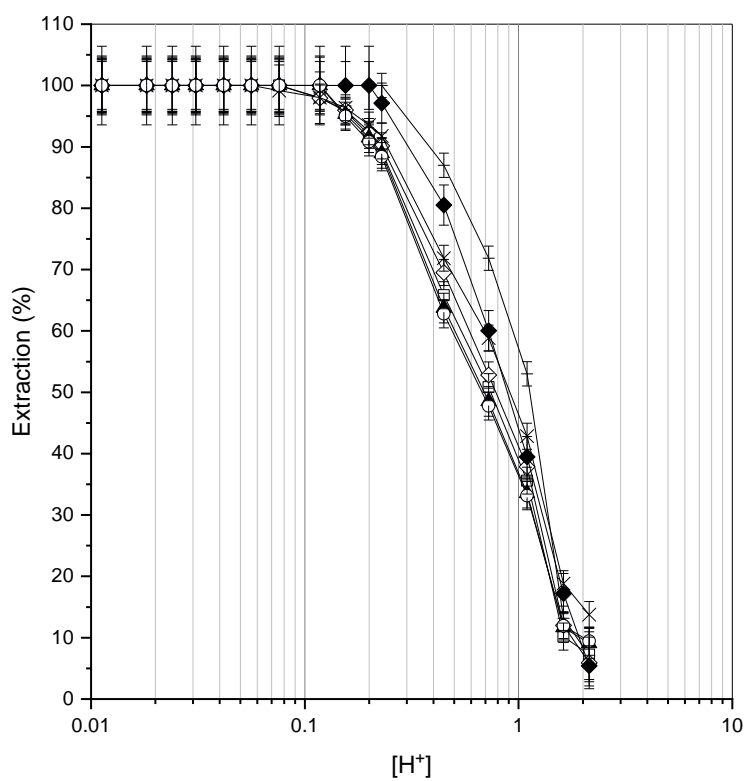
Figure 5.14. Extraction of metal ions as a function of sulfuric acid concentration on M31. Al(III) = +, Co(II) = □, Cu(II) = ◇, Fe(III) = ◆, Ni(II) = ▲, Mn(II)= ✕, Zn(II) = ○.

Table 5.9. pH50 values for the extracted metal ions as a function of pH for Dowex M31.

Metal	pH$_{50}$
Al^{3+}	-0.19
Fe^{3+}	0.04
Mn^{2+}	0.05
Cu^{2+}	0.11
Co^{2+}	0.15
Zn^{2+}	0.18
Ni^{2+}	0.68
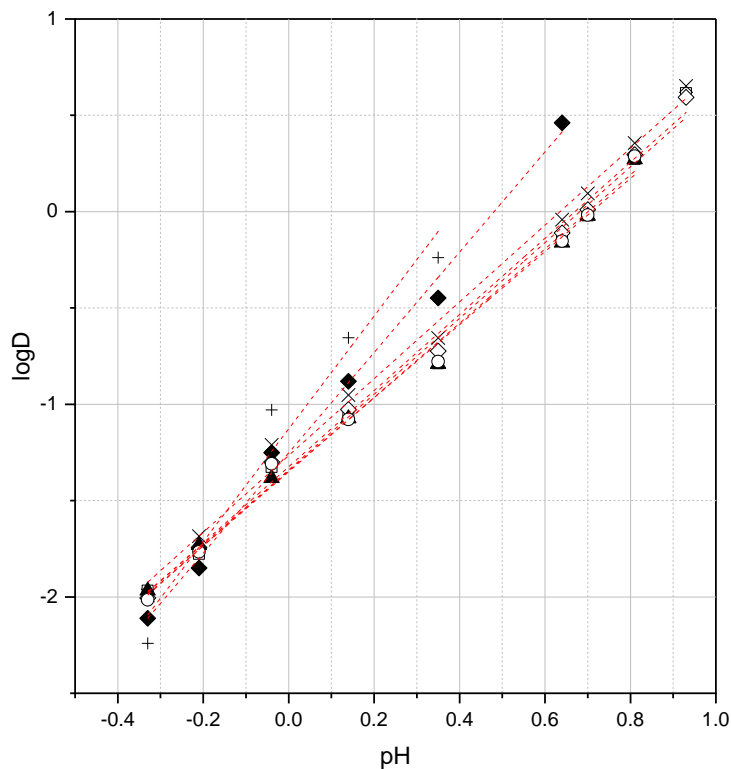
Figure 5.15. pH vs. logD for M31. Al(III) = $+$, Co(II) = □, Cu(II) = ◇, Fe(III) = ◆, Ni(II) = ▲, Mn(II)= ✕, Zn(II) = ○. Dashed lines represent portion used in linear regression analyses.

Having strongly acidic sulfonic acid functionality, the extraction of metals by M31 is most likely through a proton-cation exchange mechanism. Distribution curves for metal extraction on to M31 are provided in Figure 5.15. The results of regression analyses on these curves are presented in Table 5.10. A good fit ($R^2 > 0.95$) was achieved for the regression of distribution curves for all metal species. The slope values for most metals (Co, Cu, Mn, Ni, Zn) approximate to a value of 2, indicating an exchange of two protons per metal ion. For Al and Fe, this value was higher (approximately 3 and 2.5, respectively), suggesting a slightly different extraction mechanism for these ions. However, given the patterns in pH profiles in Figure 5.14, if Al and Fe were extracted by another mechanism, this did not significantly alter the extractive behaviour observed under these experimental conditions.

Table 5.10. Linear regression analysis of pH vs. logD curves for M31

	Al	Co	Cu	Fe	Mn	Ni	Zn
Intercept	-1.128	-1.341	-1.324	-1.252	-1.266	-1.346	-1.350
Slope	2.985	1.967	1.977	2.603	1.993	1.898	1.926
R^2	0.965	0.992	0.995	0.994	0.994	0.996	0.993

Metal extraction as a function of increased addition of ammonium sulfate, carried out at pH 1.42 (Figure 5.16) displayed a similar pattern to that of increased proton concentration. Higher sulfate concentration tended to be accompanied with a decrease in percentage extraction for all metals. As sulfate concentration increased further, a sharp increase in extraction, from approximately 5% at 1.5 M SO_4 to 25% at 4 M SO_4, was observed for Fe only (Figure 5.16).
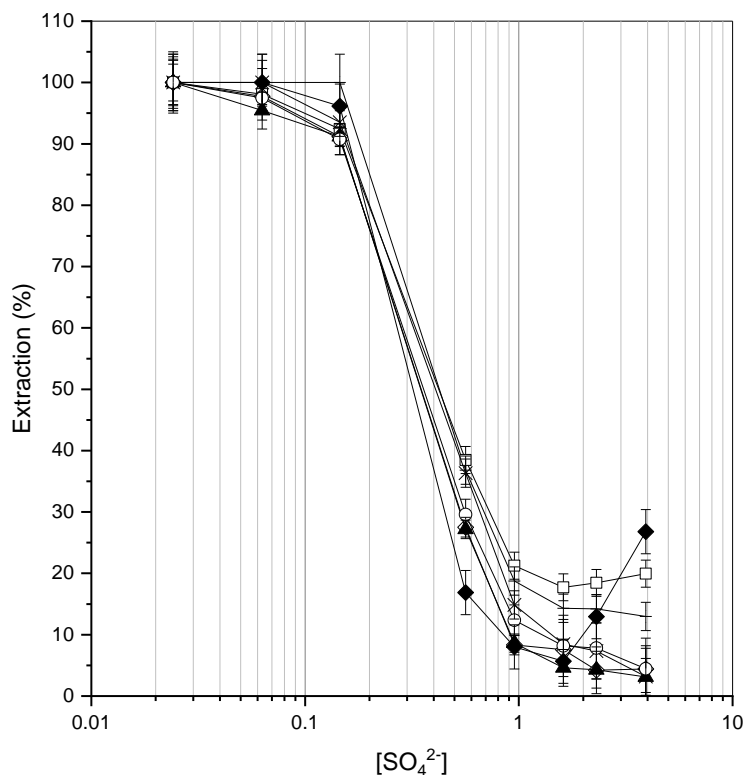
Figure 5.16. Extraction of metal ions as a function of ammonium sulfate concentration on M31 at 0.04 M H^{+}.
Al(III) = +, Co(II) = □ , Cu(II) = ◇, Fe(III) = ◆, Ni(II) = ▲, Mn(II)= ✕, Zn(II) = ○.

5.3.8   Puromet MTS9200

The isothiouronium functionalised resin Puromet MTS9200 (S920) exhibited very low adsorption of metals from the PLS under the conditions studied. As is shown in Figure 5.17, the extraction percentage for all metals remained below 10% between 0.01 and 3 M sulfuric acid concentration. As such, the isothiouronium functional group was determined not to be a suitable candidate for the proposed treatment of waste waters and was not studied further in subsequent experimentation.
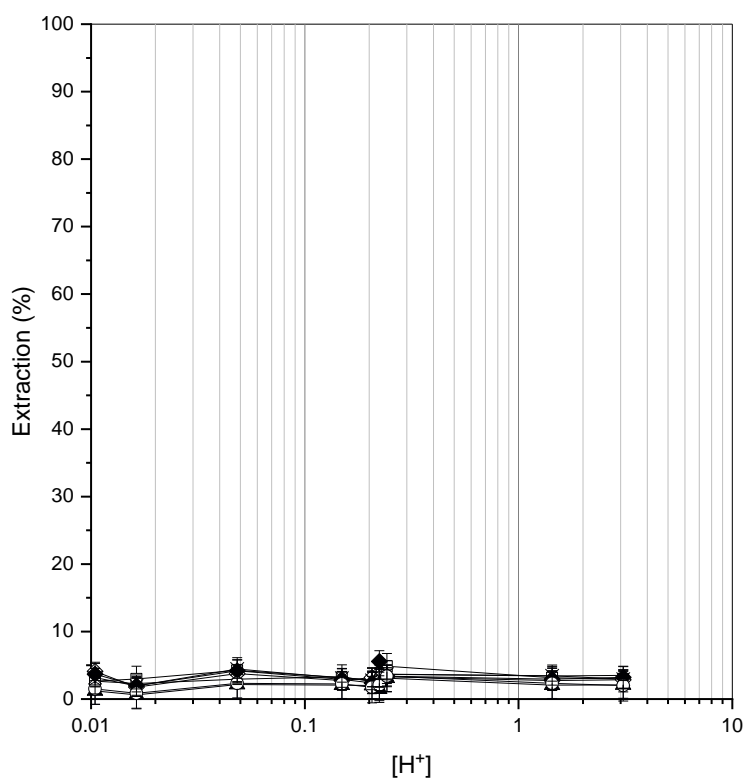
Figure 5.17. Extraction of metal ions as a function of sulfuric acid concentration on S920. Al(III) = +, Co(II) = □, Cu(II) = ◇, Fe(III) = ◆, Ni(II) = ▲, Mn(II)= ×, Zn(II) = ○.

5.3.9   Puromet MTS9140

Puromet MTS9140 (S914), a polystyrenic resin with thiourea functionality, exhibited great selectivity towards Cu under all studied conditions of pH (Figure 5.18), with Cu extraction being above 92% irrespective of increased proton concentration. Extraction of other metals present in the PLS was very low, with almost no change in extraction percentage with respect to equilibrium pH.
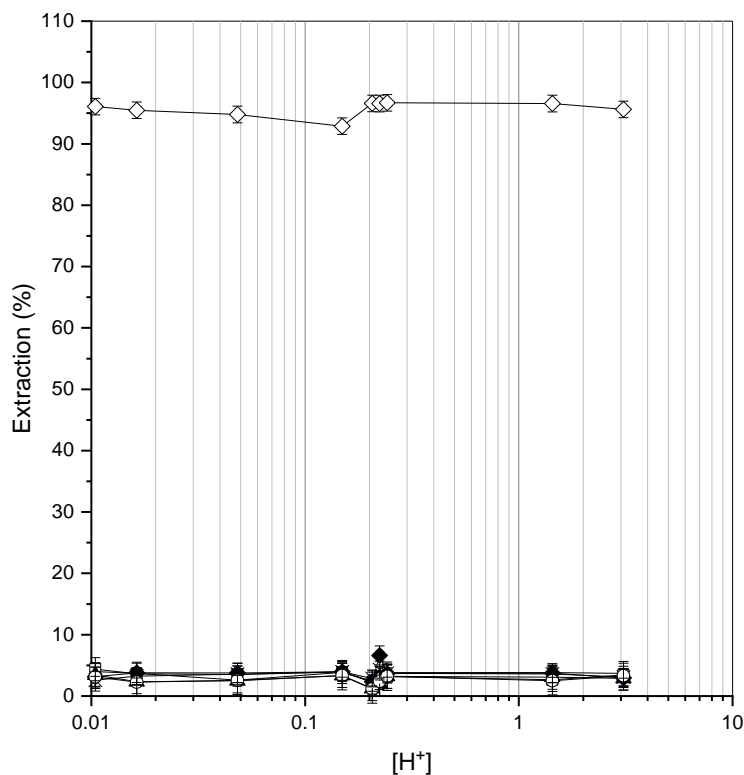
Figure 5.18. Extraction of metal ions as a function of sulfuric acid concentration on S914. Al(III) = $+$, Co(II) = $\square$, Cu(II) = $\diamond$, Fe(III) = $\blacklozenge$, Ni(II) = $\blacktriangle$, Mn(II)= $\times$, Zn(II) = $\bigcirc$.

Increased sulfate concentration in the PLS had no observable effect on the extraction of any metal species by S914, with the high capacity for Cu removal and low co-removal of other metals reported under all sulfate concentration conditions (Figure 5.19), indicating a high resilience to increased ionic strength. Given that this resin was not developed by the manufacturer for Cu separations and that true selectivity towards a single ion would be highly advantageous for treatment of mixed metal waste streams, further exploration in to the surface binding of Cu was explored for this resin by using X-Ray Photoelectron Spectroscopy (XPS) analysis.
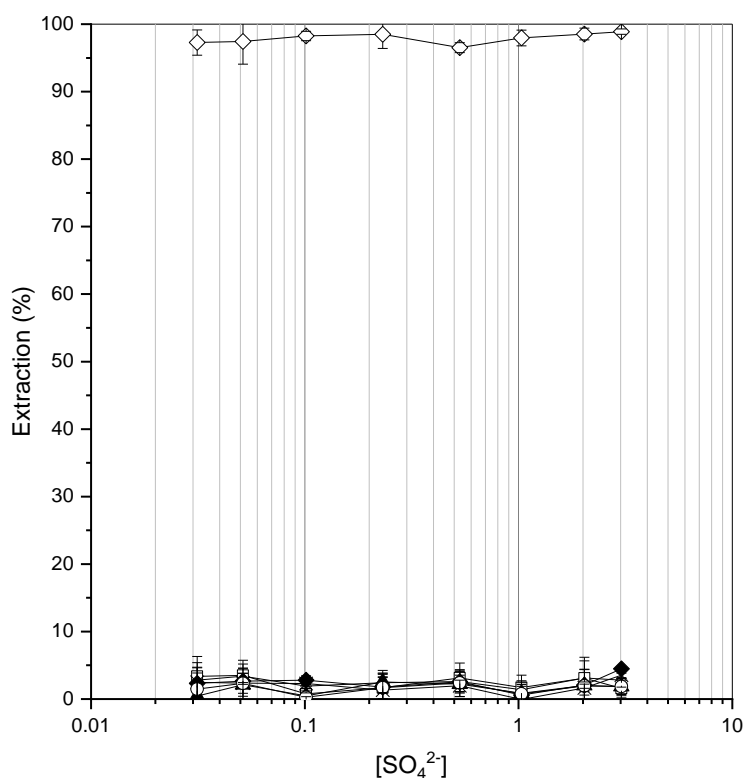
Figure 5.19. Extraction of metal ions as a function of ammonium sulfate concentration on S914 at 0.027 M H$^+$.
Al(III) = $+$, Co(II) = $\square$, Cu(II) = $\diamondsuit$, Fe(III) = $\blacklozenge$, Ni(II) = $\blacktriangle$, Mn(II)= $\times$, Zn(II) = $\bigcirc$.

The XPS survey scan was used to determine surface elemental composition of powdered sample of

Cu-loaded S914, given as atomic % (At%) in Figure 5.20. As can be expected for a resin bead with a

polystyrene-DVB backbone, the most abundant element quantified was C (63.77 At%). In decreasing

abundance, the remaining composition was determined to be O (16.98 At%), N (7.62 At%), Si (7.10

At%), S (4.28 At%), and Cu (0.25 At%) (Figure 5.20). All metal peaks were clearly detected, as

evidenced by the low 'full width at half maximum' (FWHM) values reported in the table within Figure

5.20.
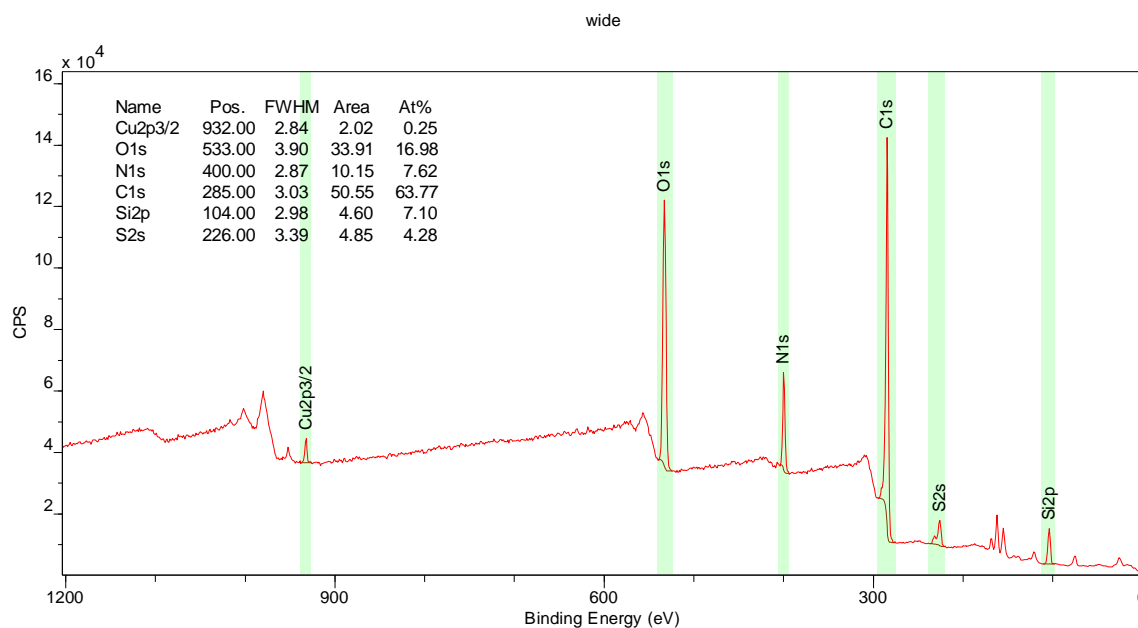
Figure 5.20. XPS survey scan for determination of elemental composition of Cu-loaded S914.

In addition to the full survey scan to determine bulk elemental composition (Figure 5.20), a more detailed scan of the Cu 2p environment was performed to investigate the speciation of Cu when loaded to S914. Figure 5.21 indicates a clear symmetrical peak at 932.82 eV, peaking at approximately 214 counts per second (CPS). A second, less well-defined, peak was also observed in the region of 952.5 eV, with a magnitude of 166 CPS. While the emission baseline appeared noisy during the Cu 2p scan, this is a direct result of the relatively low At% of Cu in the Cu-loaded resin sample (Figure 5.20).
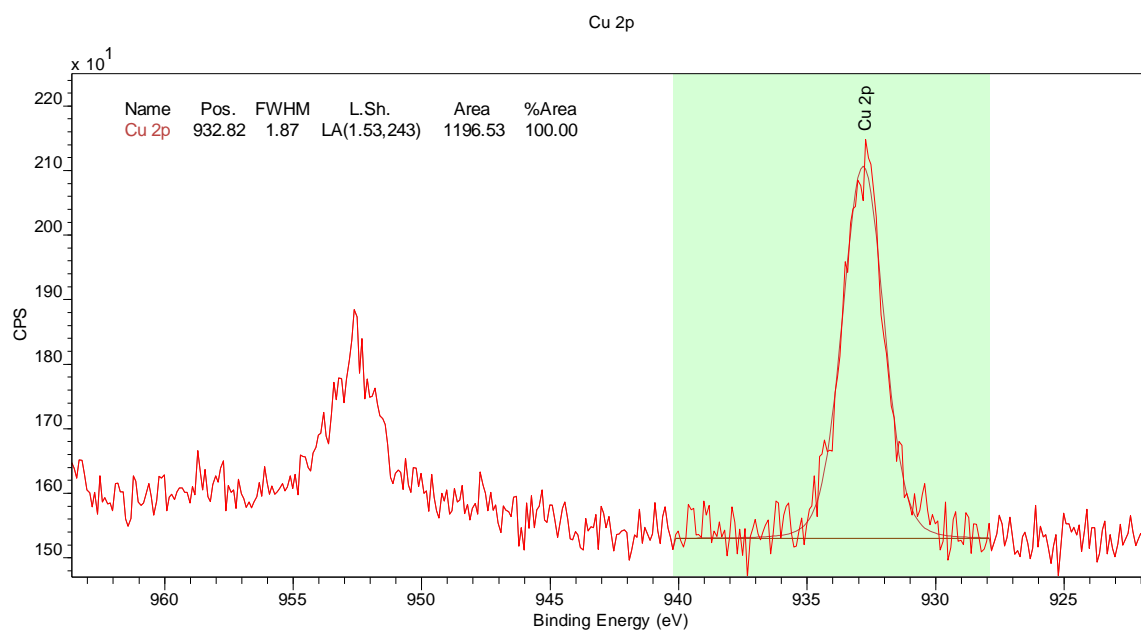
Figure 5.21. XPS Cu 2p scan for Cu-loaded S914.

5.3.10. Inter-resin Comparisons

Comparison of metal extraction profiles is crucial for determining the selectivity and potential

applications of specific resin functionalities. However, through comparison of how different resin

functionalities perform for a fixed metal, it is possible to observe how general similarities and

differences in functionality structure translate to differences in performance. The data from pH

screening experiments was replotted to produce Figure 5.22. In general, the extractive performance

of most resins suffered as a function of increased acidity. While similarities between resin

performance were not always distinct, several 'groupings' were observed between different

functionalities for specific metals. Of particular note, it tended to be the case that M31 and S957

performed quite similarly, and especially for Al, Ni, and Zn extraction. This is presumed to be related

to the shared presence of strongly-polar sulfonic acid functional groups in both resins (Figure 4.1),

which is also the likely reason behind the higher resilience of these resins to increased acidity, as

evidenced by the higher extraction efficiencies of most metals by these resins when compared to

other functionalities (Figure 5.22). Though typically less-well defined, S930 and S950 shared some

characteristics in terms of metal extraction performance, especially for Ni, which was likely due to the shared predominance of hydroxyl groups within functionality structure (Figure 4.1).
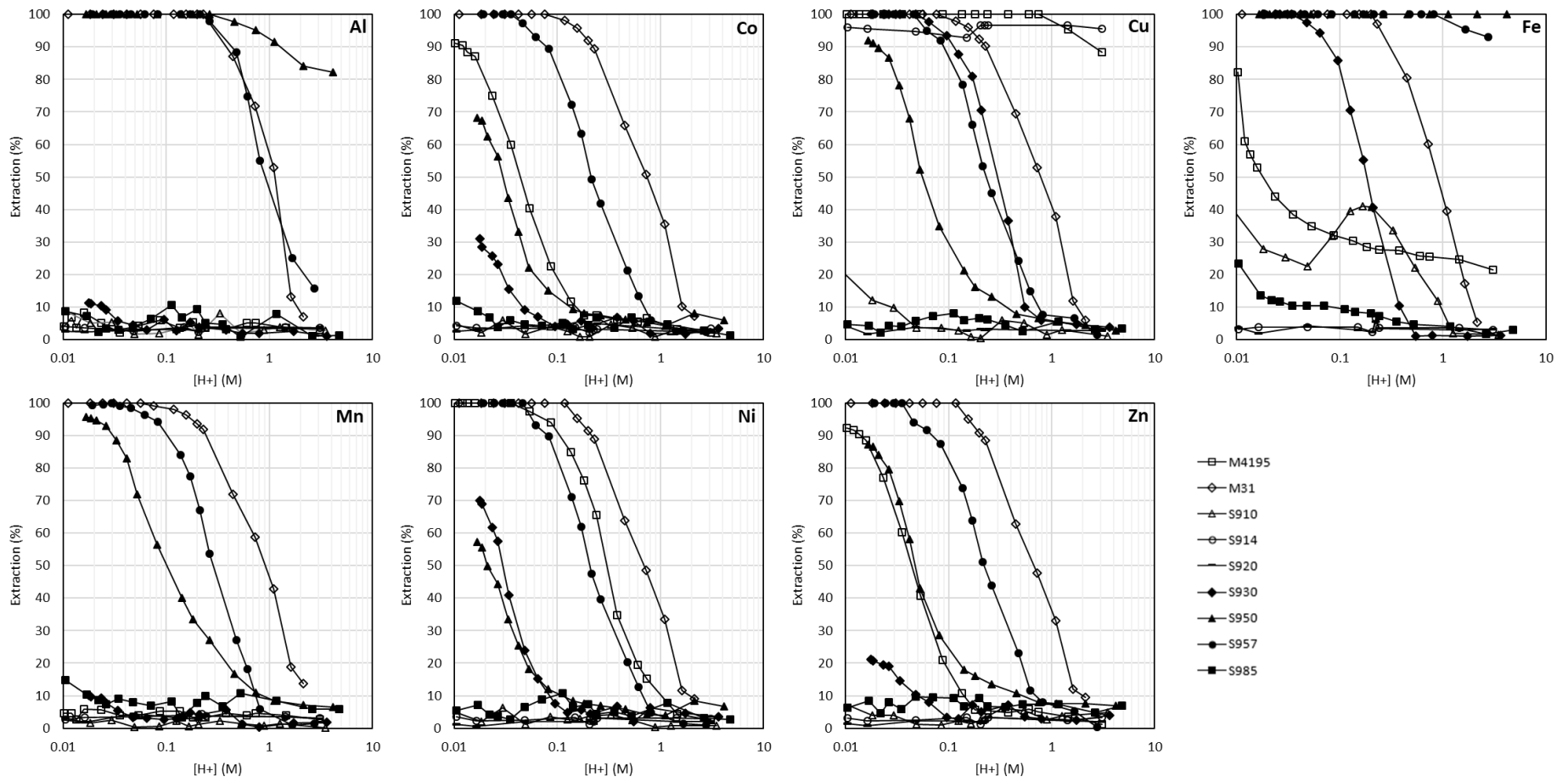
Figure 5.22. Inter-resin comparison of metal extraction efficiency (%). Data from pH screening experiments.

5.4 CHAPTER DISCUSSION

5.4.1 Dowex M4195

Dowex M4195 is a weak base chelating resin with bispicolylamine functionality which showed high

extraction efficiencies of transition metals in sulfuric acid, particularly for Cu and Ni, with good Co

extraction also (Figure 5.1). This observation conforms with previously published studies where

M4195 has been characterised by effective Cu, Co and Ni extraction from highly acidic media, with

maximal sorption capacity towards Cu (Kołodyńska, et al., 2014; Green & Hancock, 1982). The pH

dependent removal of Co, Ni, Zn, and Mn have been detailed previously for M4195 from hydrochloric

acid media (Diniz, et al., 2002), where very similar extraction trends were observed in regions where

pH range overlapped. Therefore, it can be also determined that changing from HCl to H_2SO_4 media

does little to change the extraction trends for M4195. The low extraction of Al and Mn across the

studied pH range has also been observed elsewhere for this resin (Kołodyńska, et al., 2014), and has

spurred investigations into the use of this resin to separate contaminant metals away from Mn in ore

leachates during battery production (Diniz, et al., 2005).

Increased proton concentration in solution had a detrimental effect on the extraction efficiency of all

metals, with adverse effects becoming apparent for Cu, Ni, and Co/Zn beyond 0.7 M, 0.04 M, and

0.02 M SO_4^{2-}, respectively. This behaviour is not uncommon for chelating resins and in this instance,

the weakly basic nature of bispicolylamine functional group leads to strong competition between

metal ions and H^+ ions and reduced extraction in highly acidic conditions (Sengupta, et al., 1991).

The addition of ammonium sulfate in solution had a slightly positive effect on the uptake of metals

by M4195 Figure 5.2, indicating that the most probable interaction mechanism is by chelation with

first row transition metals (Wołowicz & Hubicki, 2012), with exception of Fe. Considering the

speciation of Fe, which is most likely present as Fe^{2+} at the studied pH (Sanz, et al., 2003; Figure 11.1),

its interaction with M4195 is likely through an anion exchange mechanism. Based on Figure 5.1 and

Figure 5.2, M4195 appears to be a suitable candidate for targeted removal of Co, Ni, Cu and Zn, and some Fe away from Mn and Al in the simulant tailings leachate.

5.4.2   Puromet MTS9850

It is apparent that the anion exchange resin S985 was not well suited to extraction of metals from the acidic, sulfate-rich PLS, as evidenced by low extraction percentages in Figure 5.3. The performance of S985 in sulfate media is uncommon in the published literature, however, in chloride and mixed chloride-sulfate media, high affinity towards Ni was observed alongside Pt and Rh (Kononova, et al., 2013), and high Cu extraction away from Zn (Kononova, et al., 2014). Given that the mixed metal experiments performed by Kononova, et al. (2013) were performed at 0.01 M acid (H_2SO_4 and HCl at 1:1 ratio), it is possible that slight inaccuracies in experimental techniques meant that Ni extraction would be comparable at a slightly higher pH (note that extraction begins to increase towards the left-hand side of Figure 5.3). However, given the performance of S985 in this study in this pH range, S985 is of little value towards selective metal extraction. It has been suggested elsewhere for polyamine-functionalised resins, extraction needs to be performed in a more non-polar medium such as mixed aqueous methanol or dimethyl sulfoxide (Bukowska, et al., 2015).

5.4.3   Puromet MTS9100

The extraction of metal ions by S910 from sulfuric acid media (Figure 5.4) indicated poor performance for targeted metal recovery from the solutions tested. Under highly acidic conditions, the resin was more selective for Fe than the other metal species present. The noted change in extraction behaviour is most likely attributed to the hydrolysis of the anionic ferric sulfate species in solution under these conditions (Casas, et al., 2005), which was also confirmed during speciation modelling (Appendix Figure 11.1), where $FeHSO_4$ became the predominant Fe species (40-80% relative activity between 0.1-1M H^+). Despite Fe being the dominant metal removed by S910 in

70

Figure 5.4, previous literature has focussed on the application of amidoxime functionalised resins for the removal of Cu from waste water streams (e.g. Dąbrowski, et al., 2004; Shaaban et al., 2104; Taimur, et al., 2017), for which it has proved useful in single-metal, binary, and ternary mixtures. The reduction in metal uptake by amidoxime functional groups below pH 3 has been attributed to increased competition for active sites by H^+ ions, reducing the chelating ability of the resin (Loureiro & Rodrigues, 1998). If it is assumed that loss of chelation ability at low pH is responsible for a reduction in metal uptake, the extraction of Fe by ion exchange with anionic ferric sulfate species could be responsible for the pattern observed.

5.4.4   Puromet MTS9501

The aminophosphonic acid functionalised resin, S950, exhibited very high tendency towards Fe extraction across the entire studied range of acid concentration (Figure 5.5). While this resin is generally used industrially for copper and zinc removal from cobalt electrowinning circuit solutions, the strong attraction towards ferric ions in acidic conditions has been previously reported for this resin (Sofińska-Chmiel & Kołodyńska, 2016; Van Deventer, 2011). With the exception of Fe and Al, metal extraction efficiency was greatly hindered by increased acidity, with extraction falling below 10% beyond 1 M H^+. The low extraction of metals by S950 under highly acidic conditions is attributed to increased competition for active sites by H^+ ions in solution, resulting in partial or complete dissociation of the aminophosphonic groups (Outola, et al., 2001). The effective removal of Zn and Cu, observed at 0.01-0.02 M H^+ in Figure 5.5, and the reduction in performance of aminophosphonic acid resins at low pH was also noted by Dąbrowski, et al. (2004).

The effect of increased sulfate concentration in the PLS was investigated for S950 through addition of ammonium sulfate. With exception of Fe and Al, as noted previously, the uptake of all other metal ions by S950 was suppressed as sulfate concentrations increased. It is suggested that the formation of anionic metal sulfate complexes, incompatible with cation exchange mechanisms, is responsible

for the reduced extraction. Beyond 2 M sulfate, the extraction of Cu, Mn, and Zn begins to increase.

Given that these metals are likely in the form of anionic complexes at this point, removal by true ion

exchange is unlikely, suggesting an alternative removal process under these conditions.

5.4.5   Puromet MTS9301

Puromet MTS9301 (S930) exhibited a high selectivity towards Fe and Cu at lower acidities (100%

extraction until 0.03 and 0.05 M H$^+$, respectively), with appreciable Ni extraction alongside

(approximately 70% extraction) (Figure 5.8). As for S950, also a weak acid functionalised resin, the

role of proton competition as a limiting factor for metal extraction became apparent, which for S930

resulted in negligible extraction beyond 1 M H$^+$. Considering Cu and Ni, the extraction efficiency

curves are in agreeance with those reported by Kuz'min & Kuz'min (2014), where diminished

performance of S930 was associated with decreased pH, albeit with marginally better performance in

Figure 5.8 for Ni.

Figure 5.10 displayed results of increased PLS sulfate concentration on metal extraction by S930. As

for the pH screening, Cu and Fe were quantitatively removed at almost all sulfate concentrations,

with Fe extraction becoming only slightly suppressed at the most extreme sulfate concentration (4 M

SO$_4^{2-}$). In contrast to S950 (Figure 5.7), which also had a weak acid functionality, extraction of metals

by S930 tended to increase with increased sulfate, particularly Co, Ni, and Zn. This trend is likely a

result of increased solution ionic strength, through addition of sulfate, increasing the strength of

chelate formation, as previously reported for iminodiacetic acid functionalised silica gels in

chromatographic studies for a range of divalent transition metals (Bashir & Paull, 2002). This

phenomenon was also observed during column operation of an iminodiacetic acid resin, where

higher retention of divalent metals by Chelex 100 correlated with increased ionic strengths (Luttrell

Jr, et al., 1971).

5.4.6   Puromet MTS9570 and Dowex M31

Given the close similarities between the functionality of M31 (sulfonic acid) and S957 (bifunctional sulfonic and phosphonic acid), the joint discussion of their behaviours is appropriate. As seen from Figure 5.11 and Figure 5.14, both strong acid resins (S957 and M31) display little selectivity at higher pH. However, S957 is shown to preferentially extract trivalent metal cations below pH 1 while all metal uptake by M31 is suppressed. Similar results were found in previous literature (Chiarizia, et al., 1993) where trivalent metal cations were found to be preferentially extracted at very high acidities by Diphonix, a resin with sulfonic and gem-diphosphonic acid functional groups, in nitric acid media. The loss of selectivity at higher proton concentrations for sulfonic acid functional groups was also observed for another sulfonic acid resin, Bio-Rad AG MP-50, in alignment with observations made in Figure 5.14.

Suppression of metal uptake at higher ionic strengths by M31 (Figure 5.16) indicates a cation exchange mechanism for metal extraction. The same can be said for S957 regarding divalent metal cations, however the negligible effect of increased ionic strength on trivalent cation extraction suggests the phosphonic acid functionality has a chelating interaction with Al and Fe but does not interact strongly with the divalent cations in solution. The synthesis and use of bifunctional sulfonic-phosphonic acid resins such as S957 was introduced to improve both the selectivity and kinetics of metal ion extraction using strong acid resins (Alexandratos & Natesan, 1999). Dowex M31 has little potential regarding selective metal extraction from mine waters and wastes but has potential for bulk ion removal. The lack of selectivity by S957 also rules out this resin for specific ion removal, but results indicate potential for it to be used as a 'scrubbing' column at the tail end of a coupled-column system to remove remaining ions after selective metal removal by previous columns.

5.4.7   Puromet MTS9140

At the time of writing there has been only one published study of Puromet MTS9140 resin (including its previous name of Purolite S914), which focused only on Pt, Pd, and Rh (Abdulbur-Alfakhoury, et al., 2019). As such, interpretation of the results presented must be done with comparison to alternative thiourea-functionalised resins, and to interactions between thiourea solutions and copper. Puromet MTS9140 showed high affinity towards Cu ions, with extraction of this metal exceeding 92% under all conditions of pH (Figure 5.18), whilst co-extraction of other metals was limited (< 10%). The high capacity for Cu also remained unaffected with increased sulfate concentration, with extraction over 95% at all sample points (Figure 5.19). To assist with understanding the Cu extraction behaviour exhibited by S914, a Cu-loaded resin sample was analysed by XPS.

XPS analysis of the Cu-loaded S914 resin indicated that 63.77% of atomic mass was accounted for by C (Figure 5.20), which is not surprising given the polystyrene-divinylbenzene backbone of the resin. Nitrogen accounted for 7.62 At% of the resin composition, and with a binding energy of 400 eV is consistent with nitrogen within an organic matrix, i.e. the thiourea group within the resin matrix (Figure 4.1). While the presence of N was expected given the functionality of the resin, the high Si and O concentrations (7.10 and 16.96 At%, respectively) were unexpected. The binding energy of the Si 2p and O 1s peaks in Figure 5.20 were consistent with Si being present as silica (SiO_2), yet the percentage composition of oxygen indicates that silica was not the only oxygen source present in the sample. Close examination of the S 2s peak revealed two components; a peak consistent with thiourea (75% of S detected), and a smaller peak (25% of S) attributed to the presence of sulfate.

Considering that the resin was loaded with excess Cu in solution, the Cu surface concentration was relatively small (0.25 At%, Figure 5.20). This was likely due to a diluting effect of the bulk resin matrix, which is likely to highly overshadow functional group prevalence, meaning that the photoelectrons

emitted from Cu atoms originated too deep within the sample to escape without further collision and were less-well detected.

A more detailed scan of the Cu environment was provided in Figure 5.21. The lack of Cu satellite peaks in the 940-945 eV region eliminates the possibility for Cu(II) being present within the S914 matrix (ThermoScientific, 2019). The binding energy for the Cu 2p peak (932.82 eV, Figure 5.21) is consistent with either Cu metal or Cu(I) (933 eV for both species). The occurrence of a secondary peak, occuring in Figure 5.21 at 952.5 eV, and absence of satellite peaks is typical of Cu being present as either Cu metal or Cu(I) (Hayez, et al., 2004).

For Cu to be present on the resin surface as Cu(I), it follows that the Cu(II) present in solution must undergo reduction, with the functional group of the resin in turn being oxidised. Such redox behaviour between Cu(II) and solutions of thiourea has been previously observed (Krzewska, et al., 1980), whereby Cu(II) is immediately bonded with thiourea which is quickly oxidised by Cu(II) ions. The resulting Cu(I) ion produced as a result of this redox reaction is then complexed by thiourea to form a stable Cu(I)-thiourea complex, the form of which may involve one, two, or three thiourea ligands (Gaur, et al., 2013). Given the reported interactions of Cu(II) ions with thiourea ligands in solutions, and given that Cu metal would be expected to give a sharper and more asymmetric peak than observed in Figure 5.21 (e.g. Biesinger, et al., 2010), it is suggested that S914 removes Cu from solution through reduction to cuprous Cu(I). With Cu(I) being the only stable monocationic species formed by first-row transition metals, which is likely the reason that only Cu was extracted to a significant degree during screening studies.

5.5 CHAPTER CONCLUSIONS

Based on the results presented, several conclusions can be drawn regarding the selection of resins for water treatment through selective removal of first-row transition metals.

1. Importantly, it became apparent that Puromet MTS9140 was a very valuable resin to take forward for further investigation, given that this was the only resin studied which extracted just one metal species from the PLS (Figure 5.18). The selective removal of Cu from a mixed-metal waste stream is particularly important given that Cu was highly extracted also by M4195 (Figure 5.1), S930 (Figure 5.8), and M31 (Figure 5.14). Removing Cu from the waste stream before contact with subsequent resins would liberate a larger proportion of their capacity towards extraction of other, potentially more toxic and/or valuable, metals; resulting in a more efficient use of resin material.

2. Strong acid resins M31 and S957 were not appropriate for targeted metal recovery (Figure 5.11 and Figure 5.14), instead being more suited towards bulk metal recovery; potentially acting as a scrubbing column following the selective extraction columns to limit metal release to output waters.

3. Complete extraction of Fe by S950 was observed under all studied conditions, with only minor suppression of Al occurring beyond 0.3 M H^+ (Figure 5.5). When compared to extraction by S930 (Figure 5.8), it is evident that out-competition by Fe and Al pose a greater barrier to trace metal removal for S950, where selectivity towards Fe and Al reduces removal capacity for other, potentially more toxic, metals present. The difference in behaviour between the two weak acid resins under different sulfate concentrations could be used advantageously in an engineered process. By applying aminophosphonic acid functionalised resins where sulfate concentrations are low, and iminodiacetic acid resins where ionic strength may be a limiting factor, the removal of metals could be maximised in a range of conditions.

4. Puromet MTS985 and MTS9200 were not suitable for extracting the metals of interest in the studied leachate simulant, given the low extraction efficiencies reported in Figure 5.3 and Figure 5.17, respectively.

Based upon the pH and sulfate-dependent behaviour of the screened resins presented in this Chapter, it was possible to eliminate those with poor or undesirable performance and in doing so, select resins for further investigation by fixed-bed methods to determine operational capacities and gain an understanding of how the resins perform under non-equilibrium conditions. The resins selected for further investigation and the main reason for inclusion are as follows; 1) Dowex M4195 for Cu, Co, Ni, and Zn removal, 2) Puromet MTS9140 for selective Cu removal, 3) Puromet MTS9301 for Fe and Cu extraction and high performance with increased sulfate, 4) Puromet MTS9501 for Fe, Al, and Mn selectivity, and 5) Puromet MTS9570 for Fe selectivity and potential for bulk metal adsorption.

6 FIXED-BED ADSORPTION STUDIES[2]

6.1 CHAPTER INTRODUCTION

Batch experiments are of great value for determining resin selectivity and screening resin suitability. However, to engineer a continuous treatment process requires an understanding of adsorption behaviours under dynamic conditions; in this instance through use of fixed-bed adsorption columns. Contrary to batch experiments, where the adsorbent-solution system is left to reach equilibrium, the continuous displacement of forward reaction products in a fixed-bed column results in a system in disequilibrium (Harland, 1994). Therefore, it is not uncommon that a switch towards a dynamic set-up can alter the behaviour of functional groups towards target ions. The point at which metal ions begin to appear in effluent solutions is a critical design parameter for a treatment system and can be determined through the use of breakthrough experiments. Further to this, dynamic column operation allows exploration of the effects of flow rate on resin selectivity and determination of column operating capacities; crucial parameters for determining the rate at which solutions must be pumped, and ultimately the time required for effective waste treatment.

Given that the premise for this research is to progress to a coupled-column system, where the effluent of one column feeds directly to the inlet of the subsequent column, it was important to observe the extent to which metal ions were displaced from columns by ions with higher affinity to the adsorbent. Termed 'overshoot', this portion of the breakthrough curve, where C_t/C_o exceeds 1, is rarely studied in the ion exchange literature. Despite this, the overshoot of metals from columns is an important factor for consideration in this case given that it represents a momentary spike in pre-

---

[2] This chapter was in part published in the proceedings of *Copper Cobalt Africa 9th Southern African Base Metals Conference*, hosted by the Southern African Institute of Mining and Metallurgy in Livingstone, Zambia, July 2018.

concentrated metal ions to the following column which will progressively alter solution chemistry throughout the system.

Guided by the batch screening studies presented in Chapter 5, this chapter presents the results of dynamic breakthrough experiments and associated breakthrough modelling to assess the most-suitable resins for metal removal from a complex multi-metal synthetic waste stream. In Chapter 5, it was determined that resins with chelating groups were most appropriate for selective metal recovery, for example the selectivity towards Fe and Cu extraction exhibited by S930, the Cu and Ni extraction by M4195, and the high selectivity towards Cu exhibited by S914. It was also observed that the majority of resins were most effective in the $0.01 - 0.03$ M H^+ range, and so these optimal conditions will be used during the dynamic screening process.

Previously published works on ion exchange breakthrough tend to use single-metal solutions, with studies focussing on competitive adsorption being rare. Where published, the multiple-component systems tend to be binary solutions (e.g. Barros, et al., 2003; Escudero, et al., 2013; Shi, et al., 2018), and very occasionally ternary solutions (e.g. Barros, et al., 2006). As such, this Chapter will provide insight to competitive adsorption of metals from a complex multi-component solution under dynamic column operation. Further to this, loading flow rate will be adjusted to explore the effect that this has on the resulting breakthrough profiles and to provide insight to the most effective loading conditions to use to achieve optimum extraction.

6.2   SPECIFIC METHODS

6.2.1   Column experiments and sampling

Small-scale columns were completely packed with ion exchange resin and double-capped at either end with Teflon frits, resulting in a total BV of 5 mL wet settled resin. Columns were intermittently agitated during the packing process to temporarily fluidise the bed and promote homogeneous

distribution of resin particle size throughout the column. To ensure efficient mass transfer between solution and resin, and to reduce the risk of 'channelling' (Harland, 1994) a reverse-flow setup was employed, whereby the PLS was introduced at the bottom of the vertical column and pumped against gravity. In each experiment, the pH of PLS were adjusted to match the optimum sorption conditions identified in Chapter 5. For the two higher solution flow rates (10 BV/h, 5 BV/h), a Heidolph Hei-Flow Value 01 peristaltic pump with Heidolph SP Quick pump head was used, and for the lowest flow rate (2 BV/h), a Watson Marlow 120S peristaltic pump was used due to its more consistent performance at low revolutions per minute (RPM).

Prior to experimentation, pump flow rates were calibrated by measuring the mass of deionised water passed through a packed column over time to allow conversion of pump RPM to the equivalent flow rate in BV/h. While relative flow rates were fixed at 10, 5, and 2 BV/h, differences in the physical properties of each resin (e.g. particle size) affect the superficial velocity of the PLS as it flows through the packed bed, and so these were derived through application of the Ergun equation (Equation 6.1) using a computational tool provided by CheCalc (2019). Input data was a combination of manufacturer-specified properties of resins and measured column geometries.

Equation 6.1. Ergun equation, where ΔP = pressure drop (bar), L = height of bed (m), μf = fluid viscosity (cP), V = superficial velocity (m/s), ε = bed porosity (mm), Dp = resin particle size (mm), and Pf = fluid density (kg/m3).

$$\frac{\Delta P}{L} = 150 \left(\frac{\mu_f V (1-\varepsilon)^2}{D_p{}^2 \varepsilon^3} \right) + 1.75 \left(\frac{P_f V^2 (1-\varepsilon)}{D_p \varepsilon^3} \right)$$

A Bio-Rad Model 2110 fraction collector was used to collect samples from the column outlet prior to elemental analysis. Samples of influent and effluent solutions were collected and diluted using 1% HNO_3 prior to elemental analysis by ICP-OES (10 BV/h data) or AAS (5 BV/h and 2 BV/h data). Due to analytical limitations, data for Al concentration was only available for 10 BV/h flow rates where ICP-

OES was used. Given that effective Al analysis by AAS can only be achieved using a nitrous-oxygen flame (Perkin-Elmer, 1996), which was not accessible, Al concentrations would not be measurable at the lower flow rates. For continuity, Al was omitted from PLS solutions for 5 and 2 BV/h experiments (unless stated otherwise), and from that point onwards in all experimentation.

6.2.2   Breakthrough modelling

Concentration ratios (C_t/C_o) were calculated by dividing the effluent concentration at each time interval (C_t) by the initial PLS concentration and plotted against bed volumes of solution pumped through the column (BV). The resulting plots, termed *breakthrough curves*, were analysed using multiple breakthrough models commonly applied to ion exchange data; the modified dose-response (MDR), Bohart-Adams, Thomas, and Yoon-Nelson models. Important to note is that the models presented were not necessarily intended to describe a solid-liquid ion exchange extraction process when they were developed, and as such the calculated values may not accurately describe experimental reality (Amphlett, et al., 2018). However, given the widespread use of such models in the field, this remains the only way to consistently compare new experimental data with existing literature, and so this approach is justified.

Model fitting was performed for individual metal breakthrough in Excel using the SOLVER plugin for minimising the sum of squared errors (SSE) via a generalised reduced gradient (GRG) model. The application of a GRG model allowed local minima of SSE to be identified using the nonlinear forms of breakthrough models. It has been suggested that polynomial regression allows a better fit to be produced when compared its linear counterpart (Dytham, 2011), hence increasing the accuracy of model fits.

The MDR model is perhaps the most commonly applied breakthrough model in the literature, and is especially used to predict breakthrough behaviour at lower or higher time periods of the breakthrough curve (Dardouri & Sghaier, 2017). Its form is given in Equation 6.2 (Yan, et al., 2001),

where F_t is the cumulative flow-through (L) at a given time, and *a* and *b* are derived model constants.

From evaluating the MDR model, the maximum column loading capacity for each metal (Q_o) can be

calculated using Equation 6.3, where *m* is the mass of resin used (g).

Equation 6.2. Modified Dose Response model.

$$\frac{C_t}{C_o} = 1 - \frac{1}{1 + \left(\frac{F_t}{b}\right)^a}$$

Equation 6.3. Calculation of Q_o from MDR constant *b*.

$$Q_o = \frac{b \, C_o}{m}$$

The Bohart-Adams model is given in Equation 6.4, where the rate of adsorption is dependent on both

the concentration of sorbing species in solution, and on the remaining capacity of the adsorbent.

Assumptions are made that axial flow, the back-mixing and diffusion of solutions in the longitudinal

direction of flow, is non-existent (Chu, 2010). While originally developed for describing a gas-charcoal

adsorption system (Bohart & Adams, 1920; Hamdaoui, 2009), the model can also be applied to a

solid phase extraction system from a solution phase. In Equation 6.4, K_a is the Bohart Adams

adsorption rate constant (L mg^{-1} min^{-1}), *W* is the column adsorption capacity (mg/g), and *F* represents

the volumetric flow rate (L/hour).

Equation 6.4. Bohart-Adams model

$$\frac{C_t}{C_o} = \left(\frac{e^{K_a C_o t}}{e^{K_a C_o t} + e^{K_a \left(\frac{W}{F}\right)} - 1}\right)$$

The Thomas model (Equation 6.5, where K_t is the model constant (L min^{-1} mg$^{=1}$) is also commonly applied to ion exchange breakthrough data and was originally developed to describe adsorption to a zeolite bed (Thomas, 1944). Several assumptions are made in this model. For instance, the effects of axial dispersion are ignored (Chu, 2010), as was the case for the Bohart-Adams model. Furthermore, it is assumed that adsorption of ions follows Langmuir isotherm principles of monolayer adsorption and pseudo second order rate kinetics, that is, where the physicochemical interactions between the resin and solution phases are assumed to be rate-limiting (Robati, 2013). Therefore, a high goodness-of-fit to this model would indicate that uptake is governed by mass transfer at the resin-solution interface (Calero, et al., 2009).

Equation 6.5. Thomas model.

$$\frac{C_t}{C_o} = \frac{1}{1 + e^{\left(\frac{K_t Q_o m}{F} - K_t C_o t\right)}}$$

The final model fitted to breakthrough data is the Yoon-Nelson model, originally developed for describing the adsorption of gases to solid adsorbents, and is presented in Equation 6.6 where K_{yn} is the model constant (min^{-1}), and t_{50} is the predicted time for 50% breakthrough to be achieved. Despite not requiring input parameters based on adsorbent characteristics, and as a result not providing direct mechanistic information related to adsorption (Xu, et al., 2013), the column half-life parameter, t_{50}, is highly valued for understanding effective column operating times in engineered processes.

Equation 6.6. Yoon Nelson model.

$$\frac{C_t}{C_o} = \frac{1}{1 + e^{K_{yn}(t_{50} - t)}}$$

Equilibrium concentration data from batch contacts performed at the same pH as the breakthrough experiments presented here were used to calculate equilibrium constants for each metal and resin, using Equation 6.7, where K_{eq} is the equilibrium constant, C_o is the pre-contact PLS metal concentration, and C_{eq} is the solution metal concentration at equilibrium. Computed values are presented in Table 6.1. While fixed-bed operation does not reach equilibrium, these constants can be used to provide insight to the dynamic uptake reported in this chapter.

Equation 6.7. Calculation of equilibrium constant, K_{eq}. C_o = solution metal concentration before resin contact, C_{eq} = solution metal concentration at equilibrium.

$$K_{eq} = \left(\frac{(C_o - C_{eq})}{C_{eq}} \right)$$

Table 6.1. Computed equilibrium constant (K_{eq}) values for metals under the pH conditions used in breakthrough studies. NA = Calculation not possible due to 100% extraction.

	M4195	S930	S957	S950	S914
Al	0.022	0.062	NA	NA	0.039
Co	1.493	0.183	34.29	0.498	0.038
Cu	NA	NA	NA	2.121	21.10
Fe	0.623	NA	NA	NA	0.039
Mn	0.041	0.058	64.83	4.830	0.034
Ni	NA	0.691	NA	0.339	0.024
Zn	1.515	0.172	15.84	1.385	0.023

6.2.3. Criteria for Resin Progression

As for in Chapter 5, where batch experimental techniques were used to select the most suitable resins for study using fixed-bed techniques, the results presented here are used to identify those resins which are to be used in the final system design. As such, the criteria used for making this selection is provided in Table 6.2 alongside explanations of the importance of each on system scale

up and operation. While the influence of flow rate on capacity was investigated, this was done to find

optimum loading conditions rather than to screen out candidate resins.

Table 6.2. Criteria for resin progression/elimination following completion of breakthrough studies, and related influence on process scale-up and operation.

Characteristic	Importance for System Design	Assessment
Breakthrough point	The point at which breakthrough occurs (e.g. C_t/C_o = 0.1) directly relates to the volume of solution able to be treated before the column requires regeneration, and is crucial for determining operating regimes/timings.	The breakthrough points of 'target' metals (i.e. those for which the resin was selected for in Chapter 5) must occur beyond those of other species.

Breakthrough profiles for all metals (up to C_t/C_o = 1) should follow the standard sigmoidal shape to ensure reliable modelling of capacity can be achieved.

Overshoot of non-target metals should occur, allowing concentration of only the target metal(s) within the column. |
| Operating capacity | A high dynamic operating capacity allows for more metal to be adsorbed per column, and so directly affects the mass of resin (and therefore cost) required to achieve sufficient treatment. | Operating capacity towards target metals should be notably higher than towards non-target metals to ensure preferential extraction is maintained under dynamic operation.

Capacities should be comparable to those observed for the same resins (or similar resins) in existing literature. |

6.3   RESULTS

6.3.1   Dowex M4195

The breakthrough of metals from the M4195-packed column at 10 BV/h is presented in Figure 6.1.

Little interaction with Mn, Fe, and Al ions was evidenced by the relatively low retention of these ions

within the column, with complete breakthrough (C_t/C_o = 1) reached after 5 and 6 BV for Mn/Al and

Fe, respectively. Modified Dose Response (MDR) modelling of metal breakthrough (Table 6.3)

revealed an operational column loading capacity (Q_o) for Mn, Al, and Fe of 1.54, 1.84, and 1.64 mg/g, respectively, confirming low adsorption of these metals by M4195.

Suppressed breakthrough of Zn and Co indicated a higher affinity of these metals towards the bis-picolylamine functional group (Figure 6.1). The concentration ratio (C_t/C_o) of most metals in Figure 6.1 exceeded 1 shortly after reaching complete breakthrough; the reason for which being the increased loading of Ni and Cu to the column which displaced previously bound metal ions. For Zn and Co, the Thomas breakthrough model was able to achieve the highest goodness of fit, indicating operating capacities of 2.65 mg/g for Zn (R^2 = 0.964), and 4.59 mg/g for Co (R^2 = 0.982) (Table 6.3).

Ni breakthrough was low throughout the experiment, with a maximum C_t/C_o of 0.19 reached by 29 BV throughput, equating to a loading capacity of 17.28 mg/g Ni (Thomas model, R^2 = 0.978). Results of Yoon-Nelson modelling predicted a column half-life towards Ni of 256.7 minutes (Table 6.3), considerably longer than for other metals. Given that Cu concentration remained below limits of detection, it can be assumed that the highest selectivity exhibited by M4195 is towards Cu, resulting in its very low concentration in effluent solutions. Modelling of Cu adsorption was not possible due to the limited breakthrough observed.
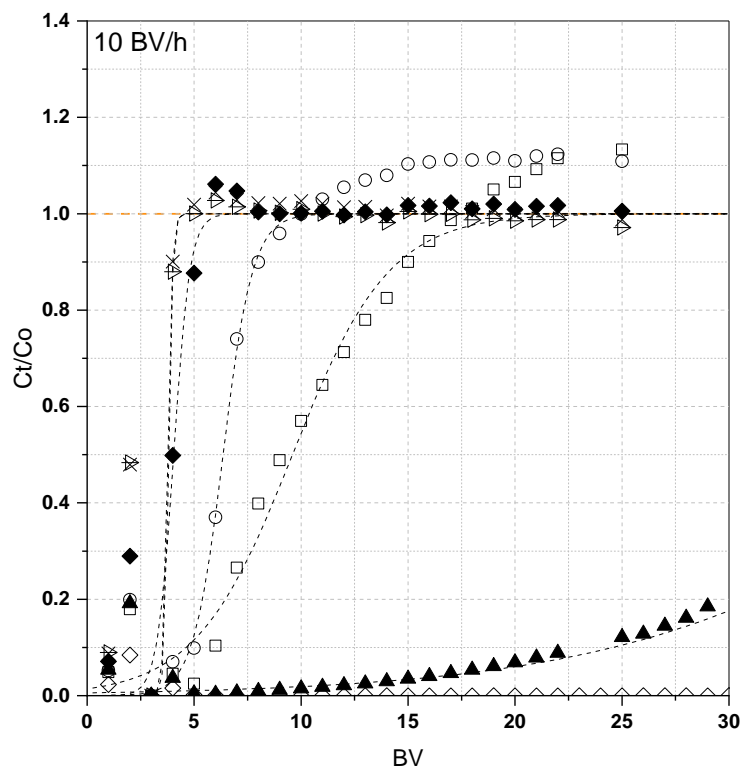
Figure 6.1 . Breakthrough curves of metals from PLS pumped through M4195 at 10 BV/h (1.8 x10^{-4} m/s) (pH 1.55). Al = ▷, Co = □, Cu = ◊, Fe = ◆ , Mn = ×, Ni = ▲ , Zn = ○. Dotted lines = best-fitting breakthrough model (see Table 6.3).

Table 6.3. Breakthrough model parameters for M4195 at 10 BV/hour flow rate.

	Modified Dose Response				Bohart-Adams			Thomas			Yoon-Nelson		
	a	b	Q_o	R^2	K_a	W	R^2	K_t	Q_o	R^2	K_{yn}	t_{50}	R^2
Al	35.75	19.3	1.84	*0.997*	0.45	4.42	*0.997*	0.4	1.84	*0.997*	NA	NA	*NA*
Co	4.63	47.04	3.99	*0.971*	0.02	9.97	*0.985*	0.02	4.59	*0.982*	0.07	57.54	*0.972*
Fe	11.29	20.51	1.64	*0.989*	0.14	3.94	*0.992*	0.14	1.64	*0.992*	0.40	24.23	*0.937*
Mn	45.39	19.43	1.54	*0.993*	0.51	3.64	*0.996*	0.51	1.52	*0.996*	NA	NA	*NA*
Ni	5.76	208.24	16.96	*0.964*	0.01	41.42	*0.978*	0.01	17.28	*0.978*	0.02	256.68	*0.984*
Zn	9.66	32.19	2.63	*0.955*	0.08	6.34	*0.964*	0.08	2.65	*0.964*	0.24	38.11	*0.967*

When solution flow rate was decreased to 5 BV/hour, a distinct sharpening of the breakthrough curves for Mn, Fe, Co, and Zn was observed when compared to those for at 10 BV/hour (Figure 6.2). Additionally, the 'overshoot', the displacement area where C_t/C_o exceeds 1, is more pronounced,

particularly for Co, Fe, and Zn, which reach maximum values of 1.2, 1.5, and 2.6, respectively (note

the y-axis break in Figure 6.2).
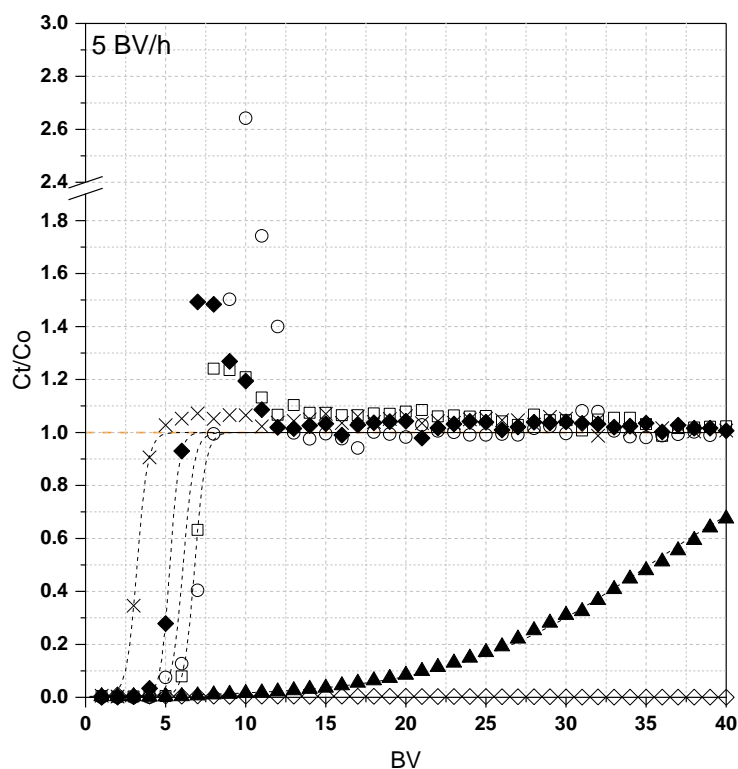
Figure 6.2. Breakthrough curves of metals from PLS pumped through M4195 at 5 BV/h (8.81 x10^{-5} m/s) (pH 1.55). Co = □, Cu = ◊, Fe = ◆, Mn = ×, Ni = ▲, Zn = ○. Dotted lines = best-fitting breakthrough model (see Table 6.4).

Table 6.4. Breakthrough model parameters for M4195 at 5 BV/hour flow rate.

	Modified Dose Response				Bohart-Adams			Thomas			Yoon-Nelson		
	a	b	Q_o	R^2	K_a	W	R^2	K_t	Q_o	R^2	K_{yn}	t_{50}	R^2
Co	19.46	34.04	4.21	*0.999*	0.07	7.65	*0.999*	0.07	3.19	*0.999*	0.25	82.11	*0.999*
Fe	75.65	25.31	3.13	*0.999*	0.10	4.67	*0.999*	0.10	1.95	*0.999*	0.29	63.46	*0.999*
Mn	68.56	15.14	1.67	*0.991*	0.09	2.74	*0.995*	0.09	1.14	*0.997*	NA	NA	*NA*
Ni	5.43	173.10	21.43	*0.990*	0.003	38.03	*0.997*	0.004	15.87	*0.997*	0.01	423.11	*0.996*
Zn	69.19	30.16	3.33	*0.973*	0.09	5.18	*0.979*	0.09	2.16	*0.980*	0.24	85.39	*0.980*

Despite being the first metal to reach breakthrough, negligible overshoot was observed for Mn, indicating that no interaction between Mn and the bispicolylamine functional groups occurred, and the resulting breakthrough curve was a gradual result of the PLS displacing interstitial water from within the column. While Cu concentration ratios remained minimal throughout the experiment, the breakthrough curve for Ni did exhibit a slightly sharper curve when flow rate was reduced to 5 BV/hour, reaching a maximum concentration ratio of 0.69. Comparisons at 30 BV throughput confirm a faster breakthrough at reduced flow rate (0.19 in Figure 6.1, 0.31 in Figure 6.2). Ni breakthrough was most adequately described by the Adams-Bohart and Thomas models (R^2 = 0.997), which predicted a column loading capacity of 15.87 mg/g Ni (Table 6.4). Given the assumptions of the Thomas model, the high goodness-of-fit for M4195 to this model suggested that the rates of adsorption of most metals were likely governed by mass transfer limitations (Calero, et al., 2009).

Reduction of solution flow rate further, to 2 BV/h, had a profound effect on the behaviour of Zn adsorption and displacement from the M4195-packed column. While Zn began to appear in effluent solutions at a similar point as during the 10 and 5 BV/hour experiments, the subsequent overshoot was much higher and sharper (Figure 6.3), reaching a maximum concentration ratio of 3.69 at 8 BV throughput. Considering the influent Zn concentration of 170.01 ppm, this maximum data point suggests a momentary concentration of 627.37 ppm in the effluent solution. Following maximum displacement, Zn concentration ratios quickly reduced and stabilised at approximately 1.25. The displacement of Fe also became more pronounced when flow rate was reduced to 2 BV/h and reached a maximum value of 1.99, equating to a concentration of 363.4 ppm, before returning to a C_t/C_o of approximately 1 (Figure 6.3).

The point at which Ni began to appear in effluent solutions was significantly delayed when running the PLS at the lowest flow rate, with 10 % breakthrough (C_t/C_o) not being surpassed until 32.5 BV at 2 BV/hour flow rate, compared to 22 and 24 BV for 5 and 10 BV/hour flow rates, respectively. Further to this, when comparing breakthrough at 30 BV (as done for 2 BV/h and 5 BV/h), Ni breakthrough

was considerably lower at 0.05, compared to 0.31 at 5 BV/h and 0.19 at 10 BV/h. Highest goodness-of-fit was achieved using the MDR model, which calculated an operational loading capacity of 28.50 mg/g for Ni at 2 BV/h (Table 6.5).
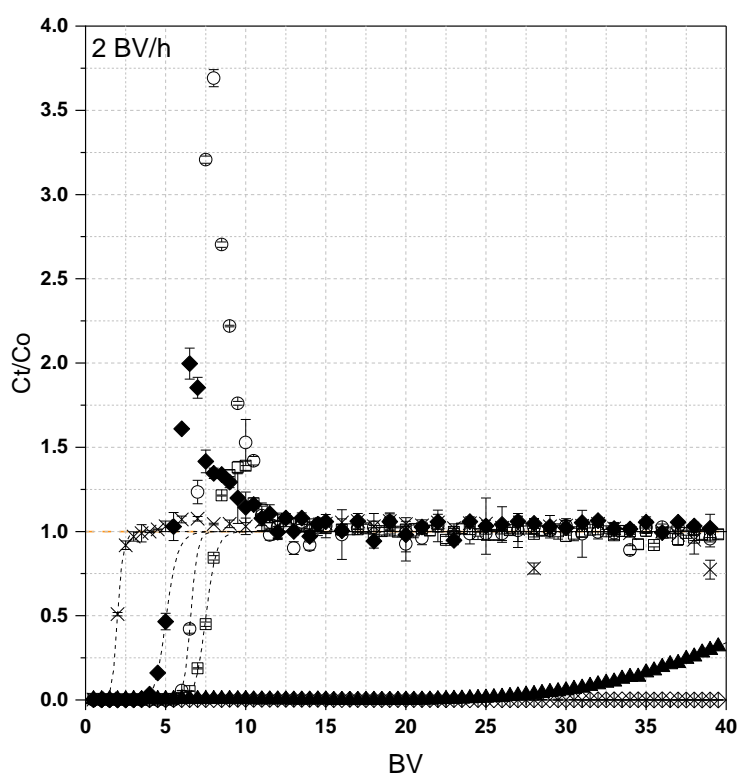
Figure 6.3. Breakthrough curves of metals from PLS pumped through M4195 at 2 BV/h (3.54 x10^{-5} m/s) (pH 1.55). Co = □, Cu = ◊, Fe = ◆, Mn = ×, Ni = ▲, Zn = ○. Dotted lines = best-fitting breakthrough model (see Table 6.5).

Table 6.5. Breakthrough model parameters for M4195 at 2 BV/hour flow rate.

	Modified Dose Response				Bohart-Adams			Thomas			Yoon-Nelson		
	a	b	Q_o	R^2	K_a	W	R^2	K_t	Q_o	R^2	K_{yn}	t_{50}	R^2
Co	23.17	37.58	4.78	*0.995*	0.03	7.18	*0.996*	0.03	4.79	*0.996*	0.10	225.97	*0.997*
Fe	14.37	25.24	3.07	*0.998*	0.03	4.61	*0.998*	0.03	3.07	*0.998*	0.17	149.82	*0.981*
Mn	14.37	25.24	3.04	*0.998*	0.07	1.81	*0.974*	0.07	1.21	*0.950*	NA	NA	*NA*
Ni	7.43	218.75	28.50	*0.998*	0.002	41.84	*0.996*	0.002	27.90	*0.996*	0.01	1284.97	*0.996*
Zn	31.55	32.83	3.72	*0.999*	0.06	5.56	*0.999*	0.06	3.72	*0.999*	NA	NA	*NA*

6.3.2   Puromet MTS9301

During loading of the S930-packed column at 10 BV/h (Figure 6.4), the only metal to reach complete

breakthrough was Zn, which exceeded C_t/C_o after 7 BV of solution was pumped through the column.

Adsorption of other metals in solution exhibited the typical sigmoidal breakthrough curve shape, yet

concentration ratios remained below 1. This suggested that multiple metals were bound to the resin

upon termination of the experiment. Beyond 20 BV throughput, an increase in concentration ratio

was observed for all metals, which for Zn resulted in a slight period of displacement; likely a result of

the steadily increasing Cu loading. It is expected that as Cu loading increases, the bound metals

would be displaced in the order of Ni > Co > Mn > Fe, according to the concentration ratios at 27 BV

throughput. Given that concentration ratios for most metals plateaued below 1, model R^2 values

were generally low and not able to satisfactorily describe metal loading. However, for Cu the MDR

model had the highest goodness-of-fit and indicated a column loading capacity of 34.89 mg/g (R^2 =

0.997, Table 6.6).
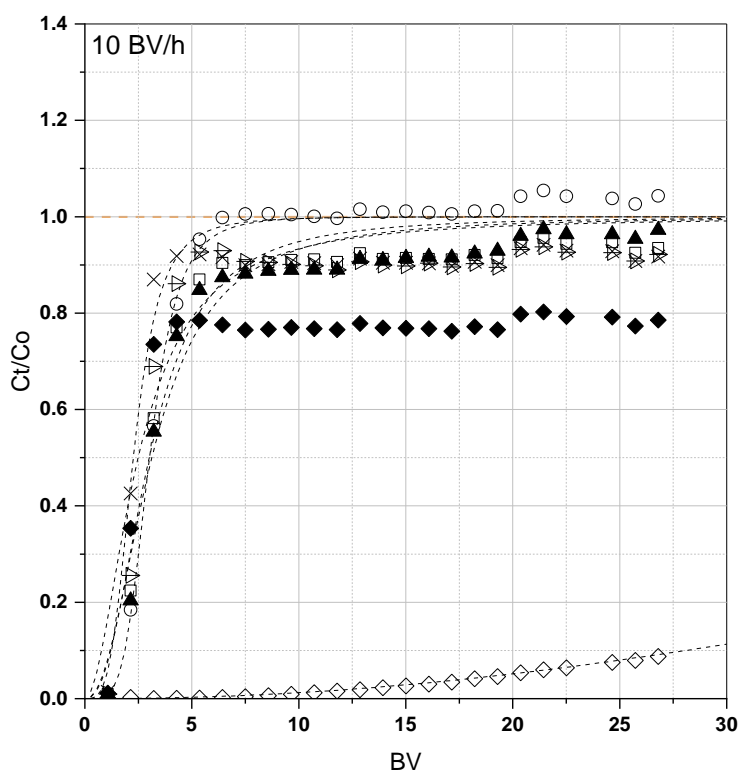
Figure 6.4. Breakthrough curves of metals from PLS pumped through S930 at 10 BV/h (1.9 x10^{-4} m/s) (pH 1.45).

Al = ▷, Co = □, Cu = ◊, Fe = ◆ , Mn = ×, Ni = ▲ , Zn = ○. Dotted lines = best-fitting breakthrough model (see

Table 6.6).

Table 6.6. Breakthrough model parameters for S930 at 10 BV/hour flow rate.

	Modified Dose Response				Bohart-Adams			Thomas			Yoon-Nelson		
	a	b	Q_o	R^2	K_a	W	R^2	K_t	Q_o	R^2	K_{yn}	t_{50}	R^2
Al	1.9	12.45	1.31	*0.884*	0.07	3.18	*0.855*	0.08	1.48	*0.855*	0.28	15.78	*0.848*
Co	2.42	15.02	1.43	*0.938*	0.06	3.26	*0.897*	0.06	1.51	*0.897*	0.19	17.76	*0.892*
Cu	2.11	397.82	34.89	*0.997*	0.004	55.31	*0.969*	0.005	25.8	*0.969*	0.01	326.68	*0.973*
Fe	0.81	13.28	1.15	*0.630*	0.004	8.43	*0.289*	0.005	0	*0.284*	NA	NA	*NA*
Mn	3.74	11.32	1.00	*0.841*	0.12	2.18	*0.828*	0.13	1.02	*0.828*	0.39	12.97	*0.820*
Ni	2.26	15.64	1.44	*0.951*	0.05	3.29	*0.897*	0.06	1.52	*0.897*	0.18	18.52	*0.892*
Zn	4.65	15.09	1.4	*0.992*	0.08	3.1	*0.991*	0.08	1.45	*0.991*	0.26	17.44	*0.991*

During the 5 BV/h flow rate loading experiment (Figure 6.5), the breakthrough of Mn, Co, Zn, and Ni was rapid, with concentration ratios reaching 1 within 2 BV of first detection. Following this point, Zn, Co, and Ni experienced a brief period of displacement from the column, with maximum values of 1.42, 1.32, and 1.23 mg/g, respectively, at 6 BV throughput. Such patterns of breakthrough and overshoot indicated minimal interaction between these ions and the iminodiacetic acid functional groups of S930. Beyond 3 BV, Fe concentration ratios immediately jumped to approximately 0.4, after which the ratio gradually increased linearly during the remainder of the experiment; reaching a final value of 0.82 at 76 BV throughput.
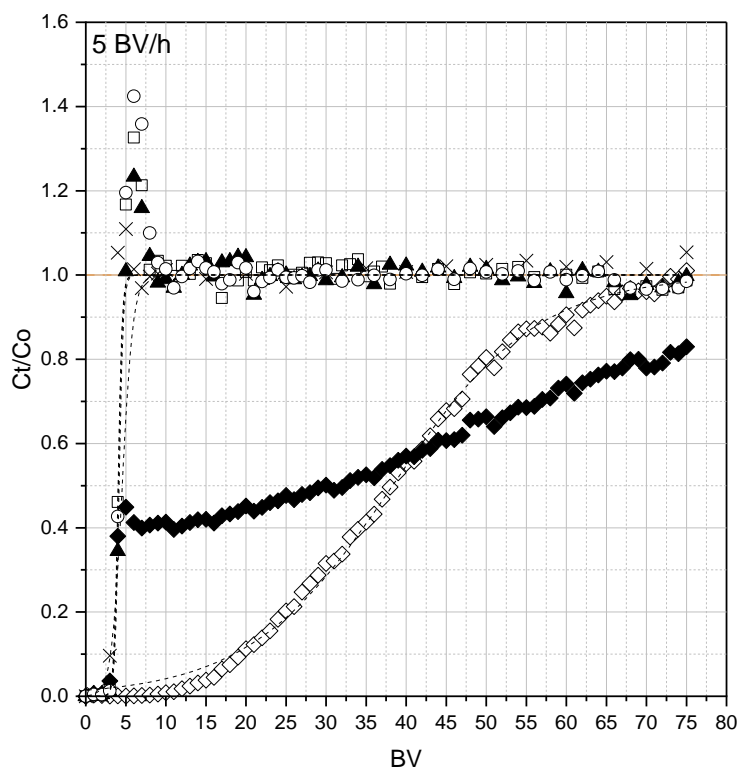
Figure 6.5. Breakthrough curves of metals from PLS pumped through S930 at 5 BV/h (8.28 x10^{-5} m/s) (pH 1.45). Co = □, Cu = ◊, Fe = ◆, Mn = ×, Ni = ▲, Zn = ○. Dotted lines = best-fitting breakthrough model (see Table 6.7).

Interestingly, a switch in selectivity by the resin was observed throughout the experiment. At 41 BV throughput, the breakthrough curves for Fe and Cu intercepted (Figure 6.5), after which Fe appeared beneath Cu, indicating preferential Fe extraction beyond this point. Modelling of Cu breakthrough indicated a loading capacity of 18.91 mg/g (Table 6.7). While this value is below that of Fe (13.38 mg/g), it is important to note that model predictions for Fe are less accurate given the abnormal curve shape and low maximum R^2 value of 0.884 (Thomas model).

Table 6.7. Breakthrough model parameters for S930 at 5 BV/hour flow rate.

	Modified Dose Response				Bohart-Adams			Thomas			Yoon-Nelson		
	a	b	Q_o	R^2	K_a	W	R^2	K_t	Q_o	R^2	K_{yn}	t_{50}	R^2
Co	13.90	20.22	2.05	*0.999*	0.09	4.06	*0.999*	0.09	2.05	*0.999*	0.31	51.78	*0.999*
Cu	4.16	184.62	18.22	*0.995*	0.003	38.61	*0.997*	0.003	18.91	*0.997*	0.01	491.07	*0.997*
Fe	0.80	109.69	9.85	*0.867*	0.001	36.05	*0.857*	0.001	13.38	*0.884*	0.003	389.66	*0.855*
Mn	6.88	20.78	1.73	*0.999*	0.04	3.87	*0.999*	0.04	1.90	*0.999*	NA	NA	*NA*
Ni	13.56	20.97	2.15	*0.999*	0.09	4.34	*0.999*	0.09	2.13	*0.999*	NA	NA	*NA*
Zn	14.06	20.42	1.70	*0.999*	0.11	3.46	*0.999*	0.11	1.70	*0.999*	0.32	52.22	*0.999*

Reduction of flow rate to 2 BV/h (Figure 6.6) had only a slight effect on the breakthrough and overshoot behaviour of Mn, Zn, Co, and Ni, which displayed similar patterns to those observed at 5 BV/h, evidenced also by the similarity in model parameters between Table 6.8 and Table 6.7 for these metals. Where the most notable dissimilarities occurred was in the breakthrough of Fe and Cu. Whereas for the 5 BV/h flow rate Fe breakthrough linearly progressed from C_t/C_o 0.4 to 0.55 over the first 40 BV, at 2 BV/h Fe concentration ratio rapidly reached 0.7 before reducing to 0.6 and remaining constant until experiment termination. When comparing Cu breakthrough at a common point (40 BV throughput), much lower breakthrough was observed at 2 BV/h (C_t/C_o = 0.19) when compared to that at 5 BV/h (C_t/C_o = 0.55). Comparing the results of MDR breakthrough modelling (Table 6.8), the operational loading capacity at 2 BV/h (33.36 mg/g Cu) was almost double the capacity under 5 BV/h loading conditions (18.22 mg/g Cu).
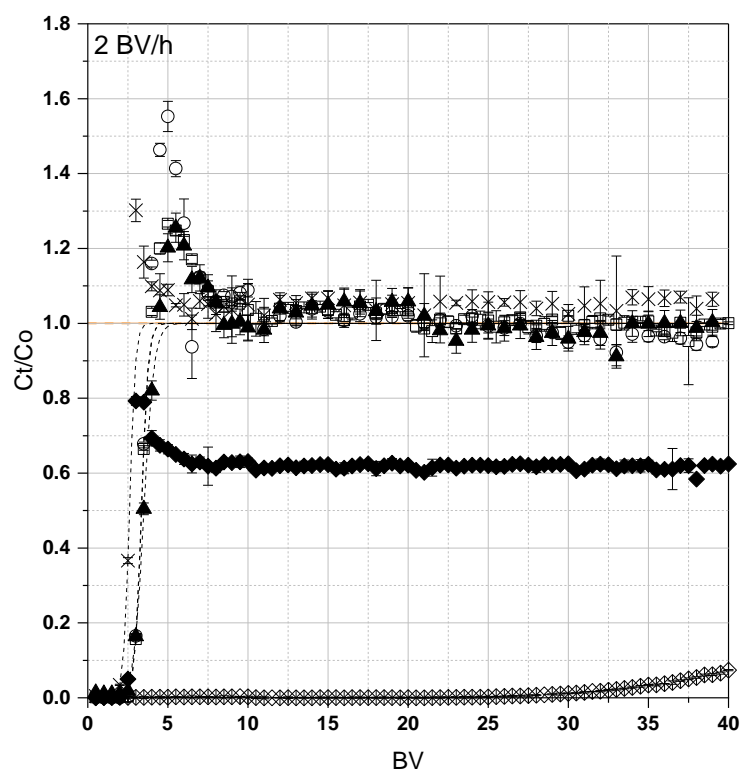
Figure 6.6. Breakthrough curves of metals from PLS pumped through S930 at 2 BV/h (3.67 x10^{-5} m/s) (pH 1.45).

Co = □, Cu = ◊, Fe = ◆ , Mn = ×, Ni = ▲, Zn = ○. Dotted lines = best-fitting breakthrough model (see Table 6.8).

Table 6.8. Breakthrough model parameters for S930 at 2 BV/hour flow rate.

| | Modified Dose Response | | | | Bohart-Adams | | | Thomas | | | Yoon-Nelson | | |
	a	b	Q_o	R^2	K_a	W	R^2	K_t	Q_o	R^2	K_{yn}	t_{50}	R^2
Co	15.42	16.75	1.79	*0.998*	0.04	3.94	*0.998*	0.04	2.21	*0.998*	0.17	97.01	*0.999*
Cu	6.91	287.49	33.36	*0.995*	0.002	63.31	*0.992*	0.002	35.54	*0.992*	NA	NA	*NA*
Fe	NA	NA	NA	*NA*	NA	NA	*NA*	NA	NA	*NA*	NA	NA	*NA*
Mn	12.43	13.07	1.32	*0.999*	0.06	2.35	*0.999*	0.06	1.32	*0.999*	NA	NA	*NA*
Ni	10.99	17.45	1.91	*0.999*	0.04	3.14	*0.999*	0.04	1.76	*0.999*	0.12	100.94	*0.996*
Zn	15.42	16.68	1.75	*0.992*	0.05	3.14	*0.993*	0.05	1.76	*0.993*	0.20	96.42	*0.968*

6.3.3 Puromet MTS9570

A relatively high volume of solution was passed through the S957-packed column before any metals

were detected in effluent solutions (approximately 12 BV or 60 mL). During this initial period, it was

assumed that all metal species were being adsorbed to the phosphonic and sulfonic acid functional

groups. The breakthrough pattern of metals from the column (Figure 6.7) can be described as three

distinct groups. Ni, Co, and Zn were the first metals to reach complete breakthrough, with Ni and Co

beginning to be displaced from the column after 20 BV throughput. Breakthrough modelling

indicated similar operating capacities for these metals; 9.61 mg/g for Ni, 10.4 mg/g for Co, and 10.14

mg/g for Zn (Table 6.9). The displacement of these metals is due to increased loading of Cu, Fe, and

Mn, which had column operating capacities of 10.71, 11.67, and 11.80 mg/g, respectively, according

to MDR and Thomas models (Table 6.9). Cu, Fe, and Mn did not reach complete breakthrough in

Figure 6.7, but they are anticipated to eventually be displaced by Al given a sufficient loading period.

Concentration ratios of Al did not exceed 0.09 throughout the experiment, suggesting a very high

operating capacity for Al by S957. Model fits were generally poor for Al given the low C_t/C_o values,

but were likely in the region of 32.40 mg/g according to the MDR model (R^2 = 0.846, Table 6.9).

Figure 6.7. Breakthrough curves of metals from PLS pumped through S957 at 10 BV/h (1.49 x10^{-4} m/s) (pH 1.35). Al = ▷, Co = □, Cu = ◊, Fe = ◆ , Mn = ×, Ni = ▲ , Zn = ○. Dotted lines = best-fitting breakthrough model (see Table 6.9).

Table 6.9. Breakthrough model parameters for S957 at 10 BV/hour flow rate.

	Modified Dose Response				Bohart-Adams			Thomas			Yoon-Nelson		
	a	b	Q_o	R^2	K_a	W	R^2	K_t	Q_o	R^2	K_{yn}	t_{50}	R^2
Al	2.46	255.08	32.40	*0.846*	0.01	32.02	*0.795*	0.01	21.6	*0.795*	0.02	249.35	*0.738*
Co	14.54	91.58	10.37	*0.988*	0.04	15.41	*0.991*	0.03	10.4	*0.991*	0.11	130.91	*0.991*
Cu	13.28	101.57	10.67	*0.962*	0.03	15.86	*0.964*	0.03	10.71	*0.964*	0.08	145.48	*0.993*
Fe	7.92	109.56	11.67	*0.999*	0.02	17.12	*0.995*	0.02	11.56	*0.995*	0.06	154.66	*0.995*
Mn	7.58	111.89	11.80	*0.997*	0.02	17.25	*0.992*	0.02	11.65	*0.992*	0.06	157.39	*0.992*
Ni	17.64	88.96	9.66	*0.969*	0.05	14.35	*0.972*	0.04	9.69	*0.972*	0.12	127.40	*0.992*
Zn	13.01	92.71	10.11	*0.995*	0.04	15.02	*0.997*	0.03	10.14	*0.997*	0.1	132.55	*0.997*

Metal breakthrough under a 5 BV/h loading flow rate began to occur at approximately 14 BV – comparable to breakthrough during the 10 BV/h loading experiment. As per Figure 6.7, the first

metals to reach complete breakthrough were Ni, Co, and Zn (Figure 6.8), which equated to loading capacities of 8.44, 8.93, and 8.57 mg/g, respectively. After reaching a concentration ratio of 1, a large displacement curve was observed for each of these metals, with maximum values in the region of 1.9 – 2.1 at 22 BV throughput. Following these maxima, concentration ratios slowly declined and did not return to 1 during the experimental period; the last sample having C_t/C_o values between 1.3 and 1.5 for these metals. The overshoot region for Mn was also very broad, beginning at 25 BV throughput and reaching a maximum of 1.83 at 37 BV throughput, after which the decline was minimal. Fe was the only metal which was not displaced from the column and reached complete breakthrough at 25 BV throughput. The Thomas model best-described Fe breakthrough (R^2 = 0.997, Table 6.10) and indicated an operating capacity of 9.08 mg/g Fe for the S957 column.
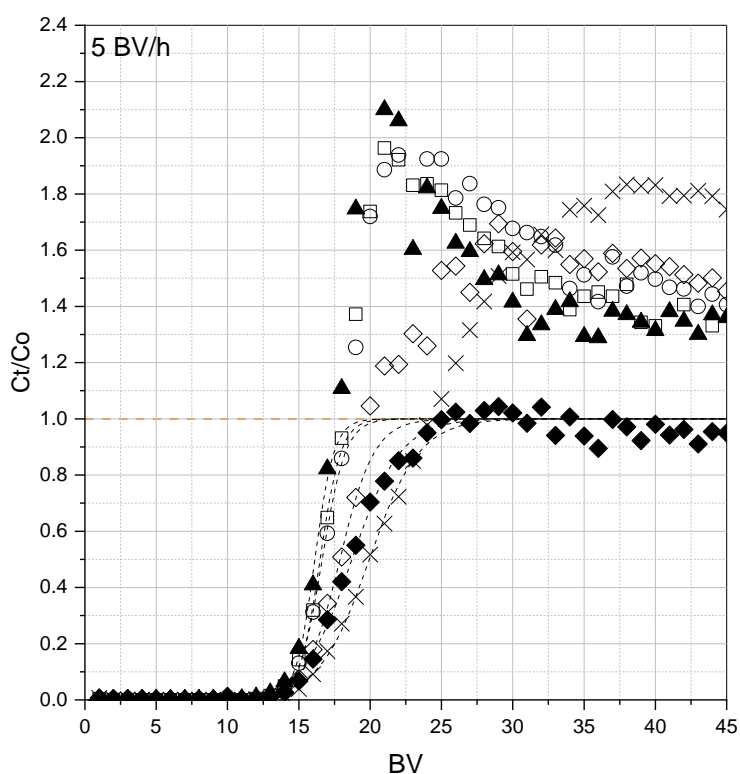
Figure 6.8. Breakthrough curves of metals from PLS pumped through S957 at 5 BV/h (8.14 x10^{-5} m/s) (pH 1.35). Co = □, Cu = ◊, Fe = ◆, Mn = ×, Ni = ▲, Zn = ○. Dotted lines = best-fitting breakthrough model (see Table 6.10). Note: Al was present in PLS, but could not be analysed for by AAS – see Section 6.2.1)

Table 6.10. Breakthrough model parameters for S957 at 5 BV/hour flow rate.

	Modified Dose Response				Bohart-Adams			Thomas			Yoon-Nelson		
	a	b	Q_o	R^2	K_a	W	R^2	K_t	Q_o	R^2	K_{yn}	t_{50}	R^2
Co	22.71	82.38	8.92	*0.995*	0.03	16.04	*0.997*	0.03	8.93	*0.997*	0.13	214.6	*0.940*
Cu	14.18	89.26	9.46	*0.999*	0.02	16.89	*0.996*	0.02	9.47	*0.999*	0.06	232.99	*0.999*
Fe	10.85	93.13	9.03	*0.975*	0.02	17.70	*0.941*	0.02	9.08	*0.997*	0.05	244.02	*0.997*
Mn	11.18	99.24	9.19	*0.997*	0.02	15.90	*0.968*	0.02	9.23	*0.997*	0.04	259.90	*0.996*
Ni	23.89	80.57	8.44	*0.992*	0.04	15.15	*0.994*	0.04	8.44	*0.994*	0.12	210.13	*0.993*
Zn	11.18	99.24	9.19	*0.997*	0.03	15.39	*0.999*	0.03	8.57	*0.999*	0.09	216.85	*0.999*

Reduction of flow rate to 2 BV/h had little effect on the point at which breakthrough began to occur (approximately 15 BV throughput) and the gradient of frontal curves when compared to 5 BV/h breakthrough curves. Most notably, reducing solution flow rate increased the overshoot maximum for Ni (C_t/C_o = 2.3, 19 BV, Figure 6.9). Additionally, the overshoot of Mn was highly exaggerated in comparison to Figure 6.8, which in Figure 6.9 reached a maximum of 2.35 at 38 BV throughput. The breakthrough behaviour of Fe also changed substantially when loaded at 2 BV/h compared to higher flow rates. Beyond 15 BV, when Fe was first detected in the effluent, a gradual increase in concentration ratio was observed which reached a maximum of 0.54 at approximately BV 25 before showing gradual decline towards 40 BV (Figure 6.9).
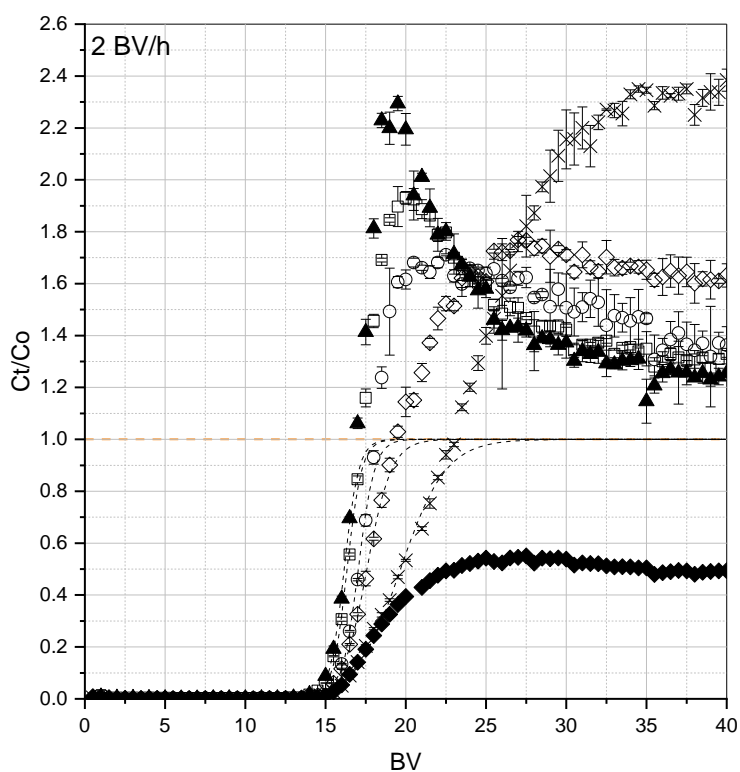
Figure 6.9. Breakthrough curves of metals from PLS pumped through S957 at 2 BV/h (3.86 x10^{-5} m/s) (pH 1.35). Co = □, Cu = ◊, Fe = ◆, Mn = ×, Ni = ▲, Zn = ○. Dotted lines = best-fitting breakthrough model (see Table 6.11).

Table 6.11. Breakthrough model parameters for S957 at 2 BV/hour flow rate.

	Modified Dose Response				Bohart-Adams			Thomas			Yoon-Nelson		
	a	b	Q_o	R^2	K_a	W	R^2	K_t	Q_o	R^2	K_{yn}	t_{50}	R^2
Co	35.91	81.66	12.4	*0.995*	0.02	16.21	*0.996*	0.02	12.41	*0.996*	0.08	449.81	*0.996*
Cu	22.85	87.76	13.08	*0.998*	0.01	17.12	*0.999*	0.01	13.10	*0.999*	0.05	483.72	*0.999*
Fe	NA	NA	NA	*NA*	NA	NA	*NA*	NA	NA	*NA*	NA	NA	*NA*
Mn	13.77	97.97	10.89	*0.994*	0.01	14.29	*0.995*	0.01	10.93	*0.995*	0.03	541.37	*0.995*
Ni	35.45	80.76	11.44	*0.997*	0.03	14.97	*0.997*	0.03	11.45	*0.997*	0.08	444.05	*0.995*
Zn	20.14	83.10	12.22	*0.916*	0.02	16.37	*0.994*	0.02	12.52	*0.994*	0.07	468.92	*0.994*

6.3.4   Puromet MTS9501

Metal adsorption to the aminophosphonic acid functional groups of S950 appeared to favour the

trivalent transition metals, Fe and Al (Figure 6.10). The order that metals reached complete

breakthrough (C_t/C_o = 1) from the column was Ni (at BV 5), Co (BV 6), Zn (BV 9), Mn (BV 11), then Cu

(BV 18). For Fe and Al, breakthrough did not exceed a C_t/C_o value of 0.8 over the studied range,

indicating higher selectivity towards these ions. During the first 5 BV, Fe breakthrough followed a

similar pattern to Mn, yet began to plateau prematurely at a concentration ratio of around 0.75. As a

result, numerical modelling of Fe breakthrough was not possible given the abnormal curve

characteristics. The modelling of dynamic adsorption to S950 highlighted the effectiveness of Al

removal by S950, with the Thomas model operating capacity for Al (12.42 mg/g) being an order of

magnitude higher than that for the other metal species (Table 6.12). Despite the Fe breakthrough

curve being above that of Al, and therefore more likely to be displaced by Al, it is suggested that

beyond 26 BV, Al would be displaced by Fe given the trajectory of Al breakthrough in Figure 6.10.
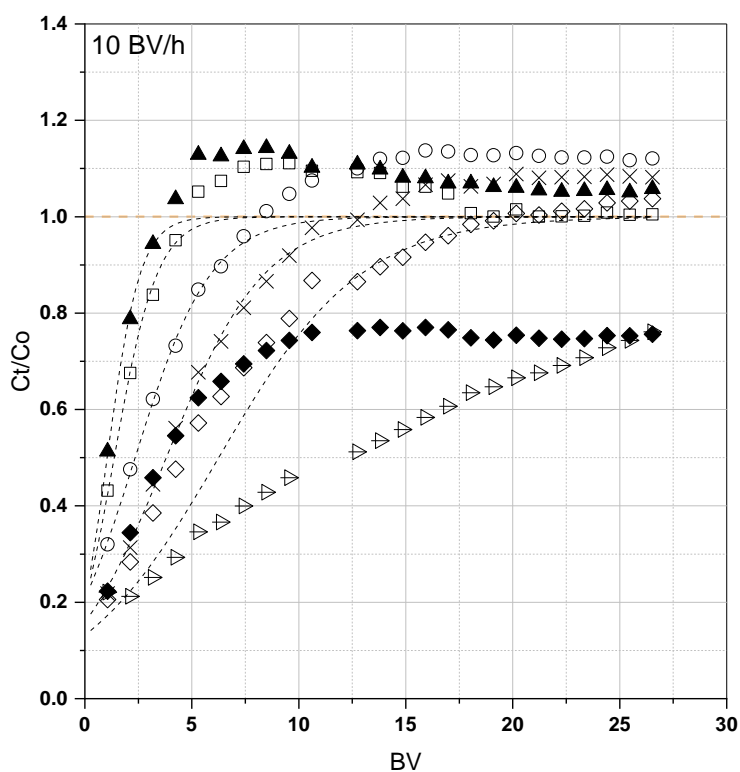
Figure 6.10. Breakthrough curves of metals from PLS pumped through S950 at 10 BV/h (1.88 x10^{-4} m/s) (pH 1.40). Al = ▷, Co = □, Cu = ◊, Fe = ◆ , Mn = ×, Ni = ▲, Zn = ○. Dotted lines = best-fitting breakthrough model (see Table 6.12).

Table 6.12. Breakthrough model parameters for S950 at 10 BV/hour flow rate.

| | Modified Dose Response | | | | Bohart-Adams | | | Thomas | | | Yoon-Nelson | | |
	a	b	Q_o	R^2	K_a	W	R^2	K_t	Q_o	R^2	K_{yn}	t_{50}	R^2
Al	1.07	55.61	8.86	*0.959*	0.005	34.94	*0.983*	0.005	12.42	*0.983*	0.02	73.17	*0.980*
Co	3.33	11.62	1.67	*0.914*	0.06	5.11	*0.936*	0.06	2.08	*0.936*	0.18	7.74	*0.968*
Cu	2.21	26.62	3.53	*0.972*	0.02	11.98	*0.991*	0.02	4.66	*0.991*	0.05	27.38	*0.989*
Fe	NA	NA	NA	*NA*	NA	NA	*NA*	NA	NA	*NA*	NA	NA	*NA*
Mn	2.84	22.61	3.01	*0.935*	0.03	9.53	*0.964*	0.03	3.82	*0.995*	0.08	21.52	*0.996*
Ni	3.7	10.13	1.41	*0.832*	0.08	4.2	*0.853*	0.08	1.72	*0.853*	0.23	5.89	*0.971*
Zn	2.94	16.09	2.26	*0.851*	0.03	7.18	*0.880*	0.03	2.86	*0.880*	0.1	13.28	*0.998*

Reducing the flow rate to 5 BV/h resulted in a notable sharpening of the breakthrough profiles for all metals in the PLS (Figure 6.11). Additionally, a large overshoot was observed for Mn, which started at 10 BV and reached a maximum concentration ratio of 1.65 at 15 BV before stabilising beyond 30 BV. Overshoot was also observed for Ni, Co, Zn, and Cu but to a lesser extent than for Mn. Thomas model operating capacities indicated highest capacity for Cu followed by Mn, Zn, Co, and Ni (Table 6.13). The Fe breakthrough profile at 5 BV/h was similar to that observed at the 10 BV/h flow rate, whereby the concentration ratio plateaued at approximately 0.75 beyond 10 BV throughput.
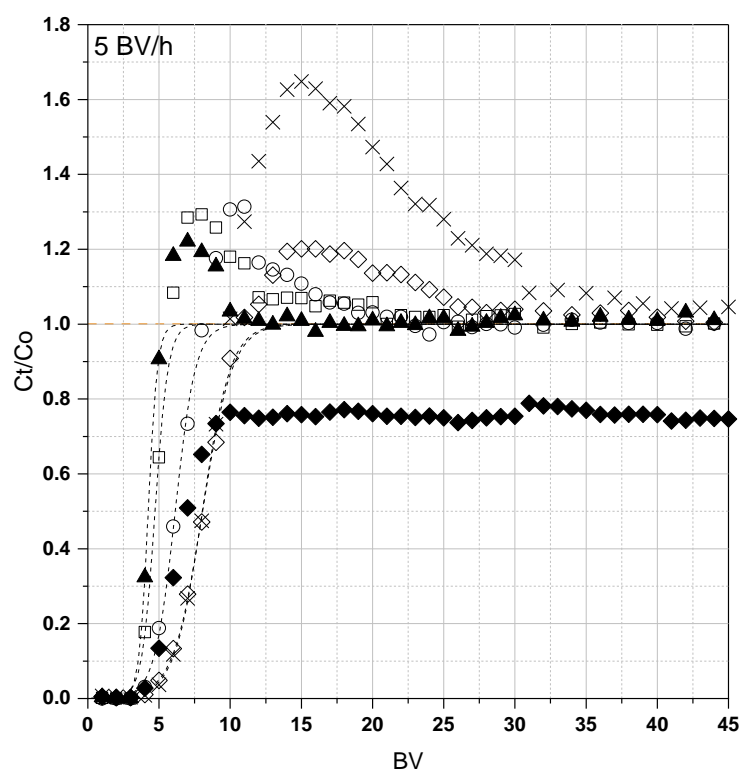
Figure 6.11. Breakthrough curves of metals from PLS pumped through S950 at 5 BV/h (9.29 x10^{-5} m/s) (pH 1.40). Co = □, Cu = ◊, Fe = ◆ , Mn = ×, Ni = ▲, Zn = ○. Dotted lines = best-fitting breakthrough model (see Table 6.13).

Table 6.13. Breakthrough model parameters for S950 at 5 BV/hour flow rate.

	Modified Dose Response				Bohart-Adams			Thomas			Yoon-Nelson		
	a	b	Q_o	R^2	K_a	W	R^2	K_t	Q_o	R^2	K_{yn}	t_{50}	R^2
Co	9.63	23.49	3.10	*0.999*	0.06	4.56	*0.998*	0.06	3.39	*0.998*	0.22	53.7	*0.979*
Cu	7.51	39.93	5.67	*0.993*	0.02	8.39	*0.997*	0.02	6.24	*0.997*	0.08	92.08	*0.996*
Fe	NA	NA	NA	*NA*	NA	NA	*NA*	NA	NA	*NA*	NA	NA	*NA*
Mn	7.57	39.99	4.51	*0.999*	0.03	6.64	*0.999*	0.03	4.94	*0.999*	0.10	91.05	*0.987*
Ni	13.56	21.12	2.86	*0.999*	0.08	4.20	*0.999*	0.08	3.12	*0.999*	0.27	48.47	*0.999*
Zn	8.49	30.38	3.77	*0.993*	0.04	5.58	*0.995*	0.04	4.15	*0.996*	0.12	70.06	*0.995*

Figure 6.12 presents the breakthrough of metals from S950 when loaded at 2 BV/h. Most notably, the reduction in flow rate resulted in substantial increases in the magnitude of the overshoot profiles for all metals, with the exception of Fe. Maximum Mn displacement remained largely unaffected by the reduction in flow rate when compared to that at 5 BV/h, but maximum values for Cu (1.59) and Zn (1.55) were of much higher magnitude under 2 BV/h loading conditions (1.25 and 1.31, respectively). For all metals which were able to be modelled, the Thomas adsorption model provided the highest goodness-of-fits, with considerably lower calculated Thomas constants (K_t, Table 6.14). The Fe breakthrough curve was similar in shape to those previously observed under higher loading flow rates. However, at 2 BV/h the point at which the concentration plateaued occurred much sooner (7 BV throughput) and stabilised at a lower concentration ratio (0.5, compared to approximately 0.75 at higher flow rates).
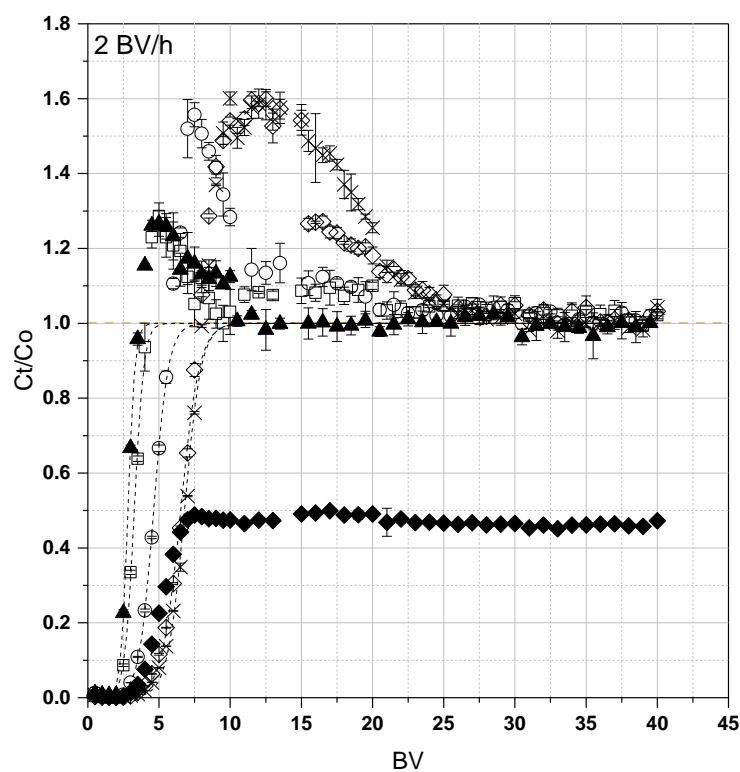
Figure 6.12. Breakthrough curves of metals from PLS pumped through S950 at 2 BV/h (3.54 x10^{-5} m/s) (pH 1.40). Co = □, Cu = ◊, Fe = ◆ , Mn = ×, Ni = ▲, Zn = ○. Dotted lines = best-fitting breakthrough model (see Table 6.14).

Table 6.14. Breakthrough model parameters for S950 at 2 BV/hour flow rate.

	Modified Dose Response				Bohart-Adams			Thomas			Yoon-Nelson		
	a	b	Q_o	R^2	K_a	W	R^2	K_t	Q_o	R^2	K_{yn}	t_{50}	R^2
Co	9.70	16.20	2.11	*0.997*	0.03	3.15	*0.998*	0.03	2.15	*0.998*	0.10	97.77	*0.996*
Cu	9.62	32.47	4.59	*0.994*	0.01	6.78	*0.997*	0.01	4.63	*0.997*	0.05	195.53	*0.993*
Fe	NA	NA	NA	*NA*	NA	NA	*NA*	NA	NA	*NA*	NA	NA	*NA*
Mn	11.50	33.82	3.81	*0.980*	0.02	5.60	*0.987*	0.02	3.82	*0.987*	0.06	203.49	*0.986*
Ni	11.46	14.01	1.87	*0.998*	0.04	2.78	*0.998*	0.04	1.90	*0.998*	0.14	84.46	*0.998*
Zn	8.70	23.00	2.86	*0.999*	0.02	4.21	*0.999*	0.02	2.87	*0.999*	0.07	138.76	*0.999*

6.3.5   Puromet MTS9140

It was observed that under dynamic operation, S914 continued to exhibit exclusive Cu selectivity and extraction from the synthetic PLS, evidenced by the almost immediate breakthrough of all other ions from the column, which reached complete breakthrough within the first 5 BV throughput (Figure 6.13). Numerical modelling for these metals indicated very low loading capacities for these ions (2.02-2.15 mg/g, MDR, Table 6.15), but considering the speed at which these metals broke through and considering the lack of displacement following complete breakthrough, this is likely an overestimation of loading capacity.

Cu breakthrough began to occur at around 5 BV throughput and gradually increased, following a slightly sigmoidal pattern, until reaching a concentration ration of 0.92 at BV 80 (Figure 6.13). While the breakthrough curve was not sharp, Cu extraction appeared unaffected by other metal ions in solution and was best-defined by the MDR model, which indicated a loading capacity of 19.84 mg/g.
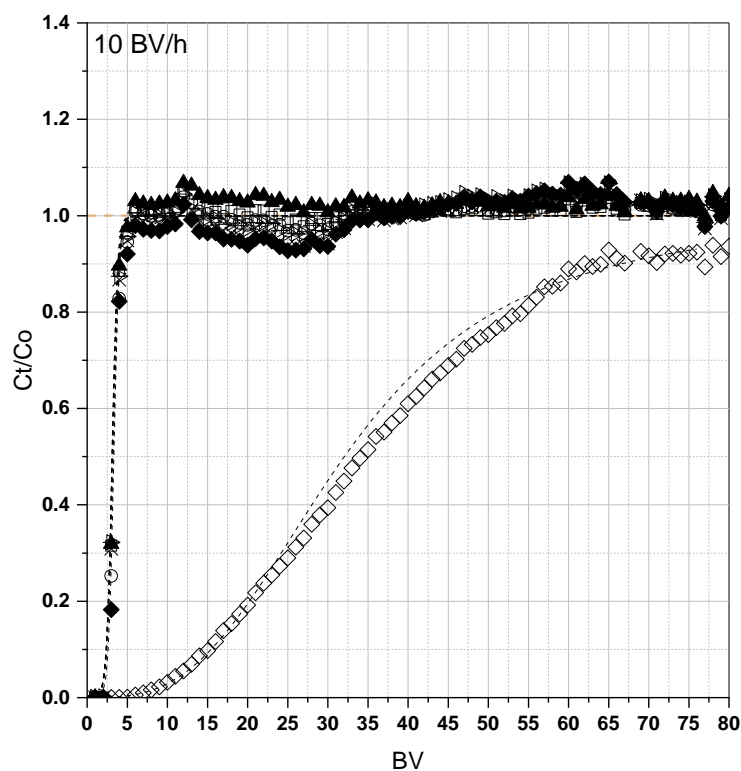
Figure 6.13. Breakthrough curves of metals from PLS pumped through S914 at 10 BV/h (1.82 x10^{-4} m/s) (pH 1.56). Al = ▷, Co = □, Cu = ◊, Fe = ◆ , Mn = ×, Ni = ▲, Zn = ○. Dotted lines = best-fitting breakthrough model (see Table 6.15).

Table 6.15. Breakthrough model parameters for S914 at 10 BV/hour flow rate.

	Modified Dose Response				Bohart-Adams			Thomas			Yoon-Nelson		
	a	b	Q_o	R^2	K_a	W	R^2	K_t	Q_o	R^2	K_{yn}	t_{50}	R^2
Al	9.15	15.45	2.10	*0.996*	0.14	3.27	*0.996*	0.14	2.12	*0.996*	0.49	18.22	*0.998*
Co	9.64	15.44	2.15	*0.999*	0.14	3.34	*0.999*	0.14	2.17	*0.999*	0.52	18.20	*0.996*
Cu	3.01	160.26	19.84	*0.998*	0.005	33.07	*0.989*	0.005	21.20	*0.989*	0.02	199.98	*0.989*
Fe	9.97	16.48	2.13	*0.980*	0.16	3.31	*0.979*	0.16	2.15	*0.979*	0.53	19.44	*0.995*
Mn	9.06	15.57	2.02	*0.986*	0.15	3.14	*0.985*	0.15	2.04	*0.985*	0.49	18.36	*0.997*
Ni	10.07	15.37	2.10	*0.999*	0.15	3.26	*0.999*	0.15	2.11	*0.999*	0.54	18.11	*0.997*
Zn	10.07	15.37	2.01	*0.999*	0.14	3.27	*0.997*	0.14	2.12	*0.997*	0.48	18.96	*0.999*

Changing solution flow rate to 5 BV/h had little effect on the uptake of Co, Fe, Mn, Ni, and Zn, which

passed through the column with little to no interaction with the thiourea-functionalised resin (Figure

6.14). For Cu, which was exclusively extracted by S914, the breakthrough profile appeared sharper than it did when loaded at 10 BV/h, which was confirmed by an associated increase in the MDR model constant 'a' (Table 6.16). Complete Cu breakthrough was also achieved earlier at the 5 BV/h flow rate, where Cu concentration ratio reached 1 at 68 BV throughput and corresponded to a Q_o value of 20.68-22.77 mg/g according to the breakthrough modelling (MDR and Thomas model had equal goodness-of-fit, R^2 = 0.998).
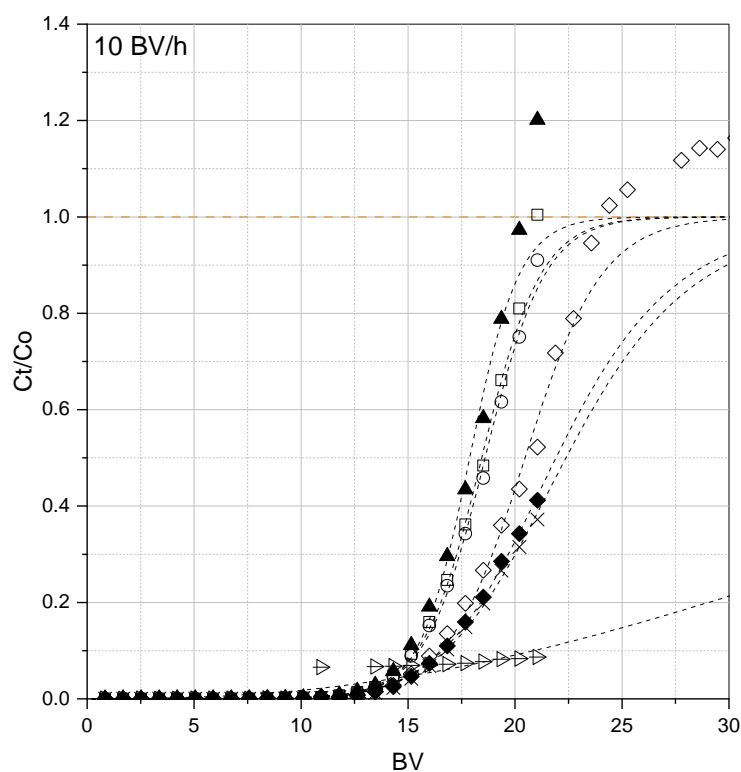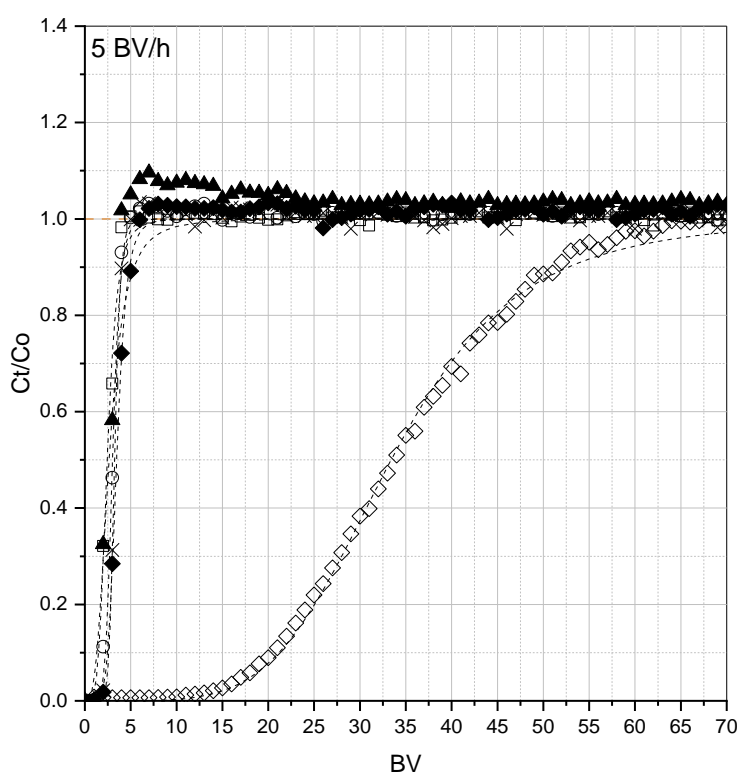

Figure 6.14. Breakthrough curves of metals from PLS pumped through S914 at 5 BV/h (1.01 x10^{-4} m/s) (pH 1.56). Co = □, Cu = ◊, Fe = ◆, Mn = ×, Ni = ▲, Zn = ○. Dotted lines = best-fitting breakthrough model (see Table 6.16).

Table 6.16. Breakthrough model parameters for S914 at 5 BV/hour flow rate.

	Modified Dose Response				Bohart-Adams			Thomas			Yoon-Nelson		
	a	b	Q_o	R^2	K_a	W	R^2	K_t	Q_o	R^2	K_{yn}	t_{50}	R^2
Co	4.49	12.15	1.69	*0.994*	0.05	2.72	*0.995*	0.05	1.76	*0.995*	0.18	26.52	*0.992*
Cu	4.81	167.02	20.68	*0.998*	0.004	35.13	*0.998*	0.004	22.77	*0.998*	0.01	360.37	*0.998*
Fe	6.45	17.32	2.23	*0.999*	0.05	3.50	*0.997*	0.05	2.27	*0.997*	0.18	36.91	*0.996*
Mn	10.29	16.18	2.10	*0.999*	0.09	3.26	*0.999*	0.09	2.12	*0.999*	0.28	34.22	*0.998*
Ni	3.09	13.20	1.80	*0.987*	0.04	2.85	*0.956*	0.04	1.84	*0.956*	0.17	27.37	*0.992*
Zn	7.35	15.07	1.87	*0.995*	0.07	3.05	*0.999*	0.07	1.98	*0.999*	0.23	31.79	*0.998*

When reduced to 2 BV/h, a further sharpening of the breakthrough of ions was observed. For all metals other than Cu, almost immediate complete breakthrough occurred, after which concentration ratios plateaued at values between 1 and 1.1 (Figure 6.15). It is important to note that a decision was made to increase sampling resolution during all 2 BV/h flow rate studies to increase the number of data points during the breakthrough frontal curve. Given the limited space for sample collection in fraction collectors, this resulted in only the first 40 BV to be sampled. Nevertheless, enough Cu breakthrough was captured to allow effective modelling and comparison to other flow rates. Cu was first detected in effluent solutions beyond 25 BV throughput (Figure 6.15), much later than observed for 10 and 5 BV/h (BV 5 and 10, respectively).
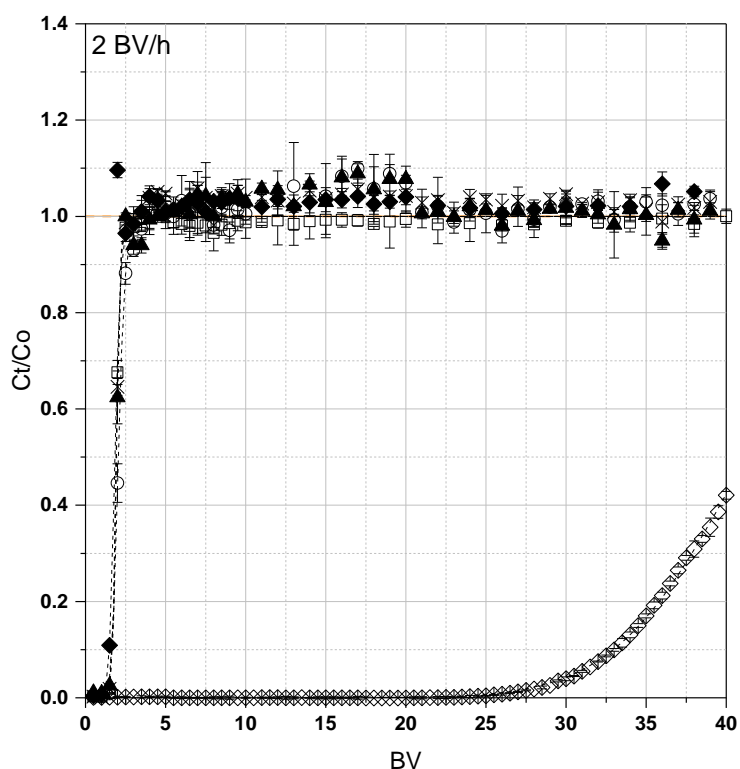
Figure 6.15. Breakthrough curves of metals from PLS pumped through S914 at 2 BV/h (3.54 x10^{-5} m/s) (pH 1.56). Co = □, Cu = ◊, Fe = ◆ , Mn = ×, Ni = ▲ , Zn = ○. Dotted lines = best-fitting breakthrough model (see Table 6.17).

Table 6.17. Breakthrough model parameters for S914 at 2 BV/hour flow rate.

	Modified Dose Response				Bohart-Adams			Thomas			Yoon-Nelson		
	a	b	Q_o	R^2	K_a	W	R^2	K_t	Q_o	R^2	K_{yn}	t_{50}	R^2
Co	16.67	9.56	1.46	*0.996*	0.09	2.25	*0.997*	0.09	1.46	*0.997*	0.333	57.52	*0.999*
Cu	9.74	206.45	32.04	*0.999*	0.002	48.75	*0.997*	0.002	31.66	*0.997*	0.01	1223.93	*0.997*
Fe	10.46	9.16	0.94	*0.999*	0.07	1.48	*0.999*	0.07	0.96	*0.999*	NA	NA	*NA*
Mn	16.14	9.63	1.08	*0.999*	0.10	1.66	*0.999*	0.10	1.08	*0.999*	0.30	57.72	*0.999*
Ni	16.57	9.69	1.18	*0.999*	0.09	1.81	*0.999*	0.09	1.18	*0.999*	0.29	57.94	*0.999*
Zn	9.97	10.25	1.13	*0.996*	0.06	1.73	*0.996*	0.06	1.13	*0.996*	0.17	61.52	*0.996*

6.4 CHAPTER DISCUSSION

6.4.1 Dowex M4195

Dowex M4195 exhibited low retention of Al, Fe, and Mn under column operation at a 10 BV/h flow rate (Figure 6.1), which was in agreeance with the trends observed during static resin screening in Chapter 5 at the pH used. When solution flow rate was reduced, the tendency for Zn and Co extraction also reduced, with M4195 being more selective towards extraction of Ni and Cu (Figure 6.2 and Figure 6.3). The general trends of low Fe retention, intermediate Co uptake, and high selectivity towards Ni observed in Figure 6.1 are in agreeance with trends reported elsewhere for this resin (Canner, et al., 2017; Diniz, et al., 2005). The preferential extraction of Ni over Co was also observed for M4195 in acidic sulfate solutions by Mendes & Martins (2004), albeit not under dynamic conditions.

For Ni it was noted that reducing solution flow rate had the effect of delaying the point at which it was detected in effluent samples (BV 5 at 10 BV/h, BV 11 at 5 BV/h, BV 27 at 2 BV/h), i.e. resulting in a delayed breakthrough. This was also associated with an increase in the calculated operating capacities for Ni of 16.96, 21.43, and 28.50 mg/g at 10, 5, and 2 BV/h, respectively (Table 6.3 -Table 6.5). Such operating capacities are in agreeance with other published studies on M4195, where capacities of 22.7 – 30.8 mg/g were observed under various conditions in sulfuric acid media (Liebenberg, et al., 2013). Earlier detection in effluent solutions at increased flow rates is observed in other fixed-bed flow rate investigations (e.g. Yilmaz Ipek, et al. (2013)), and the reason for this is related to the dynamic kinetics of extraction.

The overall rate at which ion exchange occurs is dependent on a number of sequential processes; the diffusion of ions from the bulk solution to the resin film layer (advective transport), diffusion across the film layer (film diffusion), the diffusion of ions from the surface of the resin to the interior (intraparticle diffusion), and adsorption/exchange at functional sites (Patel, 2019). During column operation, where feed solutions are presented at a constant rate, a single resin bead has a limited

time to extract the target metal before the solution has passed that point within the column. This time is inversely proportional to the superficial velocity of the solution flowing over the resin beads, with higher velocities reducing effective contact time between concentrated PLS and the thin film of lower-concentration PLS surrounding resin surfaces (Coulson & Richardson, 2002). Depending upon the rate of the specific mechanism which governs mass transport, the resin may not have sufficient time to remove the target ion at higher flow rate, which passes through the column and appears sooner in the effluent. This would especially be the case for metals with lower K_{eq} values given their lower adsorption to the resin, and their extraction would be affected to a higher degree by increased flow rate as the influence of internal physical mass transport limitations (i.e. intraparticle diffusion) plays an increasingly greater role. This is seen for M4195, where metals with lower K_{eq} values (e.g. Fe; Table 6.1) appear in effluents sooner as flow rate is increased, and with a lower degree of overshoot (Figure 6.1 - Figure 6.3), indicating less initial adsorption to functional sites.

Considering the column as a whole, if the feed solution is passing through the column at a rate higher than the rate of extraction, the exchangeable metals will begin to exit the column outlet prematurely. As such, at lower flow rates the target ion has a higher residence time within the column, allowing more time for exchange at a set point before proceeding through the column, resulting in delayed breakthrough. This is especially apparent when comparing the column half-lives determined through Yoon-Nelson modelling, where an inverse relationship between half-life and flow rate was observed (t_{50} = 256.7, 423.1, 1284.9 seconds for 10, 5, and 2 BV/h, respectively; Table 6.3, Table 6.4, and Table 6.5).

Another general observation associated with the reduction of flow rate was the increase in the magnitude of overshoot periods. For M4195, this was most notable for Zn at flow rates lower than 10 BV/h, where maximum concentration ratios reached 2.64 at 5 BV/h (Figure 6.2) and 3.69 at 2 BV/h (Figure 6.2). Despite the nature of real-life complex waste streams, a paucity of studies been completed where the focus has been on fixed-bed metal sorption from multiple-component

solutions, and as such the overshoot period (when effluent concentrations exceed influent concentrations, $C_t/C_o > 1$) has rarely been described. Occurring as a result of competitive adsorption and interaction between metals for a finite number of functional exchange sites (Escudero, et al., 2013; Chiavola, et al., 2012), the overshoot period often takes the form of a sharp curve occurring directly after analyte concentration ratios reach 1. Following the point of maximum overshoot, concentration ratios would in theory reduce until $C_t/C_o = 1$, at which point all of the previously bound metal ions would have been displaced and column effluent concentrations would resemble those of the influent.

For Zn, the overshoot region was not only greater at 2 BV/h but also much sharper, meaning that the previously bound Zn was displaced over a short time period. This sharpening was attributed to a narrower, more-highly concentrated band of Zn-enriched PLS travelling through the column, which formed as a result of longer residence time allowing a greater degree of metal-metal exchange at resin functional sites.

6.4.2   Puromet MTS9301

During loading at 10 BV/h, S930 exhibited high selectivity towards Cu, given that the remaining metals in the PLS quickly began to pass through the column (Figure 6.4). However, despite the initially rapid breakthrough of ions, only Zn reached a concentration ratio of 1. When flow rates were reduced to 5 BV/h and further to the 2 BV/h, complete breakthrough of most ions occurred within the first 5 bed volumes, yet it became apparent that abnormal breakthrough behaviour occurred for Fe, which along with Cu were the only ions extracted by this resin (Figure 6.5, Figure 6.6).

The high selectivity towards Cu by iminodiacetic acid resins has previously been attributed towards the presence of two carboxyl groups and the tertiary nitrogen atom within the resin functionality (Marhol & Cheng, 1974), which at the pH used here would likely be protonated (Hubicki & Kołodyńska, 2012). The Cu recovery potential by S930 in a fixed-bed column was explored by Bleotu

et al. (2015), which indicated favourable sorption. However, given that only single-metal solutions were used, this was not able to provide insight to competitive fixed-bed adsorption. In chloride media, the selectivity towards Cu and Fe was reported for S930 (Canner, et al., 2017). Interestingly, in that case Cu and Fe exhibited almost identical breakthrough profiles, whereas in Figure 6.5 and Figure 6.6 breakthrough curves for these ions were dissimilar, with particularly abnormal profiles for Fe.

In general, abnormal breakthrough profiles are the result of unfavourable equilibrium between the ion and resin. Under favourable equilibrium, where kinetics of exchange would be governed by film diffusion, it is reported that a sharp breakthrough pattern would be observed regardless of changes in flow rate, with uniform profile shape occuring at different points on the x-axis (Harland, 1994). However, for ion exchange with poor kinetics the exchange zone within the column is lengthened, resulting in a broader breakthrough profile. The result of which is a curve which is not self-sharpening, and closer resembles a linear breakthrough. Further to this, for weakly functional resins it has been suggested that the operating capacity of resins for which exchange is governed by slow particle diffusion decreases with increased solution flow rate (Harland, 1994). While breakthrough models in this instance were not able to describe Fe loading capacities for the lowest flow rate (Table 6.8), and achieved low R^2 at other flow rates, MDR Q_o values were lower for 10 BV/h than 5 BV/h (Table 6.6 and Table 6.7). While this alone is not conclusive, the general trends in breakthrough profiles suggest lower capacity at 10 BV/h given the near-complete breakthrough, a higher capacity at 5 BV/h whereby a gradual breakthrough was observed, and higher still at 2 BV/h, where concentration ratios plateaued and showed no upward trend. It is therefore suggested that the abnormal breakthrough profiles exhibit by Fe are a result of unfavuorable particle diffusion-controlled kinetics, and its extraction highly rate-sensitive.

6.4.3   Puromet MTS9570

At all studied flow rates, the point at which metal ions were detected in effluent solutions was much later when compared to the other resins screened, with breakthrough generally not occurring until after 13 BV throughput (Figure 6.7, Figure 6.8, and Figure 6.9). The high volume of solution throughput prior to effluent breakthrough suggested a high capacity for all metals, which was confirmed by similar Q_o values between all metals determined by breakthrough modelling (Table 6.9, Table 6.10, and Table 6.11). In a separate study of metal uptake using fixed-bed columns, the high capacity of S957 when compared to other resins during competitive adsorption was also shown (Canner, et al., 2017). The operating capacities determined through breakthrough modelling in Tables 6.7 – 6.9, which were generally in the region of 9 – 12 mg/g, compared favourably to those reported by Canner *et al.* (2017), but were generally lower by 1 – 3 mg/g. The lower values determined in the present study is likely due to the fact that the capacities reported in Canner *et al.* (2017) were calaculated from static isotherm experiments, as ion breakthrough from S957 was not sufficient for modelling in their study. It is expected that capacities calculated during isotherm experiments would generally be higher than those determined through breakthrough modelling given that equilibrium is attained during isotherm conditions.

The generally unselective extraction behaviour of S957 at low pH is typical of resins containing a sulfonic acid functional group (McKevitt & Dreisinger, 2009), which extract metals via a proton exchange mechanism. It is only through increased loading, when competition for active sites increases, that changes in breakthrough profiles between metals occurs. The preferential extraction of Al at 10 BV/h (Figure 6.7) and Fe at 2 BV/h (Figure 6.9) is expected of S957 given the strong affinity of sulfonated phosphonic functional groups towards Fe(III) (McKevitt & Dreisinger, 2009) and low Al breakthrough observed elsewhere for this resin (Lv, et al., 2019). A notable effect of decreasing flow rate to 2 BV/h was the limited breakthrough of Fe; the profile of which was not well defined and did not exceed a concentration ratio of 0.55. A slight decline towards the end of the experiment was also observed for Fe (Figure 6.9). Canner, et al. (2017) reported a similar phenomenon during their

experiments, whereby concentration ratios of Ni, Co, Cu, and Zn began to plateau in the region of C_t/C_o 0.09-0.12. It was suggested that the mechanism of extraction changed as a result of increasing resin saturation with metal cations, and theorised that given a longer contact time a period of metal displacement would occur (only 20 BV of solution was used; not enough to reach complete saturation for any metal in the PLS). In the present study, however, sufficient solution was contacted to witness complete resin saturation and overshoot for all metals except Fe. Comparing Figure 6.8, where Fe stabilised at C_t/C_o = 1, with Figure 6.9 where Fe C_t/C_o stabilised below 0.55, the overshoot profiles for Ni, Co, Cu, and Zn were reasonably similar. However, the premature flattening of the Fe breakthrough curve in Figure 6.9 was associated with a much larger and broader Mn overshoot. It is therefore suggested that it is an interaction between Fe and Mn that is responsible for the observed Fe behaviour. Under all flow conditions, Fe and Mn displayed similar profiles during the initial section of the breakthrough curve, and were responsible for the displacement of other ions from the column. At 5 BV/h as the column approached saturation, the strong affinity of the functional groups towards Fe(III) (McKevitt & Dreisinger, 2009) resulted in Mn being displaced and Fe displaying 'typical' breakthrough behaviour. However, as flow rate reduced further to 2 BV/h and the solution had longer residence time in the column, substitution of previously-loaded Mn by Fe had the dual simulataneous effects of re-adsorbing Fe from solution, hence reducing Fe C_t/C_o values, and accelarating the displacement of Mn which led to a greater degree of overshoot. The slight downward trend in concentration ratio observed for Fe in Figure 6.9 was likely a result of the rate of Fe substitution exceeding the ion presentation rate. This resulted in a steady reduction of effluent Fe concentrations relative to influent concentration, and therefore reducing C_t/C_o values, as opposed to the increasing concentration ratios encountered during typical column loading.

6.4.4   Puromet MTS9501

The chelating weak acid resin, S950, revealed a distinct affinity towards trivalent ionic Al and Fe when loaded at 10 BV/h (Figure 6.10). Such behaviour was also observed during pH screening experiments (Chapter 5), where very high extraction of these metals occurred across the entire range of [H^+] (Figure 5.6). The efficient extraction of Al and Fe was reported for S950 elsewhere when loaded with acidic PLS under dynamic conditions (Lv, et al., 2019), but little data exists regarding competitive multi-metal adsorption. Combination of the breakthrough profiles in Figure 6.10 coupled with operating capacities in Table 6.12 determined the selectivity order of S950 to be Al > Fe > Cu > Mn > Zn > Co > Ni. This selectivity series disagrees with the order published by Sofińska-Chmiel & Kołodyńska (2016) where a higher preference for Zn than Al was reported. However, it was not specified how this series was determined, and the discrepancies may be a result of the competitive loading conditions used in this work.

Reduction of solution flow rate had the effect of delaying breakthrough of all metals, as evidenced by the increased t_{50} values determined by Yoon-Nelson modelling (Table 6.12, Table 6.13, and Table 6.14). A longer time taken to reach 50% column loading implied a more effective metal removal at reduced flow and was the result of a narrowed exchange zone progressing through the column. At 10 BV/h flow rate, all metals apart from Al and Fe were displaced from the column by progressive loading of more-favoured metals, but concentration ratios remained under 1.2 (Table 6.12). As flow rate was reduced, the first metal to exhibit significant displacement was Mn (max. C_t/C_o = 1.65, 5 BV/h), followed by notable increases in Cu, Zn, Ni, and Co displacement at 2 BV/h. It therefore follows that increased solution residence time within the column leads to a delayed breakthrough, and for metals lower in the selectivity series an increased magnitude of displacement immediately following complete loading.

As for S957, the Fe breakthrough behaviour for S950 flattened at a C_t/C_o value below 1, in this case plateauing at approximately 0.8 at 10 and 5 BV/h (Figure 6.10 and Figure 6.11) and 0.5 at 2 BV/h

(Figure 6.12). The strong interaction between aminophosphonic acid functional groups and Fe (III) and Al (III) ions is well reported (Lv, et al., 2019; Page, et al., 2017). The point at which Fe begins to plateau during S950 treatment occurs concurrently with the start of Cu and Mn displacement (Figure 6.12), indicating that these may be related. During loading at 5 BV/h, when only Mn exhibited a clear displacement, Fe concentrations ratios levelled out at ~0.8. However, at 2 BV/h when both Cu and Mn exhibited similar displacement profiles, Fe concentration ratio plateaued much lower at ~0.5. This suggests that at intermediate flow rate, Fe-Mn exchange is responsible for the behaviour, with the effect amplified at 2 BV/h by additional Fe-Cu exchange when solutions have longer residence within the column.

6.4.5 Puromet MTS9140

As was the case for batch pH and sulfate concentration screening, no published data exists studying the fixed-bed adsorption of metals using Puromet MTS9140. Under dynamic operation, S914 displayed the same Cu-selective extraction properties as under previous batch experiments. All other metals present in the PLS reached complete breakthrough within the first 5 bed volumes and exhibited very little overshoot. The very small amount of overshoot observed in Figure 6.14, which increased slightly as flow rate decreased (Figure 6.15), indicated that upon entry to the column metals were momentarily adsorbed but rapidly displaced as Cu began to load. The fact that all other metals reach complete breakthrough long before Cu (BV5 compared to BV70+) indicated that it was not competition for remaining active sites that led to the displacement of metals, but perhaps instead that Cu was able extracted much faster than other metal ions. As previously described in Section 6.4.1, metal uptake is dependent on several sequential processes; 1) film diffusion of ions from the bulk solution to the resin surface, 2) diffusion of ions within the resin bead (intraparticle diffusion), and 3) the 'chemical/physical reaction' at functional sites, with the slowest of these processes controlling overall rate of extraction. Given the high concentration of the PLS, internal

mass transfer processes are likely controlling uptake rate (Helferrich, 1995). For organic exchangers which extract transition metals such as Cu via strong chelation mechanisms (e.g. iminodiacetic acid resins), it has been reported that the last of these sequential mechanisms (the interaction at functional sites) is generally rate-controlling (Harland, 1994). However, the proposed reductive Cu loading mechanism for S914, as detailed in Chapter 5, is assumed to oxidise thiourea groups very rapidly relative to diffusion given very high K_{eq} values for Cu compared to other metals (Table 6.1), thereby inhibiting their potential for concurrent uptake of other metals through slower processes, such as chelation.

All breakthrough models were able to describe metal loading to S914 with a high degree of accuracy (Table 6.15, Table 6.16, and Table 6.17), with the modified dose response generally outperforming other models for Cu. Results of MDR modelling revealed Cu operating capacities of 19.84 mg/g at 10 BV/h, 20.68 mg/g at 5 BV/h, and 32.04 mg/g at 2 BV/h. While Cu capacity at the high and intermediate flow rates were comparable, a notable increase in capacity was observed at the lowest flow rate. This was the result of a more effective extraction efficiency at the low flow rate, evidenced by delayed breakthrough point and longer column half-life (20.4 minutes) when compared to 5 BV/h (6 minutes) and 10 BV/h (3.3 minutes) operation.

Interesting to note is that despite the selectivity towards Cu, S914 did not have the highest Cu loading capacity of all the studied resins. Other resins with high calculated Cu loading capacities were S957 (max. 13.1 mg/g), S930 (max. 34.89 mg/g), and M4195, which was not able to be modelled for Cu given very limited breakthrough. Of these, S930 had a considerably higher Cu operating capacity at 10 BV/h (34.89 vs. 19.84 mg/g), with similar loading capacities at other flow rates. M4195 would be expected to have an even higher Cu operating capacity than S914 or S930 given a suitably loading period after Ni displacement. However, despite not having the highest operating capacity, the truly selective nature of Cu extraction by this resin under the tested conditions highlights the uniqueness and necessity of this resin for selective metal removal.

6.5   CHAPTER CONCLUSIONS

The results presented in this Chapter provided insight to the behaviour of selected resins towards metals under dynamic operation, and the effects that flow rate had on their extraction. Additionally, the experiments generated plentiful data on fixed-bed breakthrough behaviour using complex multi-component solutions; a rarity in the published scientific literature. A number of conclusions can be drawn from this work in terms of; a) general observations on the effect of competitive adsorption on breakthrough profile characteristics, which are of value to the wider ion exchange community, and b) resin characterisation and selection for the purpose of the current work.

1. Reduced flow rate had the general effects of delayed analyte detection in effluent solutions, and a sharpening of subsequent breakthrough curves. This was attributed to higher solution residence time in the column which allowed more time for metal extraction, especially for particle diffusion-controlled extraction. Curve sharpening was linked to the narrowing of exchange zones progressing through the column, resulting in total breakthrough ($C_t/C_o = 1$) occurring over fewer bed volumes.

2. Competitive adsorption resulted in a period of displacement (overshoot) for metals for which the resin was less selective. The magnitude and sharpness of the overshoot, where concentration ratios exceeded 1, was inversely proportional to flow rate; a result of the narrowed exchange zone also responsible for breakthrough curve sharpening.

3. The competitive extraction metals led to abnormal breakthrough behaviour for weak acid resins S930 and S950, and for mixed-functionality resin S957, particularly for Fe. This was attributed to Fe displacing previously bound ions, which in effect progressively increased the capacity of the resin for Fe, and so limited its breakthrough. The large overshoot periods for counter-ions during this phase of breakthrough supported this theory.

4. Three resins were selected for further study due to their applicability towards the treatment of the mine water PLS and potential for resource recovery. Puromet MTS9140 exhibited sole extraction of Cu from the simulant mine water, which along with its high operating capacity shows its usefulness for selective metal removal from mixed-metal waste streams. It is important to consider the effects of resin order when planning a coupled column system. By placing S914 first in the series, the second column will receive a much lower concentration of Cu; allowing a greater portion of resin capacity for other metals which may either be more ecotoxic or have higher recovery value. M4195 exhibited high selectivity and capacity towards Ni, alongside reasonable Co capacity. In the absence of Cu, these capacities are likely to increase following solution treatment by S914. For this reason, M4195 was also selected for further investigation. The final resin selected, Puromet MTS9570, was chosen for its ability to remove metals from a high volume of solution before breakthrough. This high capacity lends well to inclusion at the end of a coupled-column system to act as a 'scrubber' to limit metal release to the environment following water treatment.

Puromet MTS9501 was not selected for further study. While it did exhibit selectivity towards Fe, there is little value associated with selectively recovering this metal. Puromet MTS9301 was also disregarded for the final treatment system. Despite the identified high capacity for Cu, the selectivity towards Cu did not compete with that of S914.

The breakthrough studies presented allowed selection of resins based on their metal removal capabilities under fixed-bed operation. To determine the recoverability of metals after extraction by resins, it was deemed necessary to investigate the effectiveness of metal elution from loaded resins, and to determine the reusability of adsorbents over multiple treatment cycles; both of which could reduce treatment costs through revenue generation and reduction of material costs. The results of elution studies are presented in the following Chapter.

7   METAL ELUTION AND RESIN REUSABILITY STUDIES

7.1   CHAPTER INTRODUCTION

The previous chapter of this thesis has shown how metals may be selectively extracted from a complex mixed metal sulfate waste stream via dynamic column operation, and how the effects of flow rate affected recovery. Specifically, slower flow rates were associated with delayed breakthrough of metal ions and sharper ion breakthrough profiles but had only marginal effects on metal capacity. Of the resins selected from Chapter 6, favourable capacities were determined towards the metals for which they will be primarily used to target; S914 having a Cu operating capacity of 21 mg/g (MDR), M4195 having a Ni capacity of 21 mg/g (MDR), and S957 showing fairly uniform capacities (in the region of 9.2 mg/g) for Fe, Mn, and Zn at 5 BV/h.

Having quantified and identified suitable resins for this application, attention here shifts to recovering the extracted metals from the loaded resins. An effective resin elution process will ideally produce a concentrated metal product stream and regenerate the resin for re-use. The aim of this chapter is to identify suitable eluents and determine the concentration ranges in which metal recovery is maximised for each of the three resins. Investigations of resin re-usability were performed to quantify changes in metal uptake and recovery over multiple adsorption, desorption, and regeneration cycles; a key consideration for process design and system longevity.

The effectiveness of metal recovery from loaded ion exchange resins is a critical parameter for the assessment of resin suitability towards an engineered process. While not required for processes where spent adsorbent is directly converted to a waste form (e.g. direct vitrification or concrete encapsulation of functionalised silica adsorbents in nuclear waste remediation/ fuel reprocessing (e.g. Amphlett, et al., 2020; Garino, et al., 2011), efficient elution is essential for a system whereby the adsorbent is intended for re-use. Regeneration of resins allows for reduction in the costs of waste treatment through the reduced requirement for adsorbent replacement, and by allowing the capital

expenditure of adsorbent procurement to be offset over multiple treatment cycles through the production of a concentrated metal-rich effluent (Ebrahimi & Roberts, 2013).

7.2   SPECIFIC METHODS

7.2.1   Elution Profile Identification and Analysis

The loading of columns prior to elution experiments was carried out using 200 mg/L solutions which only contained the target metals for each resin, namely; Cu for S914, Co and Ni for M4195, and Fe, Mn, Zn for S957. Columns were loaded at 5 BV/h as standard, with further details provided in each respective section below.

Plotting effluent metal concentration (mg/L) as a function of eluent throughput (L) allowed visualisation of elution profiles, from which the area beneath the curve was indicative of the mass of metal (mg) recovered. To calculate this area, the Peak Analyzer tool of OriginPro 2018b graphing software was used to identify the start and end points of each elution curves using the following procedure. First, peaks were identified using a 'local maximum' approach, although given the nature of the resulting elution profiles, these were also easy to identify visually. After the base markers for each peak were identified, area was quantified by integration using the minimum y-value as a constant baseline to account for detection limits in AAS analysis.

Integration was used to determine the mass of metal ions adsorbed to the resin during the loading phase also, using the influent metal concentration as a boundary to calculate the area above the loading curve. While in the previous chapter this was done by breakthrough modelling, resins in this chapter were not necessarily loaded to an extent which would facilitate such numerical analysis. The calculated loading and elution masses were used to determine elution efficiency as per Equation 7.1. For M4195 elution experiments, two consecutive eluents were used on each column; the first to recover Co, the second to target Ni. Recovery of Co was calculated as per Equation 7.1, but Ni

recovery efficiencies were calculated accounting for the mass of Ni co-eluted during the first eluent

contact (Equation 7.2). Using this formula, it was possible to factor in only the loaded Ni which was

available to the second eluent, and therefore provide a more accurate assessment of the efficiency

of the Ni-targeted eluent.

Equation 7.1. Recovery efficiency calculation; M_E = mass of metal eluted, M_L = mass of metal loaded.

$$Recovery\ (\%) = \left(\frac{M_E}{M_L}\right) \times 100$$

Equation 7.2. Ni recovery efficiency calculation for M4195 elution experiments; M_C = mass of Ni co-eluted during previous eluent contact.

$$Recovery\ (\%) = \left(\frac{M_E}{M_L - M_C}\right) \times 100$$

7.2.2   Ion Chromatography (IC) Analysis

Samples from the elution of Puromet MTS9140 using 0.5 M $NaClO_3$ were analysed for their anion

concentrations; specifically, Cl^-, ClO_3^-, and SO_4^{2-}. To avoid interference by the presence of a nitrate

peak, effluent samples were diluted using 18 MΩ DI water. The IC eluent (4.5 mM Na_2CO_3 and 803

µM $NaHCO_3$ in 18 MΩ DI water) and acid regenerant (0.1 M H_2SO_4) were freshly prepared prior to

analysis. Instrument calibration was performed using four mixed-anion (Cl^-, ClO_3^-, and SO_4^{2-})

standards prepared by dilution of certified single-metal IC standards to a range of $0 - 200$ mg/L using

18 MΩ DI water. Before calibration, the IC detector was allowed to equilibrate for 20 minutes until

detector readings stabilised. 1 mL of standard was injected to the IC such that the sample loop was

completely flushed of the previous solution and filled with the solution to be analysed, eliminating

contamination between analytical runs. This same protocol was followed during sample analysis after

instrument calibration. Good linear calibration was achieved for Cl^-, ClO_3^-, and SO_4^{2-} using this

method, with R^2 values of 0.9999, 0.9995, and 0.9994, respectively. Elution peaks for each ion were clearly separated and easily distinguishable (Figure 7.1), allowing for accurate integration of peak area and determination of anion concentrations. The negative peak in Figure 7.1 at 2.25 min, termed the 'water dip', is not an uncommon phenomenon when using an anion analysis method on samples diluted with water, and is the result of the sample ionic strength being lower than the ionic strength of the eluent (Dionex Corporation, 1998; Lachat Instruments, 2009). However, as the elution of chloride occurred well beyond the water dip, the water dip did not interfere with analyte peak identification.
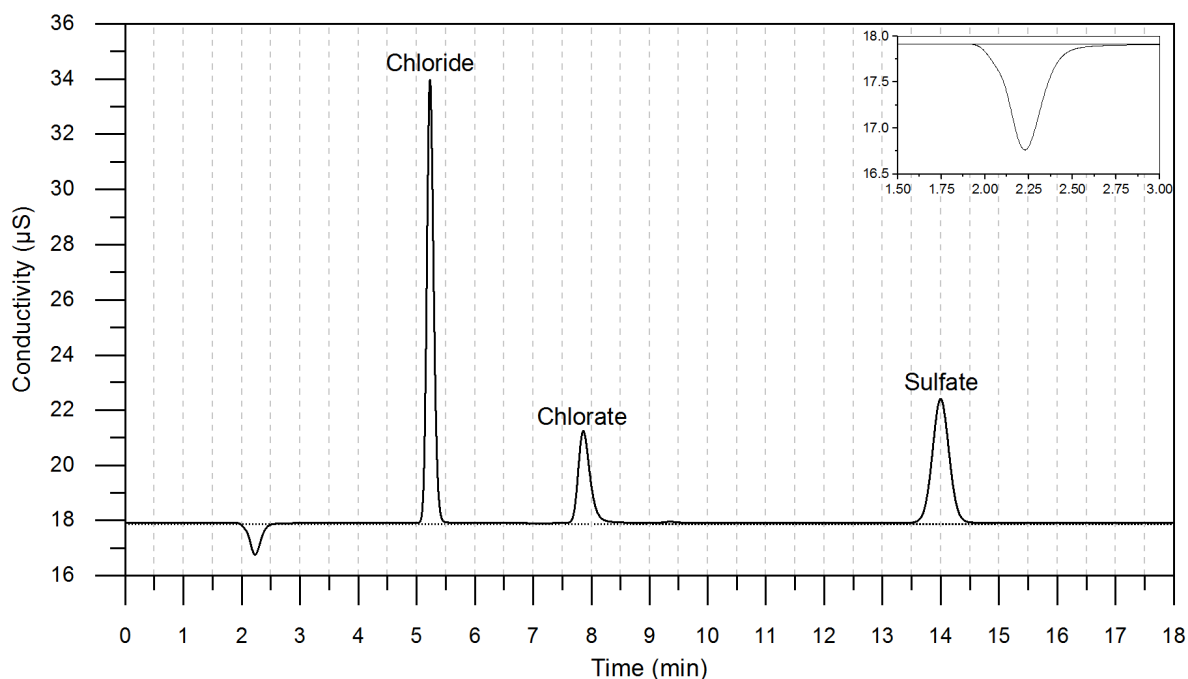
Figure 7.1. Example IC chromatogram of a 10 mg/L mixed anion standard for example. Note the clear separation of peaks allowing for accurate concentration determination. Subset graph (top right) better displays the water dip phenomenon. Flow rate: 0.7 mL/min, pressure: 10.3 MPa.

7.3   RESULTS

7.3.1   Elution of Copper from Puromet MTS9140 using Sodium Chlorate (NaClO₃)

The reductive extraction mechanism of Puromet MTS9140 (Chapter 5) required an oxidative eluent

to be applied to liberate Cu(I) as Cu(II) from the resin functionality. While no literature exists on the

elution of Cu from Puromet MTS9140 specifically, a limited number of articles do exist that explore

the elution of Cu from non-commercial dual-functionalised resins containing, among other groups,

thiourea functionality. One such paper reports effective batch Cu recovery from a thiourea/acyl

bifunctional resin using concentrated nitric acid (equivalent to 3.0 M) as an eluent (Huang, et al.,

2017). While nitric acid was explored for its potential application for Cu elution from S914, these

results are provided in the Appendix given concerns over gas formation. Sodium chlorate, an

alternative oxidant, was explored in detail in place of HNO_3.

A packed column of S914 was fully loaded using a 200 mg/L solution of $CuSO_4$ and rinsed thoroughly

using deionised water before introduction of the sodium chlorate eluent. The elution profile of Cu

from S914 using a 0.5 M solution of $NaClO_3$ at pH 2 is presented in Figure 7.2. The concentration of

Cu in effluent solutions increased sharply beyond 4 BV throughput, reaching a maximum

concentration of 511 mg/L at 20 mL (~14 BV) throughput. Following the maximum, Cu concentration

exhibited a steep decline, which gradually levelled out to below 10 mg/L by the end of the

experimental run; allowing the complete profile to be captured. Integration of the area below the

curve (Table 7.1) revealed effective Cu elution by this eluent, with an overall Cu recovery percentage

of 78.91 %.
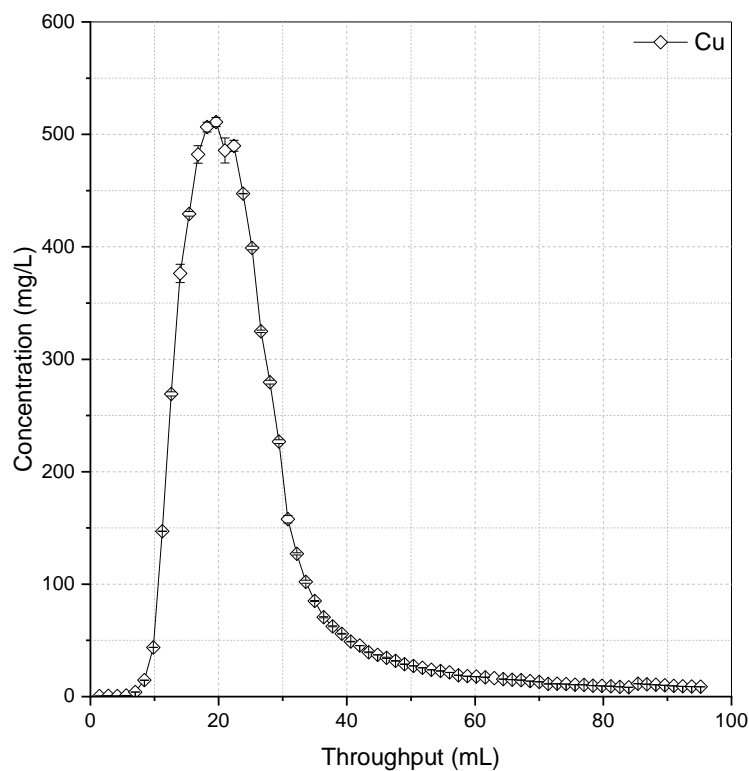
Figure 7.2. Elution of Cu from S914 using 0.5 M NaClO$_3$ at pH 2 (HCl matrix, 2 BV/h).

Doubling the concentration of sodium chlorate had the effect of increasing the maximum Cu concentration to 612 mg/L (Figure 7.3). Despite the higher maximum Cu concentration recorded, the width of the elution curve (FWHM) was smaller than that in Figure 7.2, resulting in a recovery efficiency of 81.86%; fairly similar to the Cu recovery using 0.5 M NaClO$_3$ (Table 7.1). Following elution using 1 M NaClO$_3$, a slight but notable colour change was observed, with the 1M-contacted S914 taking on a grey hue when compared to the 0.5 M-contacted resin (Figure 7.4). It is theorised that this grey colouration is the result of copper oxide formation on the surface of the resin bead.
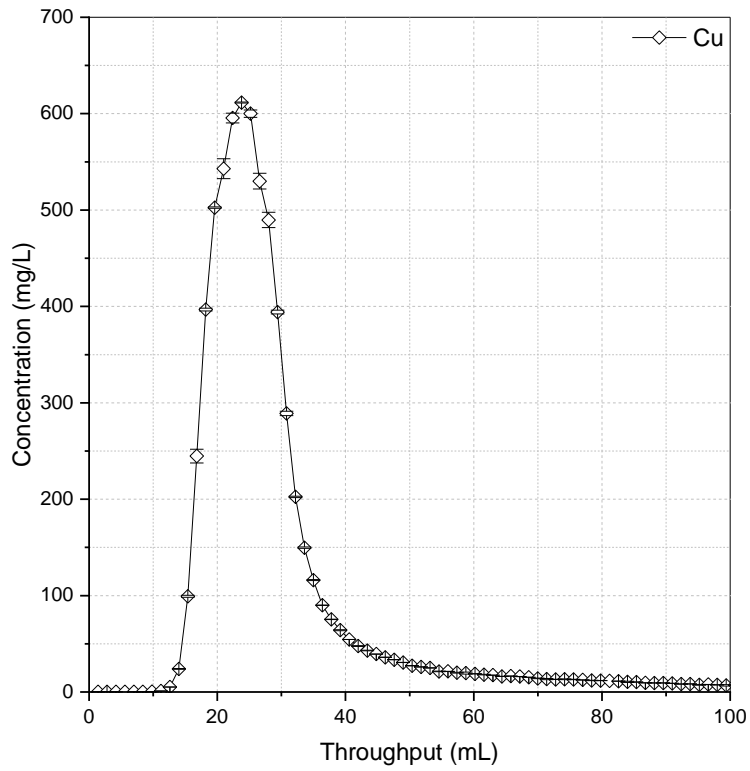
Figure 7.3. Elution of Cu from S914 using 1 M NaClO$_3$ at pH 2 (HCl matrix, 2 BV/h).
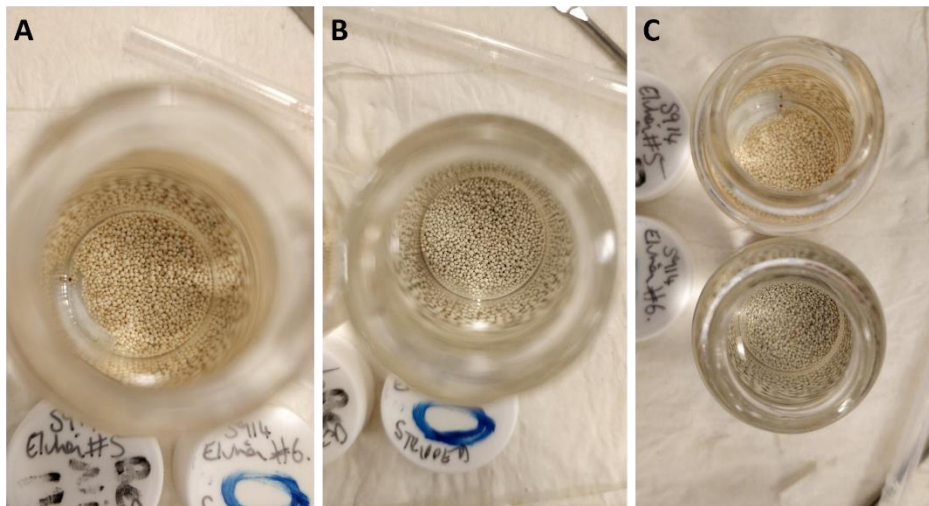
Figure 7.4. S914 colour after Cu elution using sodium chlorate; A) 0.5 M NaClO$_3$, B) 1 M NaClO$_3$, C) comparison of 0.5 M (top) and 1 M (bottom) NaClO$_3$ treatment.

Table 7.1. Details of Cu elution investigations using NaClO₃ (FWHM = Full width at half maximum; provided for comparison of curve widths).

Eluent	Loading Method	Cu loading	Bed Volume	Total Cu available	Cu recovered	FWHM	Recovery efficiency
		mg/mL	mL	mg	mg	mL	%
0.5 M NaClO₃	Batch	8.6405	1.4	12.10	9.55	16.2	78.91
1 M NaClO₃	Batch	8.3577	1.4	11.70	9.58	13.2	81.86

7.3.2   Stability of Puromet MTS9140 over Repeated Loading/Elution Cycles

To determine the reusability of S914 resin for the selective extraction of Cu, repeated loading, elution, and preconditioning cycles were performed. The 0.5 M NaClO₃ eluent was used given its effectiveness in eluent screening experiments (Figure 7.2). While the 1 M eluent did have a marginally higher recovery efficiency, the lack of resin discolouration indicated that 0.5 M NaClO₃ was a better option for investigating reusability. The resulting breakthrough curves are presented in Figure 7.5.

During the first loading cycle, typical Cu adsorption behaviour was observed, with complete breakthrough encountered at 40 BV throughput (Figure 7.5). Analysis of the area above the breakthrough curve (with an upper boundary of PLS concentration) indicated the adsorption of 7.95 mg Cu during the first loading cycle. Following Cu elution, the resin bed was loaded again using the 400 mg/L Cu solution, but exhibited very low adsorption of Cu, with only 1.55 mg of Cu removed before complete breakthrough occurred during both the second and third loading cycles (Table 7.2).
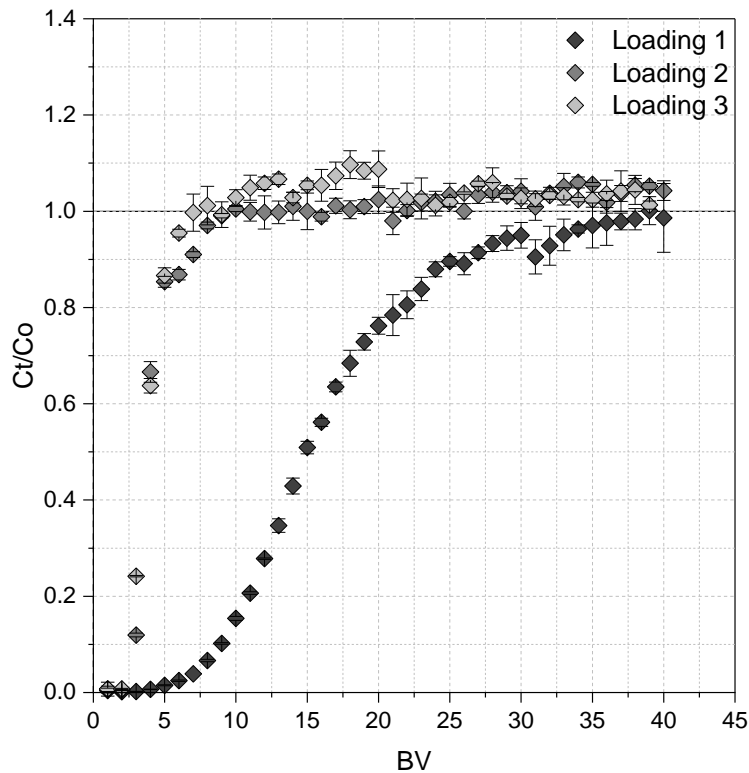
Figure 7.5. Breakthrough curves of Cu from S914 over repeated loading cycles (1.4 mL BV, 5 BV/h; 400 mg/L Cu, pH 1.55).

Comparison of elution curves using 0.5 M $NaClO_3$ (Figure 7.6) revealed that for the first cycle, where 7.95 mg Cu was loaded to the resin bed, 6.79 mg was recovered, equating to a recovery efficiency of 85.34 % (Table 7.2). The elution profile generated increased sharply, reaching a maximum Cu concentration of 418 mg/L after 0.028 L, before decreasing in an almost-symmetrical fashion, indicating effective desorption.

The considerably lower extent of Cu extraction during the second and third loading cycles (Figure 7.5) was reflected in the elution profiles for the respective cycles (Figure 7.6). Analysis of loading and elution curves (Table 7.2) revealed a decrease in the mass of Cu loaded during each cycle (from 7.95 to 1.55 mg), coupled with a decrease in the total amount of Cu adsorbed to the column (from 7.95 to

1.73 mg). The mass of Cu eluted declined greatly, with a recovery efficiency dropping from 85.34 % in

cycle one to only 41.61 % during elution cycle three (Table 7.2).
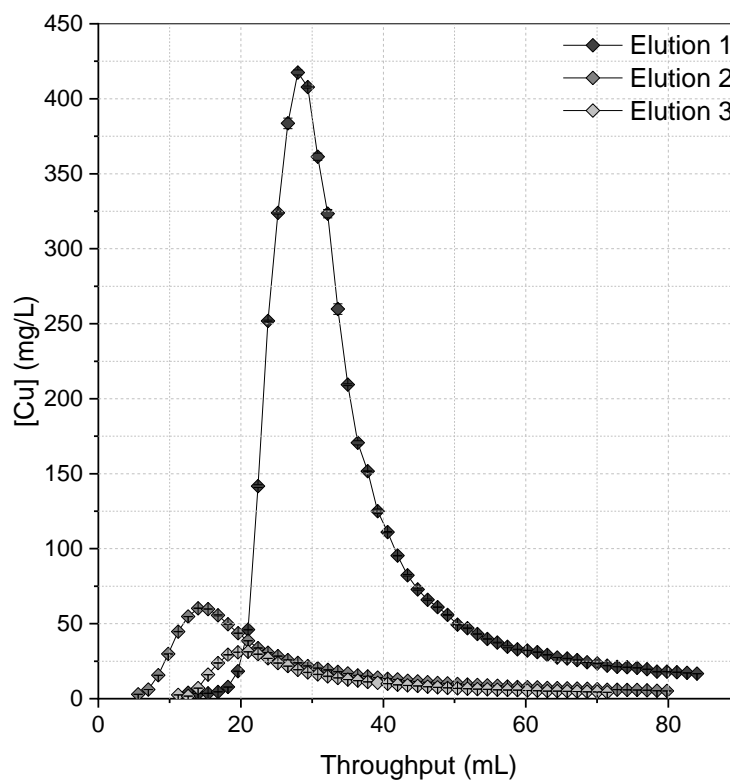
Figure 7.6. Elution of Cu from S914 using 0.5 M NaClO$_3$ (pH 2, HCl matrix, 2 BV/h) over repeated elution cycles.

Table 7.2. Masses of Cu loaded and eluted from S914, and residual Cu following elution over multiple
operational cycles. 'Total Cu' refers to amount of Cu on resin at end of each loading cycle. Recovery calculated
as percentage of Total Cu liberated during each elution cycle.

	Residual mg	Loaded mg	Total Cu mg	Eluted mg	Recovery %
Cycle 1	-	7.95	7.95	6.79	85.34
Cycle 2	1.16	1.55	2.71	1.37	50.55
Cycle 3	0.18	1.55	1.73	0.72	41.61

7.3.2.1 Degradation Mechanism of S914 During NaClO₃ Elution

It is evident that while Cu can successfully and efficiently be recovered from S914, a cuprous

oxidation approach to elution is unsuitable for maintaining the functionality of the resin for reuse. To

better understand the degradation of S914, Cu elution using 0.5 M $NaClO_3$ was repeated on a Cu-

loaded column (Figure 7.7), with effluent bed volumes being sampled and analysed by anion

chromatography.
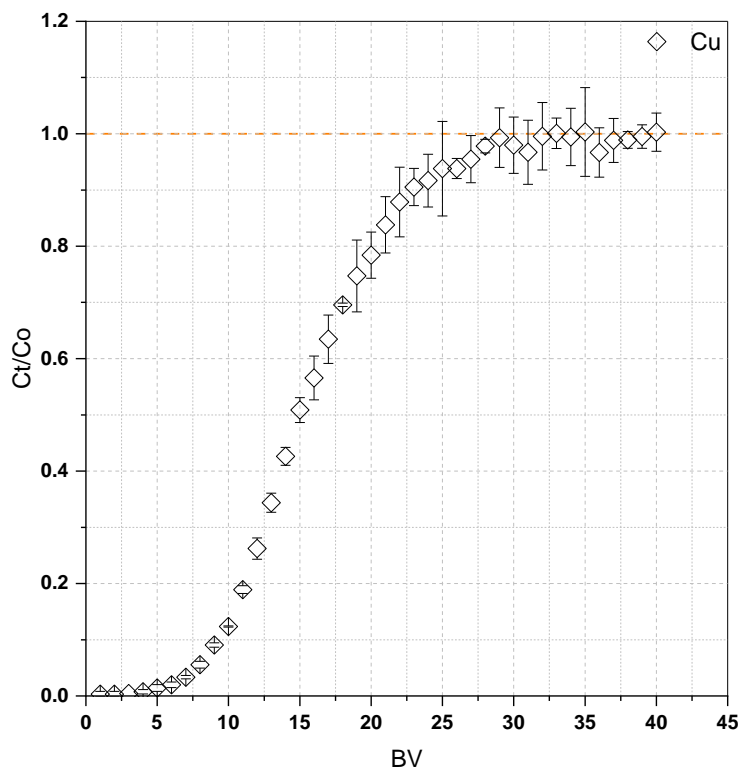
Figure 7.7. Breakthrough curve of Cu loading to S914 for resin degradation experiment ([Cu] 200 mg/L, pH 1.55,
BV: 1.4 mL, 5 BV/h. Thomas model Q_o 20.5 ± 0.11 mg/g, R^2 = 0.998).

During elution of Cu, an increase in pH was observed in effluent solutions, reaching pH 3.13 at 7 BV

throughput (Figure 7.8); an increase of 1.18 pH units from the native pH of the eluent used (pH 1.95).

A lag of 5 BV was observed until peak Cu elution, which occurred after 12 BV and reached a

concentration of 604 mg/L.
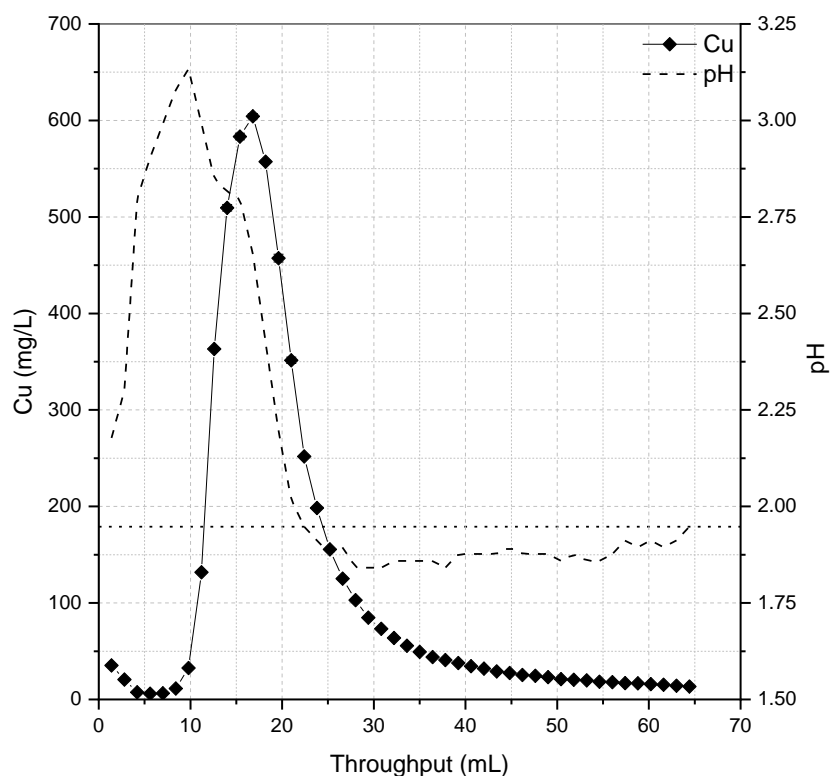
Figure 7.8. Cu concentration and pH of effluent solutions during elution of Cu from S914 at 2 BV/h using 0.5 M NaClO$_3$ (pH 1.95, HCl media: dotted horizontal line represents pH of eluent).

Given that the chlorate ion is fundamental to the oxidation of the Cu(I) centre, it was theorised that a peak in chloride would occur alongside Cu elution, and so this was analysed for by IC, as well as sulfate concentrations. The concentrations of Cl$^-$ and SO$_4^{2-}$ are presented alongside the Cu elution profile below in Figure 7.9. A spike in chloride concentration was observed simultaneously with maximum Cu elution, with a concentration of 0.02 M Cl$^-$ (714 mg/L). A substantial increase in sulfate concentration (maximum 0.085 M SO$_4^{2-}$ (5646 mg/L)) was also detected, occurring prior to the maxima of Cu and Cl, and before the period of increased pH.
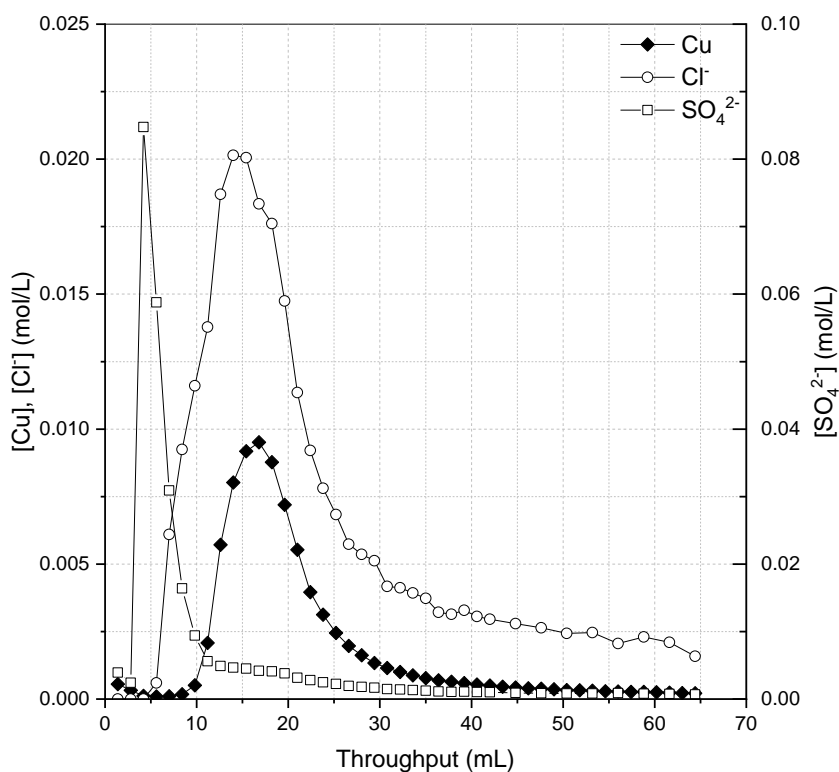
Figure 7.9. Concentrations of Cu, chloride, and sulfate in effluent solutions during elution of S914 at 2 BV/h using 0.5 M $NaClO_3$ (pH 1.95, HCl media, same Cu elution profile as presented in Figure 7.8).

7.3.3   Selective Elution of Co and Ni from Dowex M4195 through pH Control

Given the notable effect that solution pH had on the batch extraction of metals from solution by Dowex M4195 (Figure 5.2), a pH-controlled approach to metal elution was investigated to selectively elute cobalt and nickel as distinct product streams. The use of an acid elution also had the dual benefit of reconditioning the resin to its proton form, allowing immediate reuse of the resin for metal extraction without the requirement of a separate preconditioning cycle. The pH conditions at which 50, 25, and 10 % extraction of the metals was achieved were selected for eluent solutions.

7.3.3.1   *Elution Using pH$_{50}$ Values*

Batch pH screening results presented in Chapter 5 were used to calculate the pH$_{50}$ values of Co and Ni extraction by M4195. These were identified as 0.04 M H$^+$ and 0.3 M H$^+$ for Co and Ni, respectively, and so sulfuric acid eluents at these concentrations were initially used for M4195 regeneration.

Upon introduction of the first eluent to the loaded column, a distinct and sharp Co elution profile was observed, reaching 289 mg/L after 18 mL throughput (Figure 7.10). Following maximum elution, Co concentrations in effluent solutions rapidly declined, reaching approximately 0.3 mg/L by the time the second eluent was pumped through the column. Analysis of the area indicated the elution of 1.94 mg Co, equating to a recovery efficiency of 82.16 % (Table 7.3). During the Co elution cycle, minimal Ni concentrations were recorded in the eluent streams (0.03 mg/ 1.44 %).

The Ni-targeted eluent was introduced to the column immediately following the previous eluent. While a Ni elution peak was present shortly after eluent contact with the bed, the profile indicated a less-efficient recovery. Ni concentration in effluent solutions reached 58.7 mg/L, after which a long trailing decay in concentration occurred which was not fully captured during the experimental period. Analysis of the curve areas during this phase revealed a recovered mass of 1.55 mg Ni, equating to a recovery percentage of 67.39 %. During elution using 0.3 M H$^+$, contamination of the Ni product stream by Co was observed, evidenced by a small but sharp elution profile (max. 17.6 mg/L) at 56 mL throughput, which corresponded to 0.06 mg Co – 2.39 % of the Co initially loaded to the column.
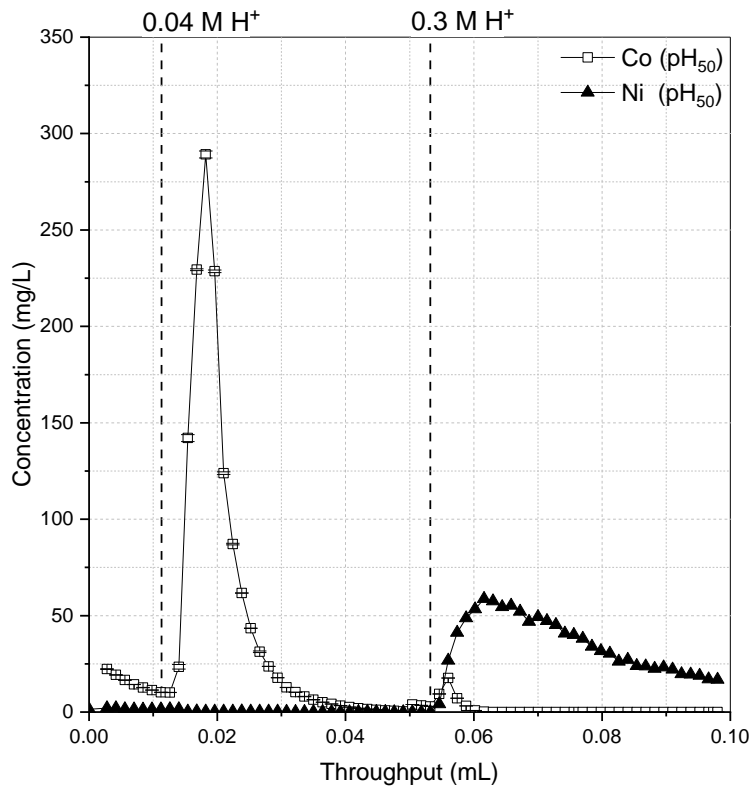
Figure 7.10. Elution of Co and Ni from M4195 at 2 BV/h using sulfuric acid at pH_{50} values (0.04 and 0.3 M H^+).

Table 7.3. Masses recovered and efficiency of Co and Ni elution from M4195 using sulfuric acid eluents at pH_{50} values.

	Cobalt		Nickel	
	Elution (mg)	Recovery (%)	Elution (mg)	Recovery (%)
Eluent 1	1.94	82.16	0.03	1.44
Eluent 2	0.06	2.39	1.55	67.39

7.3.3.2   Elution Using pH_{25} Values

Sulfuric acid solutions of 0.08 M and 0.5 M H^+ were used to represent the conditions under which 25

% extraction of Co and Ni occurred during batch screening experiments. During contact with 0.08 M

H^+ acid, a sharp elution profile for Co was recorded, reaching a maximum concentration of 548 mg/L

136

before quickly dropping below detection limits by 0.03 L throughput (Figure 7.11). Curve integration revealed that 2.22 mg of Co was eluted, which indicated a recovery efficiency of 95.82 %.

While Co recovery was high, the increased acidity of the first eluent also had the effect of displacing a small but considerable amount of Ni from the column. This was calculated to be 0.68 mg, or 27.12 % of the Ni loaded to the column. However, it was noted that most of this Ni was displaced from the column after the Co elution profile had stabilised, and so through careful optimisation of eluent cycle times, the release of Ni during the Co elution phase could be minimised.

During the Ni-targeted elution phase using 0.5 M H^+ sulfuric acid, a Ni elution curve with a sharp frontal profile was observed. The maximum Ni concentration encountered was 130.7 mg/L, accounting for 92.88 % (1.70 mg) of the extracted Ni (Table 7.4). While Ni recovery during the second eluent phase was high, it is worthwhile to note that this could have been improved through better experimental operation. It was apparent that following the decay of the Co elution profile, the concentrations of Ni in effluents steadily increased before introduction of the second eluent (in the range of 20 – 50 mL throughput; Figure 7.11). Had the second eluent been introduced at the 20 mL throughput point, a higher mass of Ni would have been present in the effluent of the second elution step and therefore would have improved the overall efficiency of the 0.5 M eluent.
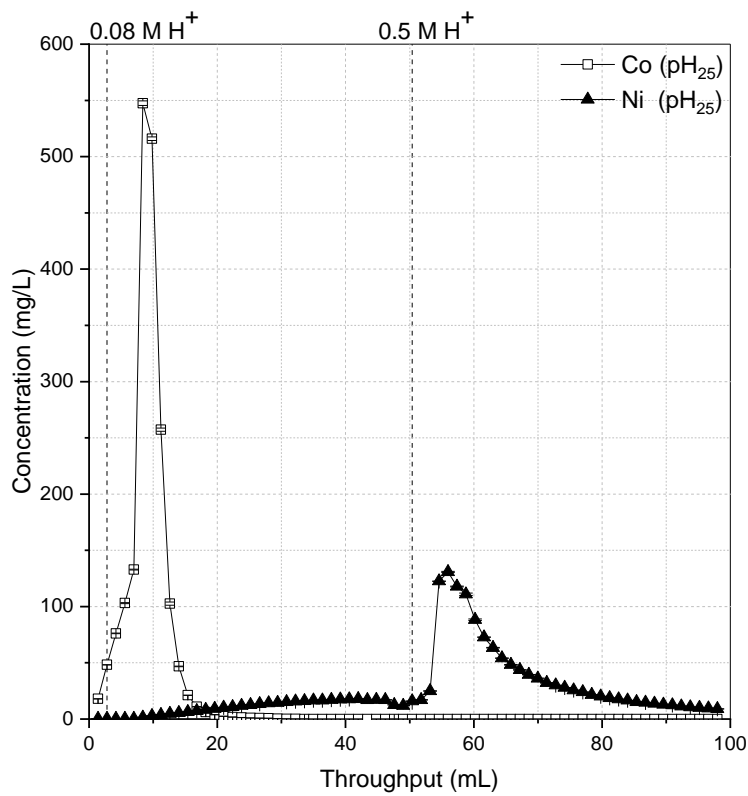
Figure 7.11. Elution of Co and Ni from M4195 at 2 BV/h using sulfuric acid at pH_{25} values (0.08 and 0.5 M H^{+}).

Table 7.4. Masses recovered and efficiency of Co and Ni elution from M4195 using sulfuric acid eluents at pH_{25} values.

	Cobalt		Nickel	
	Elution (mg)	Recovery (%)	Elution (mg)	Recovery (%)
Eluent 1	2.22	95.82	0.68	27.12
Eluent 2	0.00	0.00	1.70	92.88

7.3.3.3   Elution Using pH_{10} Values

Elution of Co and Ni from M4195 using sulfuric acid solutions at 0.15 M and 1 M H^{+}, respectively, proved highly effective. During the first eluent contact, a sharp and reasonably symmetrical elution profile for Co was observed, indicating the movement of a high-concentration gradient through the

column during elution (Figure 7.12). Maximum Co concentration during this eluent phase was 574 mg/L, and accounted for 100 % of the Co loaded to the column (Table 7.5). As for Figure 7.11, the presence of Ni in the Co-targeted effluents occurred while using 0.15 M H$^+$ sulfuric acid, with release of 0.65 mg Ni, equal to 23.13 % of the total available Ni.

Ni elution using 1 M H$^+$ sulfuric acid resulted in a well-defined elution profile with a steep frontal curve and short decay length (Figure 7.12). Integration of the area revealed that 2.12 mg of Ni was eluted using this eluent, equivalent to a 98.60 % recovery efficiency when factoring in the co-eluted Ni from the previous eluent (Table 7.5). Over the entire elution cycle (both eluents), 98.93 % of all extracted Ni was recovered, again indicating that with proper process optimisation the proportion of Ni in the Ni-targeted eluent stream could be improved. Given the complete elution of Co during the first eluent phase, very little Co was present in the second, more concentrated eluent (Table 7.5).
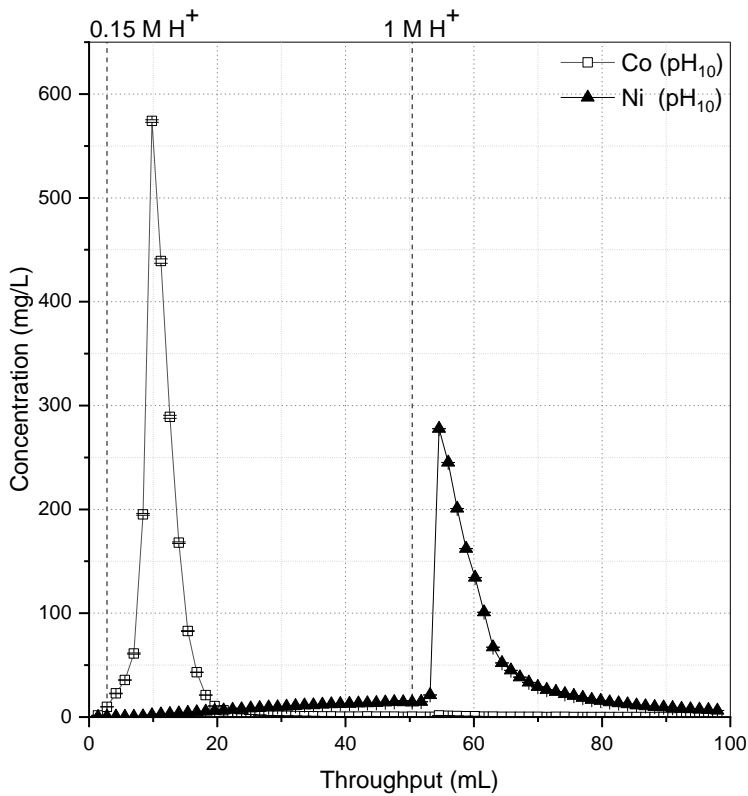
Figure 7.12. Elution of Co and Ni from M4195 at 2 BV/h using sulfuric acid at pH_{10} values (0.15 and 1 M H$^+$).

Table 7.5. Masses recovered and efficiency of Co and Ni elution from M4195 using sulfuric acid eluents at pH_{10} values.

	Cobalt		Nickel	
	Elution (mg)	Recovery (%)	Elution (mg)	Recovery (%)
Eluent 1	2.64	107.44	0.65	23.13
Eluent 2	0.01	0.35	2.12	98.60

7.3.3.4   Comparison of M4195 pH-controlled Elution

When viewed alongside each other, the differences between Co and Ni elution profiles as a function

of eluent acid concentration became more apparent (Figure 7.13). For Co, a distinction between the

lateral position of profile maxima can be observed, with the highest Co concentration for the pH_{50}

eluent occurring 5-6 bed volumes later than for the other two eluents. The maximum concentration recorded for the pH_{50} eluent also differed substantially compared to the two more concentrated eluents, which showed relatively little variation (548 mg/L and 574 mg/L for the pH_{25} and pH_{10} eluents, respectively). When considering Co recovery, a direct relationship between increased eluent concentration and higher elution efficiencies can be observed (Figure 7.14).

Comparison of Ni elution profiles (Figure 7.13) revealed a clear trend in profile shape, magnitude, and position. A distinct increase in height is apparent with higher acidity eluents, with maximum concentrations reaching 58.7, 130.7, and 277.7 mg/L Ni for the pH_{50}, pH_{25}, and pH_{10} eluents, respectively. Alongside this height increase, a narrowing of profile width was observed, with the FWHM values (in order of increased acidity) being 25, 9, and 6 mL. Increased height and narrowing of elution profiles indicated more favourable Ni elution as a function of increased proton concentration in eluent solutions. This is further backed up by the gradual increase in Ni recovery efficiency during each eluent screening (Figure 7.14).
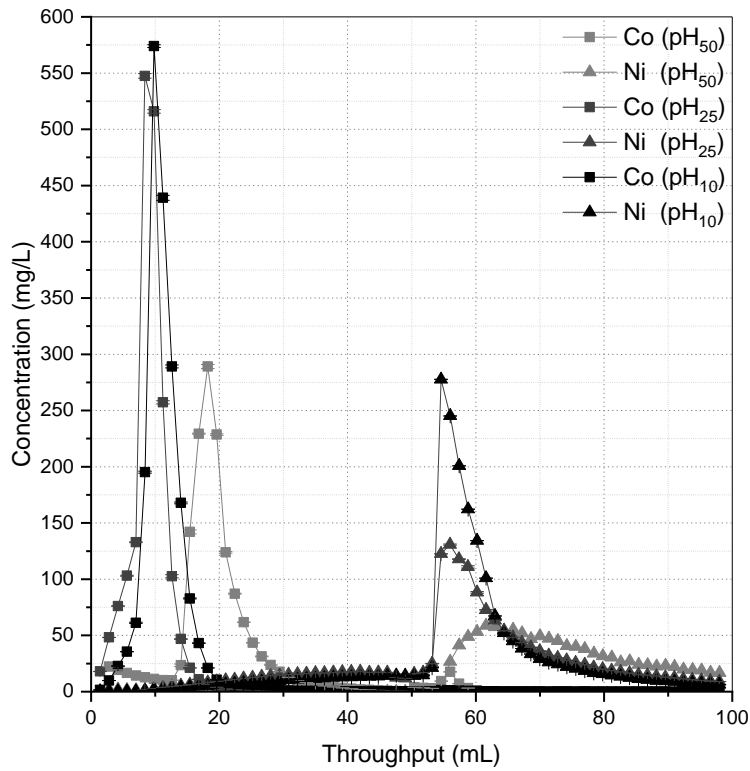
Figure 7.13. Comparison of Co and Ni elution profiles using H_2SO_4 solutions at varying pH values (2 BV/h).
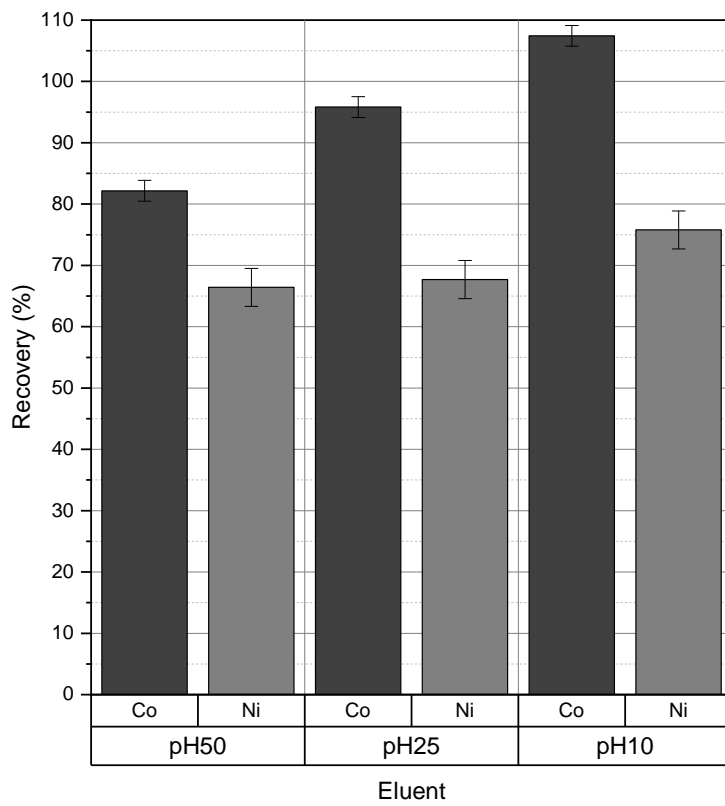
Figure 7.14. Comparison of calculated Co and Ni recovery efficiencies from M4195.

7.3.4   Stability of Dowex M4195 over Repeated Loading/Elution Cycles

To investigate the durability and reusability of M4195 during repeated loading and elution cycles, it was first necessary to select the most appropriate eluents for each targeted metal elution. For Co, the pH_{25} eluent (0.08 M H^+) was chosen given the high recovery efficiency (95.82 % (Table 7.4)). Despite Co recovery being higher for the 0.15 M H^+ eluent (Figure 7.14), 0.08 M H^+ was selected given the reduced extent of Ni co-elution observed during for this eluent during screening experiments (Table 7.4 and Table 7.5). For Ni elution, the pH_{10} eluent (1 M H^+) was selected given superior recovery efficiencies (Table 7.5 and Figure 7.14) and highest concentrations of effluent solutions (Figure 7.13). Additionally, the use of 1 M H^+ during the second elution cycle ensured that in the case of no degradation, functional sites were more effectively regenerated to their proton form prior to the subsequent resin loading cycle.

Figure 7.15 revealed that M4195 was resilient towards repeated loading and elution, with very little variation between elution profiles over the four cycles. As in prior screening results, the Co and Ni profiles produced by the 0.08 and 1.0 M H^+ eluents were very sharp in the lead up to concentration maxima, followed by a rapid decay to negligible concentrations. Additionally, the masses of Co and Ni loaded to and eluted from the M495 column remained reasonably consistent over each experimental cycle (Table 7.6), as do the percentage recoveries of both metals (Figure 7.16). The higher Ni recovery percentage during elution cycle 4 is attributed to a different batch of eluent being used for Ni elution during that particular cycle.
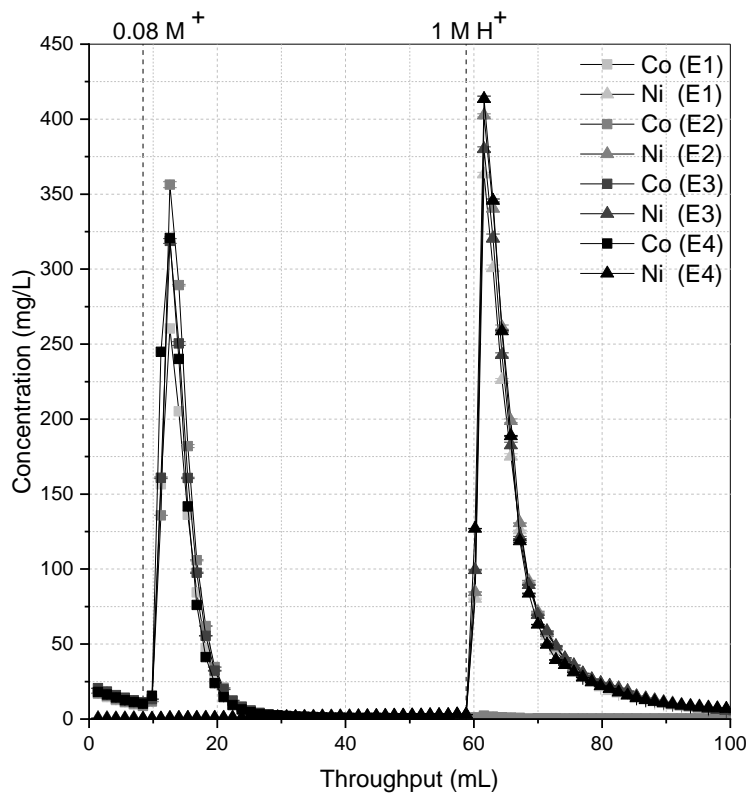
Figure 7.15. Elution of Co and Ni from M4195 at 2 BV/h using 0.08 and 1 M H+ (as H_2SO_4) over repeated loading and elution cycles.

Where Figure 7.15 does differ from previous elution screening results is in the fact that more Ni and less Co was initially loaded to the columns during the loading cycle, as evidenced by lower maximum concentrations for Co than Ni as compared to the higher concentrations for Co on previous elution Figures (e.g. Figure 7.13). This has been attributed to probable human error when measuring the resin quantity for column packing, resulting in slightly more displacement of Co by Ni during the loading cycle (i.e. a loading cycle of 10 BV was performed assuming a bed volume of 1.4 mL, however, if the bed volume was smaller, a relatively higher volume of PLS passed through the column during the loading phase). This does not affect the legitimacy of the results presented in Figure 7.15, but does explain the differences when contrasted with prior elution screening Figures.

Table 7.6. Masses of Co and Ni loaded and eluted from M4195 over multiple operational cycles.

Cycle	Metal	Loading (mg)	Elution (mg)
1	Co	2.731	1.374
	Ni	3.334	2.562
2	Co	2.733	1.742
	Ni	3.298	2.819
3	Co	3.017	1.731
	Ni	3.366	2.714
4	Co	2.908	1.732
	Ni	2.867	2.787
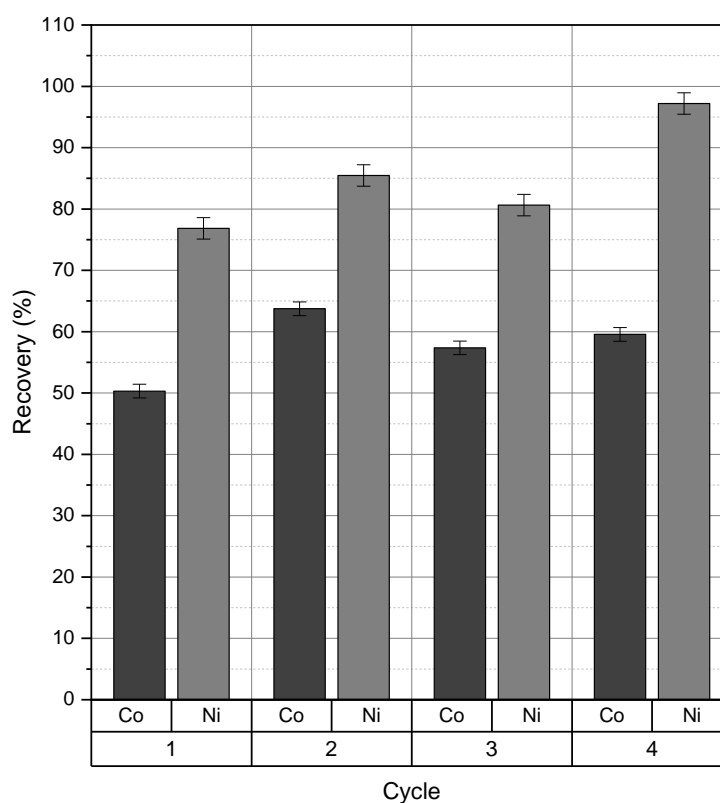
Figure 7.16. Recovery efficiencies (%) of Co and Ni from M4195 during each elution cycle.

7.3.5 Extraction of Iron, Manganese, and Zinc by Puromet MTS9570

It was revealed in Chapters 5 and 6 that S957 had high potential for the indiscriminate removal of metals from solution, with a high dynamic operating capacity for all studied metals. Working under

the assumption that S914 targets Cu, and M4195 removes Ni and Co prior to the PLS reaching the

S957 column, the dynamic adsorption characteristics of S957 in a tri-component solution of Fe, Mn,

and Zn was first determined.

Figure 7.17 presents the breakthrough curves of Fe, Mn, and Zn from a 1.4 mL column of S957, with

influent metals concentrations of 200 mg/L at pH 1.56. During the first 25 BV of solution, effluent

concentrations were negligible for all three metal ions, after which breakthrough occurred at

different rates. For Mn, the resulting breakthrough curve was the least-sharp of all metals and

displayed an almost linear increase in concentration ratio before reaching C_t/C_o of 1 after 70 BV

throughput. The Fe breakthrough curve was reasonably sharp and reached a value of 1 after 49 BV of

solution were pumped through the column. After reaching a C_t/C_o value of 1, the concentration ratio

of Fe appeared to stabilise; the slight drop being attributed to analytical discrepancies during AAS

analysis, as evidenced by the larger error bars on data points towards the end of the experiment.

After reaching complete breakthrough, Zn began to be displaced from the column by the continued

loading of Fe and Mn, resulting in a large overshoot beyond BV 40 (maximum C_t/C_o = 1.73, 46 BV).

For subsequent elution experiments, a loading cycle of 30 BV was selected, given the similar degree

of loading between the three metal ions at this point.
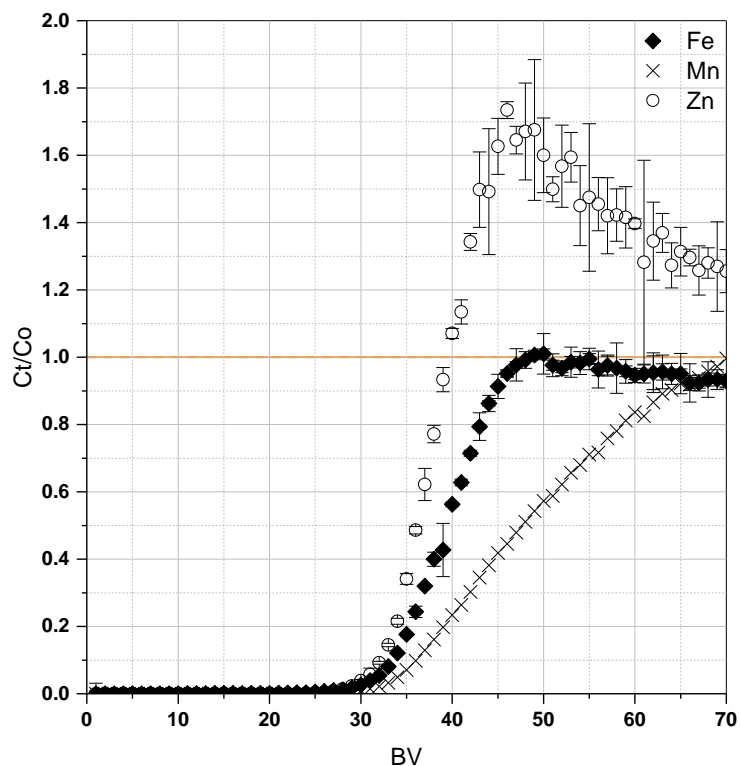
Figure 7.17. Breakthrough of Fe, Mn, and Zn during the loading of S957 (PLS concentration: 200 mg/L, pH 1.37, 1.4 mL BV, 5 BV/h).

7.3.6 Recovery of Fe, Mn, and Zn from S957 using Sodium Chloride Eluent

Static screening metal extraction by S957 as a function of sulfate concentration in Chapter 5 revealed

a distinct decrease in extraction efficiency with increased sulfate concentration, except for Fe which

was not affected (Figure 5.14). Given this trend, the use of a sulfate-based eluent could be successful

for metal elution. In addition to sulfate, the increase of chloride concentration was also previously

shown to adversely affect extraction of metals to S957 (Canner, et al., 2017). A comparison of the

sulfate/chloride concentration required to achieve 50, 20, and 10 % metal extraction revealed that

greater suppression of uptake could be achieved using substantially lower concentrations of chloride

than sulfate (Table 7.7), indicating that chloride elution would be the more effective approach.

Following a 30 BV loading cycle to achieve approximate breakthrough of 10% for all ions, the elution

of Fe, Mn, and Zn from S957 was explored using NaCl solutions with concentrations ranging from 0.1

M to 1.0 M.

Table 7.7. Comparison of anion concentrations required to affect bulk metal extraction (except Fe) by S957.
Sulfate data from Chapter 5, chloride data from Canner, et al. (2017).

	Extraction Efficiency		
	50 %	20 %	10 %
SO_4^{2-}	0.2 – 0.3	0.4 – 2	N/A
Cl^-	0.05	0.1	0.75

Upon introduction of 0.1 M NaCl to the loaded column, concentrations of all three metal ions

reached their maximum within the first 5 BV, with concentrations of 73.1 mg/L, 27.3 mg/L, and 127.1

mg/L for Fe, Mn, and Zn, respectively (Figure 7.18). Elution profiles for all ions occurred

simultaneously, with no lateral separation in occurrence. The magnitude of each ion profile

correlated well with the order of selectivity exhibited during breakthrough of ions in Figure 7.17, with

the ions that reached breakthrough first producing larger curves. Integration of elution areas

suggested low rates of recovery for each metal, with the largest area (Zn; 3.397 mg) only equating to

46.7% recovery (Table 7.8).
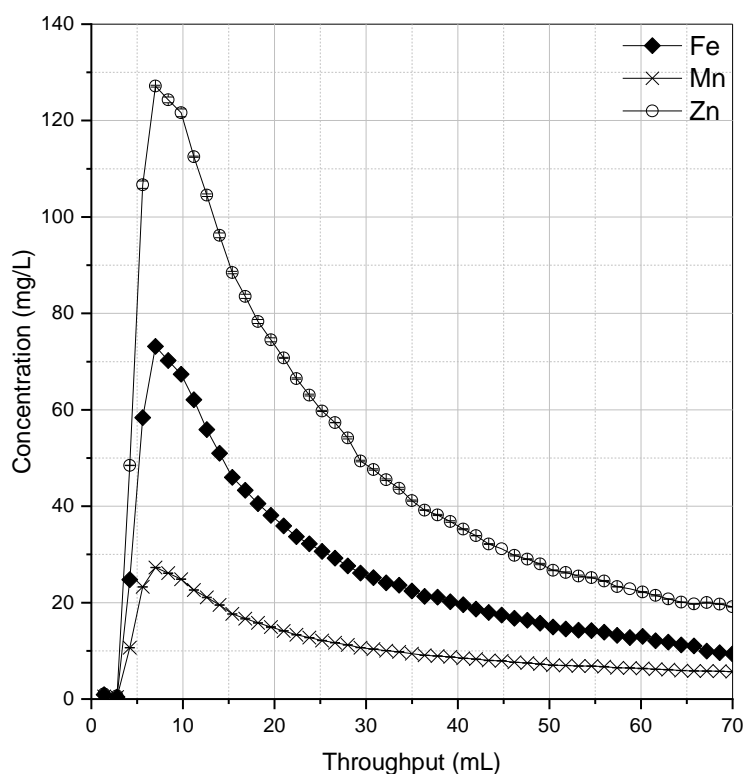
Figure 7.18. Elution of Fe, Mn, and Zn from S957 at 2 BV/h using 0.1 M NaCl eluent (pH 7).

Table 7.8. Recovery efficiencies of Fe, Mn, and Zn from S957 using 0.1 M NaCl eluent.

	Loading (mg)	Elution (mg)	Recovery (%)	FWHM (mL)
Fe	8.366	1.831	21.89	15.9
Mn	8.766	0.756	8.62	17.3
Zn	7.275	3.397	46.69	19

Increasing eluent NaCl concentration to 0.5 M greatly increased the maximum concentration of each of the three metals in solution. Additionally, elution profiles were considerably sharper than for 0.1 M elution and occurred within a much lower volume of eluent. Maximum concentrations for Zn were higher than other metals (1435 mg/L; Figure 7.19), and as such corresponded to a higher recovery efficiency of 99.73 % (Table 7.9). As for elution at 0.1 M NaCl the points of highest concentration coincided, confirming that selective elution was not possible with this eluent. Despite the maximum

concentration of Fe (845 mg/L) being higher than that of Mn (406 mg/L), recovery efficiencies were

relatively similar (66.49 and 67.74 %, respectively; Table 7.9) given the more gradual reduction of Mn

concentration following the height of elution.
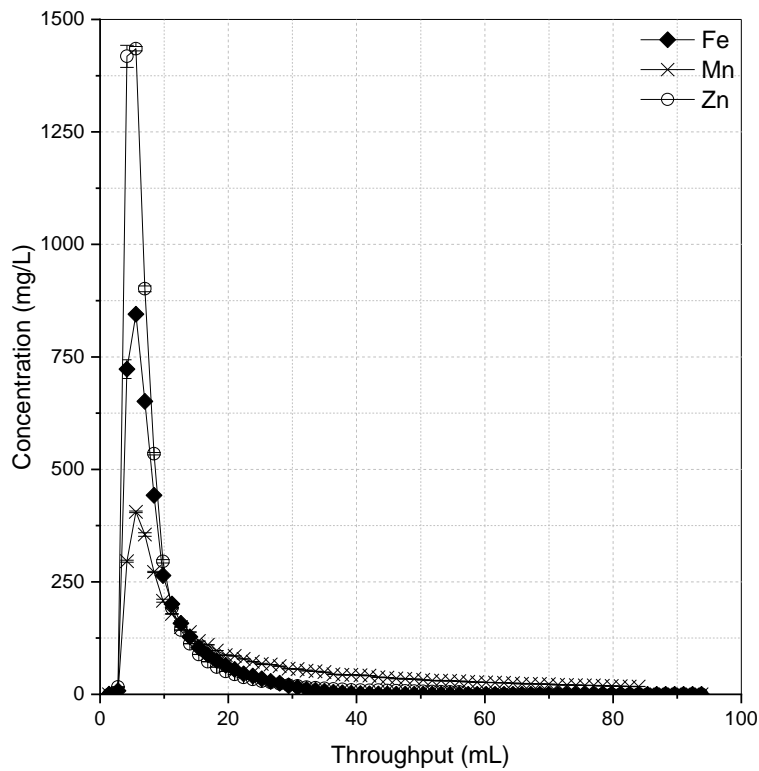
Figure 7.19. Elution of Fe, Mn, and Zn from S957 at 2 BV/h using 0.5 M NaCl eluent (pH 7).

Table 7.9. Recovery efficiencies of Fe, Mn, and Zn from S957 using 0.5 M NaCl eluent.

	Loading (mg)	Elution (mg)	Recovery (%)	FWHM (mL)
Fe	8.556	5.689	66.49	5
Mn	8.502	5.751	67.74	6.3
Zn	8.025	8.003	99.73	4.2

The treatment of loaded S957 with 0.75 M NaCl resulted in a sharp elution profile for Zn and Fe, with

maximum concentrations in effluent solutions of 1318 mg/L and 1129 mg/L, respectively (Figure

7.20). Metal concentrations rapidly decreased beyond this point, indicative of effective Fe and Zn

elution from S957 using this eluent. For Mn, the resulting elution profile was of lower magnitude,

reaching a concentration of 666 mg/L. Despite the height for the Mn profile being lower than those

for Fe and Zn, the concentration during the tail of the curve was higher due to a slower decay of

concentration, indicating that Mn was liberated from the resin functional site over a longer period

than for the other ions. Analysis of curve areas indicated very high metal recovery rates using 0.75 M

NaCl (Table 7.10), ranging from 84-92 %.
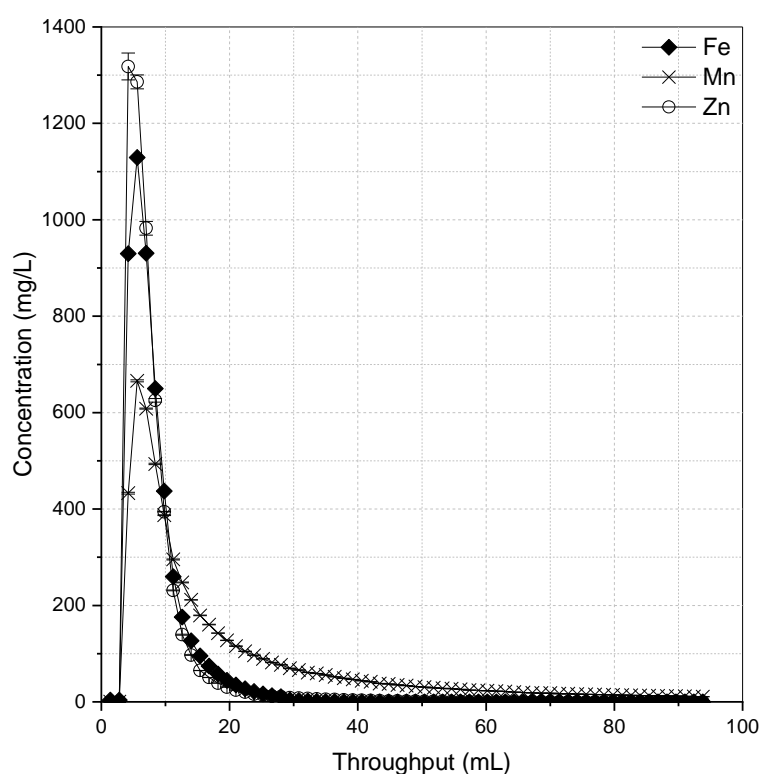
Figure 7.20. Elution of Fe, Mn, and Zn from S957 at 2 BV/h using 0.75 M NaCl eluent (pH 7).

Table 7.10.Recovery efficiencies of Fe, Mn, and Zn from S957 using 0.75 M NaCl eluent.

	Loading (mg)	Elution (mg)	Recovery (%)	FWHM (mL)
Fe	8.428	7.074	83.93	5.3
Mn	8.863	8.144	91.89	6.8
Zn	8.457	7.598	89.84	4.8

The elution of S957 using 1.0 M NaCl resulted in very sharp elution profiles for Fe and Zn (Figure

7.21), as was the case for 0.75 M treatment. However, maximum concentrations for these ions were

notably higher in this instance, with maximum heights of 1335 mg/L and 2104 mg/L after 3 and 4 BV

for Fe and Zn, respectively. After maximum heights were reached, concentrations declined rapidly for

both ions, reaching negligible concentrations beyond 20 mL eluent throughput. A reasonably sharp

elution profile for Mn was also observed, but with a longer decay curve than those for the other two

metal ions. Recovery efficiencies for this eluent were very high, with 83 % extraction for Fe, 96 % for

Mn, and ~100 % recovery of Mn from the resin. High recovery of each metal from S957 indicates that

the use of NaCl as an eluent can provide effective, almost complete, regeneration of the resin, albeit

with proton preconditioning being required before subsequent loading cycles.
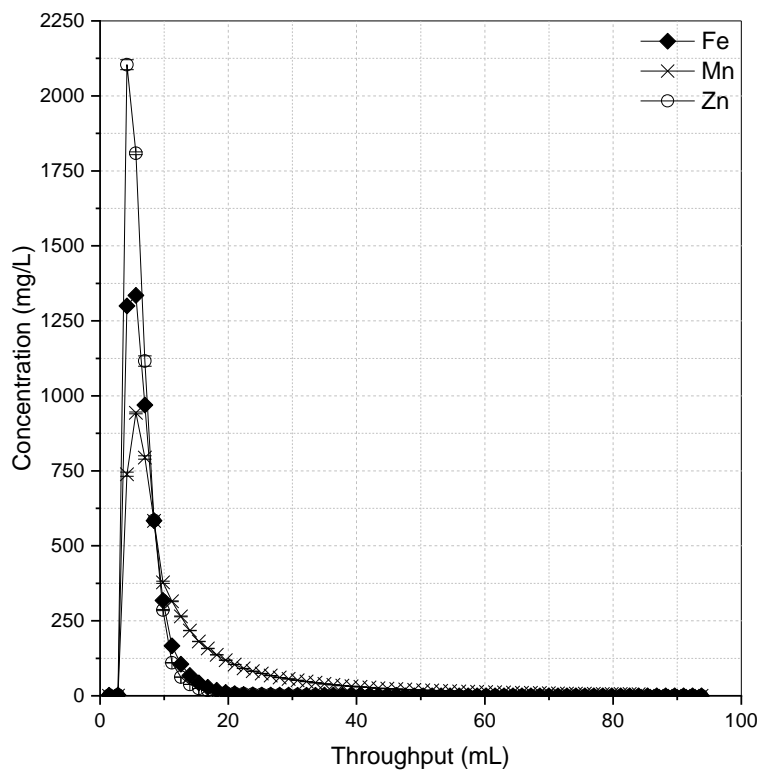
Figure 7.21. Elution of Fe, Mn, and Zn from S957 at 2 BV/h using 1.0 M NaCl eluent (pH 7).

Table 7.11. Recovery efficiencies of Fe, Mn, and Zn from S957 using 1.0 M NaCl eluent.

	Loading (mg)	Elution (mg)	Recovery (%)	FWHM (L)
Fe	8.436	7.004	83.03	4.6
Mn	8.858	8.515	96.13	5.5
Zn	8.405	8.717	103.71	3.7

7.3.6.1 *Comparison of Puromet MTS9570 Elution using NaCl Eluents*

Comparison of elution profiles for the three metal ions (Figure 7.22) as a function of eluent

concentration indicated a distinct positive trend between increased sodium chloride concentration

and the height of profiles for Fe and Mn. The exception to this trend was the maximum Zn

concentrations for 0.50 M and 0.75 M, whereby the concentration during the 0.75 M was slightly

lower than for the 0.50 M elution (1318 mg/L and 1435 mg/L, respectively). Increases in eluent

concentration were also accompanied by a narrowing of profile widths, as evidenced by reductions in

FWHM values (Table 7.8, Table 7.9, Table 7.10, and Table 7.11), indicating a more efficient exchange

of loaded metals under higher eluent concentrations.
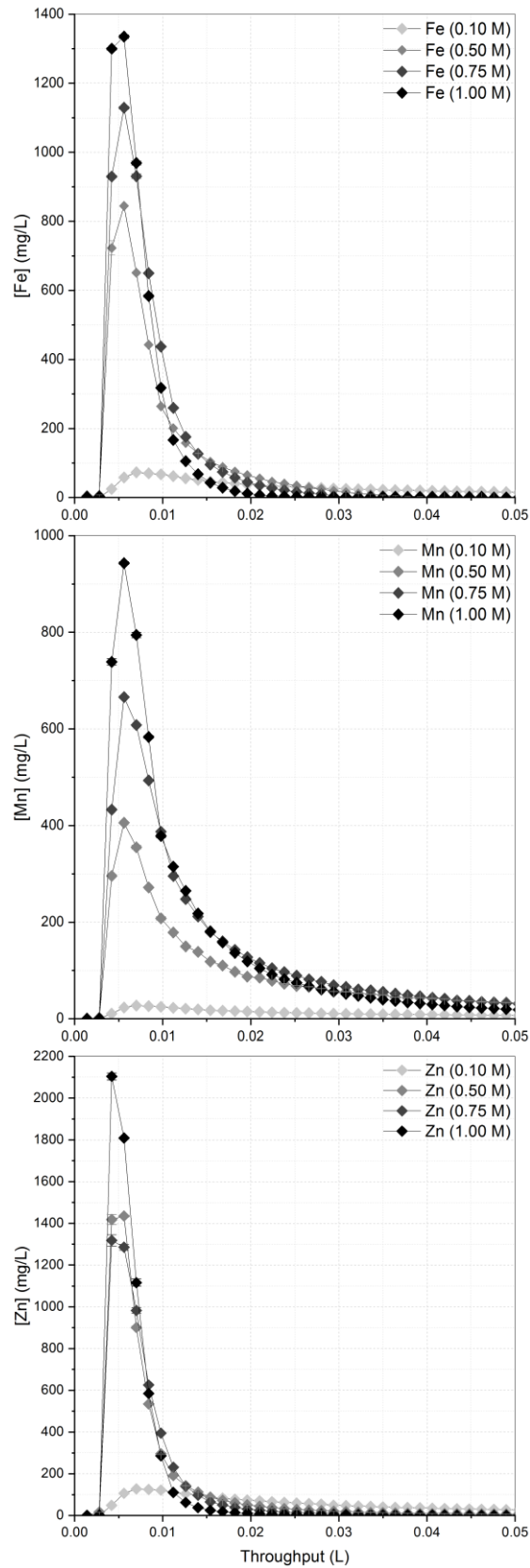
Figure 7.22. Comparison of NaCl eluent concentration (pH 7) on Fe, Mn, and Zn elution from S957 at 2 BV/h.

In general, higher NaCl concentrations were associated with higher percentage recoveries of each metal ion (Figure 7.23). However, this was not the case for Zn, where a decreased recovery of approximately 10 % was observed during elution using 0.75 M NaCl. In terms of overall trends in metal recovery, for the higher concentration eluents where more favourable recoveries were observed, Zn was recovered most efficiently followed by Mn then Fe (Figure 7.23). Considering that the elution profiles of Mn were generally wider than those for Fe, it was unexpected that the recoveries of Mn were greater. Given that for eluent concentrations greater than 0.1 M the entire Fe elution period was recorded (i.e. effluent concentrations reached zero within sampled range) and given that no real difference in recovery for 0.75 and 1.0 M was observed (approximately 83%, Figure 7.23), it is suggested that there remains a portion of loaded Fe that is unable to be recovered from S957 functional sites using this method of elution.
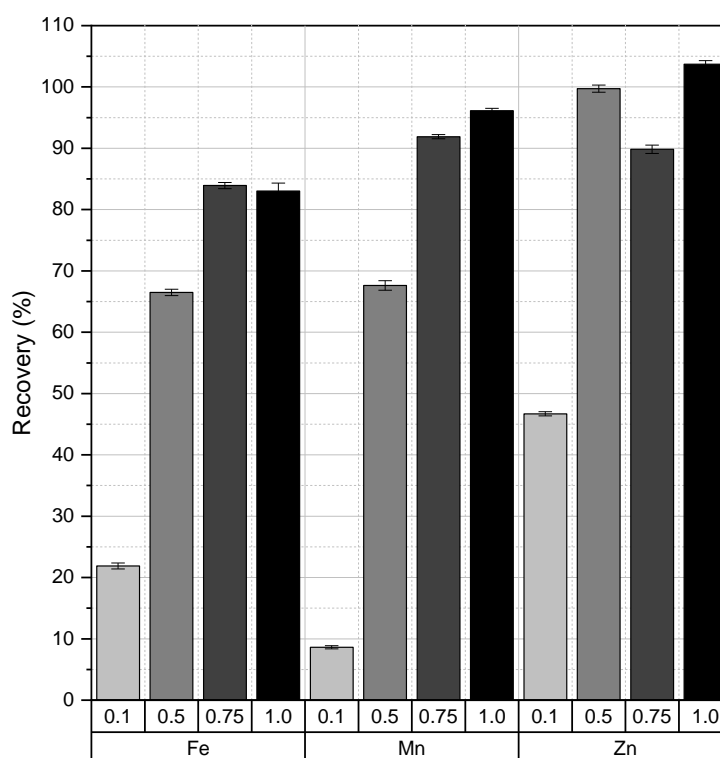
Figure 7.23. Comparison of calculated Fe, Mn, and Zn recovery efficiencies from S957 as a function of NaCl concentration (M).

7.3.7   Stability of Puromet MTS9570 over Repeated Loading and Elution Cycles

In general, the highest recovery efficiencies were encountered using a 1 M NaCl eluent, and as such this was used for repeated loading and elution experiments. As per eluent screening experiments, a 30 BV loading phase was used, followed by a 5 BV rinse cycle to remove residual PLS, and a minimum 36 BV elution phase to ensure complete elution profile capture. After elution, a 10 BV proton conditioning step was performed using 1 M H_2SO_4 to regenerate the resin in preparation for the next loading cycle.

It can be seen in Figure 7.24 that S957 was suitable for repeated loading and elution cycles using an NaCl eluent. Maximum recorded Fe concentrations did decrease slightly during the second elution cycle (from 1376 mg/L in the first cycle to 1355 mg/L in the second). However, the highest effluent Fe concentration was recorded during the third elution cycle (1503 mg/L). This trend was also reflected in recovery efficiencies for Fe, which for the three elution cycles were 78.1 %, 73.9 %, and 86.4 % (Figure 7.25). As expected from previous experimentation, the concentrations encountered for Mn were the lowest of the three metals. As for Fe, a reduction in maximum Mn concentration was observed between the first and second elution cycle (909 mg/L to 841 mg/L), followed by an increase during the final elution cycle (1035 mg/L). Despite this, elution profiles were of similar width and lateral occurrence, indicating no significant deterioration in extractive ability of the resin over repeated cycles. Concentration maxima and recovery efficiencies were highest for Zn, with similar elution profiles over the three cycles. While recovery efficiency did decrease slightly during the second elution cycle (96.05 %; Figure 7.25), recovery during the first and third cycle was 100 %. As such, it was confirmed that S957 was an appropriate resin for multiple loading cycles and was not adversely affected by the 1.0 M NaCl eluent.
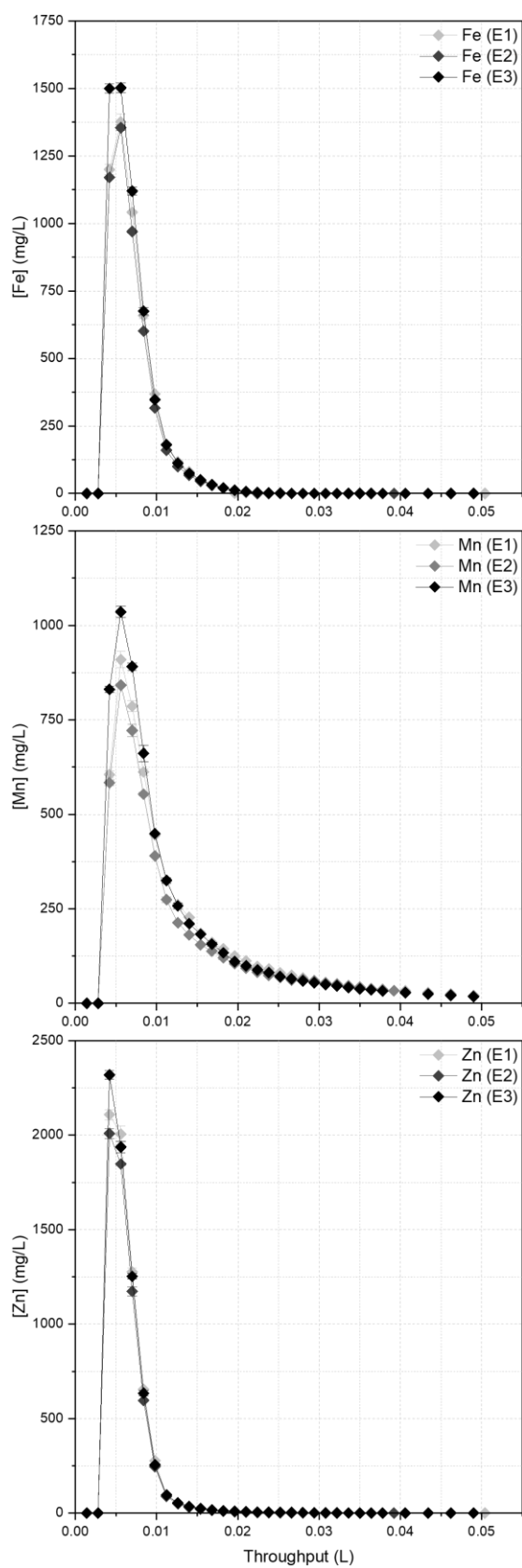
Figure 7.24. Elution of Fe, Mn, and Zn from S957 using 1 M NaCl over repeated elution cycles at 2 BV/h.
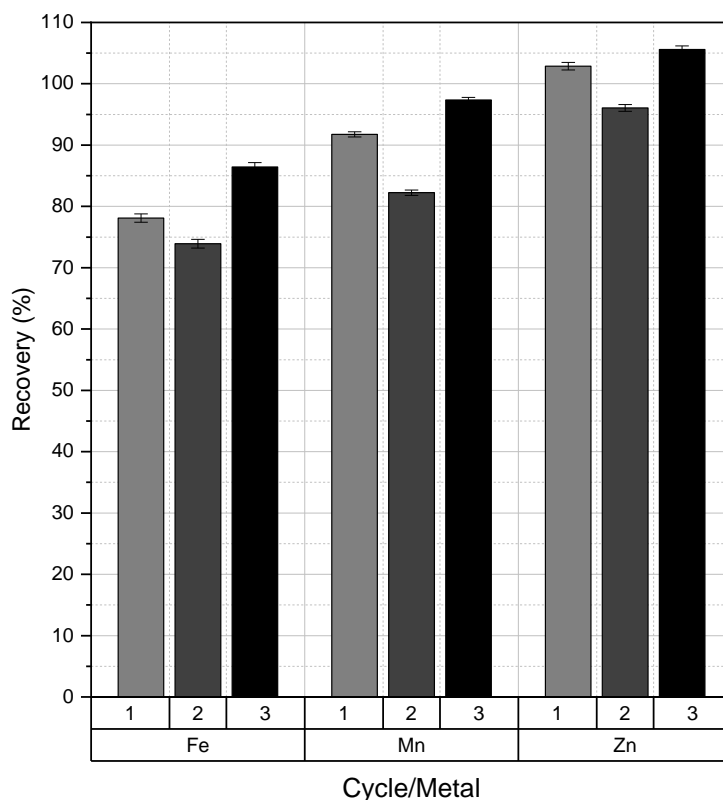
Figure 7.25. Recovery efficiencies (%) of Fe, Mn, and Zn from S957 during each elution cycle.

7.4 CHAPTER DISCUSSION

7.4.1 Copper recovery from Puromet MTS9140

It was previously determined through XPS analysis (Figure 5.21) that after loading, Cu was present on

S914 as Cu(I), and so the mechanism of Cu extraction on to S914 involved the reduction of Cu(II) from

solution to Cu(I) on the resin. According to hard/soft acid-base theory, strong coordination

interaction is exhibited between ligands (bases) and metals (acids) that are of the same type (i.e.

soft-soft, or hard-hard). Given that thiourea acts as a soft base and copper as a soft acid, the

resulting complexes are predicted to be highly stable (Fakhar, et al., 2017). Further evidence for the

presence of Cu(I) complexes was gained visually, through colour change of loaded resins. When other

resins which exhibited Cu selectivity (e.g. M4195, S930) were loaded with Cu, a distinct blue/green

colour change was observed, which was not the case during S914 Cu loading. Given that most Cu(II) compounds absorb light in the blue/green spectrum (600-900 nm), and that Cu(I) complexes are generally colourless, further evidence was provided to justify that redox to Cu(I) had occurred given the lack of colour change in Cu-loaded S914.

As such, an oxidative elution approach using $NaClO_3$ was explored. While HNO_3 was initially considered (see Appendix), $NaClO_3$ was selected given the higher reduction potential of chlorate (1.152 – 1.451 V) over nitrate (0.803 – 0.934 V) in acidic media (Vanýsek, 2010). In addition to acting as a stronger oxidising agent, the use of $NaClO_3$ over HNO_3 allowed elution to be performed under less-acidic conditions, in this case at approximately pH 2.

Cu elution using $NaClO_3$ solutions proved effective for both eluent concentrations (Figure 7.2 and Figure 7.3), with recovery efficiencies of 78.91 % at 0.5 M and 81.86 % at 1 M (Table 7.1). Importantly, no gas formation was observed during chlorate elution, which was also evidenced by the more regular shape of elution profiles when compared to those obtained during HNO_3 elution (Appendix Figure 11.3). Cu elution profiles were fairly symmetrical with a steep frontal curve and slightly longer tail-end. This curve profile is often observed where effective elution is achieved (e.g. Korak et al., 2017; Jeffrey et al., 2010; Tavakoli et al., 2013), and implies a favourable exchange (or removal) of the target ion in favour of the eluent counter-ion. It was decided that the 0.5 M eluent would be used for resin reusability investigations given the potential CuO formation at 1 M concentration (Figure 7.4), and similar Cu recovery efficiencies.

The observed decrease in resin performance was highlighted by reductions in Cu extraction from 7.95 mg in the first loading cycle to only 1.55 mg adsorption during the following two loading cycles (Figure 7.5). The degradation of resin functionality was also apparent during the respective elution cycles, where decreases in profile magnitude were observed (Figure 7.6). Interestingly, although the same mass of Cu was loaded to the column during the second and third loading cycles, the percentage recovery of Cu dropped significantly during the third elution cycle, from 50.55 to 41.61 %

when residual Cu from previous elution cycles was factored in (Table 7.2). The lower mass of Cu

recovered from S914 during the third elution cycle could potentially be explained by progressive loss

of resin functionality during elution cycles. It could be assumed that as the eluent contacts the

exterior of resin beads before diffusing through the resin pores, the functional groups at the surface

of each bead would be the first to be degraded, explaining the loss of capacity between cycle one

and two. Assuming this 'shrinking-core' hypothesis for loss of functionality is true, it holds that during

the later elution cycles the remaining functionality is located deeper within the resin beads and

therefore less accessible to the eluent. While the ionic radii of Cu(I) (0.46-0.77 Å) is substantially

smaller than that of ClO_3^- (1.71 Å), it is unlikely that Cu residing in pores inaccessible to ClO_3 was

responsible for this observation given the flexibility of gelled polymers (Harland, 1994). Instead, this

is more likely a result of kinetic limitations inherent to column operation, i.e. the limited residence

time within the column is hindering sufficient mass transfer between the bulk eluent and resin and in

doing so reduces eluent efficiency (Oliveira, et al., 2015). It is expected that such effects are amplified

when coupled with functionality degradation on resin outer surfaces.

To better understand the mechanism behind S914 functionality degradation, effluent samples from

0.5 M $NaClO_3$ elution were analysed by ion chromatography and AAS, revealing a spike in pH and

SO_4^{2-} concentration before Cu elution, which occurred concurrently with increased Cl^- concentrations

(Figure 7.8 and Figure 7.9). The increase in Cl^- is not unexpected, and the parallel occurrence of Cu

and Cl^- elution confirmed that the method of Cu liberation is a redox interaction between ClO_3^- and

Cu(I), whereby ClO_3^- is reduced to Cl^- and Cu(I) oxidised to Cu(II).

However, the large spike in sulfate concentration is particularly significant given that no sulfate was

introduced to the system during the elution cycle. While the PLS used for loading did contain sulfate,

a thorough rinse cycle was performed prior to elution using 18 MΩ deionised water such that

residual sulfate concentration was below 0.002 M at the start of Figure 7.9. It is important to note

that anion concentrations presented in Figure 7.9 have been corrected to consider the

concentrations in both the calibration blank and eluent solution, such that the presented data represents only *additional* anions introduced to the system. Therefore, the sulfate detected in effluent solutions could have only originated as a result of resin degradation. While not specifically recorded for chlorate, the oxidation of thiourea compounds by other halogenic oxidants such as bromate, chlorite, and iodate has been shown to form sulfate through substitution of sulfur for oxygen on the thiourea group, and subsequent sulfur oxidation (Sahu, et al., 2011). It is therefore expected that oxidation by chlorate is also able to produce such by-products during degradation of thiourea functional groups.

7.4.2   Selective Co and Ni recovery from Dowex M4195

A pH-controlled elution process was chosen for investigating the potential for selective recovery of Ni and Co from M4195. Sulfuric acid has previously been suggested as a suitable eluent for Co and Ni recovery from picolylamine-functionalised resins (Diniz, et al., 2005; Mendes & Martins, 2004; Nagib, et al., 1999; Rosato, et al., 1984). As such, the static pH screening results from Chapter 5 were used to inform the eluent acid concentrations studied during elution experiments.

It is immediately apparent from Figure 7.10 - Figure 7.12 that a two-step elution process using different concentrations of sulfuric acid was highly successful in selectively recovering Co and Ni, as evidenced by the clear separation in each set of elution profiles. As sulfuric acid concentrations were increased from the pH_{50} values towards pH_{10} values, the elution profiles tended to become sharper and reach a higher maximum concentration for both metals. Additionally, the recovery efficiency of both metals was positively correlated with increased eluent acidity (Figure 7.14). However, this was also accompanied by a higher degree of co-elution of Ni during the Co targeted elution phase (Table 7.3 - Table 7.5). The increased extent of co-elution can be explained by referring to the previously reported pH profile for M4195, where increased proton concentration resulted in a lower affinity of the bispicolylamine groups towards both metals. The sharpening of elution profiles as eluent

concentration increased is related to the rate at which ions are desorbed from the resin functionality. An eluent with higher efficiency will desorb metal ions faster, and therefore increase the concentration in solution faster than a less efficient eluent would. This results in a sharper frontal curve to the elution profile with higher maximum concentration, and given the finite mass of metal ions available for desorption, a shorter period of elution before effluent metal concentrations returned to zero.

Investigations into M4195 reusability were performed through repeated loading and elution cycles to determine whether any significant loss of functionality was encountered during operation. Eluent acid concentrations were informed by eluent screening results, resulting in the selection of 0.08 M H^+ for Co, and 1.0 M H^+ for Ni. The use of these eluents ensured maximum potential metal recovery and minimal co-elution of Ni during the Co-targeted elution cycles. It was determined that M4195 was very durable for re-use under the selected loading and elution regime. Analysis of metal loading revealed that similar masses of Co and Ni were loaded during each cycle (Table 7.6), indicating no significant loss of capacity as a result of elution. Elution profiles for Co and Ni were well-separated, with minimal co-elution, and profile maxima and magnitude remained fairly consistent over four loading and elution cycles (Figure 7.15). The similarity between elution profiles not only highlighted the robustness of this resin for re-use, but also confirmed that using a 1.0 M H^+ eluent during the second elution phase was sufficient for adequate regeneration of resin functional groups for the subsequent loading cycle. The successful repeated use of M4195 over repeated loading and elution cycles was noted elsewhere for the recovery of As, Cr, and Cu from chromated copper arsenate treated wood leachates using a NH_4OH eluent (Janin, et al., 2009). In this case also, the requirement of a separate re-conditioning (protonation) step was negated by using an eluent which encourages proton-metal exchange. While different metals and eluents were used by Janin *et al.* (2009) than in the present study, the common finding that M4195 was robust during multiple operational cycles further emphasised the durability of this resin.

7.4.3   Recovery of Fe, Mn, and Zn from Puromet MTS9570

Based on the assumption that S914 would target Cu and M4195 would extract Co and Ni from the

PLS, it was assumed that the S957 resin would be mostly used for extraction of Fe, Mn, and Zn. As

such, the recovery of these metals from S957 after loading were explored by elution using NaCl

solutions, given the negative effect that increased Cl^- concentration has on metal extraction by this

resin (Canner, et al., 2017). As for the elution of Co and Ni from M4195, an increase in eluent

concentration had the effect of increasing the maxima of elution profiles for Fe, Mn, and Zn from

S957 (Figure 7.18 - Figure 7.21). The increase of maxima was accompanied with a narrowing of

widths, as evidenced by reductions in FWHM values of elution profiles with increased NaCl

concentration (Table 7.8 - Table 7.11). As previously discussed, the increased maxima and reduced

width is related to the kinetics of elution, whereby more efficient elution conditions allowed more

metal to be liberated from the resin in a smaller total volume of eluent; resulting in increased spot

concentrations and a less-prolonged period of elution.

Comparing the recovery efficiencies of Mn and Zn, it was observed that recovery efficiencies

increased as a result of increased NaCl concentration (Figure 7.23). However, this was not the case

for Fe, where the recovery efficiency stabilised around 83 % for both 0.75 M and 0.1 M eluents. This

suggested that not all of the loaded Fe was able to be recovered from the resin using this eluent. A

possible explanation for this could lie in the fact that S957 is a dual-functionalised resin, with both

sulfonic acid and phosphonic acid functional groups responsible for metal extraction. Strong sulfonic

acid resins are known for their unselective extraction of cations at low pH (McKevitt & Dreisinger,

2009), which was previously observed during static screening studies for Dowex M31. Phosphonic

acid functionalised resins on the other hand are known to have preference towards the extraction

Fe^{3+} ions, particularly under acidic conditions (McKevitt & Dreisinger, 2009). It is therefore a

reasonable assumption that the Fe extracted by S957 is distributed between the two resin

functionalities, each with different strengths of attraction towards Fe. In terms of elution, the difficulty of recovering iron from phosphonic acid resins is reportedly a common barrier to their industrial application (Zhang, et al., 2016). Conversely, the extraction of Fe by sulfonic acid functionalised resins has been shown to be negatively affected by increased chloride concentrations, which would allow for effective elution using chloride eluents (Littlejohn & Vaughan, 2012). For this reason, it is assumed that the inability to achieve Fe elution beyond 83%, regardless of increased eluent concentration, is due to a portion of the loaded Fe remaining bound to the phosphonic acid groups of S957, which would be more difficult to recover using a simple chloride eluent than the Fe loaded to sulfonic acid groups.

Repeated loading and elution cycles were performed using a 1.0 M NaCl eluent at neutral pH and reconditioned to proton form using 1.0 M H_2SO_4 between each cycle. Comparison of elution profiles over each cycle revealed that S957 was very durable to repeated use and regeneration, with minimal change in profile character (Figure 7.24), and no notable deterioration in elution efficiency over the three repeated cycles (Table 7.11). The reusability of S957 towards Fe was also detailed by Lv *et al.* (2019), where elution profiles of Fe remained unchanged over four cycles during using a 6.0 M HCl eluent. While it is likely that an HCl eluent would also be effective in the current work, the decision to use NaCl was made to reduce the hazards and costs that would be associated with using a 6.0 M HCl eluent at a larger scale. The results of S957 elution were promising in their simplicity and effectiveness, with potential to recover metals from the column at a low cost, which would be beneficial for final system design given that the S957 column is intended as a final 'scrubbing' column before effluent release and may not necessarily have the highest monetary value associated with the recovered metals.

7.5 CHAPTER CONCLUSIONS

This chapter provided a detailed exploration of metal recovery potential from selected ion exchange resins and explored the optimisation of eluent solution composition to achieve the most-suitable metal recoveries. In the context of the wider literature, the presented elution profiles are of notably higher data resolution than many other published studies, and as such allowed better examination of metal elution behaviour as a function of eluent composition. A number of specific conclusions can be drawn from the results of these experiments;

- Efficient Cu recovery from S914 was possible by using an oxidative elution approach to oxidise the Cu(I) present on the resin after loading. While concentrated HNO_3 was suitable in terms of total Cu recovery (100 %), nitric oxide gas formation was problematic for system operation, and predicted to be a limiting factor for process scale-up. The use of a sodium chlorate eluent circumvented the issue of gas formation and was able to achieve good Cu recovery efficiencies (82 %). However, the oxidation of the thiourea functional groups led to a loss of resin capacity, as evidenced by the identification of degradation by-products in effluent solutions. The almost-complete loss of Cu capacity during elution limits the possibility for resin reuse, and as such this column would be considered single-use in future system design. However, given the relatively low-cost nature of this resin (approx. $20/L, compared to approx. $140/L for bispicolylamine (M4195 equivalent)[3]), this may not be a limiting factor in terms of financial feasibility.

- A pH control approach was suitable for the selective elution of Co and Ni from M4195 following non-selective adsorption, and careful optimisation of eluent concentrations and combinations allowed minimisation of co-elution. The selective elution of Co and Ni resulted in relatively pure (single metal) effluent streams; a highly desirable outcome given the value of these resources. The bispicolylamine functional groups were resilient to reuse and were

---

[3] Prices given as estimates through personal communication with Purolite Ltd representative, July 2019. Actual wholesale prices dependent upon order quantity.

not affected by repeated loading and elution cycles, indicating that this resin was a suitable candidate for inclusion in a selective treatment system.

- Fe, Mn, and Zn were successfully recovered from S957 using an NaCl eluent, although separation of the three metals was not possible with this approach. Maximum recovery efficiencies of 83 %, 96 %, and 100 % were achieved for Fe, Mn, and Zn, respectively. Increasing the concentration of the eluent had the dual effect of increasing the concentration of profile maxima and reducing the volume of solution required for maximum recovery. Despite increasing from 0.75 to 0.1 M NaCl, no further increase in Fe recovery was observed, indicating a limit to the maximum recovery (83 %) using this eluent. Repeated loading and stripping of the resin did little to affect its performance, and as such it was deemed that S957 was suitable for use, and that the use of a 1.0 M NaCl eluent did not adversely affect resin performance.

The results presented in this Chapter provide the means for recovering metals from resins after they have been extracted from the simulant mine water PLS, and therefore allowing production of a product for downstream processing. While this has allowed an understanding of the unit operations that will be employed in treatment, the following Chapter will address the coupled-column operation of the resins when used in series.

8 COUPLED-COLUMN SYSTEM

Up to this point, the focus of work has been; a) to identify and characterise resins capable of selective metal recovery from a mixed-metal PLS, b) to determine optimum loading and elution conditions, and c) to assess the reusability of the resins for this purpose. In Chapter 7, it was proven that high recovery efficiencies for Cu (79-82 %), Co (95.8 %), Ni (98.6 %), Fe (83 %), Mn (96 %), and Zn (100 %). Furthermore, for M4195 and S957 it was shown that the resin beds are suitable for repeated use without significant deterioration in extractive ability.

Given that the aim of this work was to progress towards a coupled-column treatment system for mine water treatment, this final data chapter presents the initial results of a benchtop-scale version of the process. The aim of this chapter was to determine the effectiveness of a coupled-column approach, which has never been published before for three columns of distinct resin functionality. Most importantly, given the novelty of this approach, this was done to allow insight to the problems which may arise from such a setup, and to determine whether the study of breakthrough from single-column systems is adequate for predicting the behaviour of resins when operated in series, and to identify possibilities for future work.

8.1 CHAPTER INTRODUCTION

The coupling of multiple ion exchange columns with distinct functionalities is a novel process within the scientific literature. Through arranging columns of different functionality in series, it is theoretically possible to control the fate of metals within the coupled system. A benefit of coupling different resins in series is that the available capacity of resins towards targeted metals can be readily optimised. Consider an ion exchange resin, X, which exhibits equally high capacity for ions A and B, and a second resin, Y, which shows preferential selectivity for ion A but not B. By ordering

resin Y before X, it is possible to remove the bulk of ion A from solution in the first column, and allow

a greater extent of the capacity of resin X to be used for ion B, as indicated schematically in Figure

8.1.
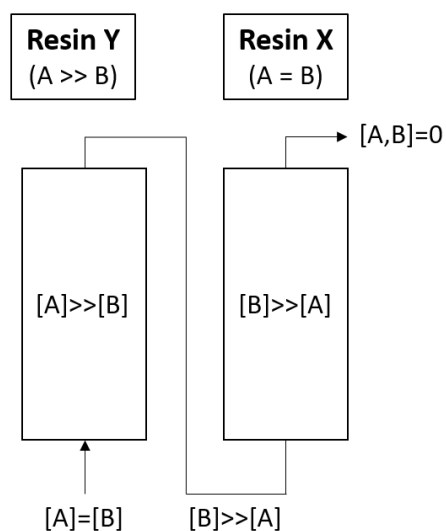
Figure 8.1. The effect of column order on metal concentrations within a coupled-system. Curved brackets indicate resin selectivity, square brackets represent solution/column concentration of ions A and B.

Further to this example, where ion B is of considerably greater recovery value than A, this approach

would allow for a more concentrated solution of ion B to be recovered; increasing the value of

effluent product solutions and improving the efficiency of downstream metal purification processes.

The selection of resins must be based on a thorough understanding of the selectivity of these resins

towards metals under competitive dynamic adsorption conditions. As such, the order of resins used

in this chapter is based upon the previously determined metal removal behaviours observed in

previous chapters.

8.2 SPECIFIC METHODS

8.2.1 Loading Conditions

For the coupled-column system, three small-scale columns were packed such that a 1.4 mL BV of wet settled resin was achieved per column. Following packing, columns were directly coupled such that the effluent of the first column passed directly to the influent of the following column. Minimisation of the space between resin beds allowed for a more controlled loading cycle, as it was not necessary to factor in the volume of solution between columns during subsequent mass balance calculations. Based on the existing knowledge of resin performance identified through prior experimentation, the order of resins and their target metals was as follows; S914 to exclusively target Cu, M4195 to extract Ni and Co, and S957 to act as a final catch-all (predominantly for extraction of Fe, Mn, and Zn under optimum operation, but also for extracting ions breaking through from previous columns). The system was loaded at 5 BV/h such that the first column of the three received 15 BV of PLS. This loading extent was chosen as it roughly corresponded to a Co breakthrough between 10 and 50 % from M4195 (the first metal likely to be displaced from the target column, as per breakthrough screening studies at this flow rate).

8.2.2 Elution Conditions

After loading, columns were detached and rinsed separately using DI water to prevent further metal loading before the elution process was started. Elution of metals was achieved through use of the optimised eluents identified in Chapter 7 at a flow rate of 2 BV/h and collected using a fraction collector prior to dilution with 1% HNO_3 and analysis by ICP-OES. Elution profiles were presented as per Chapter 7, but with additional analyses of metal concentrations within combined effluent streams. This was calculated as a rolling average of metal concentrations leaving each column, and was provided to represent the chemical composition of effluent product solutions assuming that all effluent bed volumes were collected and combined from the start of the elution cycle.

Following the elution cycles, which were not 100% effective, it was necessary to attempt to quantify the residual metal bound to the resin beds for mass balance purposes. This was completed using 10 BV of 3 M HNO_3 for S914 and 3 M HCl for S957, given previous observations of the adverse effect of these solutions on resin performance (Chapter 7 and Canner, *et al.*, 2017). Residual masses bound to the M4195 column were inferred by difference.

The aim of this experiment was primarily to identify any potential issues encountered through coupled-column operation which may not be immediately apparent through single-column breakthrough screening, and to assess the accuracy of using single-resin breakthrough curves as predictors for coupled-system performance. Additionally, the extent of co-elution of non-targeted metals was an important consideration as this will directly affect product stream purity, and hence the costs and efficacy of downstream processing.

8.3 RESULTS

8.3.1 System Loading

During the system loading cycle metal breakthrough was minimal with only trace concentrations of Mn and Ni detected in effluent solutions such that extraction of both was calculated at beyond 99.9%. Concentration of other metals were below detectable limits using ICP-OES and so were assumed to be completely adsorbed. Given the lack of breakthrough, curve analysis was not possible for loading calculation, however, the masses of adsorbed metals were calculated through multiplication of the volume of solution pumped through the system (L) by the influent concentration of each metal (mg/L). The calculated masses are presented in Table 8.1. Masses of metals loaded to the column system were fairly similar, ranging from approximately 3.9 to 4.3 mg, which was expected given the similar concentration of each metal in the PLS. Calculation of loading to each discrete column are provided later during mass balance estimates.

Table 8.1. Total masses of metals input to the coupled-column system (PLS metal concentration: 200 mg/L each, pH 1.56, flow rate: 5 BV/h)

Metal	Mass Input (mg)	Metal	Mass Input (mg)
Cu	4.305	Mn	3.954
Co	4.332	Ni	3.935
Fe	4.286	Zn	4.186

8.3.2   Coupled-Column Elution Profiles

8.3.2.1   *Column No. 1: Puromet MTS9140*

The introduction of 0.5 M $NaClO_3$ to the S914 column resulted in a sharp Cu elution profile (Figure 8.2). There was an initial delay before Cu concentration began to increase, but beyond 11 BV throughput the increase in concentration was rapid, reaching a maximum of 159.06 mg/L at 20 BV PLS throughput. Immediately following this maximum, concentration decreased quickly before slowing to a gradual decline towards the end of the elution curve. Because of this gradual decline in concentration, the final section of the tail was not captured during the sampling regime. While this will result in a slight under-estimation of the Cu recovery from the S914 column, it remains possible to calculate the likely mass loaded to the column given the known Cu recovery efficiency of 78.91 % using this eluent identified in Chapter 7. The integrated area beneath the curve in Figure 8.2 corresponds to a recovery of 2.57 mg of Cu, which if assumed to be 78.91 % of the total, indicates a mass of 3.26 mg Cu was adsorbed by this column. As expected considering the selectivity of S914 towards Cu, no other metals were detected in effluent solutions during the elution cycle (Figure 8.2).
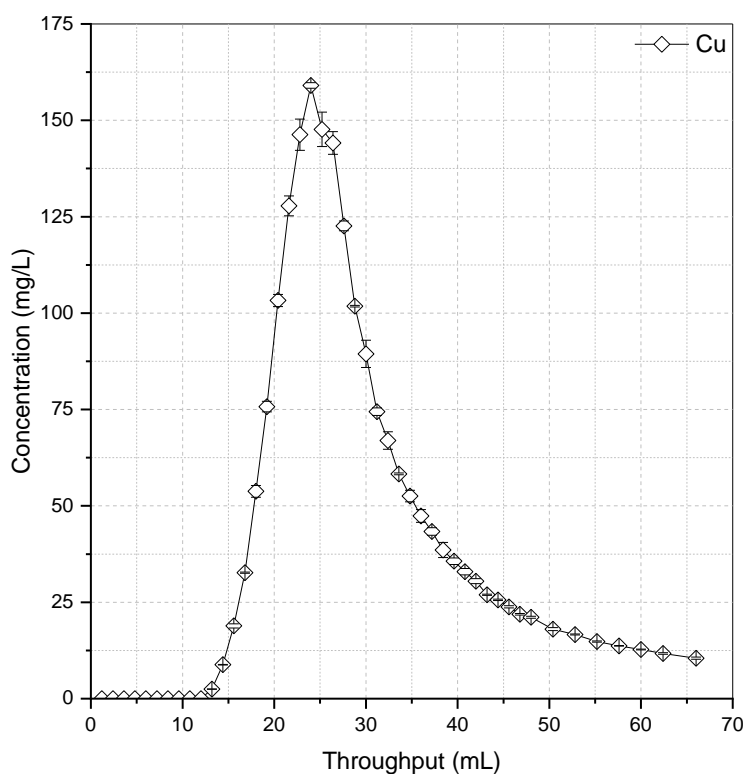
Figure 8.2. Elution of Cu from the S914 column at 2 BV/h using 0.5 M NaClO$_3$ at pH 2 (FWHM = 11.43 mL).

To better investigate the usability of eluted product streams, a rolling average of effluent metal concentrations was plotted as a function of eluent throughput. This allowed for a more realistic interpretation of the quality of product streams and gave an indication of solution composition at each point during the elution cycle (assuming that all effluents were collected and combined from the start of the elution process). For the elution of the S914 column in the coupled system, it was observed that combined effluents reached a concentration of 89 mg/L after 30 mL eluent throughput (Figure 8.3). Considering the whole elution profile captured in Figure 8.2, should all effluents be collected, the resulting Cu product solution would have a concentration of 55 mg/L (Figure 8.3).
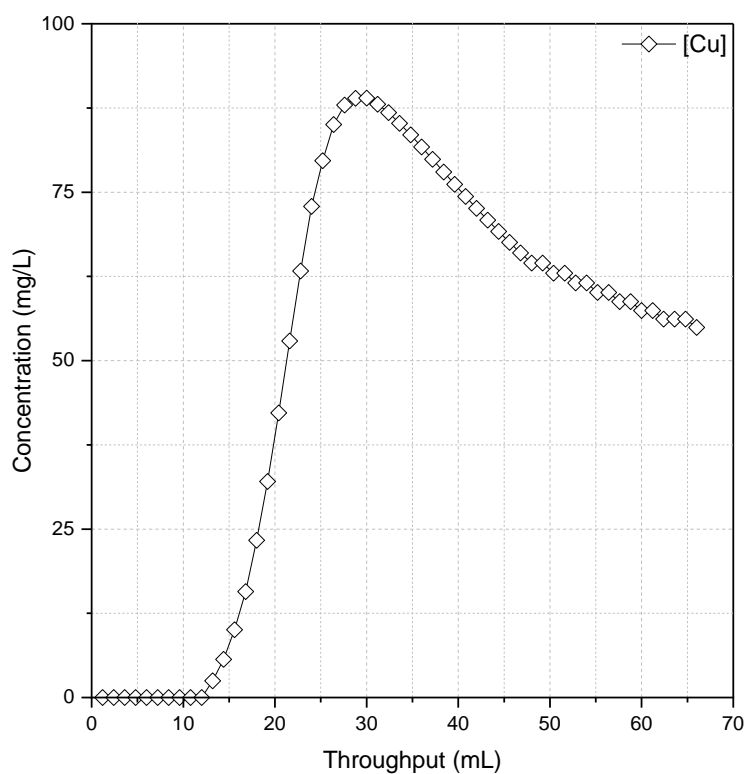
Figure 8.3. Combined effluent concentrations during the Cu-targeted elution of S914 presented in Figure 8.2.

8.3.2.2   Column No. 2: Dowex M4195 - Elution 1

During the first elution cycle of M4195, a 0.08 M H$^+$ solution of H$_2$SO$_4$ was used to target the recovery of Co. A distinct spike in Co concentration was observed beyond 4 BV eluent throughput, which reached a maximum concentration of 299.53 mg/L at 9 BV (Figure 8.4). Following this, concentrations reduced rapidly such that detection limits were reached after 21 BV. Through curve integration, the mass of Co recovered was calculated to be 2.19 mg, which when considering a Co recovery efficiency of 95.82 % for this eluent (Table 7.5) indicates that 2.29 mg of Co was initially loaded to this column.
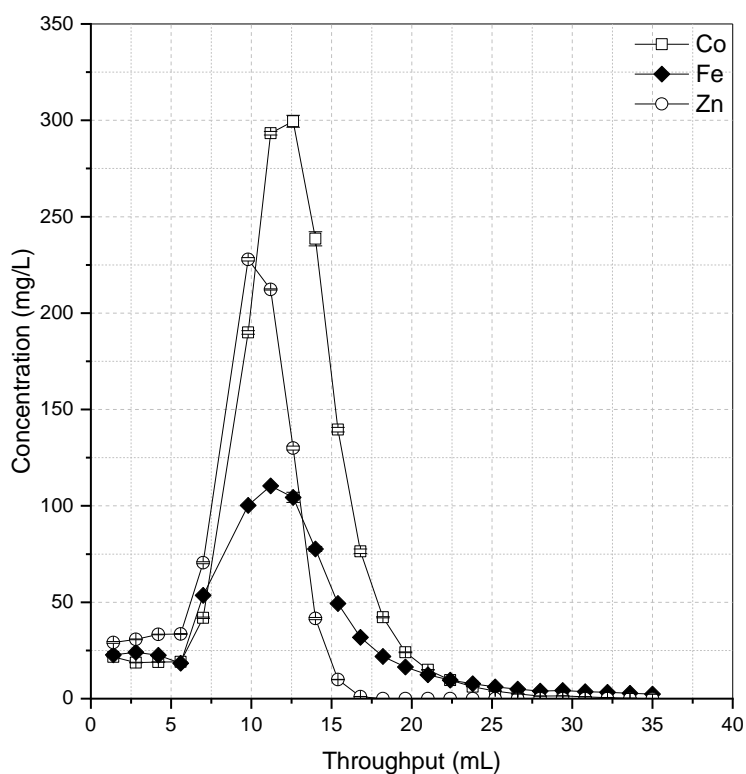
Figure 8.4. Cobalt-targeted elution of the M4195 column at 2 BV/h using 0.08 M H$^+$ (as H$_2$SO$_4$).

Important to note is that despite the M4195 column being used to target Co and Ni only, notable masses of Zn and Fe were adsorbed to the resin and resulted in elution of these ions in Figure 8.4. For Zn, the elution profile maximum occurred 2 BV prior to that of Co, reached a maximum concentration of 227.90 mg/L, and equated to a loaded mass of 1.34 mg Zn. For Fe, the extent of co-elution was lower than for Zn, reaching a concentration of 110.33 mg/L at 8 BV throughput and equating to a recovered mass of 1.07 mg Fe. As these were non-target metals, the efficiency of the 0.08 M H$^+$ eluent on their recovery was not determined in prior experimentation, and so it was not possible to estimate the extent of co-loading to the column. Promisingly, no Ni was detected during the initial elution of the M4195 column Figure 8.4, which indicates that the eluent was successful in leaving the Ni bound to the resin for subsequent elution using the more-concentrated eluent.

In terms of the composition of combined effluents, the point at which Co concentrations were highest was at 15.4 mL throughput, where Co concentration was 128 mg/L (Figure 8.5). However, given the unexpected presence of other metals in the effluent solution, the concentration of Fe and Zn in combined effluents at the point of highest Co concentration would be 58.3 mg/L and 81.9 mg/L, respectively.
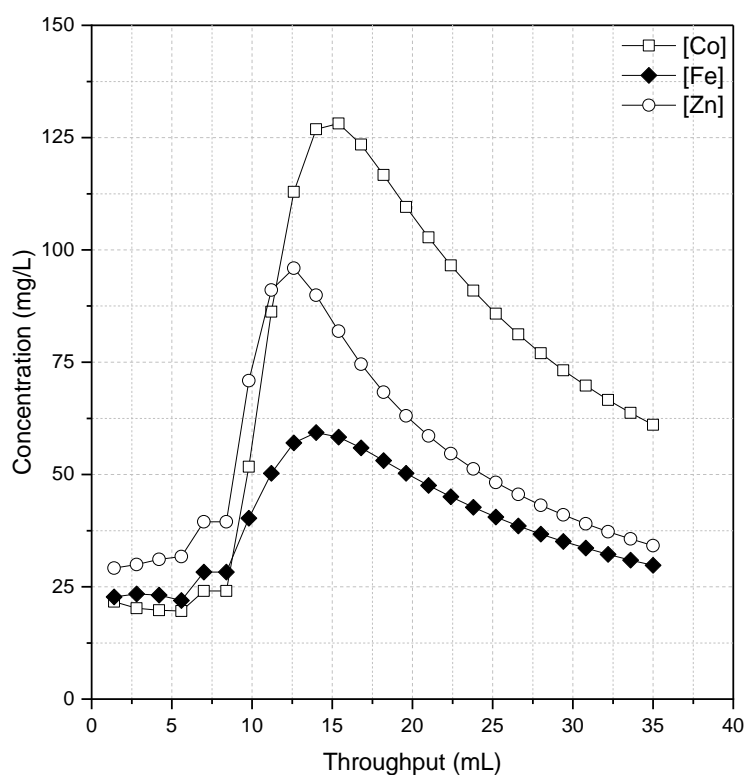
Figure 8.5. Combined effluent concentrations during the Co-targeted elution of M4195 presented in Figure 8.4.

8.3.2.3   Column No. 2: Dowex M4195 - Elution 2

Following the cobalt-targeted elution, the M4195 column was subjected to elution using a 1.0 M H$^+$ solution of H$_2$SO$_4$ with the aim of recovering Ni. Almost immediately upon eluent introduction, the

concentration of Ni detected in effluent solutions rose sharply to reach a concentration of 529.84

mg/L after 5.6 mL (4 BV) throughput (Figure 8.6). Calculation of the area beneath this elution profile

indicated a recovered mass of 3.35 mg Ni. Using the previously determined recovery efficiency of this

eluent for Ni (98.60 %; Table 7.6), the recovery of 3.35 mg here indicates an initial loading of 3.40 mg

to the M4195 column.
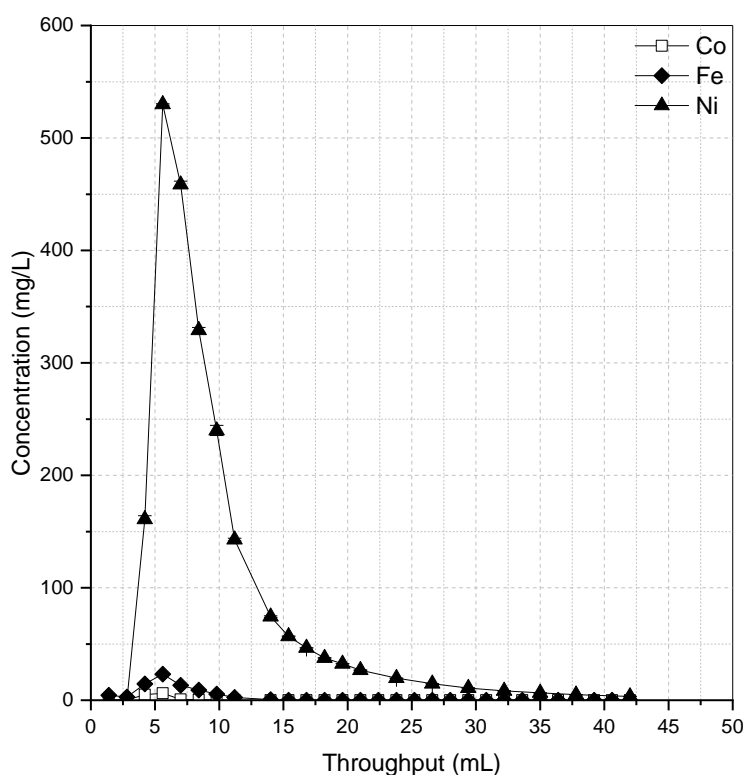
Figure 8.6. Nickel-targeted elution of the M4195 column at 2 BV/h using 1.0 M H^+ (as H_2SO_4).

Co-elution of other metals was very low, with only Fe and Co being detected in the effluent.

Maximum concentrations of Fe and Co both occurred simultaneously with that of Ni, but at much

lower concentration (23.18 mg/L and 6.17 mg/L for Fe and Co, respectively; Figure 8.6). Despite the

peaks being present, the low magnitude meant that contamination of the Ni eluate was minimal,

with only 0.10 mg of Fe and 0.02 mg of Co being eluted. This is further evidenced by examination of

combined effluent volumes (Figure 8.7), where at the maximum Ni concentration (246 mg/L, 8.4 mL

eluent) Fe and Co concentrations were considerably lower (11.2 mg/L and 2.1 mg/L, respectively).
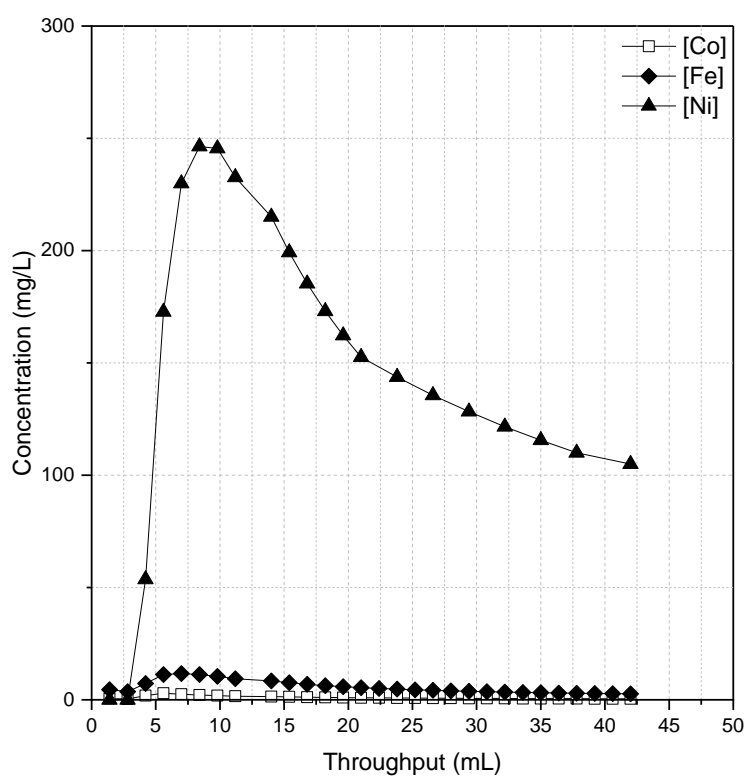
Figure 8.7. Combined effluent concentrations during the Ni-targeted elution of M4195 presented in Figure 8.6.

8.3.2.4   Column No. 3: Puromet MTS9570

The final column in the coupled system, Puromet MTS9570, was intended to act as a non-selective

'scrubbing' step to extract any metals which either; a) were not target species of the previous two

adsorbents, or b) had partially broken through from the previous columns. Previous experimental

work identified 1.0 M NaCl as a suitable eluent for Fe, Mn, and Zn (Chapter 7). During the elution of

S957, a very prominent profile for Zn was observed (Figure 8.8), which reached a maximum

concentration of 245.90 mg/L after 7 mL (5 BV) throughput.
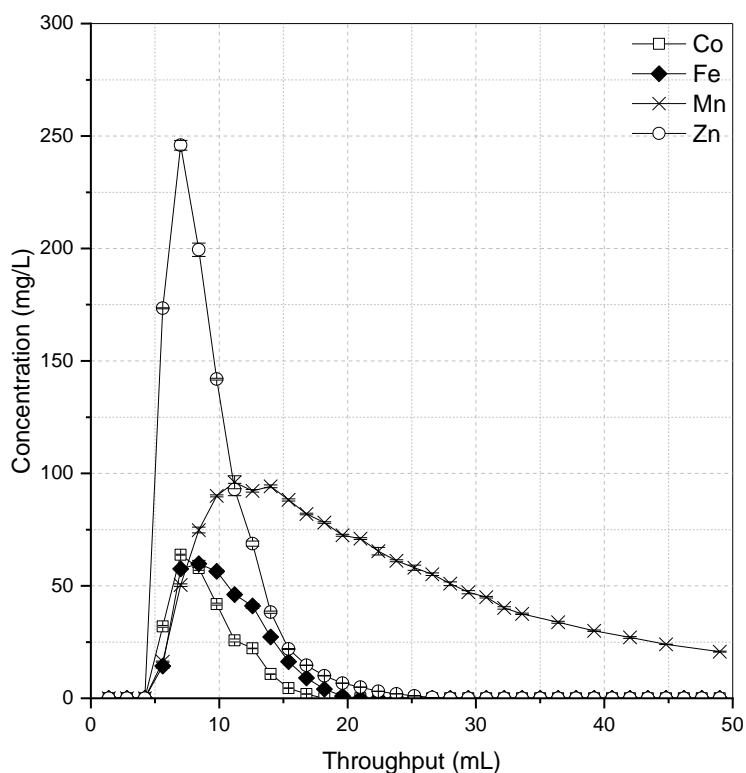
Figure 8.8. Elution of the S957 column at 2 BV/h using 1 M NaCl.

Integration of the area beneath the Zn profile indicated a recovery of 1.44 mg, which when

considering that 1.0 M was able to recover 100% of loaded Zn in screening studies (Table 7.12),

suggests that this was the total amount of Zn loaded to the S957 column. The maximum

concentration recorded for Fe was much lower than for Zn, reaching 59.79 mg/L across a broader

peak (Figure 8.8). The elution profile area represented a recovery of 0.47 mg Fe, which indicated an

initial loading of 0.57 mg Fe to the column when considering the eluent efficiency of 83.03 % for Fe.

As in previous elution screening results, the profile for Mn was of low magnitude but accounted for a

high mass. In this instance, maximum Mn concentration was encountered at 11.2 mL (8 BV) throughput and reached 92.81 mg/L. Following this point, concentrations decayed slowly resulting in a long tail portion of the curve. While the final portion of the curve was not captured during the sampling regime, the area under the curve represented a recovered mass of 2.32 mg Mn in total. Considering that the 1.0 M NaCl solution was known to recover 96.13 % of Mn from S957 (Table 7.12), this suggested that at least 2.41 mg of Mn was adsorbed to the S957 column during the system loading cycle. Alongside Fe, Mn, and Zn, there was also present a Co profile of similar magnitude to that of Fe. The maximum Co concentration encountered in the effluent solution was 63.83 mg/L at 7 mL (5 BV) eluent throughput. Integration of the area beneath the curve suggested a recovered mass of 0.36 mg Co.

Combined effluent concentrations indicated that for Zn, Fe, and Co, highest concentrations were attained at 11.2 mL throughput, with a maximum Zn concentration of 127 mg/L (Figure 8.9). At the point of maximum Zn concentration, the concentration of other metals was significantly lower (28 – 41 mg/L), suggesting a Zn-rich product stream at this point of the elution process. Towards the end of the elution phase, Mn was most concentrated in the combined effluent (51 mg/L) followed by Zn (31 mg/L), Fe (9.5 mg/L), and Co (7.4 mg/L), as shown in Figure 8.9.
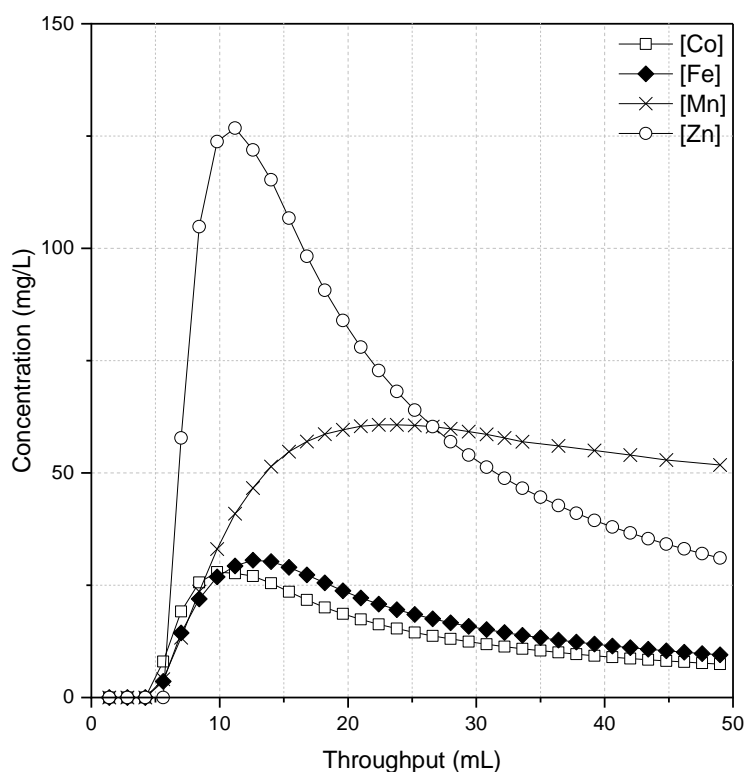
Figure 8.9. Combined effluent concentrations during the elution of S957 presented in Figure 8.8.

8.3.3   System Mass Balance

To understand how well the system performed during this initial trial, it was useful to determine the

extent to which metals were bound to the anticipated columns. The percentage of each metal which

was adsorbed to their respective target columns (i.e. Cu on S914, Co/Ni on M4195, Fe/Mn/Zn on

S957) is presented in the final column of Table 8.2. Given the nature of the experimental setup,

whereby multiple columns were operated in series, there was a 'lag' of 1 BV in PLS throughput for

each additional column, such that the third column received two fewer BV of PLS than the first. The

percentage of metal successfully loaded to their target columns was calculated taking this into

account, in addition to the masses recovered during the elutions (Figure 8.2 -Figure 8.8), and eluent

efficiencies. It can be seen that despite the elution processes being fairly effective towards their

target metal species, the loading cycle used was not optimised for properly controlling the fate of

metals within the system. The percentages of metals loaded to their *target* columns ranged from

88.2 % for Ni loading on M4195 down to only 12.9 % of Fe successfully loaded to S957. Mn loading to

S957 was achieved moderately successfully (76.5 % of all loaded Mn was on S957), as was Cu to S914

(75.7 %). It was apparent that the loading cycle employed did not maximise the potential capacity of

each resin bed, but despite this it was still possible to perform a chemical mass balance on the

system.

Table 8.2. Calculation of metal masses received, loaded, and eluted from each column of the coupled system, and the percentage of metal mass which was loaded to the intended column. [1]Calculated from PLS concentration and volume received by each column, [2]calculated from effluent composition during elution, [3]determined in Chapter 7, [4]back-calculated using known eluent efficiencies.

| | IN | | | OUT | | LOADING | | | |
| | Mass Received (mg)[1] | | | Mass Eluted[2] (mg) | Eluent Efficiency[3] (%) | Mass Loaded[4] (mg) | | | Loading Success (%) |
	S914	M4195	S957			S914	M4195	S957	
Co	4.33	4.02	3.71	2.20	95.82	-	2.30	-	57.1
Cu	4.30	3.99	3.69	2.57	78.91	3.26	-	-	75.7
Fe	4.29	3.98	3.67	0.47	98.60	-	-	0.47	12.9
Mn	4.26	3.96	3.66	2.32	83.03	-	-	2.80	76.5
Ni	4.26	3.95	3.65	3.35	96.13	-	3.49	-	88.2
Zn	4.19	3.89	3.59	1.44	100	-	-	1.44	40.0

Further to the mass of metals recovered during targeted elution, a certain portion of metals were

recovered due to co-elution, for example the Fe and Zn eluted during M4195 elution stages (Figure

8.4 - Figure 8.6), and the Co present in effluents from the S957 elution stage (Figure 8.8).

Additionally, a portion of the metals which were not recovered during the elution processes were

liberated during the final strip of each column, which when combined can give a better estimation of

the total metal mass which was accounted for during mass balance estimates, as shown below in

Table 8.3. In terms of mass balance, good accountability was achieved for Mn, Cu, and Ni, for which

over 95 % of the masses were accounted for in the calculated loading and observed elution

processes. Reasonable accountability was made for Zn and Co also, at 78.2 % and 72.1 %,

respectively. For Fe, however, only 45.4 % of the initial mass introduced to the system was

accounted for during the elution and stripping processes, indicating that the majority of Fe remained

bound to the system at the end of the experiment.

Table 8.3. Masses of metals co-eluted during system regeneration and final resin strip, and summary of the masses of metals accounted for during the mass balance exercise (mg and %). *Measured experimentally, M_A = amount of metal accounted for during mass balance calculations (mg, %), M_U = mass unaccounted for in calculations (mg, %).

	Mass co-eluted* (mg)	Final Strip* (mg)	M_A (mg)	M_A (%)	M_U (mg)	M_U (%)
Co	0.38	0	2.68	72.1	1.04	27.9
Cu	0	0.31	3.57	96.7	0.12	3.3
Fe	1.2	0	1.67	45.4	2.01	54.6
Mn	0	0.74	3.53	96.8	0.12	3.2
Ni	0	0	3.49	95.5	0.16	4.5
Zn	1.34	0.03	2.81	78.2	0.78	21.8

8.4   CHAPTER DISCUSSION

8.4.1   System Loading

Analysis of effluent metal concentrations from the coupled-column system revealed that

breakthrough of metals from the system were negligible, indicating that despite planning for

columns to reach 10 % breakthrough, this was not the case. While the loading period of 15 BV was

selected based on the point at which metals reached 10 % breakthrough during single column

loading studies (Chapter 6), this had not sufficiently accounted for the amount of metals adsorbed to

subsequent columns, and so while the loading of the first column (S914) was to the correct extent,

the Cu exiting this column did not reach the exit point of the system and as such was not detected.

While this oversight and lack of sampling points between columns hindered breakthrough analysis,

not reaching the desired loading extent on each column did not prevent useful findings from being

attained. Although overall metal loading to each column was lower than anticipated, it was still possible to gain insight as to how the system behaved during this early stage of loading in terms of elution effectiveness, the extent of co-elution, and the location of bound metals within the system.

8.4.2   S914 Elution

It was confirmed that effective Cu extraction and recovery was achieved using S914 as part of the coupled-column system, with production of a pure Cu product stream following resin elution. While this result is promising for effective treatment, this behaviour was not unexpected given that the composition of solution received by the first column of a coupled system is identical to the solution received during single-column screening experiments. Nevertheless, the quality of the Cu product stream is of high value in terms of resource recovery and provides a means for truly selective metal recovery from a complex waste stream.

Comparison of the elution profile in Figure 8.2 to that determined in Chapter 7 (Figure 7.8) revealed a lower maximum concentration in this instance (159 mg/L versus 511 mg/L). The lower concentration in Figure 8.2 is the result of the lesser extent of loading reached during the coupled system test and is not indicative of lower eluent effectiveness. In both instances, the point at which Cu concentrations reached their maximum was approximately 9 BV after first detection of Cu in the effluent solutions, indicating a similar elution behaviour in each case.

In the context of recovering an optimum value-added product stream from the system, there are several factors to take into consideration to decide how best to operate an ion exchange treatment system. For example, Figure 8.3 revealed that if all column effluents during the elution cycle were collected together, as would most likely be the case, a combined effluent Cu concentration of 89 mg/L could be obtained if collection were stopped after 30 mL eluent throughput. While this approach would result in the highest copper concentration in the product stream, and potentially more effective post-treatment of Cu (e.g. recovery by precipitation), only 60.2 % of the total eluted

Cu was recovered by this point of the elution cycle (Figure 8.2). It is therefore apparent that a trade-off exists between product stream concentration and total mass of metal recovered. However, given the single metal product stream and the reasonably high concentration of Cu after all of the elution profile was captured (55 mg/L), it is unlikely that this trade-off would cause significant issues during industrial operation.

8.4.3   M4195 Elution

As was identified in Chapter 7, a two-stage approach to metal elution from M4195 was effective for separately eluting Co and Ni product streams from the resin bed. The results of the Co-targeted elution from the M4195 column of the coupled system were provided in Figure 8.4, where it was shown that despite a clear Co elution profile, Fe and Zn were also present in the effluent solutions. The reason for the presence of Fe and Zn can be explained using the breakthrough behaviour previously observed in Chapter 6, where the order of metal breakthrough from M4195 at 5 BV/h (the same loading condition used for the coupled system) was Mn, Fe, Zn, Co, then Ni (Figure 6.2). Further to this, the breakthrough of Cu was negligible throughout M4195 dynamic screening experiments. While it was correctly assumed that the Cu would have been removed from solution by S914 prior to the PLS reaching the M4195 column, and that this would have made more capacity available for Co and Ni, it was overlooked that this would delay Fe and Zn displacement from the resin to the point where by the end of the loading cycle these metals remained bound to M4195. As such, the under-loading of the system is likely responsible for their presence on the M4195 column and in subsequent eluent solutions.

In terms of the composition of product streams, while the predominant constituent was Co (128 mg/L at the maximum point), significant concentrations of Fe and Zn were also encountered (Figure 8.5). Although it is anticipated that under more-optimised loading conditions this would not be the case, further treatment of the combined effluent obtained here would be required in order to

produce a Co product stream, be that through further ion exchange treatment or a selective precipitation approach. Most importantly, however, no Ni was detected in the elution profiles or combined effluent, which proves that despite the contamination of the Co product stream with Fe and Zn, no co-elution of Ni occurred and so remained on the resin for the subsequent elution process.

Following the elution of Co from the M4195 resin bed, the bed was subject to elution using a more concentrated acid eluent to target Ni, the results of which were presented in Figure 8.6. The Ni-targeted elution step was highly effective for the removal of Ni from the column, with the resulting elution curve reaching approximately 530 mg/L. Despite the highly effective removal of Ni using the 1.0 M H^+ eluent, the co-elution of Fe and Co was minimal (Figure 8.6), as also evidenced by the very low concentrations for these metals in Figure 8.7. Analysis of combined effluents revealed the great potential for this resin in terms of being able to produce a concentrated (246 mg/L) Ni-eluent solution of high purity. Such an outcome is desirable in terms of separations processes and would allow for simpler post-processing and recovery of a value-added product stream. Further to this, the minimal co-elution of metals in Figure 8.6 verifies that even under sub-optimal loading conditions where the Co product stream was contaminated, the two-stage elution process protects the Ni product stream and maintains its purity.

8.4.4 S957 Elution

Using the 1.0 M NaCl eluent previously determined to be most appropriate for S957 elution in Chapter 7, the elution profiles presented in Figure 8.8 were generated. While the overall curve heights were lower than in Chapter 7 due to lesser extent of column loading, the general trends in elution were similar, with a very pronounced profile for Zn and a lower and wider Mn profile (Figure 8.8, Figure 7.27). Where the results of elution from the coupled S957 column differ is in the Fe elution profile. Whereas for single-column studies the Fe maximum was higher than for Mn, under

coupled-column operation the Fe maximum was notably smaller, indicating that less Fe was present on the S957 column than expected, and therefore present elsewhere within the system. Further to this, the presence of a Co profile with similar magnitude to that of Fe was observed. While this does indicate that the M4195 column alone was not adequate for capturing all of the Co from solution, it does imply that the S957 column was performing successfully in capturing metal ions from previous resin beds and limiting their release to effluent waters.

While the purpose of using the sulfonic/phosphonic acid functionalised resin at the end of the system was not necessarily for the recovery value of eluted metals, Figure 8.9 revealed that depending upon the point at which elution was stopped, it was possible to recover a concentrated Zn solution from the resin. At the point where Zn concentrations in combined effluents was highest (11.2 mL throughput), the concentration was notably higher than other metals in the solution (Zn: 127 mg/L, Mn: 41 mg/L, Fe and Co: 29 mg/L). However, given that at this point the elution of Mn was only 16.9 % complete and that the effluent still contained several metals, it would be more appropriate to only consider the combined effluent for resource recovery following complete regeneration of the resin.

8.4.5   Mass Balance and Overall Performance

The presence of unanticipated metals in effluent samples during elution stages was able to give indication to the location of metals bound to the coupled-column system. The percentage of each metal which was loaded to the intended resin bed was provided in Table 8.2, where it was revealed while for certain metals their fate was properly controlled (e.g. Ni, Mn, Cu), for other metals this was not the case.

In particular, the percentage of Fe properly loaded to S957 was only 12.9 % of the Fe received by the system (Table 8.2). The significant Fe elution profile resulting from the first elution of M4195 (Figure 8.4), which represented a higher mass than that following S957 elution (Table 8.3), indicated that a

large portion of the Fe within the system had been loaded to the M4195 column and did not reach the S957 bed. However, when taking this mass of Fe into account, there still remained a mass of 2.01 mg of Fe which was unaccounted for in elution processes, equating to 54.6 % of the total Fe introduced to the system. Given that S914 exhibited no extraction of Fe in any experiment performed, it is only possible that the unaccounted Fe remained on the M4195 column after the Ni and Co-targeted elution cycles. Unfortunately, as the efficiency of the sulfuric acid eluents on M4195 was not explored, the mass recovered due to co-elution cannot be back-calculated to determine loading. However, considering the effect that increased H_2SO_4 concentration had on the extraction of Fe by M4195 in batch screening experiments (Figure 5.2), it is certainly possible that some Fe would remain associated with M4195 functional groups during contact with the 1 M H^+ eluent given that Fe was still extracted at this acidity in Chapter 5.

Another metal which was not sufficiently loaded to the target column was Co, for which only 57.1 % was loaded to M4195 (Table 8.2). While the Co which was adsorbed to M4195 was effectively recovered, a significant portion was loaded elsewhere; which considering the extent of co-elution was determined to be on S957. Whereas Fe was bound to a column preceding the target column, the additional Co was bound the final column of the system, indicating that it was displaced from M4195. This result was not ideal considering that it has been proved that selective Co and Ni recovery is possible from M4195. However, this observation of Co displacement from the target column is vital information for future refinement of the coupled system, where one possibility could be the use of two M4195 columns in series; the first of which would become gradually more-concentrated with Ni, and the second predominantly Co (in addition to Ni breakthrough from the first).

A visual overview of the system and its performance during this initial study is presented in Figure 8.10, alongside details of the composition of solutions used and generated throughout the loading and elution cycles.

		Description		Notes	
PLS		Mine water Cu,Co,Fe,Mn,Ni,Zn	21 mL 200 mg/L	–	
C1		S914	1.4 mL	–	
C2		M4195	1.4 mL	–	
C3		S957	1.4 mL	–	
E1		$NaClO_3$ HCl	0.5 M 0.01 M	Cu: 79%	
E2		H_2SO_4	0.08 M	Co: 96%	
E3		H_2SO_4	1.0 M	Ni: 99%	
E4		NaCl	1.0 M	Zn: 100% Fe: 83% Mn: 96%	
P1		Product stream	Cu: 89 mg/L	–	
P2		Product stream	Co: 128 mg/L Zn: 82 mg/L Fe: 58 mg/L	–	
P3		Product stream	Ni: 246 mg/L Fe: 11 mg/L Co: 2 mg/L	–	
P4		Product stream	Zn: 127 mg/L Mn: 61 mg/L Fe: 31 mg/L	–	
X		Peristaltic pump	–	X1: 7 mL/min X2: 2.8 mL/min	
OUT		Treated Water	Mn <0.01 mg/L Ni <0.01 mg/L	–	

Figure 8.10. Process flowsheet for the initial run of the coupled-column system (black solid lines = loading cycle, grey dashed lines = elution cycle, percentages represent eluent efficiencies towards specified metal ion (as per Chapter 7).

8.4.6. Preliminary Technoeconomic Assessment

Despite experimentation being performed solely at benchtop scale, it was desirable to understand the basic economic limitations of the process at a theoretical larger scale in order to understand economic limitations which may become apparent during future works. This was achieved by performing economic costings of the process based on; a) the cost of resin packing, b) the cost of eluent preparation, and c) the value of metals recovered. In all instances, a hypothetical column of 50 L bed volume was considered, with input data of resin capacities and eluent volume demand to achieve total recovery being scaled from data presented in Chapters 6 and 7, respectively, assuming that characteristics scale linearly. While extrapolating from such small-scale data is unlikely to yield results accurate to real-world operation, such calculations are valuable for highlighting areas of focus for future research and process optimisation.

Table 8.4. Preliminary technoeconomic assessment of resin bed packing and elution costs, and estimated metal recovery value based on linear scale up to 50 L bed capacity. [1]using estimated prices from manufacturer, [2]scaled from eluent volume required to achieve maximum recovery (Chapter 7), [3]based on chemical cost (Sigma-Aldrich website – not wholesale), [4]based on modelled operating capacities (Chapter 6) and eluent efficiencies, [5]data from London Metal Exchange.

	Resin Cost[1] (/bed)	Eluent Demand[2] (/cycle)	Eluent Cost[3] (/cycle)	Metal Recovered[4] (/cycle)	Metal Value[5] (/t)	Recovered Value (/cycle)
S914	£750	1000 L	£9,203	Cu: 3.5 kg	£5,329	£18.65
M4195	£7,000	715 L	£83.70	Co: 0.7 kg	£33,980	£23.79
		1070 L	£1,568	Ni: 3.57 kg	£11,391	£40.67
S957	£1,250	1070 L	£18.76	Fe: 1.50 kg	£94	£0.14
				Mn: 1.53 kg	£1,611	£2.46
				Zn: 1.53 kg	£1,888	£2.89

The preliminary technoeconomic assessment revealed that, based on extrapolation of the benchtop-scale process, the projected cost of column elution far exceeded the value of metals returned. Such a result was not entirely unexpected given that the previous optimisation of elution processes (Chapter 6) were not based on cost-minimisation, and so did not optimise for reduced eluent demand. However, these results do show that for S914, the regeneration of the resin bed may not be an economically feasible approach given that the resin was not able to be reused after elution with sodium chlorate, therefore preventing the cost of resin procurement to be offset. For M4195 and S957, however, good reusability potential was observed (Figure 7.13, Figure 7.24), and so despite resin packing costs being high, there remains potential for offsetting these costs over multiple treatment cycles, particularly after further optimisation of elution processes.

In terms of anticipated system operating regimes, it may be beneficial for two of each type of column to be used for treatment such that one may be regenerated while the other is being loaded to reduce system down-time. Such an approach may also allow for exhausted columns to be regenerated *ex-situ* using potentially lower-cost elution approaches to improve the overall economic viability of the process. For example, while the continuous requirement for mine water treatment lends itself well

for fixed-bed adsorption, it may be more cost-effective, through reduced eluent demand, to regenerate resins and recover metals using a batch-wise process. Rather than being prohibitive to the viability of the proposed system, the results of this preliminary technoeconomic assessment open avenues for future work, particularly in the optimisation of elution cycles by reducing overall eluent demand, either through the reuse of eluent batches, or through exploration of lower-cost eluent solutions.

8.5 CHAPTER CONCLUSIONS

This chapter presented the initial investigations into the effects that coupling ion exchange columns together has on metal extraction and the efficiency of elution when compared to single-column experiments. To the author's knowledge this represents the first study of three discrete resin beds of different functionalities being coupled together to achieve effective metal separations. As such, the data and insights generated here, while not entirely successful in light of the experimental aim, provided a groundwork for future studies on coupled-column treatment and highlighted the potential difficulties in designing a coupled system based on single-column screening experiments. From the results presented, a number of conclusions can be drawn, as detailed below;

- Observation of breakthrough from single-column experiments alone was not appropriate for determining the most ideal loading regime for the multi-column system. Despite this, however, useful observations were still able to be made of the effect that operating resins of different functionality in series had upon metal extraction and recovery.

- The previously observed Cu-specific extraction and recovery from S914 was maintained when operated in a coupled system and was shown to perform effectively as the lead-column, as evidenced by the absence of Cu in the elution profiles of subsequent columns.

- The insufficient loading period employed led to contamination of the Co product stream generated from the M4195 column by significant quantities of Fe and Zn. Further refinement of the loading process, and potentially bed volume of M4195, may help to optimise Co adsorption by this column. The Ni product stream was of high purity and was not significantly impacted by co-elution of other metals, and as such a highly effective separation of Ni was achieved from the PLS.

- The S957 column was effective in its role as a final 'scrubbing' column, to the extent where no metals were detected in system effluents over the studied period. The column adsorbed Fe, Mn, and Zn as expected, but also extracted the Co which had previously been displaced from the prior column.

- Overall, the mass balance exercise provided key insight to the location of metals bound within the system and was able to account for most of the metals within the PLS to a good degree. It was evident that the coupled-column system should undergo further optimisation before any future attempts are made at process scale-up.

9 CONCLUSIONS AND FUTURE WORK

This thesis has presented the results of novel work addressing four aspects of ion exchange resin behaviour and operation with respect to selective metal removal, namely; a) the identification of suitable resin functionalities and their limitations with respect to solution composition, b) the influence of flow rate upon metal removal characteristics under fixed-bed column operation, c) the feasibility of recovering bound metals from resins in an effective, sustainable, and selective manner, and d) the effectiveness of a novel coupled-functionality system for selective metal recovery. This closing chapter recaps the initial motivation behind the work, reviews how well the research aims were satisfied, and suggests which steps could be taken during future works.

9.1 MOTIVATION FOR WORK

As was introduced in Chapter 1, the issue of freshwater pollution resulting from the mining industry is a major factor contributing to the global scarcity of clean and safe drinking water. It is also the case that for many affected areas, the impacts of this pollution continue to occur long after mining operations have ceased, via the long-term hydrogeological processes governing mine water release and the atmospheric weathering of legacy waste deposits. The results of which are severe environmental degradation of local watercourses, and in some cases the contamination of groundwater aquifers designated for drinking water abstraction.

An emerging trend in the environmental management of these sites is to begin to view the metals responsible for the pollution as potential resources. The recovery of metals from mining wastes, be that through heavily-engineered leaching processes or in-situ leachate capture, has the potential to provide solutions to the mine waste problems for active *and* historic mines through; a) providing a means to improve overall operational efficiency in active mining operations, and b) attracting

investors to remediate legacy mine sites by providing opportunity to view the wastes as a resource. Regardless of application, it is clear that the removal of metals from mine wastes is a critical priority in limiting subsequent environmental damage and raises the possibility of simultaneous resource recovery.

In light of current mine water treatment techniques, where the emphasis has been on bulk metal removal via precipitation (whether through active chemical addition or passive biological processes), an ion exchange-based system was proposed whereby metals could be extracted selectively to increase the resource recovery potential of the final aqueous product stream. In researching this topic, it was found that not only were publications focused on ion exchange treatment of mine waters scarce, but also the selective removal of metals by resins in mixed metal sulfate media was rarely studied.

9.2 REVIEW OF RESEARCH AIMS

It is the author's view that the overall research aim of this work has been satisfied, as it has been shown that the metals present in mine waters can be removed, through selective dynamic adsorption, and effectively recovered as high-purity product streams through targeted elution. A review of the hypotheses presented in Chapter 3 are provided below.

The first aim of this work was to determine which resin functionalities were most appropriate for selective metal recovery, and to what extent this was controlled by solution composition. This work was completed under static conditions, as this allowed for understanding of equilibrium behaviour and facilitated the screening of a large number of resin functionalities concurrently. Nine resins of different functionality were screened under batch contact conditions to determine their extractive ability and selectivity towards metals encountered in mine wastes. It was immediately apparent that not all resins were appropriate for this application, with poor performance exhibited by Puromet MTS9100 and MTS9200. Strong acid resins, while capable of bulk metal extraction, were not

appropriate for selective metal recovery, whereas the weak acid and weak base chelating resins tended to perform more favourably. These results satisfied the first research aim of the work, proving that selective metal extraction from the synthetic mine water was achievable through careful selection of resin functionality. Furthermore, it was shown that effective recovery efficiencies were attained under the typical conditions within acid mine drainage, namely low pH and high sulfate concentrations, and for chelating resins the increased sulfate concentrations had a beneficial effect on performance.

The most promising finding of this chapter was the exclusive extraction of Cu by Puromet MTS9140, which was determined to be due to the electrochemical reduction of Cu(II) to Cu(I); a phenomenon that has not previously been described for an ion exchange resin in the literature. Such a finding has high potential for improving selective copper recovery and removal within a wide range of applications and industries.

Given that mine waters are released continuously, the treatment of them would also most likely be done in a continuous manner. This led to development of the second aim of the project, which was to determine any changes in performance of the most-suitable resins under dynamic conditions. A fixed-bed method was selected to investigate this, with flow rate investigations providing information on optimal operating conditions during loading phases, and also the effect of inter-metal competition for active sites during dynamic loading.

The five most suitable resins identified in Chapter 5 were studied under fixed-bed dynamic conditions at multiple flow rates to determine their applicability for continuous water treatment. Flow rate studies suggested a sharpening of the frontal portion of breakthrough curves with reduced flow rate, in addition to delayed breakthrough and higher modelled operating capacities. Slower flow rates were also associated with increased magnitude of metal displacement (overshoot) resulting from increased rates of inter-metal exchange on resin surfaces.

The results generated satisfied the second aim of the research, which was to determine whether acceptable performance was maintained under continuous treatment conditions. In assessing the selected resins, it became apparent that while Puromet MTS9501 and MTS9301 were promising under batch conditions, the abnormal interaction with Fe under dynamic conditions, and the under-performance for metal removal when compared to other resins, limited their applicability.

Because of the overarching aim of valorising mine wastes through metal recovery, it was vital to explore the possibility for recovering loaded metals from resin beds following removal from the synthetic mine water. As such, the fourth aim was developed to identify suitable eluents for this purpose, and where necessary determine the most appropriate technique for selectively eluting metals from resin beds where multiple metals were bound. In the context of process valorisation, it was necessary to maximise the concentration of metal within effluents to increase the economic value of recovered solutions. Furthermore, the reusability of each selected resin was determined, given that the longevity of a system is a major consideration in assessing appropriate technologies for water treatment.

A viable and sustainable resource recovery system cannot be achieved without the ability to recover the extracted metals. As such, a variety of elution approaches were trialled to maximise the recovery of metals from loaded columns. For Puromet MTS9140, the recovery of a pure Cu product stream was successfully achieved using an oxidative elution approach, albeit at the expense of repeated operation. A dual-eluent pH-controlled approach was successful in recovering distinct Co and Ni product streams from Dowex M4195, which was loaded with both metals. This process was optimised to minimise co-elution and shown to be repeatable over four cycles with no effect on performance. *Selective* metal elution from loaded Puromet MTS9570 was not achieved. However, given the lower value of metals targeted by this resin and the simplicity of the eluent, this was not considered an issue. Regeneration of this resin was highly effective and stable over repeated operating cycles.

As such, the third aim of the research was achieved, given that concentrated product streams were generated from resin beds following mine water treatment. Furthermore, a novel selective elution approach was observed to separate two valuable product streams (Ni and Co) directly from the M4195 bed – a major benefit in terms of reducing post-processing requirements.

The final aim of the project was to determine the effectiveness and suitability of a coupled-column system approach to selective metal removal. This has not been previously studied in the academic literature, and so provided a challenge.

An attempt was made to describe the operation of a triple-column coupled ion exchange system in terms of metal loading, metal recovery, and overall mass balance. Despite no previous research being available on systems such as this, the attempt was reasonably successful in its aims despite requiring further optimisation. In each instance of elution, the targeted metals were the most concentrated component of each effluent composition. However, it was observed that the metals which were not expected to be present on the columns were co-eluted alongside target metals during the first elution of M4195 and MTS9570. It was suggested that a longer loading period was required in order for metals to reach their designated locations within the coupled system prior to switching to the elution phase.

In light of the fourth research aim, the data presented showed that the fate of metals can be partially controlled when using a coupled system, and it is expected that this is achievable given further optimisation of the loading phase. Additionally, the eluents which were previously explored remained effective for metal recovery from the coupled system, particularly for Cu and Ni where a high degree of purity was achieved in recovered product solutions.

In terms of mine water treatment, a properly optimised coupled-column approach would provide the benefit of being tailorable towards the specific hydrochemical conditions encountered at different mine sites. The rationale for this approach was that by understanding the elemental composition of

leachates and the behaviour of resin metal extraction in complex solutions, systems installed at treatment sites may be tailored to provide maximum targeted recovery at that particular site.

Given the limited environmental budget allocated within the UK, private investment in remediation schemes is highly beneficial, and so the focus taken in this work has been primarily on selectively targeting those metals with higher market values to incentivise mine water treatment. Of particular value are Co ($33,980/tonne), Ni ($14,908/tonne), and Cu ($6833/tonne, as of September 2020 (LME, 2020)), and as such the selective recovery of these metals, and optimisation of their purity and concentration was particularly important. By having options in place for the recovery of these valuable metals, financial scope is afforded for the removal of other, less economically-attractive metals such as Mn (~ $2000/tonne) and Fe (~$120/tonne), which can be removed alongside to satisfy the environmental standards of residual effluents. In this sense, two often competing ideologies, the desire for financial gain and the desire for environmental protection, may be satisfied concurrently in line with 'green accounting' principles. By showing that the recovery of high-value resources is possible while also improving the environment, it is hoped that the treatment of legacy wastes may become sufficiently incentivised.

9.3 FUTURE WORK

It is suggested that future efforts focus on improving the operation and optimisation of laboratory scale coupled-column ion exchange systems to ensure that system loading and the location of metals within the system are better understood. A possible approach for this would be to engineer a setup whereby samples could be taken between columns at regular intervals to allow plotting of breakthrough from each discrete column rather than the whole system. However, this would likely require scale-up to minimise the effect that solution volumes lost to sampling would have upon loading of the subsequent column.

System scale-up would also have benefits in terms of better understanding the costs (material and energy) of treatment, and a more detailed technoeconomic assessment would allow exploration of economic feasibility at a scale more similar to real-world applications. Furthermore, the effects of system operating regimes on economic feasibility and resource maximisation may be explored. As an example, the effectiveness of reusing the same batch of eluent for regenerating multiple cycles of a column could be investigated to determine at which point the maximum value (environmental or monetary) could be gained from the materials used and improve overall resource efficiency.

Maximisation of resource efficiency is particularly desirable in terms of eluent volume minimisation, and so an avenue of potential exploration could be the use of batch-wise for resin regeneration, which may be a more sustainable and economically viable approach to system operation, not only through minimised eluent demand, but also reduced pumping requirements.

Once the proof of concept for a coupled-system approach has been provided, the next major step of work would involve the use of real mine water samples. This would allow for a more realistic assessment of system performance and would introduce variables such as differences in relative metal composition, and depending on the source waters, potential microbiological factors which were not included in this work. The use of real mine waters would advance the technological readiness level of the system and bring it a step closer to real-world application.

Finally, the work presented here has potential for benefitting other branches of the hydrometallurgy sector through knowledge transfer. While the selective removal of metals from sulfate media is important in environmental remediation and mineral processing industries, the overall strategic approach to resin screening and system development employed in this research may be applied to metals in other media (e.g. acidic chloride solutions) to frame research in other growing research areas, such as in nuclear decommissioning. This would also be beneficial in understanding how a selective ion exchange approach may be applied to a wider range of environmental pollutant sources, where metal speciation may be different to that encountered in acidic mine waters.

9.4 CONCLUSION

In conclusion, the presented work has addressed and achieved the research aims originally set out. Appropriate resin functionalities for selective metal removal from mine waters have been identified and proved to be effective for continuous water treatment. The recovery of metals from these resins has been shown to be achievable and viable in terms of generating a value-added product stream, particularly for Cu, Co, and Ni. Furthermore, initial steps were made in progression towards coupled-column treatment, with preliminary data suggesting that this approach is viable for the discrete pre-concentration of metals within the system *in-situ*.

Much work remains to be done to remedy the effects that mining has upon the water environment, and it is unlikely that there is one 'silver bullet' approach to achieve this. However, through its potential to combine resource recovery with environmental remediation, it is evident that selective ion exchange should be part of the solution.

10 REFERENCE LIST

Abdulbur-Alfakhoury, E., Van Zupten, S. & Leermakers, M., 2019. Development of the diffusive gradients in thin films technique (DGT) for platinum (Pt), palladium (Pd), and rhodium (Rh) in natural waters. *Talanta,* Volume 203, pp. 34-48.

Alexandratos, S. D., 2009. Ion-Exchange Resins: A Retrospective from Industrial and Engineering Chemistry Research. *Industrial Engineering Chemistry Research,* Volume 48, pp. 388-398.

Alexandratos, S. D. & Natesan, S., 1999. Ion-selective polymer-supported reagents: the principle of bifunctionality. *European Polymer Journal,* 35(3), pp. 431-436.

Al-Zoubi, H. et al., 2010. Optimization Study for Treatment of Acid Mine Drainage Using Membrane Technology. *Separation Science and Technology,* 45(14), pp. 2004-2016.

Amphlett, J. T. M. et al., 2018. Polyamine functionalised ion exchange resins: Synthesis, characterisation and uranyl uptake. *Chemical Engineering Journal,* Volume 334, pp. 1361-1370.

Amphlett, J. T. M. et al., 2020. Impact of Copper(II) on Activation Product Removal from Reactor Decommissioning Effluents in South Korea. *Journal of Industrial and Engineering Chemistry,* Volume 82, pp. 261-268.

Aqion, 2020. *Hydrochemistry & Water Analysis.* [Online]
Available at: https://www.aqion.de/
[Accessed 09 2020].

Armitage, P. D., Bowes, M. J. & Vincent, H. M., 2007. Long term changes in macroinvertebrate communities of a heavy metal polluted stream: The River Nent (Cumbria, UK) after 28 years. *River Research and Application,* Volume 23, pp. 997-1015.

Banks, D., Athresh, A., Al-Habaibeh, A. & Burnside, N., 2017. Water from abandoned mines as a heat source: practical experiences of open- and closed-loop strategies, United Kingdom. *Sustainable Water Resources Management,* pp. 1-22.

Banks, D. et al., 1997. Mine-water chemistry: the good, the bad and the ugly. *Environmental Geology,* 32(3), pp. 157-174.

Barros, M. A. S. D. et al., 2003. Binary ion exchange of metal ions in Y and X zeolites. *Brazilian Journal of Chemical Engineering,* 20(4), pp. 413-421.

Barros, M. A. S. D. et al., 2006. Chromium uptake from tricomponent solution in zeolite fixed bed. *Adsorption,* 12(4), pp. 239-248.

Bashir, W. & Paull, B., 2002. Ionic strength, pH and temperature effects upon selectivity for transition and heavy metal ions when using chelation ion chromatography with an iminodiacetic acid bonded silica gel column and simple inorganic eluents. *Journal of Chromatography A,* 942(1-2), pp. 73-82.

Bezzina, J. P., Ogden, M. D., Moon, E. M. & Soldenhoff, K. L., 2018. REE behavior and sorption on weak acid resins from buffered media. *Journal of Industrial and Engineering Chemistry,* Volume 59, pp. 440-455.

Biesinger, M. C., Lau, L. W. M., Gerson, A. R. & Smart, R. S. C., 2010. Resolving surface chemical states in XPS analysis of first row transition metals, oxides and hydroxides: Sc, Ti, V, Cu and Zn. *Applied Surface Science,* Volume 257, pp. 887-898.

Bleotu, I. et al., 2015. Removal of copper from diluted aqueous solutions using an iminodiacetic acid chelating ion exchange resin in a fixed-bed column. *Studia Universitatis Babes-Bolyai Seria Chemia,* Volume 3, pp. 163-172.

Blowes, D., Ptacek, C., Lambor, J. & Weisener, C., 2013. The Geochemistry of Acid Mine Drainage. In: H. D. Holland & K. K. Turekian, eds. *Treatise on Geochemistry.* 2nd ed. s.l.:Elsevier Science, pp. 149-204.

Blowes, D. W. et al., 2000. Treatment of inorganic contaminants using permeable reactive barriers. *Journal of Contaminant Hydrology,* 45(1-2), pp. 123-137.

Bohart, G. S. & Adams, E. Q., 1920. Some Aspects of the Behaviour of Charcoal with Respect to Chlorine. *Journal of the American Chemical Society,* 42(3), pp. 523-544.

Boss, B. C. & Fredeen, K. J., 2004. *Concepts, Instrumentation and Techniques in Inductively Coupled Plasma Optical Emission Spectrometry.* 3rd ed. Shelton, CT: Perkin Elmer.

Bradshaw, D. K., 2013. *The Analysis of Water and Wastes by U.S. EPA Method 200.7,* Waltham, MA: Perkin Elmer, Inc..

Brown, M., Barley, B. & Wood, H., 2002. *Minewater Treatment: Technology, Application and Policy.* 1st ed. London: IWA Publishing.

Bukowska, A., Bukowski, W. & Pytel, M., 2015. Scavenging properties of the polyamine functionalized gels based on the glycidyl methacrylate terpolymers. *Open Journal of Polymer Chemistry,* Volume 5, p. 63.

Calero, M. et al., 2009. Study of Cr(III) biosorption in a fixed-bed column. *Journal of Hazardous Materials,* 171(1-3), pp. 886-893.

Canner, A. J., Pepper, S. E., Hayer, M. & Ogden, M. D., 2017. Removal of radionuclides from a HCl steel decontamination stream using chelating ion exchange resins - Initial studies. *Progress in Nuclear Energy,* Volume 104, pp. 271-279.

Casas, J. M., Crisóstomo, G. & Cifuentes, L., 2005. Speciation of the Fe(II)–Fe(III)–H2SO4–H2O system at 25 and 50 °C. *Hydrometallurgy,* 80(4), pp. 254-264.

CheCalc, 2019. *Packed Bed Pressure Drop.* [Online]
Available at: https://checalc.com/solved/packed_bed.html
[Accessed 10 September 2020].

Chen, T., Yan, B., Lei, C. & Xiao, X., 2014. Pollution control and metal resource recovery for acid mine drainage. *Hydrometallurgy,* Volume 147-148, pp. 112-119.

Chiarizia, R. et al., 1993. Uptake of metal ions by a new chelating ion-exchange resin. Part 2. Acid dependencies of transition and post-transition metal ions. *Solvent Extraction and Ion Exchange,* 11(5), pp. 967-985.

Chu, K. H., 2010. Fixed bed sorption: Setting the record straight on the Bohart-Adams and Thomas models. *Journal of Hazardous Materials,* 177(1-3), pp. 1006-1012.

Cortina, J.-L.et al., 2003. Passive In Situ Remediation of Metal-Polluted Water with Caustic Magnesia: Evidence from Column Experiments. *Environmental Science and Technology,* 37(9), pp. 1971-1977.

Coulson, J. M. & Richardson, J. F., 2002. *Chemical Engineering Volume 2: Particle Technology & Separation Processes.* 5th ed. Oxford: Butterworth-Heinemann.

Dąbrowski, A., Hubicki, Z., Podkościelny, P. & Robens, E., 2004. Selective removal of the heavy metal ions from waters and industrial wastewaters by ion-exchange method. *Chemosphere,* 56(2), pp. 91-106.

Dardouri, S. & Sghaier, J., 2017. A comparative study of adsorption and regeneration with different agricultural wastes as adsrobents for the removal of methylene blue from aqueous solution. *Chinese Journal of Chemical Engineering,* Volume 25, pp. 1282-1287.

Deepatana, A. & Valix, M., 2006. Recovery of nickel and cobalt from organic acid complexes: Adsorption mechanisms of metal-organic complexes onto aminophosphonate chelating resin. *Journal of Hazardous Materials,* 137(2), pp. 925-933.

Diniz, C., Ciminelli, V. & Doyle, F., 2005. The use of the chelating resin Dowex M-4195 in the adsorption of selected heavy metal ions from manganese solutions. *Hydrometallurgy,* 78(3-4), pp. 147-155.

Diniz, C. V., Ciminelli, V. S. T. & Doyle, F. M., 2005. The use of chelating resin Dowex M-4195 in the adsorption of selected heavy metal ions from manganese solutions. *Hydrometallurgy,* 78(3-4), pp. 147-155.

Diniz, C. V., Doyle, F. M. & Ciminelli, V. S. T., 2002. Effect of pH on the adsorption of selected heavy metal ions from concentrated chloride solutions by the chelating resin Dowex M-4195. *Separation Science and Technology,* 14(3169-3185), p. 37.

Dionex Corporation, 1998. *DX-120 Ion Chromatograph Operator's Manual,* USA: Dionex Corporation.

Djoudi, N., Mostefa, M. L. P. & Muhr, H., 2019. Precipitation of Cobalt Salts for Recovery in Leachates. *Chemical Engineering & Technology,* 42(7), pp. 1492-1499.

Dupont, D., Raiguel, S. & Binnemans, K., 2015. Sulfonic acid functionalized ionic liquids for dissolution of metal oxides and solvent extraction of metal ions. *Chemical Communications,* Volume 51, pp. 9006-9009.

Dytham, C., 2011. *Choosing and Using Statistics: A Biologist's Guide.* 3rd ed. Sussex: Wiley & Blackwell.

Ebrahimi, S. & Roberts, D. J., 2013. Sustainable nitrate-contaminated water treatment using multi-cycle ion-exchange/bioregeneration of nitrate selective resin. *Journal of Hazardous Materials,* Volume 262, pp. 539-544.

Eldridge, D. S., Crawford, R. J. & Harding, I. H., 2015. The role of metal ion-ligand interactions during divalent metal ion adsorption. *Journal of Colloid and Interface Science,* Volume 454, pp. 20-26.

Fakhar, I., Yamin, B. M. & Hasbullah, S. A., 2017. A comparative study of the metal binding behaviour of alanine based bis-thiourea isomers. *Chemistry Central Journal,* Volume 11, p. 76.

Falagán, C., Grail, B. M. & Johnson, D. B., 2017. New approaches for extracting and recovering metals from mine tailings. *Minerals Engineering,* Volume 106, pp. 71-78.

Feng, D., Aldrich, C. & Tan, H., 2000. Treatment of acid mine water by use of heavy metal precipitation and ion exchange. *Minerals Engineering,* 13(6), pp. 623-642.

Filimonov, E. V. & Shcherbakov, A. I., 2004. Catalytic Effect of Copper Ions on Nitrate Reduction. *Protection of Metals,* 40(3), pp. 280-284.

Fu, F. & Wang, Q., 2011. Removal of heavy metal ions from wastewaters: A review. *Journal of Environmental Management,* 92(3), pp. 407-418.

Gandy, C. & Jarvis, A., 2006. *Attenuation of mine pollutants in the hyporheic zone,* Bristol: Environment Agency.

García, V. et al., 2014. Purification techniques for the recovery of valuable compounds from acid mine drainage and cyanide tailings: application of green engineering principles. *Journal of Chemical Technology and Biotechnology,* 89(6), pp. 803-813.

Garino, T. J., Nenoff, T. M., Krumhansl, J. L. & Rademacher, D. X., 2011. Low-Temperature Sintering Bi-Si-Zn-Oxide Glasses for Use in Either Glass Composite Materials or Core/Shell 129I Waste Forms. *Journal of the American Ceramic Society,* 94(8), pp. 2412-2419.

Gaur, A. et al., 2013. X-ray absorption of fine structure study of multinuclear copper(I) thiourea mixed ligand complexes. *The Journal of Chemical Physics,* 139(3).

Gillespie, W. B. et al., 1999. Transfers and Transformations of Zinc in Flow-Through Wetland Microcosms. *Ecotoxicology and Environmental Safety,* 43(2), pp. 126-132.

Gombert, P. et al., 2019. An overview of priority pollutants in selected mine discharges in europe. *Mine Water and the Environment,* 38(1), pp. 16-23.

Green, B. R. & Hancock, R. D., 1982. Useful resins for the selective extraction of copper, nickel and cobalt. *Journal of the Southern African Institute of Mining and Metallurgy,* p. 303.

Hamdaoui, O., 2009. Removal of copper(II) from aqueous phase by Purolite C100-MB cation exchange resin in fixed bed columns: Modeling. *Journal of Hazardous Materials,* Volume 161, pp. 737-746.

Hardwick, E. & Hardwick, J., 2016. *An overview of the use of Ion Exchange to extract wealth from mine waters.* Freiberg, Germany, International Mine Water Association.

Harland, C. E., 1994. *Ion Exchange: Theory and Practice.* 2nd ed. Cambridge: Royal Society of Chemistry.

Hayez, V., Franquet, A., Hubin, A. & Terryn, H., 2004. XPS study of the atmospheric corrosion of copper alloys of archaeological interest. *Surface and Interface Analysis,* 36(8), pp. 876-879.

Helferrich, F., 1995. *Ion Exchange.* New York: Dover Publications, Inc..

Huang, X. et al., 2017. Preparation of a novel resin with acyl and thiourea groups and its properties for Cu(II) removal from aqueous solution. *Journal of Environmental Management,* Volume 204, pp. 264-271.

Hubicki, Z. & Kołodyńska, D., 2012. Selective Removal of Heavy Metal Ions from Waters and Waste Waters Using Ion Exchange Methods. In: A. Kilislioglu, ed. *Ion Exchange Technologies.* Rijeka, Croatia: InTech, pp. 193-240.

Janin, A., Blais, J. F., Mercier, G. & Drogui, P., 2009. Selective recovery of Cr and Cu in leachate from chromated copper arsenate treated wood using chelating and acidic ion exchange resins. *Journal of Hazardous Materials,* 169(1-3), pp. 1099-1105.

Jarvis, A. P. et al., 2014. *Mitigation of pollution from abandoned metal mines. Part 1: Review of passive treatment technologies for metal mine drainage remediation,* Bristol: Environment Agency.

Jarvis, A. P., Gandy, C. J. & Gray, N. D., 2012. *Mitigation of pollution from abandoned metal mines; Part 1: Review of passive treatment technologies for metal mine drainage remediation,* Bristol: Environment Agency.

Jarvis, A. P. & Younger, P. L., 1997. Dominating chemical factors in mine water induced impoverishment of the invertebrate fauna of two streams in the Durham coalfield, UK. *Chemistry and Ecology,* 13(4), pp. 249-270.

Jarvis, A. P. & Younger, P. L., 2000. Broadening the scope of mine water environmental impact assessment: a UK perspective. *Environmental Impact Assessment Review,* 20(1), pp. 85-96.

Jeffrey, M. I., Hewitt, D. M., Dai, X. & Brunt, S. D., 2010. Ion exchange adsorption and elution for recovering gold thiosulfate from leach solutions. *Hydrometallurgy,* 100(3-4), pp. 136-143.

Johnson, D. B. & Hallberg, K. B., 2003. The microbiology of acidic mine waters. *Research in Microbiology,* 154(7), pp. 466-473.

Johnson, D. B. & Hallberg, K. B., 2005. Acid mine drainage remediation options: a review. *Science of The Total Environment,* 338(1-2), pp. 3-14.

Johnston, D. et al., 2008. *Abandoned mines and the water environment. Science Project SC030136-41,* Bristol: Environment Agency.

Jones, A. et al., 2013. Mine water geochemistry and metal flux in a major historic Pb-Zn-F orefield, the Yorkshire Pennines, UK. *Environmental Science and Pollution Research,* Volume 20, pp. 7570-7581.

Jouini, M., Neculita, C. M., Genty, T. & Benzaazoua, M., 2020. Environmental behavior of metal-rich residues from the passive treatment of acid mine drainage. *Science of The Total Environment,* Volume 712, p. 136541.

Kefeni, K. K., Msagati, T. A. M. & Mamba, B. B., 2017. Acid mine drainage: Prevention, treatment options, and resource recovery: A review. *Journal of Cleaner Production,* Volume 151, pp. 475-493.

Khatri, N., Tyagi, S. & Rawtani, D., 2017. Recent strategies for the removal of iron from water: A review. *Journal of Water Process Engineering,* 19(13), pp. 291-304.

Kirchnerova, J. & Purdy, W. C., 1981. The mechanism of the electrochemical oxidation of thiourea. *Analytica Chimica Acta,* 123(1), pp. 83-95.

Kołodyńska, D., Sofińska-Chmiel, W., Mendyck, E. & Hubicki, Z., 2014. DOWEX M 4195 and LEWATIT MonoPlus TP 220 in Heavy Metal Ions Removal from Acidic Streams. *Separation Science and Technology,* 49(13), pp. 2003-2015.

Konno, H., 2016. Chapter 8 - X-ray Photoelectron Spectroscopy. In: M. Inagaki, ed. *Materials Science and Engineering of Carbon.* s.l.:Elsevier, pp. 153-171.

Kononova, O. N. et al., 2014. Sorption recovery of copper(II) and zinc(II) from aqueous chloride solutions. *Journal of the Serbian Chemical Society,* 79(8), pp. 1037-1049.

Kononova, O. N., Melnikov, A. M. & Demitrichenko, D. S., 2013. Simultaneous ion exchange recovery and subsequent separation of platinum (II, IV), Rhodium (III), and Nickel (II) from chloride and sulfate-chloride solutions. *Solvent Extraction and Ion Exchange,* 31(3), pp. 306-319.

Korak, J. A., Huggins, R. & Arias-Paic, M., 2017. Regeneration of pilot-scale ion exchange columns for hexavalent chromium removal. *Water Research,* 118(1), pp. 141-151.

Kruse, N. A. et al., 2013. The role of remediation, natural alkalinity sources and physical stream parameters in stream recovery. *Journal of Environmental Management,* Volume 128, pp. 1000-1011.

Krzewska, S., Podsiadly, H. & Pajdowski, L., 1980. Studies on the Reaction of Copper(II) with thiourea - III: Equilibrium and Stability Constants in Cu(II)-Thiourea-HClO4 Redox System. *Journal of Inorganic and Nuclear Chemistry,* 42(1), pp. 89-94.

Kusin, F. M., Jarvis, A. P. & Gandy, C. J., 2010. Hydraulic residence time and iron removal in a wetland receiving ferruginous mine water over a 4 year period from commissioning. *Water Science and Technology,* 62(8), pp. 1937-1946.

Kuz'min, V. & Kuz'min, D., 2014. Sorption of nickel and copper from leach pulps of low-grade sulfide ores using Purolite S930 chelating resin. *Hydrometallurgy,* Volume 141, pp. 76-81.

Lachat Instruments, 2009. *QuikChem with Ion Chromatography Option.* [Online]
Available at: http://www.lachatinstruments.com/products/quik-chem-ion-chromatography/faq.asp#4
[Accessed 09 July 2019].

Lèbre, É., Corder, G. & Golev, A., 2017. The Role of the Mining Industry in a Circular Economy: A Framework for Resource Management at the Mine Site Level. *Journal of Industrial Ecology,* 21(3), pp. 662-672.

Lèbre, É., Corder, G. & Golev, A., 2017. The Role of the Mining Industry in a Circular Economy: A Framework for Resource Management at the Mine Site Level. *Journal of Industrial Ecology,* 21(3), pp. 662-672.

Liebenberg, C. J. et al., 2013. *The recovery of nickel and cobalt from a sulphate bioleach solution using Dow M4195.* Mpumalanga, The Southern African Institute of Mining and Metallurgy.

Littlejohn, P. & Vaughan, J., 2012. Selectivity of commercial and novel mixed functionality cation exchange resins in mildly acidic sulfate and mixed sulfate-chloride solution. *Hydrometallurgy,* Volume 121-124, pp. 90-99.

LME, 2020. *London Metal Exchange: Home.* [Online]
Available at: https://www.lme.com/
[Accessed September 2020].

Loureiro, J. M. & Rodrigues, A. E., 1998. Sorption of Metals by an Amidoxime Chelating Resin. Part I: Equilibrium. *Separation Science and Technology,* 33(11), pp. 1585-1604.

Luttrell Jr, G. H., More, C. & Kenner, C., 1971. Effect of pH and Ionic Strength on Ion Exchange and Chelating Properties of an Iminodiacetate Ion Exchange Resin with Alkaline Earth Ions. *Analytical Chemistry,* 43(11), pp. 1370-1375.

Lv, R. et al., 2019. Removal of Fe3+ and Al3+ ions from phosphoric acid-nitric acid solutions with chelating resins. *Hydrometallurgy,* Volume 188, pp. 194-200.

Lv, R. et al., 2019. Removal of iron (III) and aluminium ions from phosphoric acid-nitric acid solutions by S957 chelation resin: kinetics, dynamic adsorption and elution. *Industrial and Engineering Chemistry Research,* XX(XX), pp. XXX-XXX.

Mackie, A. L., Laliberte, M. & Walsh, M. E., 2016. Comparison of Single and Two-Stage Ballasted Flocculation Processes for Enhanced Removal of Arsenic from Mine Water. *Journal of Environmental Engineering,* 142(2), pp. 1-8.

Marhol, M. & Cheng, K. L., 1974. Some chelating ion-exchange resins containing ketoiminocarboxylic acids as functional groups. *Talanta,* Volume 21, pp. 751-762.

Mayes, W. M. et al., 2009. Wetland treatment at extremes of pH: A review. *Science of the Total Environment,* 407(13), pp. 3944-3957.

Mayes, W. M. et al., 2009. Wetland treatments at extremes of pH: A review. *Science of the Total Environment,* 407(13), pp. 3944-3957.

Mayes, W. M., Johnston, D., Potter, H. A. B. & Jarvis, A. P., 2009. A national strategy for identification, prioritisation and management of pollution from abandoned non-coal mine sites in England and Wales. I. Methodology development and initial results W.M.. *Science of the Total Environment,* 407(21), pp. 5435-5447.

Mayes, W. M., Johnston, D., Potter, H. & Jarvis, A., 2009. A national strategy for identidication, prioritisation and management of pollution from abandoned non-coal mine sites in England and Wales. I. Methodology development and initial results.. *Science of the Total Environment,* 407(21), pp. 5435-5447.

Mayes, W. M., Potter, H. A. B. & Jarvis, A. P., 2009. Novel approach to zinc removal from circum-neutral mine waters using pelletised recovered hydrous ferric oxide. *Journal of Hazardous Materials,* 162(1), pp. 512-520.

Mayes, W. M., Potter, H. & Jarvis, A., 2010. Inventory of aquatic contaminant flux arising from historical metal mining in England and Wales. *Science of the Total Environment,* 408(17), pp. 3576-3583.

McKevitt, B. & Dreisinger, D., 2009. A comparison of various ion exchange resins for the remova of ferric ions from copper electrowinning electrolyte solutions part I: Electrolytes containing no other impurities. *Hydrometallurgy,* 98(1-2), pp. 116-121.

McKevitt, B. & Dreisinger, D., 2009. A comparison of various ion exchange resins for the removal of ferric ions from copper electrowinning electrolyte solutions part I: Electrolytes containing no other impurities. *Hydrometallurgy,* 98(1-2), pp. 116-121.

Mendes, F. D. & Martins, A. H., 2004. Selective sorption of nickel and cobalt from sulphate solutions using chelating resins. *International Journal of Mineral Processing,* 74(1-4), pp. 359-371.

Mendes, F. & Martins, A., 2004. Selective soprtion of nickel and cobalt from sulphate solutions using chelating resins. *International Journal of Mineral Processing,* 74(1-4), pp. 359-371.

Mohajane, G. B., Maree, J. P. & Panichev, N., 2014. Treatment of iron(II)-rich acid mine water with limestone and oxygen. *Water Science and Technology,* 70(2), pp. 209-217.

Monteagudo, J. M. & Ortiz, M. J., 2000. Removal of inorganic mercury from mine waste water by ion exchange. *Journal of Chemical Technology and Biotechnology,* Volume 75, pp. 767-772.

Moustafa, Y. M. & Morsi, R. E., 2013. Ion Exchange Chromatography - An Overview. In: D. Martin & B. Martin, eds. *Column Chromatography.* s.l.:IntechOpen, pp. 1-30.

Muraviev, D., Noguerol, J. & Valiente, M., 1997. Application of the reagentless dual-temperature ion-exchange technique to a selective separation and concentration of copper versus aluminum from acidic mine waters. *Hydrometallurgy,* Volume 44, pp. 331-346.

Nagib, S., Inoue, K., Yamaguchi, T. & Tamaru, T., 1999. Recovery of Ni from a large excess of Al generated from spent hydrodesulfurization catalyst using picolylamine type chelating resin and complexane types of chemically modified chitosan. *Hydrometallurgy,* 51(1), pp. 73-85.

Nariyan, E., Sillanpää, M. & Wolkersdorfer, C., 2017. Electrocoagulation treatment of mine water from the deepest working European metal mine - Performance, isotherm and kinetic studies. *Separation and Purification Technology,* Volume 177, pp. 363-373.

Neymeyer, A., Williams, R. T. & Younger, P. L., 2007. Migration of polluted mine water in a public supply aquifer. *The Quarterly Journal of Engineering Geology and Hydrogeology,* 40(1), pp. 75-84.

Oh, C. et al., 2015. Efficiency assessment of cascade aerator in a passive treatment system for Fe(II) oxidation in ferruginous mine drainage of net alkaline. *Environmental Earth Sciences,* 73(9), pp. 5363-5373.

Oliveira, L. M. et al., 2015. Fixed-bed column process as a strategy for separation and purification od cephamycin C from fermented broth. *Industrial & Engineering Chemistry Research,* 54(11), pp. 3018-3026.

Outola, P., Leinonen, V., Ridell, M. & Lehto, J., 2001. Acid/Base and Metal Uptake Properties of Chelating and Weak Base Resins. *Solvent Extraction and Ion Exchange,* 19(4), pp. 743-756.

Page, M. J., Soldenhoff, K. & Ogden, M. D., 2017. Comparative study of the application of chelating resins for rare earth recovery. *Hydrometallurgy,* Volume 169, pp. 275-281.

Parkhurst, D. L. & Apello, C. A. J., 1999. *User's guide to PHREEQC - A computer program for speciation, batch-reaction, one-dimensional transport, and inverse geochemical calculations,* Denver: U.S. Geological Survey Water-Resources Investigations Report.

Patel, H., 2019. Fixed-bed column adsorption study: a comprehensive review. *Applied Water Science,* Volume 9, p. 45.

Pérez-Gallent, E., Figueiredo, M. C., Katsounaros, I. & Koper, M. T. M., 2017. Electrocatalytic reduction of Nitrate on Copper single crystals in acidic and alaline solutions. *Electrochemica Acta,* Volume 227, pp. 77-84.

Perez, I. D., Botelho Junior, A. B., Aliprandini, P. & Espinosa, D. C. R., 2019. Copper recovery from nickel laterite with high-iron content: A continuous process from mining waste. *The Canadian Journal of Chemical Engineering,* Volume 1, pp. 1-12.

Perkin Elmer, Inc., 1996. *Analytical Methods for Atomic Absorption Spectroscopy,* s.l.: Perkin Elmer, Inc..

Perkin-Elmer, 1996. *Analytical Methods for Atomic Absorption Spectroscopy,* s.l.: The Perkin-Elmer Corporation.

Phillips, D. H., 2009. Permeable reactive barriers: A sustainable technology for cleaning contaminated groundwater in developing countries. *Desalination,* 248(1-3), pp. 352-359.

PIRAMID Consortium, 2003. *Engineering guidelines for the passive remediation of acidic and/or metalliferous mine drainage and similar wastewaters,* Newcastle Upon Tyne: Hydrogeochemical Engineering Research and Outreach.

Robati, D., 2013. Pseudo-second-order kinetic equations for modeling adsorption systems for removal of lead ions using multi-walles carbon nanotube. *Journal of Nanostructure in Chemistry,* Volume 3, p. 55.

Roehl, K. E., Meggyes, T., Simon, F. G. & Stewart, D. I., 2005. *Long-Term Performance of Permeable Reactive Barriers.* 1st ed. Amsterdam: Elsevier B.V..

Rosato, L., Harris, G. B. & Stanley, R. W., 1984. Separation of Nickel from Cobalt in Sulphate Medium by Ion Exchnge. *Hydrometallurgy,* Volume 13, pp. 33-44.

RoyChowdhury, A., Sarkar, D. & Datta, R., 2015. Remediation of Acid Mine Drainage-Impacted Water. *Current Pollution Reports,* 1(3), pp. 131-141.

Sahu, S., Sahoo, P. R., Patel, S. & Mishra, B. K., 2011. Oxidation of thiourea and substituted thioureas: a review. *Journal of Sulfur Chemistry,* 32(2), pp. 171-197.

Sanz, J., Lombraña, J. I. & De Luis, A. M., 2003. Microwave and Fenton's reagent oxidation of wastewater. *Environmental Chemistry Letters,* 1(1), pp. 45-50.

Sapsford, D. et al., 2007. Low Footprint Passive Mine Water Treatment: Field Demonstration and Application. *Mine Water and the Environment,* 26(4), pp. 243-250.

Sapsford, D., Cleall, P. & Harbottle, M., 2016. In Situ Resource Recovery from Waste Repositories: Exploring the Potential for Mobilization and Capture of Metals from Anthropogenic Ores. *Journal of Sustainable Metallurgy,* 3(2), pp. 375-392.

Scholes, L. et al., 1998. The treatment of metals in urban runoff by constructed wetlands. *The Science of the Total Environment,* 214(1-3), pp. 211-219.

Schwarzenbach, R. P. et al., 2010. Global Water Pollution and Human Health. *Annual Review of Environment and Resources,* Volume 35, pp. 109-136.

Scott, K. & Hughes, R., 1996. *Industrial Membrane Separation Technology.* 1st ed. s.l.:Springer Netherlands.

Sengupta, A., Zhu, Y. & Hauze, D., 1991. Metal(II) Ion Binding onto Chelating Exchangers with Nitrogen Donor Atoms: Some New Observations and related Implications. *Environmental Science and Technology,* 25(3), pp. 481-488.

SeQuant, 2007. *A Practical Guide to Ion Chromatography: An Introduction and Troubleshooting Manual,* Umeå, Sweden: SeQuant AB.

Shaaban, A. F. et al., 2014. Synthesis of a new chelating resin bearing amidoxime group for adsorption of Cu(II), Ni(II) and Pb(II) by batch and fixed-bed column methods. *Journal of Environmental Chemical Engineering,* 2(1), pp. 632-641.

Shi, Q. et al., 2018. Binary adsorption equilibrium and breakthrough of toluene and cyclohexane on macroporous and hypercrosslinked polymeric resins. *Microporous and Mesoporous Materials,* Volume 271, pp. 73-82.

Simate, G. S. & Ndlovu, S., 2014. Acid mine drainage: Challenges and opportunities. *Journal of Environmental Chemical Engineering,* 2(3), pp. 1785-1803.

Sofińska-Chmiel, W. & Kołodyńska, D., 2016. Purolite S940 and Purolite S950 in heavy metal ions removal from acidic streams. *Separation Science and Technology,* 51(15-16), pp. 2528-2538.

Sofińska-Chmiel, W. & Kołodyńska, D., 2016. Purolite S940 and Purolite S950 in heavy metal ions removal from acidic streams. *Separation Science and Technology,* 51(15-16), pp. 2528-2538.

Sole, K. C., Mooiman, M. B. & Hardwick, E., 2018. Ion exchange in hydrometallurgical processing: An overview and selected applications. *Separation & Purification Reviews,* 47(2), pp. 159-178.

Song, Y. et al., 2001. Lead and Zinc Removal by Laboratory-Scale Constructed Wetlands. *Water Environment Research,* 73(1), pp. 37-44.

Taimur, S., Hassan, M. I. & Yasin, T., 2017. Removal of copper using novel amidoxime based chelating nanohybrid adsorbent. *European Polymer Journal,* Volume 95, pp. 93-104.

Tavakoli, H., Sepehrian, H., Semnani, F. & Samadfam, M., 2013. Recovery of uranium from UCF liquid waste by anion exchange resin CG-400: Breakthrough curves, elution behavior and modeling studies. *Annals of Nuclear Energy,* 54(1), pp. 149-153.

Taylor, K., Banks, D. & Watson, I., 2016. Characterisation of hydraulic and hydrogeochemical processes in a reducing and alkalinity-producing system (RAPS) treating mine drainage, South Wales, UK. *International Journal of Coal Geology,* Volume 164, pp. 35-47.

Teignmouth Science and Technology Centre, 2017. *A Beginner's Guide to XPS,* Teignmouth: Teignmouth Science and Technology Centre.

ThermoScientific, 2019. *XPS: Copper.* [Online]
Available at: https://xpssimplified.com/elements/copper.php
[Accessed 26 June 2019].

Thomas, H. C., 1944. Heterogeneous Ion Exchange in a Flowing System. *Journal of the American Chemical Society,* 66(10), pp. 1664-1666.

Tolonen, E.-T.et al., 2014. Acid mine drainage treatment using by-products from quicklime manufacturing as neutralization chemicals. *Chemosphere,* 117(1), pp. 419-424.

Upreti, P. D., Tangyie, G. C., Huddersman, K. & Isla, S., 2016. *Field trial of an ion exchange based metal removal technology in the treatment of mine waters.* s.l., IMWA Symposium 2016.

Van Deventer, J., 2011. Selected Ion Exchange Applications in the Hydrometallurgical Industry. *Solvent Extraction and Ion Exchange,* 29(5-6), pp. 695-718.

Vanýsek, P., 2010. Electrochemical Series. In: W. M. Haynes, ed. *CRC Handbook of Chemistry and Physics.* Boca Raton: CRC Press, pp. 20-29.

Vilensky, M. Y., Berkowitz, B. & Warshawsky, A., 2002. In Situ Remediation of Groundwater

Contaminated by Heavy- and Transition-Metal Ions by Selective Ion-Exchange Methods.

Environmental Science and Technology, 36(8), pp. 1851-1855.

Westermann, S. et al., 2017. *Evaluation of mine water rebound processes in European Coal Mine*

Districts to enhance the understanding of hydraulic, hydrochemical and geomechanical processes.

Lappeenrata, Finland, International Mine Water Association.

WHO/UNEP, 1997. *Water Pollution Control - A Guide to the Use of Water Quality Management*

Principles, London: E. & F. Spon.

Williams, B. K., 2011. Passive and active adaptive management: Approaches and an example. *Journal*

of Environmental Management, 92(5), pp. 1371-1378.

Wolkersdorfer, C., 2008. *Water Management at Abandoned Flooded Underground Mines.* 1st ed.

Freiberg: Springer-Verlag.

Wołowicz, A. & Hubicki, Z., 2012. The use of the chelating resin of a new generation Lewatit

MonoPlus TP-220 with the bis-picolylamine functional groups in the removal of selected metal ions

from acidic solutions. *Chemical Engineering Journal,* Volume 197, pp. 493-508.

Xu, Z., Cai, J.-G. & Pan, B.-C., 2013. Mathematically modeling fixed-bed adsorption in aqueous

systems. *Journal of Zhejiang University SCIENCE A,* Volume 14, pp. 155-176.

Yan, G., Viraraghavan, T. & Chen, M., 2001. A New Model for Heavy Metal Removal in a Biosorption

Column. *Adsorption Science and Technology,* 19(1), pp. 25-43.

Yilmaz Ipek, I., Kabay, N. & Yüksel, M., 2013. Modeling of fixed bed column studies for removal of

boron from geothermal water by selective chelating ion exchange resins. *Desalination,* Volume 310,

pp. 151-157.

Younger, P. L., 2000. Holistic remedial strategies for short- and long-term water pollution from abandoned mines. *Mining Technology,* 109(3), pp. 210-218.

Younger, P. L., 2000. The Adoption and Adaptation of Passive Treatment Technologies for Mine Waters in The United Kingdom. *Mine Water and the Environment,* 19(2), pp. 84-97.

Younger, P. L., 2001. Mine water pollution in Scotland: Nature, extent and preventative strategies. *Science of the Total Environment,* 265(1-3), pp. 309-326.

Younger, P. L., Banwart, S. & Hedin, R., 2002. *Mine Water: Hydrology, Pollution, Remediation.* s.l.:Kluwer Academic.

Younger, P. L. et al., 2003. Passive treatment of acidic mine waters in subsurface-flow systems: exploring RAPS and permeable reactive barriers. *Land Contamination and Reclamation,* 11(2), pp. 127-135.

Zainol, Z. & Nicol, M. J., 2009. Ion-exchange equilibria of Ni2+, Co2+, Mn2+ and Mg2+ with iminodiacetic acid chelating resin Amberlite IRC 748. *Hydrometallurgy,* 99(3-4), pp. 175-180.

Zhang, Y., Liu, Q. & Li, L., 2016. Removal of iron from synthetic copper leach solution using a hydroxy-oxime chelating resin. *Hydrometallurgy,* Volume 164, pp. 154-158.

11 APPENDICES

11.1 MANUFACTURER SPECIFICATIONS OF RESINS

To provide further detail of the characteristics of the nine resins used during the static screening studies presented in Chapter 5, manufacturer-supplied specifications are summarised in Table 11.1. A range of functionalities were selected, but where possible, differences in the polymer matrix were kept to a minimum.

Because the exact methods used by manufacturers to determine total capacity were not declared, and given that capacities were reported using inconsistent units, the specified capacities have been uniformly converted to equivalents per litre (Eq/L) using the relationship in Equation 11.1. It is important to note that because the methods used to generate total capacity values were not detailed by manufacturers, and were evidently generated using a range of techniques (e.g. different metal loadings and titrations) the values reported in specification sheets should only be used as approximate guidelines, and actual operating capacities can only be determined experimentally (e.g. through isotherm or fixed-bed studies) using the solutions for which treatment is intended.

Equation 11.1. Relationship used for unit conversion of reported total capacities (from g to Eq)

$$E_q = \frac{Mass\ of\ Metal\ (g)}{Atomic\ Mass\ (g/mol)} \times Valency$$

Table 11.1. Manufacturer-specified characteristics of ion exchange resins used (PS = polystyrene, PA = polyacrylic, DVB = divinylbenzene; *based on feedstock of 6 g/L Cu at pH2, **unknown feedstock and/or methodology, capacities converted to Eq/L where necessary).

Name	Alias	Functionality	Reported Capacity	Converted Capacity (Eq/L)	Polymer Matrix	Moisture Content (%)	Particle Size (μm)
Dowex M4195	M4195	Bis-picolylamine	35-42 g/L Cu*	1.1-1.3	PS-DVB	40-60	297-841
Puromet MTS9301	S930	Iminodiacetic acid	45 g/L Cu**	1.42	PS-DVB	52-60	425-1000
Puromet MTS9100	S910	Amidoxime	40 g/L Cu**	1.26	PA-DVB	52-60	300-1200
Puromet MTS9501	S950	Aminophosphonic acid	26 g/L Ca**	1.30	PS-DVB	60-68	300-1200
Puromet MTS9570	S957	Phosphonic/sulfonic acid	18 g/L Fe**	0.64	PS-DVB	55-70	315-850
Puromet MTS9140	S914	Thiourea	1 Eq/L**	1	PS-DVB	50-56	300-1200
Puromet MTS9200	S920	Isothiouronium	275 g/L Hg**	2.74	PS-DVB	48-54	300-1200
Puromet MTS9850	S985	Polyamine	2.3 Eq/L**	2.3	PA-DVB	52-57	300-1200
Dowex M31	M31	Sulfonic acid	1.95 Eq/L**	1.95	PS-DVB	50-54	420-1190

11.2 Metal Speciation as a Function of pH

To provide insight to the behaviour of resins observed during static screening experiments in Chapter 5, the speciation of metals (Al, Cu, Fe, Mn, Ni, Zn) was modelled using the Aqion 7.1.5 GUI (Aqion, 2020) for PhreeqC geochemical modelling software (Parkhurst & Apello, 1999). Model calculations were performed at 9 intervals for each metal across a proton concentration range of 0.001-10 M H^+, with charge balances satisfied by addition of SO_4^{2-} to represent pH alteration using sulfuric acid. Calculations were made at a simulated temperature of 25°C, using an open CO_2 system to simulate the headspace above solutions during resin contacts. Data for each metal species were presented as a percentage of total concentration to represent the relative activity of each species as a function of pH. Given the high ionic strength of solutions used during sulfate screening experiments, it was not possible to accurately resolve PhreeqC calculations, and so this data is not presented. Furthermore, the absence of Co data within the native Aqion 7.1.5 dataset did not allow for Co speciation to be calculated under the studied conditions.
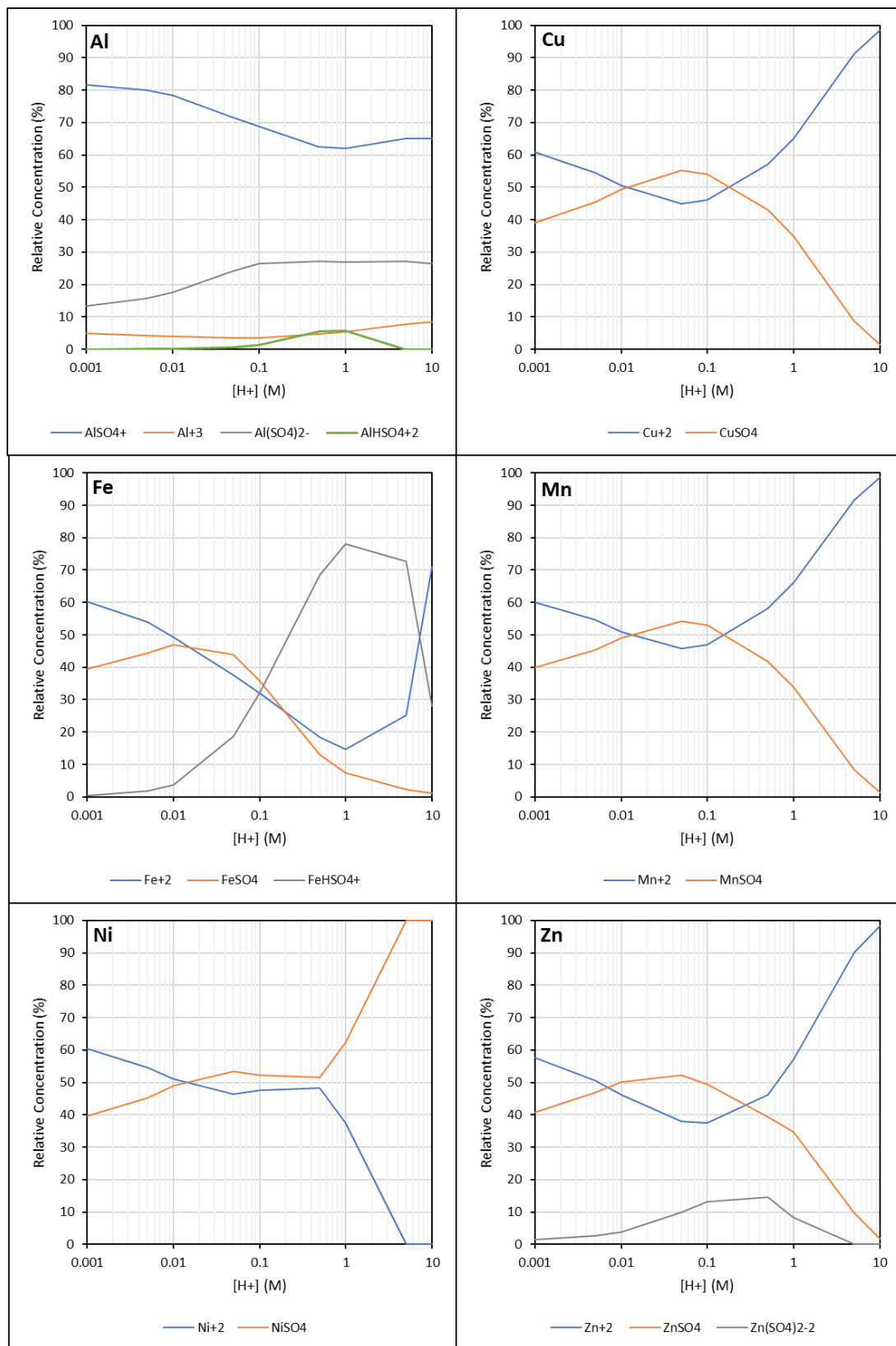
Figure 11.1. Speciation of Al, Cu, Fe, Mn, Ni, and Zn as a function of [H$^+$] in H$_2$SO$_4$ media. Modelling performed using Aqion 7.5.1. interface for PHREEQC.

11.3 NITRIC ACID ELUTION OF COPPER FROM PUROMET MTS9140

SAFETY WARNING: The use of concentrated nitric acid for the oxidation of Cu(I)

resulted in reduction of nitric acid (HNO_3) and subsequent formation of nitric

oxide (NO) gas. NO gas is hazardous (see hazard statements H270, H330, H314),

and the generation of gases in a closed column system may result in explosive

pressure release. As such, this procedure is not advised to be repeated.

Results

To quantify the extent to which nitric acid could act as a suitable eluent for Cu-loaded thiourea resin,

a 5 mL column of S914 was loaded dynamically (Figure 11.2), after which aliquots of the 5 mL bed

volume were used for subsequent elution experiments. Integration of the area above the loading

curve suggested a total of 29.03 mg Cu adsorbed to the column, equating to a loading of 5.81 mg
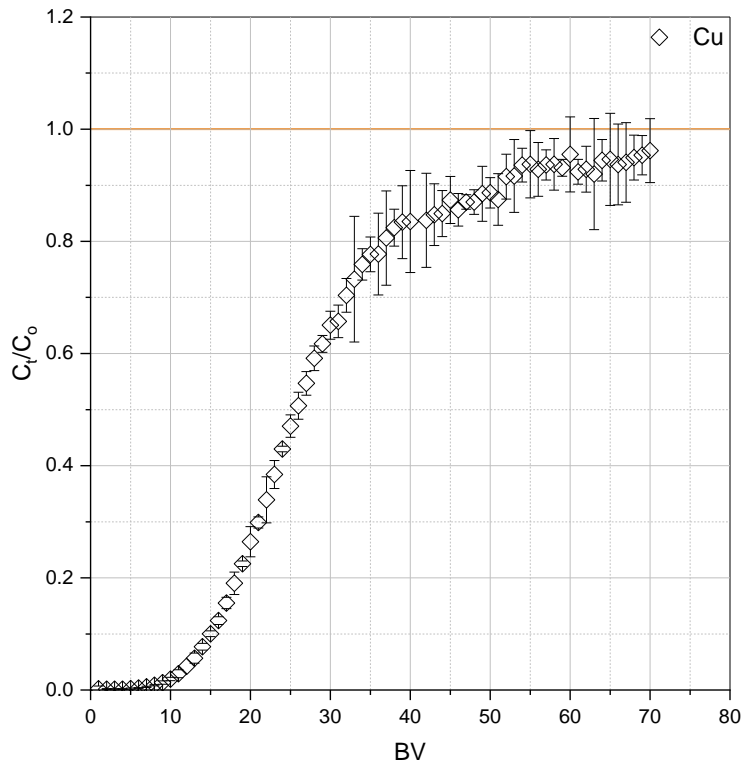
Cu/mL S914 for this batch of resin.

Figure 11.2. Breakthrough curve of Cu from S914 (5 mL BV, 5 BV/h, 400 mg/L Cu, pH 1.55).

Figure 11.3 presents three elution profiles of Cu from S914 using a 3 M HNO$_3$ solution as an eluent. The first elution profile (labelled Elution 1) occurred at 27 mL throughput (31 BV) and was very sharp, with a maximum Cu concentration of 2853.6 mg/L (2.85 g/L). Prior to the elution curve, Cu concentrations are negligible in effluent solutions, as is the case for effluent solutions following the point of maximum elution. The 1.6 mL BV column was calculated to be loaded with 9.29 mg Cu, with analysis of elution curve area suggesting a 109% Cu recovery. While recovery beyond 100% is an impossibility, such a result is attributed to the loading procedure, whereby variation in the loading profile within the larger 5 mL may cause discrepancy between the calculated loading of the 5 mL column and the smaller aliquots. Nevertheless, given the sharpness and magnitude of the profile it is assumed that a near-total recovery was achieved.

Inconsistencies in sample collection were observed, with the bed volume immediately prior to Cu elution being overfilled, and empty 'missed' fractions during the Cu elution stage (hence the low data

resolution during the Elution 1 in Figure 11.3). This was initially attributed to a malfunction of the fraction collector during the experimental run, and so the elution was repeated using a separate aliquot of Cu-loaded S914.

Repetition of Cu elution with 3 M HNO_3 also yielded a sharp curve and high maximum concentration (Elution 2 in Figure 11.3), yet this occurred sooner than during the first elution attempt (11 mL throughput). The maximum Cu concentration was also much higher; 5208 mg/L compared to 2853 mg/L. As for the previous elution, the issue of 'missed' and overfilled fractions surrounding the elution phase was encountered, but in this case was observed to be due to the formation of gas during the elution cycle which caused an airlock within the small column used.

Given the inconsistencies of previous elution experiments, the 3 M HNO_3 elution experiment was repeated once more using a batch-loaded resin (loaded to 8.64 mg Cu/mL resin), the results of which are also presented in Figure 11.2 (Elution 3). In this instance, the highest Cu concentration (5400 mg/L) occurred at 10 mL throughput, comparable to Elution 2. Again, the formation of gas bubbles within the column and tubing caused the airlock issues previously encountered and resulted in low data resolution during the Cu elution event. Comparison of the three elution curves concurrently clearly exhibits the variation in their position and magnitude, despite comparable recoveries (Table 11.2).
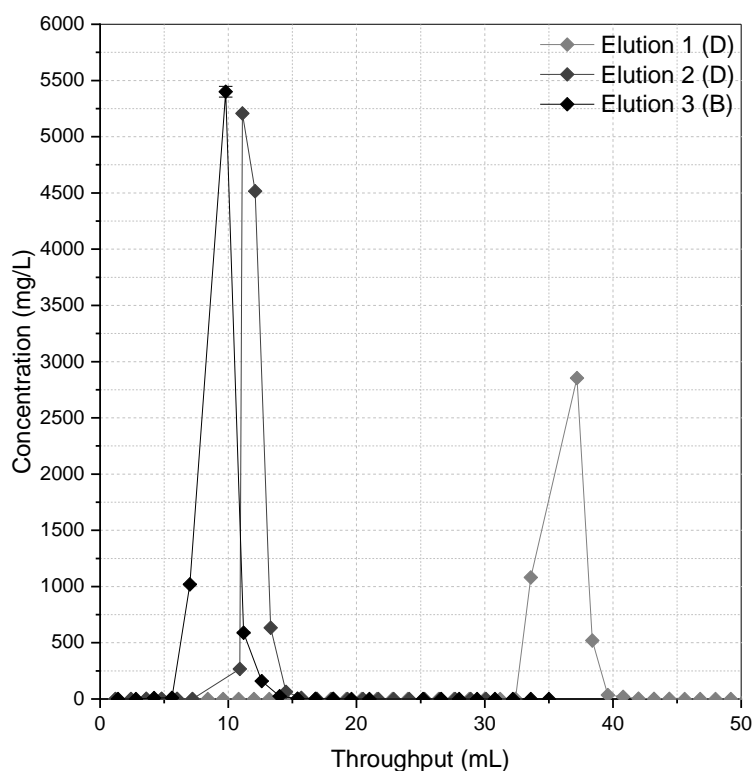
Figure 11.3. Comparison of Cu elution profiles from S914 using 3 M HNO3 at 2 BV/h (D = dynamically-loaded resin, B = batch-loaded resin).

Table 11.2. Details of Cu elution investigations using HNO_3 (FWHM = Full width at half maximum; provided for comparison of profile widths).

	Eluent	Loading Method	Cu loading	Bed Volume	Total Cu available	Cu recovered	FWHM	Recovery efficiency
			mg/mL	mL	mg	mg	mL	%
Elution 1	3 M HNO$_3$	Dynamic	5.805	1.6	9.289	10.142	3.6	109.2
Elution 2	3 M HNO$_3$	Dynamic	5.805	1.6	9.289	9.465	1.7	101.9
Elution 3	3 M HNO$_3$	Batch	8.641	1.6	13.825	14.580	2.5	105.5
Elution 4	1 M HNO$_3$	Batch	8.641	1.4	12.097	0.837	-	6.92

The use of lower concentration nitric acid was investigated to attempt to minimise the gas formation

issues encountered. Elution was repeated using 1 M HNO$_3$ and a fresh aliquot of batch loaded S914

packed in to a 1.4 mL BV column. The resulting Cu elution profile indicated poor potential of this
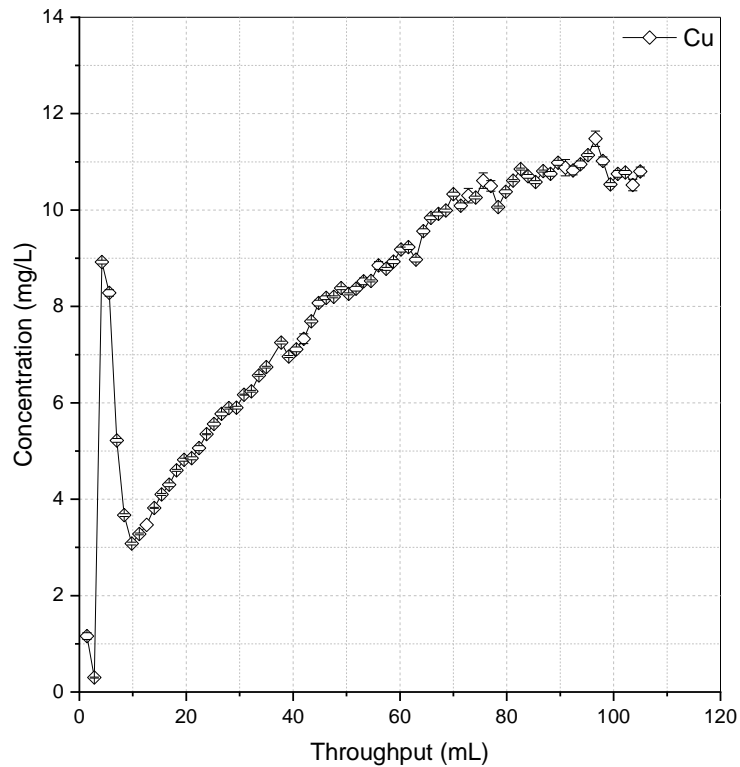
eluent for Cu recovery (Figure 11.4).

Figure 11.4. Elution of Cu from S914 using 1 M HNO3 at 2 BV/h.

Despite an initial spike, Cu concentrations remained relatively low over the experimental run, with no complete elution profile captured over a 75 BV period. Analysis of the curve suggested recovery of under 7% over the studied period (Table 11.2). While it is anticipated that given enough time, a higher recovery efficiency would be achieved, the relatively low definition of the elution curve when compared to those presented in Figure 11.3 suggested that 1 M HNO_3 would not be a suitable eluent for effective resource recovery given the lower concentration product stream that would result from such an elution profile.

Discussion

The recovery of Cu from S914 using 3 M HNO_3 was highly effective, with complete recovery achieved during every repetition (Table 11.2). Despite the high efficiency of this eluent, problems were encountered due to gas formation which led to airlocks within the column and resulted in highly

varied elution profiles (Figure 11.3). The formation of gas within the column was likely a product of

the redox interaction between nitrate and Cu(I). The half-reactions for the reduction of Cu(I) and

nitrate, and standard reduction potentials ($\varepsilon°$) are provided in Equation 11.2 and Equation 11.3.

Equation 11.2. Reduction half-reaction of Cu(II) to Cu(I) and standard reduction potential (V).

$$Cu^{2+} + e^- \rightarrow Cu^+ \quad (\varepsilon° = 0.153\ V)$$
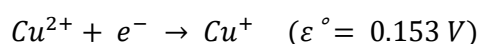
Equation 11.3. Reduction half-reaction of nitrate and standard reduction potential (V).

$$NO_3^- + 4H^+ + 3e^- \rightarrow NO + 2H_2O \quad (\varepsilon° = 0.957\ V)$$
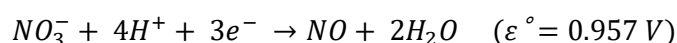
When the above Equations are combined, with Cu(I) being oxidised to Cu(II), and NO_3 being oxidised,

the resulting balanced redox reaction is formed, requiring three moles of cuprous ions per mole of

nitrate (Equation 11.4).

Equation 11.4. Proposed redox reaction between Cu^+ and NO_3^- during the HNO_3 elution of Cu from S914.

$$3Cu^+_{(resin)} + NO_3^-{}_{(aq)} + 4H^+{}_{(aq)} \rightarrow 3Cu^{2+}{}_{(aq)} + NO_{(g)} + 2H_2O_{(l)}$$
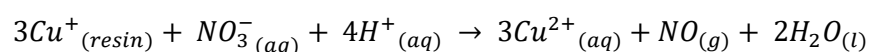
Considering the products of Equation 11.4, nitric oxide (NO) gas was likely responsible for the airlock

problems encountered in columns when using 3 M HNO_3 as an eluent. Electrochemical nitrate

reduction by copper has been reported elsewhere, particularly in acidic media where the products

were NO and NH_4^+ (Pérez-Gallent, et al., 2017). The reduction of nitrate cannot be initiated by Cu

metal or Cu(II) ions, but the catalytic effect of Cu(I) ions does allow nitrate to reduce and form NO

gas, as reported by Filimonov & Shcherbakov (2004), further suggesting that this was the case during

3 M HNO_3 elution. It was also likely that the nitric acid oxidised not only the Cu(I) loaded to the resin

but also the thiourea functional groups. At high acidity it is known that thiourea may be completely oxidised by HNO_3 to form NO gas (Kirchnerova & Purdy, 1981), which may also have contributed to the observed behaviour.

Reducing the concentration of the eluent was explored to minimise the extent of NO formation (Figure 11.4). However, a low Cu recovery efficiency was obtained (Table 11.2), potentially due to the lower acidity of the eluent not being able to provide the protons required for nitrate reduction, as per Equation 11.4. It was deemed that the use of concentrated nitric acid as an eluent for S914 would be unsuitable for two main factors; a) the observed formation of NO gas could hinder process scale-up and pose a health and safety hazard, and b) the safety concerns of handling large volumes of highly concentrated nitric acid at a larger scale.